FORCED CONVECTIVE EVAPORATION AT SUB-ATMOSPHERIC PRESSURE

by

Leong Wan Cheah

A thesis submitted in fulfilment of the requirements for the degree of Doctor of Philosophy of the University of London and for the Diploma of Imperial College of Science, Technology and Medicine

Department of Chemical Engineering and Chemical Technology, Imperial College of Science, Technology and Medicine, London, SW7 2AZ

December 1995

In memory of my late-grandmother,

for my parents and my whole family

Abstract

This thesis is the culmination of a research programme on forced convective evaporation at sub-atmospheric pressures in the vertical upward flow of water. The objectives of the work were: (i) the design, construction, commissioning and operation of a new industrial scale, electrically heated, single tube, sub-atmospheric evaporator (SAE) rig and its instrumentation, (ii) to conduct steady state experiments using the SAE rig with exit pressures as low as 250 mbar abs., and finally, (iii) to design and program a framework/methodology for the phenomenological modelling of two-phase flow and heat transfer for these conditions. These three objectives were successfully achieved and the conclusions drawn are reported.

From the experimental results, several interesting features and effects were observed, namely; heat transfer coefficient maxima at around zero quality for high inlet subcoolings and at low sub-atmospheric pressures which were attributed to local thermal non-equilibrium instability as hypothesised by Jeglic and Grace (1965); and a flow boiling hysteresis similar to that observed by Abdelmessih et al. (1974) seems to occur.

The modelling work was embodied into a computer code, SAE. The SAE code together with the Chen (1966) and the Liu and Winterton (1991) flow boiling correlations were found to be inadequate to predict the SAE experimental results as the pressure is lowered. This is to be expected since the present SAE code uses models and correlations derived from atmospheric and high pressure data. Nevertheless, the SAE code is most promising from the point of view of providing a framework for future developments and improvements, since its flow regime based structure and modularity allows alternative models to be easily substituted.

Acknowledgement

Firstly and most importantly, I would like to express my deepest gratitude to Professor G.F. Hewitt, FRS, FEng, for his patience, perseverance, guidance, support and friendship, which had been both invaluable and enlightening.

I would also like to thank members of the Academic Staff, especially Dr. P.G. Clay, who has been, not only a personal tutor but also a friend.

I am grateful to members of the Technical Services, Electronics, Computing, Workshop, Library, Secretarial and Security of the Chemical Engineering Department for their assistance and friendship, which I deeply cherish.

I would like to thank my friends and colleagues in the Multiphase Flow System Group, both past and present, for their friendship and assistance. In particular Dr. P.F. Pickering during the construction and commissioning of the sub-atmospheric evaporator (SAE) rig.

I would also like to thank British Nuclear Fuels Plc. for sponsoring this project, in the form of an Imperial College Student Bursary and industrial project account.

Finally, I would also like to take this opportunity to thank my dear friends in the Chemical Engineering and Computing departments, past and present, as well as those from University College London (UCL), for their antics, fun, laughter and support during my Ph.D. and hopefully, beyond.

Nomenclature

Latin Characters:

A	cross sectional area of channel	m^2
C	homogeneous concentration of droplets in the core	$kg\ m^{-3}$
C_0	distribution parameter	
Ch	*'churn flow'* ratio (introduced in Chapter 6)	
C_p	specific heat capacity at constant pressure	$J\ kg^{-1}\ K^{-1}$
D	diameter	m
D	deposition rate per unit peripheral area	$kg\ m^{-2}\ s^{-1}$
D_d	bubble departure diameter	m
d_i	internal tube diameter	m
E	entrainment rate per unit peripheral area	$kg\ m^{-2}\ s^{-1}$
E	two-phase flow enhancement factor (Winterton & co-workers)	
F	two-phase flow enhancement factor (Chen, 1963, 1966)	
f	friction factor	
f_i	interfacial friction factor	
g	gravitational acceleration	$m\ s^{-2}$
h	specific enthalpy	$J\ kg^{-1}$
h_{LG}	latent heat of vaporisation	$J\ kg^{-1}$
$\Delta h_{subcool}$	inlet subcooling	$J\ kg^{-1}$
k	droplet mass transfer coefficient	$m\ s^{-1}$
L	length	m
L_b	Taylor bubble length	m
L_s	liquid slug length	m
l_e	entrance length	m
M	relative molecular mass	$kg\ kmol^{-1}$
M	momentum flux	$N\ m^{-2}$
$\dot{M}$	mass flow rate	$kg\ s^{-1}$

m	mass	kg
$\dot{m}$	mass flux	kg m^{-2} s^{-1}
$\dot{m}_G$	gas mass flux	kg $m^{-2}s^{-1}$
$\dot{m}_L$	liquid mass flux	kg $m^{-2}s^{-1}$
$\dot{m}_{LF}$	liquid film mass flux	kg $m^{-2}s^{-1}$
$\dot{m}_{LFC}$	critical liquid film mass flux for onset of entrainment	kg $m^{-2}s^{-1}$
$\dot{m}_{LE}$	entrained liquid mass flux	kg $m^{-2}s^{-1}$
P	tube periphery	m
p	pressure	N m^{-2}
p_c	critical pressure	N m^{-2}
p_r	reduced pressure	
Δp_{sat}	difference in saturation pressure corresponding to saturation temperature difference	N m^{-2}
$\dot{q}$	heat flux	W m^{-2}
$\dot{q}_I$	heat flux at the point of intersection between single-phase liquid convection and fully developed nucleate boiling	W m^{-2}
R	gas constant	kJ $kmol^{-1}$ K^{-1}
R_p	surface roughness parameter (Glättungstiefe, DIN 4762)	µm
R_V	delivered gas-to-liquid volume ratio	
r_1, r_i	inner wall radius	m
r_2, r_o	outer wall radius	m
r_b	bubble radius	m
r_c	cavity radius	m
r_c'	critical cavity radius	m
S	suppression factor	
T	temperature	K
T_{sat}	saturation temperature	K
ΔT_{sat}	wall superheat	K
u	velocity	m s^{-1}
u_{GU}	mean relative velocity (drift velocity)	m s^{-1}
u_S	rise velocity of a single slug	m s^{-1}
U	superficial velocity	m s^{-1}

U^*	dimensionless superficial velocity	
$\dot{V}_L$	liquid volumetric flow rate	$m^3 s^{-1}$
$\dot{V}_G$	gas volumetric flow rate	$m^3 s^{-1}$
x	vapour quality	
x	Cartesian coordinate	m
y	Cartesian coordinate	m
z	distance along a tube, Cartesian coordinate	m

Dimensionless numbers:

Bo	Boiling Number
Co	Convective Number
Fr	Froude Number
Ku	Kutateladze Number
Nu	Nusselt Number
Pe	Peclet Number
Pr	Prandtl Number
Re	Reynolds Number
St	Stanton Number
We	Weber Number

Greek Characters:

α	heat transfer coefficient	$W m^{-2} K^{-1}$
β	volumetric flow ratio	
β	ratio of Taylor bubble length to total slug length	
Γ	film flow rate (by mass) per unit wetted perimeter	$m s^{-1}$
δ	liquid film thickness	m
ε	void fraction	
ε	surface roughness	m
η	dynamic viscosity	$kg m^{-1}s^{-1}$
θ	contact angle	°

θ	angle of inclination from the horizontal	°
κ	thermal diffusivity	$m^2 s^{-1}$
λ	thermal conductivity	$W m^{-1} K^{-1}$
λ	dimensionless scaling parameter, Baker (1954)	
ν	kinematic viscosity	$m^2 s^{-1}$
ρ	density	$kg m^{-3}$
σ	surface tension	$N m^{-1}$
τ	shear stress	$N m^{-2}$
ψ	dimensionless scaling parameter, Baker (1954)	
Ω	Baroczy (1965) two-phase multiplier ratio	

Subscripts:

A	accelerational
avg	average
b	bubble
c	cavity
c	critical
F	frictional
f	film
FC	forced convective
fdb	fully developed nucleate boiling
G	gas phase
G	gravitational
GC	gas core
GO	total mass flux flowing with gas phase properties
i	interfacial
i	inside
inlet	inlet conditions
L	liquid phase
LE	entrained liquid
LF	liquid film

LFC	critical liquid film for onset of entrainment
LO	total mass flux flowing with liquid phase properties
m, mix	mixture
max	maximum
NB, nb	nucleate boiling
NVG	net vapour generation
o	outside
ONB	onset of nucleate boiling
r	reduced properties
s	specific fluid properties with reference to water
s	slug
sat	saturation
scb	subcooled boiling
spl	single-phase liquid
TP	two-phase
w	wall

List of Figures

Chapter 6

List of Tables

Table of Contents

CHAPTER 1

INTRODUCTION

1.1 Uses and aims of the research project

Two-phase flow occurs in a diverse range of industrial plants, boilers, refrigeration systems, condensers and nuclear reactors. In the nuclear industry, heat transfer in two-phase flow in both vertical and horizontal conduits is a common process. A good understanding of the mechanisms involved both quantitatively and qualitatively is extremely important, and the need arises mainly from three key sources as classified by Shires (1977). Firstly, there is the need of the design engineers for information to help them to optimise their process designs in order to achieve higher efficiency and to produce products or provide services that is competitive in today's market. The second need is that of the operators of the process plants, who need to decide on the optimum operating conditions or, in a less fortunate case, to investigate and diagnose faults or accidents which have already occurred. Finally, the most important and crucial need is that of a safe and reliable operation of the process plant, where in some cases it is necessary to know precisely the maximum safe operating limits. This is particularly true in the nuclear industry where adequate safety margins must be allowed. Recently, an additional need has materialised in the form of environmental protection and preservation where companies are encouraged, and in some cases, required by law to minimise the impact of their industrial processes on the environment, namely in terms of waste discharge and energy consumption. It is to

fulfil these needs both directly and indirectly that most industrially sponsored research programmes are born .

The research work described in this thesis is funded by British Nuclear Fuels PLC. (BNFL), with the emphasis on the steady state hydrodynamics and heat transfer behaviour in forced convective vaporisation at sub-atmospheric pressures in vertical upward flow. BNFL operates a number of reboilers and evaporators in its various process plants. Typically such evaporators would be of the multi-tube type, with vaporisation taking place inside the stainless steel tubes (typical diameters of 1 inch and 2 inch - 25.4 and 50.8 mm) with lengths of the order of 4 to 5 metres. These tubes are heated externally by condensing steam. The fluid evaporated is normally an aqueous solution, containing nitric acid. Even with stainless steel, the nitric acid can be highly corrosive if the temperature is sufficiently high. Consequently, in order to maintain a low temperature, the evaporator systems are normally operated at sub-atmospheric pressures, as low as 0.2 bar, where the saturation temperature is low enough to minimise corrosion.

Although extensive work has been carried out on boiling heat transfer and associated fluid flow phenomena at pressures ranging from one atmosphere to the critical pressure (221.2 bars), there is a dearth of data at sub-atmospheric pressures. Therefore, this research programme was designed to redress this by producing an experimental database at sub-atmospheric conditions. Another important component of this work is to provide a framework/methodology to approach the modelling of two-phase flow at these conditions, drawing from the vast pool of knowledge and data available in the higher pressure studies and from the sub-atmospheric experimental results. The framework designed will be in the form of a FORTRAN computer program written to model the major hydrodynamics parameters (pressure drop, void fraction and quality) and the heat transfer coefficient for a vertical tube evaporator.

Hence, the objectives of this Ph.D. research programme are as follows:

1) To design, construct, commission and operate a new sub-atmospheric evaporator (SAE) rig and its instrumentation.

2) To perform and collect experimental data at sub-atmospheric pressures, as low as 250 mbar abs.

3) To design and code a framework/methodology for the phenomenological modelling of two-phase flow.

1.2 Description of the thesis

This thesis is divided into 7 major chapters and 5 appendices. After this introductory chapter, the rest of the chapters will focus on the following areas.

Chapter 2

Chapter 2 focuses on the hydrodynamics literature reviewed for this work. These reviews are presented in the form of discussions on the gas-liquid two-phase flow in general, followed closely by a section on the physical description of two-phase flow patterns and the two main methods used to classify the various flow regimes, i.e. by using flow pattern maps and semi-theoretical transitions. This is followed by reviews on pressure drop models for single and two-phase flow, and on void fraction models such as the homogenous flow model, Zuber-Findlay drift flux model and an alternative drift flux model proposed by Chexal and Lellouche (1991).

Chapter 3

This chapter presents the second major part of the literature review on flow boiling and its sub-sections of single-phase liquid convection, subcooled flow boiling and saturated flow boiling. The subcooled boiling review is divided into (1) *onset of nucleate boiling* (ONB) and *net vapour generation* (NVG), (2) partial subcooled boiling heat transfer and (3) fully developed subcooled nucleate boiling . For saturated flow boiling, the review is also classified into the heat transfer models on which the correlations such as Chen (1966) were based. The classifications used were based on those proposed by Webb and Gupte (1992) into superposition, asymptotic and enhancement models. The chapter finally concludes with a discussion on other research work on sub-atmospheric vaporisation available in published literature, most notably that of Stone (1971).

Chapter 4

In chapter 4, the sub-atmospheric evaporator (SAE) rig that was built as part of the research work is described and its operating procedures are outlined. The measurement apparatus and techniques used for measuring the wall and fluid temperatures, pressure drop along the test-section, inlet fluid flow rate and their associated calibrations are described in some detail, together with the data acquisition system devised and the programs used. The experimental matrix that was performed was discussed, noting the 4 key operating parameters present, i.e. the outlet pressure at the top of the test-section, the heat flux, the mass flux and the inlet subcooling.

Chapter 5

Chapter 5 discusses the results from the experiments, in particular the effects on pressure gradient and heat transfer coefficient values as a result of varying mass fluxes, heat fluxes, outlet pressures and inlet subcooling. The main results discussed are those in the churn and annular flow regimes whose conditions were similar to those expected in the actual BNFL evaporator systems.

Chapter 6

Chapter 6 focuses on the various sub-annular flow models for hydrodynamics and heat transfer used in constructing the computer code SUBANA and also a section on the Harwell Annular Flow Model (HANA). By combining these two codes, a flow model program is presented, known as SAE, that enables the modelling of forced convective vaporisation in a vertical tube from single-phase liquid flow to two-phase annular flow. A feature of this model is that the code is *flow regime* based rather than the normal practice of performing calculations in a predetermined number of steps with fixed intervals along the length of the tube being modelled. Another feature of this program is its modularity (in the form of independent subroutines) which will facilitate future modifications as more advancements are made in the field of multiphase flow. Improvements on some of the current sub-annular models used are presented and discussed, namely those in slug flow and churn flow. For churn flow, a new approach based on the dimensionless gas superficial velocity U_G^* for evaluating the void fraction, wall shear stress and pressure gradient is introduced. The chapter concludes with the comparison of the results obtained from the sub-atmospheric experiments against those of the modelling program and some general flow boiling correlations found in the literature, with the intention of validating the code. The main variables for comparisons will be the flow regimes encountered, the total test-section pressure drop and the heat transfer coefficient along the length of the test-section.

Chapter 7

Although some conclusions are presented at the end of each of the preceding chapters, Chapter 7 provides a summary of the most important conclusions, followed by some recommendations for future research work.

This thesis is completed by the reference section and appendices. Appendix A presents the derivation of the equation used to calculate the temperature difference across the test-section wall based on one-dimensional steady state conduction with thermal energy generation for a radial geometry. Appendix B provides the thermocouple

calibration results whilst Appendix C discusses the estimation of experimental error and its analysis. The procedures which were employed to determine the experimental matrix is discussed in Appendix D. Appendix E will list the experimental runs conducted together with their key parameters.

CHAPTER 2

LITERATURE REVIEW :

HYDRODYNAMICS

The enormous potential of boiling as a mechanism of heat transfer at low temperature differences can be said to be truly realised around the 1930s. Nukiyama's (1934) description of the "boiling curve" for boiling of water at atmospheric pressure from a horizontal wire heater, has long been cited and regarded by many researchers as the first modern investigation of the boiling transitions. This is not to say that prior to Nukiyama, there wasn't any work being done on the subject but, rather that Nukiyama's work was viewed as a progenitor for the coming growth and interest in the boiling field. Three decades later, Gouse (1964) conducted a literature survey of over 6000 citations in boiling and two-phase flow, with the aim of encompassing all the known and available literature at that time. The massive amount of literature quoted by Gouse confirmed the rapid growth of research in the field in such a short intervening period of time. Since then, no other researcher has publicly attempted to do what Gouse did, but the qualitative evidence is of a continued growth of, and publications in, the field.

Bearing in mind this perspective, the objective of the present and next chapters are to survey the published literature on two-phase flow and flow boiling heat transfer in a vertical flow channel only in sufficient detail to provide a firm basis and platform for the discussion of the analytical and experimental work in subsequent chapters. This

chapter will focus exclusively on the hydrodynamics of two-phase gas-liquid flow and then followed by the next chapter on flow boiling heat transfer.

2.1 Gas-liquid two-phase flow

As the name suggests, gas-liquid two-phase flow is the simultaneous flow of a liquid phase in direct contact with a gaseous phase in a channel. Gas-liquid two-phase flow is one of the four possible combinations of two-phase flows, the others being gas-solid, liquid-liquid and liquid-solid flows. Of these four types of two-phase flows, the gas-liquid flows are the most complex in the sense that they combine the characteristics and effects of a deformable interface together with the compressibility of one of the phases. In the case of a diabatic system, there are the added effects caused by an exchange of energy in the form of heat.

Although gas-liquid two-phase flows occur in a variety of industrial equipment and processes, there was relatively little work done on the subject until the advent and development of the nuclear power industry in the 1950s. This key industrial development led to a rapid expansion and improvement in the level of knowledge of gas-liquid two-phase flows, particularly in high pressure steam and water systems. However, despite these great strides, there is still no general model for predicting with accuracy the behaviour of two-phase flows. Consequently, many designers adopt one of the two following approaches when designing for two-phase flow systems.

1) **Empirical correlation**. This approach involves the correlation of experimental data in dimensional or non-dimensional form to produce design relationships. Empirical correlations have been fairly successful in the prediction of design parameters such as pressure gradient and heat transfer coefficient where there is a large and extensive database of measured values available. However, this approach suffers from a serious deficiency in that one cannot reliably extrapolate such correlations to conditions beyond those of the original database from which the

correlations were derived from. This limitation has led many researchers to adopt a modelling approach in trying to improve the generality of prediction of two-phase flows.

2) **Modelling.** The key element in the modelling approach is to try and improve the prediction of two-phase flows by describing mathematically the mass and heat transport phenomena that are taking place. However, because of the complex and intricate nature of two-phase flows, most of the standard methods of analysis used for two-phase flows are normally extensions (e.g. in the forms of two-phase flow multipliers) of those already well-tried and tested for single-phase flows. The procedure is to write down the basic equations governing the conservation of mass, momentum and energy, and, to solve these equations by making use of simplifying assumptions or constitutive relations. The three main types of simplifying assumptions that are usually made are:

- *Homogeneous Flow Model.* This is the simplest of the three assumptions. Here, the two-phase flow is assumed to behave as a homogeneous fluid with the velocities of the two phases being identical (velocity ratio, S = 1) and having homogeneous physical properties calculated by suitably weighting the physical properties of each individual phases. The homogeneous flow is also sometimes known in some literature as *fog flow* (for example, see Collier and Thome, 1994).

- *Separated Flow Model (Six equation model).* In this model, the basic assumption is that the two phases flow in separate zones, which may interact with each other. The two phases flow in their separate regions each with its own velocity, thus the velocity ratio S, is not equal to 1 as for the homogeneous flow. Conservation equations are written for mass, momentum and energy for each phase, giving a total of six equations. The phasic conservation equations for mass, momentum and energy respectively may be summed to give three *combined* separated flow equations.

- *Phenomenological modelling.* This is a more sophisticated approach to modelling in that the two phases are considered to be flowing in a definite prescribed geometries, i.e. it takes take account of the *flow pattern* or *flow regimes*. It is now generally accepted that this approach provides improvements in prediction, especially of pressure drop and there have been major developments (e.g. in annular flow). In order to apply these flow regime models, it is necessary to know when each model should be used and to be able to predict the transition from one flow regime to the next.

It is the phenomenological modelling approach that will be utilised in the work described in this thesis. Therefore, it is imperative as a first step in this modelling to be able to distinguish the flow regimes that one may encounter in two-phase gas-liquid flow.

2.2 Two-phase flow regimes

In a two-phase flow, the interfacial structure and distribution may take a variety of forms which are often referred to as *flow regimes* or *flow patterns* (these two terms are used interchangeably in this thesis). There are many factors which affect the type of flow regime one may encounter. The key factors are the phase flow rates, the physical properties of each phase, the heat flux and the channel geometry and orientation. Despite the crucial importance of identifying the correct flow regime for a given set of local flow conditions, there is still no clear and satisfactory method for doing so. This is because the identification and description of the type of flow regime encountered is subjective, although there has been regularly cited in literature a commonly accepted reference set, which will be described in the next section. The flow pattern can be affected by other factors such as departure from local hydrodynamic equilibrium and the presence of trace contaminants which may affect, for instance, the coalescence of bubbles in the system.

2.2.1 Physical description of flow regimes.

The commonly accepted reference set of flow regimes encountered in vertical round tubes are illustrated in Figure 2.1 (see also Hewitt and Hall-Taylor, 1970). They are :

Bubbly flow. Here, the liquid phase is continuous with a dispersions of discrete bubbles flowing within the liquid continuum. At one extreme, the bubbles may be small and spherical in shape whilst at the other extreme, they may be large with a spherical cap and a flat tail.

Slug or plug flow. At higher gas flows, there is a transition to slug or plug flow. Conventionally, this was considered to be due to bubble coalescence leading to a gradual increase in bubble diameter until the bubble size approached that of the tube diameter. However, more recent evidence indicates that coalescence is normally inhibited in flows at normal gravity due to bubble wake effects; the transition is now considered more likely to occur with the formation of void waves in the system as a precursor. In slug flow, large characteristically "bullet-shaped" *Taylor* bubbles (named after Sir Geoffrey Taylor) are formed, which may be separated by liquid regions containing dispersions of smaller entrained bubbles. The length of the Taylor bubble may vary considerably but has been found experimentally to be typically around 12-20 diameters of the tube. The Taylor bubble is separated from the tube wall by a thin falling film of liquid, although the *net* flow of both liquid and gas is upwards.

Churn flow. With increasing flow velocity, the breakdown of slug flow Taylor bubbles leads to an unstable flow regime in which there is, in wide bore tubes, an oscillatory motion of liquid upwards and downwards in the tube (i.e. time varying in character), hence the name "churn flow". However, in narrow bore tubes, this oscillatory nature may not occur and a smoother transition from slug to annular flow can be observed. Although periodic bridging of the liquid across the tube (as shown in Figure 2.1) was considered to be a common phenomena in churn flow, it now seems likely that there is a continuous passage-way for the gas through the tube and, in that

sense, churn flow has some analogy with annular flow. Recent studies on the mechanism of churn flow include those of Hewitt et al. (1985), Govan et al. (1991) and Jayanti et al. (1992). The mechanism identified by Hewitt et al., and confirmed in the later studies, is one of liquid transport upwards in the form of large waves which shed liquid behind them, this latter liquid ultimately falling down in the form of a falling film. Thus, the wall conditions are intermittent in this region and highly complex.

Annular flow. In this flow regime, the liquid flows on the wall of the tube as a film and the gas phase flows in the centre. Usually, some of the liquid phase is entrained as small droplets in the gas core; it is also possible, although less common, for bubbles to be entrained in the liquid film.

Wispy -annular flow. This flow regime has been identified as a distinct flow regime primarily as a result of the research work carried out by Bennett et al. (1965) and Hewitt and Roberts (1969). As the liquid film flow rate is increased, the concentration of drops in the gas core increases and, ultimately, droplet coalescence occurs in the core which may lead to the formation of large lumps or streaks (wisps) of liquid in the gas core. This flow regime is characteristic of flows with high mass flux and because of its highly aerated liquid film, it could be confused with high velocity bubbly flow.

Whilst the above flow regimes are normally found in vertical adiabatic co-current flow, the flow regimes in vertically heated channels are slightly different. The presence of a heat flux through the channel wall alters the flow regime from that which would have occurred in a long unheated channel at the same local flow conditions. The two main reasons for these differences are the departure from thermodynamic equilibrium coupled with the presence of radial temperature profiles in the channel, and the departure from local hydrodynamic equilibrium throughout the channel. This is hardly surprising because the physical processes which govern the changes in flow regimes such as bubble coalescence require a finite length and time to occur. Therefore, in a heated tube where the rate of change of the local flow conditions (characterised by the rate of change of quality with distance, dx/dz) is large, some of these physical

processes may not be completed. Consequently, the region where certain flow regimes occur may be either expanded or compressed and in some cases, disappear altogether.

Figure 2.2 shows a schematic representation of the flow regimes in a vertically heated tube. Starting from the tube inlet, the single-phase liquid is being heated, thereby increasing its enthalpy. At some point, the first bubble will be formed at the tube wall when the required local superheat temperature is attained. As more bubbles grow and detach from the wall, bubbly flow is formed.

Due to the difference in densities between the liquid and vapour phases, the continuous increase in enthalpy of the fluid accelerates the flow. With the production of more vapour, the bubble population increases and coalescence takes place leading to the formation of slug flow further along the tube, followed by churn flow. Further along the channel, we will obtain the annular flow regime, which consists of a liquid film flowing on the tube wall with a vapour core containing entrained liquid droplets. The liquid film continues to deplete until dryout occurs when the depletion of the liquid film due to evaporation and droplet entrainment outbalances the replenishment of the film by droplet deposition. Beyond dryout, the wall temperature rises and the entrained droplets continue evaporating until single-phase vapour flow is formed.

The probable mechanisms for the above flow regime transitions will be discussed in further detail in later sections of this chapter and also in Chapter 6, which focuses on the sub-atmospheric evaporator (SAE) modelling code.

Information on flow regimes is often expressed in terms of "flow regime" maps where the regions of operation of each of the flow regimes is indicated in terms of selected variables or coordinates. A number of such flow regime maps are presented in the next section. Despite the existence of a variety of maps, they all suffer from the same drawback in that a given set of coordinates is unlikely to describe all the flow regime transitions. Thus, the development of specific theoretical description of the transitions is also discussed in detail in what follows.

2.2.2 Flow regime maps

Flow regime maps serve a purpose in that their simplicity helps to provide a quick graphical estimation albeit its accuracy is slightly suspect when compared with theoretical models of the transitions which normally require computer implementations. The golden era of the flow regime maps was in the 1960s and 1970s. However, some earlier maps could be traced as far back as the late 1940s and early 1950s. Examples of these early flow regime maps were those proposed by Kosterin (1949) and Baker (1954).

Kosterin (1949) conducted a series of investigations into the influence of tube diameter and orientation on the hydraulic resistance and on the structure of flow of a gas-liquid mixture. Although the main bulk of his investigations were focused on horizontal and inclined pipes, he also conducted some observations on vertical flow. He presented his findings in a graphical map using the input volume fraction of the gas as the ordinate and the mixture velocity as the abscissa. He had identified the bubbly, slug and annular flow regions (although he had given these regions different names to those now commonly used, i.e. "uniform emulsion flow", "vapour lock flow" and their sub-regions and "ring flow" instead of bubbly, slug and annular respectively) Kosterin arrived at a number of conclusions, of which the most relevant ones to the current studies were that, for the vertical flow, the conditions under which the gas-liquid mixture was introduced (i.e. the design of the inlet mixer and meshes) had little influence over the size of the zone/region with a stable flow pattern and also that this sector of a stable flow pattern/structure, at the same throughputs and volume fraction of gas is smaller than in horizontal tubes, primarily due to the influence of gravity in relation to the flow direction.

Baker (1954) published a paper on flow regime maps for horizontal flow. Although his work was focused on the horizontal flow, it is acknowledged here as one of the first works to recognise the importance of identifying the flow regime as a starting point for the calculation of pressure drop, void fraction, heat and mass transfer. He

used the mapping coordinates $\dot{m}_G/\lambda$ and $\dot{m}_L \lambda \psi/\dot{m}_G$ where λ and ψ are dimensionless scaling parameters, defined below, which took into account the variations in the physical properties of the fluids from a "standard" case., where the "standard" case is for air-water under standard atmospheric pressure and room temperature.

$$\lambda = \left[\left(\frac{\rho_G}{0.075}\right)\left(\frac{\rho_L}{62.3}\right)\right]^{0.5} \tag{2.1}$$

$$\psi = \frac{73}{\sigma}\left[\eta_L\left(\frac{62.3}{\rho_L}\right)^2\right]^{1/3} \tag{2.2}$$

Contrary to what he initially intended, which is to produce a non-dimensional map, Baker only managed to produced a map with one dimensionless axis. Even so, his map is widely used and quoted as an initial reference in many subsequent works on horizontal flow.

From the 1960s, because of the practical importance of vertical flow in industry, the amount of research work on two-phase vertical flow, culminating directly or indirectly in the proposal of new flow regime maps began to grow. Many new flow regime maps were proposed, mostly based on the researchers' own experimental data or in some cases from the observations of others. The key point here is that the majority of these maps were *experimentally* based and were plotted as a two dimensional map with various dimensional or non-dimensional coordinates. Among the numerous maps available were those proposed by Griffith and Wallis (1961), Chaudhry et al. (1965), Hewitt and Roberts (1969), Govier and Aziz (1972), Oshinowo and Charles (1974), Taitel et al. (1980), Weisman and Kang (1981), Mishima and Ishii (1984), McQuillan and Whalley (1985) and Taitel (1990). The later maps were increasingly based on theoretically modelled transitions from one flow regime to another. These theoretical relationships will be reviewed in more detail in Section 2.2.3 below.

Griffith and Wallis (1961) published a paper on their investigation into two-phase slug flow. The flow regime map they proposed used $\frac{\dot{V}_L}{\dot{V}_L+\dot{V}_G}$ and $\left(\frac{\dot{V}_L+\dot{V}_G}{A}\right)^2 \Big/ gD$ as mapping coordinates where $\dot{V}_L$ and $\dot{V}_G$ are the liquid and gas volumetric flow rates and A and D are the pipe cross sectional area and pipe diameter respectively. Whilst they recognised that the coordinates they utilised were not sufficient to completely determine the flow regimes, they argued that it was still the best single pair that could be chosen for a map. It is interesting to note that in this map (see Figure 2.3), the churn flow regime was omitted. When questioned by Brown and Govier as part of the published discussion of their publication, Griffith and Wallis stressed that they agreed that the churn flow regime does occur between slug and annular flow but they defended their omission by stating that the purpose of their work was to show where slug flow regime was and to model it, rather than where the other flow regimes are, and that the omission of the churn flow regime was considered to be not too serious!

Chaudhry et al. (1965) presented a flow regime map obtained visually as part of their investigation on the mechanism of flow regime transitions for co-current upwards vertical flow of water and air. They plotted their observations using the gas and liquid superficial velocities as axes. As shown in Figure 2.4, instead of using clearly defined curves (see Govier et al. (1957) and Galegar et al. (1954)) for separating adjacent flow regimes, they opted for shaded bands representing regions where classification was uncertain but spanned across the two adjacent regimes. These bands coalesced at the liquid superficial velocity of approximately 2.2 ft./sec., which according to Chaudhry et al. corresponded to a region when the separate flow regimes could no longer be distinguished at higher liquid flows, where the system resembled a froth traversed by fast moving quasi-periodic disturbances, whatever the gas flow. From their investigations, Chaudhry et al. also noted the consistency of their findings on the slug-churn and churn-annular transitions to those proposed by Nicklin (1961) on the flooding mechanism for slug-churn transition and that of Wallis (1962) on the flow reversal transition for the churn-annular flow regime.

In 1969, Hewitt and Roberts conducted some studies on two-phase flow patterns using simultaneous X-ray and flash photography for upward flow of air-water mixture. One of the primary objectives of their studies was to obtain high-definition X-ray photographs of two-phase flow especially at high liquid flow rates which was extremely difficult to distinguish by visual observation at visible light conditions as reported earlier by Chaudhry et al. (1965). The technique applied had proved to be fairly successful in that Hewitt and Roberts were able to identify this high liquid flow region as one resembling a region of transition from bubbly flow to wispy annular flow without the intermediate stage one normally associates with slug flow. Based on these observations, it seems that the "indistinguishable" region observed by Chaudhry et al.(1965) is the wispy annular flow regime.

Using their own experimental data and those of the steam-water experiments from Bennett et al. (1965), Hewitt and Robert produced a flow regime map in terms of superficial gas and liquid momentum fluxes, $\rho_G u_G^2$ and $\rho_L u_L^2$ respectively as shown in Figure 2.5. They derived these parameters from their analyses on Baker (1954) dimensionless scaling parameters λ and ψ, which was described earlier in this section, and from the Wallis (1962) work on flow reversal transition for churn to annular flow. They noted the presence of a common factor of superficial momentum flux terms in both studies. Although they suggested that the map they proposed may not be that accurate for a wide range of fluids and channel geometries, they stressed that as a first approximation and taking into account the good fit to their experimental data and those of Bennett et al. (1965), there seems to be no strong justification for a more complex map.

Other flow regime maps proposed included those by Wallis (1969) and Govier and Aziz (1972) as shown in Figures 2.6 and 2.7 respectively. Both studies utilised the superficial velocities of the gas and liquid flows as their coordinate systems and plotted the regions for each flow regimes accordingly. Oshinowo and Charles (1974) conducted a series of experiments investigating and classifying the flow patterns in vertical upflow, downflow and in bends for the flow of air and water and air and glycerol solutions of varying concentrations. They produced flow regime maps for the

vertical upward and downward flows. Figure 2.8 reproduced the Oshinowo and Charles's map for upward vertical flow with the coordinates $(R_V)^{1/2}$ and Fr_{tp}/Λ, where R_V is the delivered gas-to-liquid volume ratio, Fr_{tp} is the mixture Froude number, and $\Lambda = \eta_S/(\rho_{LS}\ \sigma_S)^{1/4}$ in which η_S, ρ_{LS} and σ_S are specific viscosity, specific density and specific surface tension respectively of the liquid with reference to water. One of the most recent flow regime map based on experimental measurements is that of Ohnuki et al. (1995) for the upward flow of air-water two-phase flow in a large vertical pipe, with a hydraulic diameter of 0.48 m. They noted the change in flow regimes from uniform bubbly to churn bubbly flow via agitated bubbly flow, with the notable absence of the slug flow regime.

As with the other flow regime maps, these maps clearly marked out the zones for the bubbly, slug, churn and annular flow regions in addition to a few other sub-regions which they had individually distinguished and assigned. The fact remained , however, that while numerous flow regime maps are available, each with its own equally valid experimental data supporting it, such two-dimensional plots are not adequate to describe accurately all the flow regimes whose individual characteristics and transitions are governed by different hydrodynamic variables of varying importance.

Later researchers began to concentrate on the actual mechanisms for each individual flow regime transitions but continued to propose two-dimensional flow regime maps. However, the difference was that the boundaries dividing the various flow regimes depicted in these later maps, such as those by Taitel et al. (1980), Weisman and Kang (1981), Mishima and Ishii (1984), McQuillan and Whalley (1985) and Taitel (1990), are theoretically modelled. Since this is the key feature of these new maps, they are more appropriately reviewed separately in the next section under the heading of flow regime theoretical transitions.

2.2.3 Flow regime theoretical transitions

Comparisons between the various flow regime maps revealed differences both in the absolute values and trends. The problem seems to arise from the fact that in almost all cases, the transition boundaries were empirically located and were not based on suitable physical models. Consequently, it is imperative to develop a theoretical basis for the description of the transitions, with the aim of improving the generality of the predictions and for classifying the experimentally observed flow regimes. For the case of vertical flow, the key transitions are:

- Bubbly to slug flow transition
- Slug to churn flow transition
- Churn to annular flow transition

Needless to say, different workers subdivide their flow regime observations further into smaller sub-sections, but a decision was made to focus only on the above 3 major transitions and to group the other sub-divisions within the appropriate section in the following review.

2.2.3.1 Bubbly to slug flow transition

The classical view of the transition from bubbly flow to slug flow is one of bubble agglomeration or coalescence as the bubble density increases leading to larger and larger bubbles and ultimately, to bubbles of the size of Taylor bubbles and hence to slug flow. Radovcich and Moissis (1962) performed a semi-qualitative treatment of bubble coalescence by considering a cubic lattice in which the individual bubble fluctuates. They postulated that the collision frequency between the bubbles becomes very large at void fraction of approximately 0.3, and a rapid transition to slug flow is expected. Radovcich and Moissis's postulation was confirmed by Griffith and Snyder (1964) who also stated that only in an entrance condition can bubbly flow with void

fraction higher than 0.35 could be sustained and that visual observations of higher void fractions than this are most likely to be erroneous. Mishima and Ishii (1984) also supported this view and lent further support by proposing that the value 0.3 can also be obtained from simple geometrical analysis by assuming that the bubbles distribute themselves in a tetrahedral lattice pattern in which each bubble fluctuates. They also assumed that there is a sphere of influence around each bubble, and when the maximum possible gap between two bubbles becomes less than a bubble diameter, the bubbles will deform considerably with each fluctuation thereby increasing the number of collisions and probability of coalescence. They arrived to the conclusion that this condition is reached when the void fraction is approximately 0.3.

Taitel et al. (1980) also lent their weight in principle to the postulation of Radovcich and Moissis (1962), however, they extended the concept by considering not only the coalescence of the bubbles, but also their break-up in the turbulence, the latter effect becoming greater as the flow velocity increased. This turbulent break-up effect would allow the bubbly flow regime to remain stable up to higher void fractions though the maximum packing void fraction of 0.52 still formed an upper limit. They derived the following equations for these two conditions,

$$U_L = 3.0\,U_G - 1.15\left[\frac{g\sigma(\rho_L - \rho_G)}{\rho_L^{\,2}}\right]^{1/4} \tag{2.3}$$

for the transition from bubble flow to slug flow at low velocity, assuming that bubbly flow becomes unstable at a void fraction of around 0.25. The limit for bubble break-up by turbulence is given by

$$U = U_G + U_L = 4.0\left\{\frac{D^{0.429}(\sigma/\rho_L)^{0.089}}{\nu_L^{\,0.072}}\left(\frac{g(\rho_L - \rho_G)}{\rho_L}\right)^{0.446}\right\} \tag{2.4}$$

and if U is greater than this value, the bubbles break up and larger void fractions are possible before transition. However, an upper value of the transition void fraction is given by

$$\varepsilon_G = 0.52 \tag{2.5}$$

corresponding to close cubic lattice packing of the bubbles. In the above relationships,

D = tube diameter (m)

g = acceleration due to gravity (= 9.81 ms^{-2})

U_G and U_L = gas and liquid superficial velocities (ms^{-1})

ρ_G and ρ_L = gas and liquid densities (kg m^{-3})

ν_L = liquid kinematic viscosity (m^2 s^{-1})

σ = liquid surface tension (N m^{-1})

ε_G = void fraction (-)

McQuillan and Whalley (1985) proposed that the value of 0.74 for a hexagonal lattice should be used instead of 0.52 and developed a modified criteria which also took account of the work of Weisman et al. (1979). McQuillan and Whalley derived the following criterion as an alternative to equation (2.4):

$$U_L \geq \frac{6.8}{\rho_L^{0.444}} \left\{ g\sigma \left(\rho_L - \rho_G\right) \right\}^{0.278} \left(\frac{D}{\eta_L}\right)^{0.112} \tag{2.6}$$

Weisman and Kang (1981) proposed an alternative equation, (2.7), for the bubbly flow to intermittent flow transition in vertical flow based on the approach adopted for horizontal flow by Taitel and Dukler (1976) and Weisman et al. (1979), and claimed good agreement between this new equation with the experimental data of several other workers. It should be noted here that Weisman and Kang decided to group the slug flow and churn flow regimes together as the *intermittent flow* regime for vertical flow; the present author disagrees with this grouping because both flow regimes are

intrinsically different in character and behaviour. The equation proposed by Weisman and Kang for the bubbly to intermittent flow transition is as follows,

$$\frac{U_G}{\sqrt{(gD)}} = 0.45\left(\frac{U_G + U_L}{\sqrt{(gD)}}\right)(1 - 0.65\cos\theta) \qquad (2.7)$$

where θ is the angle of inclination from the horizontal. It is essentially the relationship between the gas-phase Froude number and the total volumetric flow Froude number, a parameter first suggested by Kozlov (1954).

However, a recent survey by Hewitt (1990) on non-equilibrium two-phase flow cites recent developments by L. van Wijngaarden and co-workers (van Wijngaarden (1989), Biesheuvel (1984), Biesheuvel and Gorissen (1990) and Kapteijn (1989)), which suggests that the classical picture of gradual coalescence of bubbles to form slug flow is incorrect. They suggested that the transition is associated with the rapid growth of void waves in the fluid. In their paper, Biesheuvel and Gorissen (1990) showed that above a void fraction of 0.3 or more, the waves were found to grow rapidly and it was suggested that this could lead to the transition to slug flow. Nevertheless, the value of void fraction of 0.3 seemed to be a key indicator for the bubbly to slug flow transition.

2.2.3.2 Slug to churn flow transition

There is still considerable controversy about the existence of churn flow as a distinct and separate flow regime (see Mao and Dukler (1989, 1993) and Hewitt and Jayanti (1993)), let alone its various proposed transitions from slug flow. With the aim of clarifying the situation, Jayanti and Hewitt (1992) undertook an analytical programme of study specifically on the prediction of slug to churn flow transition in vertical two-phase flow. The review in this section is, in many ways similar to and based on the rather rigorous survey carried out by Jayanti and Hewitt (1992). Jayanti and Hewitt

classified the various proposed transition criteria for slug to churn flow into four major schools of thought, namely:

- Entrance effect mechanism (Dukler and Taitel, 1986)
- Bubble coalescence mechanism (Brauner and Barnea, 1986)
- Wake effect mechanism (Mishima and Ishii, 1984)
- Flooding mechanism (Nicklin and Davidson, 1962)

Each of these models was reviewed and compared by Jayanti and Hewitt using the experimental data obtained by Owen (1986). Details on the experimental equipment used and values of the data can be found in the Ph.D. thesis by Owen (1986). Based on their analysis, Jayanti and Hewitt (1992) proposed their own improved model which will be presented later in this section. First, the four alternative models are reviewed.

Entrance effect mechanism (Dukler and Taitel, 1986)

Dukler and Taitel (1986) and Taitel et al. (1980) regarded the churn flow regime as an entrance phenomenon and as a part of the formation of stable slug flow further downstream in a pipe. They postulated that at the inlet, where both gas and liquid are introduced, short liquid slugs and Taylor bubbles are formed. Since these short liquid slugs are unstable, they "collapse" down the tube, coalesce with the next slug and so on, until liquid slugs long enough to become stable are formed. They argued that if the pipe is long enough, slug flow will be observed at the end, and this developing region appears to be "churning" due to the oscillatory motion of the rising and collapsing liquid slugs. Dukler and Taitel (1986) presented the following equation to calculate the entrance length l_e, required to form stable slug flows for a given flow condition as:

$$\frac{l_e}{D} = 42.6\left(\frac{U_m}{\sqrt{g\,D}} + 0.29\right) \tag{2.8}$$

where U_m is the mixture superficial velocity. Therefore, according to Dukler and Taitel, if the actual pipe length is less than l_e calculated from (2.8), "churn" flow would be observed in the whole pipe; otherwise slug flow should be seen near the end of the pipe.

Bubble coalescence mechanism (Brauner and Barnea, 1986)

Brauner and Barnea (1986) introduced the idea of the formation of highly aerated liquid slugs as the cause of the slug to churn flow transition. They postulated that the gas that was entrained in the liquid slugs was entrained as dispersed bubbles due to the turbulence within the liquid slugs. Consistent with earlier proposals by Taitel et al. (1980), when the void fraction reaches 0.52, these bubbles will coalesce, thereby destroying the distinct identity of liquid slugs leading to churn flow. Therefore, the transition proposed by Brauner and Barnea (1986) is that when the void fraction in the liquid slug is greater than 0.52.

Wake effect mechanism (Mishima and Ishii, 1984)

Mishima and Ishii (1984) state that the transition from slug to churn occurs when the mean void fraction in the pipe exceeds that of the Taylor bubble region. Their criterion can be visualised as follows. At a point just before the transition, the Taylor bubbles are lined up very close to each other and the tail of a preceding bubble starts to touch the nose of a following bubble. This would create a strong wake effect which would destabilise the liquid slug, causing it to destruct. Under this condition, the mean void fraction over the Taylor bubble region would be equal to the mean void fraction in the pipe. The mean void fraction, ε_{avg}, was evaluated using the standard drift flux model whilst the mean void fraction over the Taylor bubble, ε_b, was calculated by a new expression proposed by Mishima and Ishii using potential flow analysis:

$$\varepsilon_{avg} = \frac{U_G}{\left[C_0 U_m + 0.35 \sqrt{\frac{g D (\rho_L - \rho_G)}{\rho_L}} \right]} \qquad (2.9)$$

$$\varepsilon_b = 1 - 0.813\left[\frac{(C_0 - 1)U_m + 0.35\sqrt{\frac{(\rho_L - \rho_G)gD}{\rho_L}}}{U_m + 0.75\sqrt{\frac{(\rho_L - \rho_G)gD}{\rho_L}}\left(\frac{(\rho_L - \rho_G)gD^3\rho_L}{\eta_L^2}\right)^{1/18}}\right]^{3/4} \quad (2.10)$$

where

$$C_0 = 1.2 - 0.2\sqrt{\frac{\rho_G}{\rho_L}} \text{ for round tubes} \quad (2.11)$$

and

$$C_0 = 1.35 - 0.35\sqrt{\frac{\rho_G}{\rho_L}} \text{ for rectangular ducts} \quad (2.12)$$

Flooding mechanism (Nicklin and Davidson, 1962)

When the liquid film in a counter-current flow of gas and liquid breaks down due to the formation of large interfacial waves, flooding is said to have occurred and numerous studies over the years had been conducted on this phenomenon (e.g. Wallis (1961), Hewitt and Wallis (1963), McQuillan et al. (1985), literature review on flooding by Bankoff and Lee (1986), Zabaras and Dukler (1988), Govan et al. (1991) to name a few). The idea of flooding as a possible mechanism for the slug to churn flow transition was originally propounded by Nicklin and Davidson (1962). Since then, several other workers have further developed this concept, including Wallis (1969) and Govan et al. (1991) and most notably McQuillan and Whalley (1985). This view is further supported by its consistency with a few experimental studies, for example, Wallis (1961) and Chaudhry et al. (1965).

The flooding velocities can be calculated using several correlations and calculations methods that can be found in the literature (see, for example Wallis (1969) and Bankoff and Lee (1986)). McQuillan and Whalley (1985) proposed the following set

of equations for modelling their transition. They postulated that flooding occurs (and therefore the slug to churn flow transition) when,

$$\sqrt{U_{bs}^{*}} + \sqrt{U_{fs}^{*}} \geq 1 \tag{2.13}$$

where U_{bs}^{*} and U_{fs}^{*} are the superficial velocities of the Taylor bubble and the falling liquid film. Equation (2.13) is a modified version of the flooding correlation proposed by Wallis (1961) and Hewitt and Wallis (1963). Both these superficial velocities are evaluated as follows:

$$U_{bs}^{*} = U_{bs}\frac{\sqrt{\rho_G}}{\sqrt{g\,D\,(\rho_L - \rho_G)}} \text{ and } U_{fs}^{*} = U_{fs}\frac{\sqrt{\rho_L}}{\sqrt{g\,D\,(\rho_L - \rho_G)}} \tag{2.14}$$

The gas superficial velocity in the Taylor bubble, U_{bs} is calculated from the Taylor bubble rise velocity, U_b, as proposed by Nicklin et al. (1962) multiplied by the cross section occupied by the bubble as follows:

$$U_{bs} = \left(1 - 4\frac{\delta}{D}\right) U_b = \left(1 - 4\frac{\delta}{D}\right)\left[1.2\,(U_G + U_L) + 0.35\sqrt{\frac{g\,D\,(\rho_L - \rho_G)}{\rho_L}}\right] \tag{2.15}$$

U_{fs} is then calculated from the continuity expression:

$$U_{fs} = U_{bs} - (U_G + U_L) \tag{2.16}$$

The liquid film thickness, δ, in the Taylor bubble region was evaluated by McQuillan and Whalley (1985) using the Nusselt (1916) expression for a laminar falling film:

$$\delta = \left[\frac{3\,U_{fs}\,D\,\eta_L}{4\,g\,(\rho_L - \rho_G)}\right]^{1/3} \tag{2.17}$$

Analyses of mechanisms

In their analyses of all the above models, Jayanti and Hewitt (1992) arrived at the following conclusions after making comparisons with Owen's (1986) experimental results;

1) The Dukler and Taitel (1986) model on developing slug flow was found to be quantitatively inconsistent but Jayanti and Hewitt (1992) did not rule out its underlying qualitative argument, although they stated that from a practical point of view, any flow considered to be still developing after 600 diameters has to be considered as if it were a separate regime since one rarely encounter such long vertical tubes in industry.

2) The lack of agreement at low liquid flow rates for the Brauner and Barnea (1985) model is attributed by Jayanti and Hewitt (1992) to ~~be caused by~~ the inaccuracy and simplification of predicting the liquid slug void fraction, which was assumed by Brauner and Barnea to behave like dispersed bubbly flow, hence ignoring bubble entrainment at the front of the slug and subsequent dispersion of the bubbles through the body of the slug.

3) As for the Mishima and Ishii (1984) model, Jayanti and Hewitt (1992) noted that for their transition to be true, the average slug unit void fraction can only be greater than the Taylor bubble void if the void in the liquid slug region is greater than that of the Taylor bubble. This observation is based on the following relationship between the voids in the slug unit, ε_u, liquid slug, ε_s, and Taylor bubble, ε_b;

$$\varepsilon_u = \varepsilon_s (1-\beta) + \varepsilon_b \beta \text{ where } \beta = \frac{L_b}{L_b + L_s} \qquad (2.18)$$

where $0 < \beta < 1$, where ε_u can be greater than ε_b, only if $\varepsilon_s > \varepsilon_b$. They also stressed the point that Mishima and Ishii (1984) did not make any attempt to evaluate the liquid slug void fraction but used the standard drift flux model to

evaluate the mean void fraction in the pipe instead. They also noted that McQuillan and Whalley (1985) had also queried the method proposed by Mishima and Ishii (1984) for calculating the Taylor bubble void. Thus, Jayanti and Hewitt (1992) concluded that, while Mishima and Ishii (1984) model showed good superficial agreement with the Owen (1986) experimental data, it lacks a sound mechanistic basis.

4) Finally, for the McQuillan and Whalley (1985) model, Jayanti and Hewitt (1992) concurred that the flooding mechanism is the most likely transition mechanism but noted that the model proposed by McQuillan and Whalley (1985) is inconsistent with Owen (1986) data at high liquid flow rates which they attributed to 2 major shortcomings. The first is that of the assumption of a laminar film surrounding the Taylor bubble and the Nusselt (1916) relation (see equation (2.17)); Jayanti and Hewitt proposed that it should be replaced by an empirical correlation by Brotz (1954), which was found to be applicable over a wider range of film Reynolds numbers by Fulford (1964),

$$\delta\left[\frac{g\left(\rho_L-\rho_G\right)}{\nu_L^2\,\rho_L}\right]^{1/3}=0.1719Re_f^{2/3} \text{ where } Re_f=\frac{\Gamma}{\eta_L} \qquad (2.19)$$

and Γ is the film flow rate (by mass) per unit wetted perimeter. Equation (2.19) was rewritten by Jayanti and Hewitt (1992) in terms of superficial film flow rate as:

$$U_{fs}=9.916\left(1-\varepsilon_b\right)\sqrt{\frac{g\,D\left(\rho_L-\rho_G\right)\left(1-\sqrt{\varepsilon_b}\right)}{\rho_L}} \qquad (2.20)$$

where $\varepsilon_b=1-4\frac{\delta}{D}$. The second shortcoming of the McQuillan and Whalley (1985) model which was highlighted by Jayanti and Hewitt (1992) is the neglect of the effect of the falling film length on the flooding velocity. Jayanti and Hewitt (1992) proposed the use of an empirical correlation obtained from the experiments of Hewitt et al. (1965) to correct this deficiency. Upon

comparison of all their proposed modifications to the McQuillan and Whalley (1985) model, Jayanti and Hewitt (1992) found that their new proposed model gave an excellent agreement with Owen (1986) data at both low and high liquid flow rates , and is therefore used by the present author as the transition criterion for slug to churn flow in his modelling work described in this thesis in Chapter 6. The full details of the Jayanti and Hewitt (1992) model will be reviewed and presented in Chapter 6.

2.2.3.3 Churn to annular flow transition

As the gas velocity increases in churn flow, the liquid film layer becomes thinner and the violence of the oscillations and interfacial interaction decreases. This is manifested by a decrease of pressure gradient with increasing gas velocity as depicted in Figure 2.11. As the gas flow rate is further increased, the film becomes even thinner and the film flow becomes uni-directional and the annular flow pattern is established. Ripple waves and at high enough liquid velocities, disturbance waves appear and the pressure gradient begins to rise with increasing gas flow rate. These successive events raise the question as to where churn flow ends and annular flow begins. Hewitt (1989) (see also Jayanti et al., 1992) points out the following number of alternative definitions for the churn to annular flow transition:

1) **At the flow reversal point.** The transition from churn to annular flow has been identified (see Hewitt (1982)) as the point at which all the liquid injected around the periphery of the channel travels upwards in the form of a liquid film with no downflow below the injector, see Figure 2.10. However, the flow oscillations and large wave structures associated with churn flow may still be present, even though they will decrease as the gas velocity is increased beyond the flow reversal point. The most commonly used correlation for the prediction of flow reversal is that of Wallis (see Wallis 1961, Hewitt and Wallis

1963). The correlation suggested by Wallis can be characterised by the criterion,

$$U_G^* \cong 1.0 \tag{2.21}$$

where

$$U_G^* = U_G \, \rho_G^{1/2} \left[g \, D \left(\rho_L - \rho_G \right) \right]^{-1/2} \tag{2.22}$$

Jones and Zuber (1978) [see Collier and Thome (1994)] have examined the above transition for various geometries. They recommend the following correlation,

$$U_G^* = 4 \left(\frac{\rho_G}{\rho_L} \right)^{0.5} \left[U_L^* + K \right] \tag{2.23}$$

where K is the constant in the equation for the bubble rise velocity (K = 0.35 for round tubes) and

$$U_L^* = U_L \, \rho_L^{1/2} \left[g \, D \left(\rho_L - \rho_G \right) \right]^{-1/2} \tag{2.24}$$

2) **At the pressure drop minimum.** Since this point is either very close or just beyond the flow reversal point, its occurrence can also be used as the transition from churn to annular flow.

3) **At the condition of zero mean wall shear stress.** For slug flow, the *mean* wall shear stress is normally negative and this condition persists in churn flow, whilst in annular flow, the mean wall shear stress is positive. Consequently, the point of zero mean wall shear stress can be taken as the transition point.

4) **At the condition of continuously positive wall shear stress.** Although the average wall shear stress may be greater than zero, the local wall shear stress does fluctuate and therefore, may be periodically negative, which may represent

a downward flow of liquid film similar to that observed between the waves in churn flow. Since annular flow is always uni-directional, one can take the condition when wall shear stress is always positive as the transition criterion.

The wall shear stress criteria outlined in 3) and 4) are difficult to establish without detailed measurements close to the wall and therefore, they are inconvenient boundaries to use. Jayanti et al. (1992) argued against the pressure drop minimum criterion on the basis that the pressure gradient includes the hydrostatic component, and thus does not wholly represent the frictional or interfacial behaviour and also that this minimum does not correspond to the transition visually observed by other workers (see Govier et al. (1957) and also Owen (1986)).

The flow reversal criterion specified by equations (2.21) and (2.22) were shown to provide an approximately accurate transition value in later studies (e.g. Willetts et al. (1986)) and are consistent with the conclusion that the flow reversal phenomenon provides a natural transition from churn to annular flow, with the added advantages that simple equations outlined above are available for its determination.

Another view of the transition from churn to annular flow is that of the minimum gas velocity required to suspend entrained droplets and this is determined from the balance between the gravitational and the drag forces acting on the drops, see Taitel et al. (1980). The analyses of Taitel et al. (1980) yields a transition boundary whose condition is determined by the Kutateladze number (Ku_G) as:

$$Ku_G = \frac{U_G \, \rho_G^{1/2}}{\left[\sigma \, g \left(\rho_L - \rho_G\right)\right]^{1/4}} \tag{2.25}$$

The major disadvantage of Taitel's (1980) proposal is that the entrained droplet suspension mechanism does not necessarily mean a uni-directional liquid film flow as one would associate with annular flow.

Finally, an interesting recent development in flow regime predictions is that of the *unified* model covering the whole range of pipe inclination. The earliest unified models known to the author were those proposed by Barnea (1986 and 1987) and the most recent is that by Taitel (1990).

Taitel (1990) presented his "unified" model for predicting the flow regime transitions over the complete range of pipe inclinations, thereby, at one stroke, he proposed the elimination of the needs for using models which are restricted to specific angles of inclination. He also used the term *intermittent* flow to cover elongated bubble, slug and churn flows. Despite proposing such an obviously ambitious, and in parts controversial, "unified" model, Taitel did mentioned and stressed that there was no absolute guarantee that the model he proposed is the absolute "true" model since in the future, possibly better or more realistic models can be found. Nevertheless, he emphasised that the principle behind any new future models is that it should be able to be extended and applied to all pipe inclinations.

Taitel's "unified" model relied, in many ways, on the previous research work of Taitel and Dukler (1976), Taitel et al.. (1980) and Barnea et al.. (1982a, 1982b). The model considered a number of transition borders and in this thesis, the focus will be on those transitions that will affect the flow regimes one would normally encounter in vertical two-phase flow, and had been discussed in the previous sections on flow regime transitions, i.e. the category for stratified flow is omitted. Apart from providing results in graphical plots with dimensionless coordinates, Taitel recommended the usage of computer code that can be easily written to yield the flow regime for any given fluids, operational conditions, pipe diameters and inclination. To aid the user and to enable the arrival at a unique answer, he also proposed a logical sequence in order to solve the model. However, the present author disagrees with Taitel's proposal regarding the transition from slug to churn flow; Taitel disregarded the validity of this transition on the basis that the flooding criterion is not applicable in horizontal flow, even though it may be true for vertical flow! Therefore, the unified model scheme is fundamentally flawed if one is obliged to utilise only those transition mechanisms that are universally applicable to all inclinations. The flooding mechanism could in principle apply to any

flow where there are periods of countercurrent flow between the slugs. This would clearly never apply in downward flow but could occur in slug flow with any upwards inclination. This illustrate the fundamental problem of developing unified models for all inclinations.

The above review on flow regimes provides a crucial background to the attempt to develop in the work described in this thesis, a partially phenomenologically based hydrodynamic and heat transfer modelling framework. The attention will now shift on to the two key hydrodynamic variables, namely, pressure drop and void fraction.

2.3 Pressure drop and void fraction models

Pressure drop is one of the major design parameters for many process systems; in forced-circulation systems, it governs the pumping requirements whilst for natural-circulation systems, it dictates the circulation rate and, therefore, it affects the other system parameters. Void fraction is another key parameter especially for flows involving gas-liquid phases or where there is a phase change, and it is defined as either

1. The fraction of the channel volume that is occupied by the gas phase
2. The fraction of the channel cross-sectional area occupied by the gas phase.

It is commonly assumed that, on a time-averaged basis, these two definitions would give the same value. The ability to predict both the pressure drop and void fraction is, of paramount importance and this is reflected by the plethora of models and correlations that are available. Consequently, only a few widely used models are discussed in this section. However, it should be borne in mind that none of these general correlations are highly accurate and standard deviations of as much as 40% or more are very common (see Hewitt, 1982).

2.3.1 Pressure drop models.

2.3.1.1 Single-phase pressure drop.

In single-phase internal flows, such as those in pipes, apart from asking whether the flow is laminar or turbulent, one is also required to take into account of the existence of *entrance* and *fully developed* regions. Discussions of these regions can be found in many standard chemical engineering textbooks, e.g. Incropera and DeWitt (1990). For a fully developed single-phase flow in a vertical tube, the pressure drop is calculated from,

$$-\frac{dp}{dz} = \frac{2 f \rho u^2}{D} + \rho g + u^2 \rho^2 \frac{d}{dz}\left(\frac{1}{\rho}\right) \tag{2.26}$$

where f is single-phase Fanning friction factor. If the fluid density remains constant (often a good approximation in single-phase flow) then the third (accelerational) term is zero. In single-phase flow, the friction factor can be evaluated from the Moody diagram (see Figure 2.12). Clearly, it is not very convenient to use a graphical representation and so, a number of friction factor correlations had been developed to calculate value of f for known values of the Reynolds number and surface conditions, i.e. the surface roughness. For fully developed laminar flow, one can use,

$$f = \frac{16}{Re} \tag{2.27}$$

For turbulent flow, the correlations are empirically based and one of the earliest for smooth pipes is that by Blasius (1913),

$$f = 0.079\, Re^{-0.25} \tag{2.28}$$

The Blasius equation has a good degree of accuracy for the range of Reynolds number from 3000-100 000 and is typical of other correlations of this type, using different values for the constants. von Kármán (1930) correlated data for rough pipes as follows:

$$\frac{1}{\sqrt{f}} = 4.06 \log_{10}\left(\frac{D}{2\varepsilon}\right) + 3.36 \qquad (2.29)$$

where ε is roughness of the pipe. Nikuradse (1932) extended von Kármán's equation format for smooth pipes and the correlation he proposed provided an excellent fit to essentially all reliable data (see Govier and Aziz, 1972) and has the form,

$$\frac{1}{\sqrt{f}} = 4.0 \log_{10}\left(Re\sqrt{f}\right) - 0.4 \qquad (2.30)$$

Equations (2.29) and (2.30) apply over a wide range of Reynolds numbers (i.e. up to 3×10^6). Colebrook and White (1939) further developed this idea and proposed his own correlation, which has been widely accepted and adopted as follows,

$$\frac{1}{\sqrt{f}} = 4.0 \log_{10}\left(\frac{D}{2\varepsilon}\right) + 3.48 - 4.0 \log_{10}\left(1 + 9.35\frac{D}{2\varepsilon\, Re\sqrt{f}}\right) \qquad (2.31)$$

Its applicability covers not only the fully developed turbulent flow regions for smooth and rough pipes, it also covers the transition region as well. However, like the Nikuradse (1932) correlation, Colebrook's (1939) correlation suffers from a disadvantage that it is an **implicit** equation and therefore has to be solved iteratively.

To avoid the need for an implicit solution, a number of explicit friction factor correlations have been proposed over the years (e.g. Wood (1966), Churchill (1977), Chen (1979), Haaland (1983) and Zigrang and Sylvester (1985)) and each of them used the Colebrook and White (1939) equation as a benchmark in terms of accuracy. Zigrang and Sylvester (1985) presented a review of all the above mentioned explicit

equations as well as proposing one themselves. Zigrang and Sylvester (1985) concluded that despite the inherent inaccuracy associated with the Colebrook and White (1939), equation, it should continue to serve as the standard until more accurate experimental data is available. They also concluded that the present choice of explicit equation for friction factor is, therefore a matter of compromise between the degree of accuracy sought and the complexity of the correlation. Chen (1979) correlation was chosen on such a basis by the present author for his research work and is given as follows,

$$\frac{1}{\sqrt{f}} = -4.0 \log_{10}\left[\frac{\varepsilon}{3.7065\,D} - \frac{5.0452}{Re}\log_{10}\left(\frac{1}{2.8257}\left(\frac{\varepsilon}{D}\right)^{1.1098} + \frac{5.8506}{Re^{0.8981}}\right)\right] \qquad (2.32)$$

By knowing the Reynolds number and the surface roughness, the friction factor can then easily be calculated and the pressure drop for turbulent single-phase flow obtained.

2.3.1.2 Two-phase pressure drop.

For two-phase flow, the most common approach to pressure drop prediction is to assume an idealised model such as the homogeneous flow model or the separated flow model. Of the two, the separated flow model is more widely used. For a steady state flow in a constant cross-section duct, e.g. a round tube, the combined phasic momentum equations from a separated flow model analysis yield the following expression for pressure gradient (see also in Hewitt (1982) for full derivation):

$$-\frac{dp}{dz} = \frac{\tau_w P}{A} + \dot{m}^2 \frac{d}{dz}\left\{\frac{(1-x)^2}{\rho_L (1-\varepsilon_G)} + \frac{x^2}{\rho_G \varepsilon_G}\right\} + g\left\{\rho_G \varepsilon_G + \rho_L (1-\varepsilon_G)\right\}\sin\theta \qquad (2.33)$$

where τ_w is the wall shear stress, ε_G is the void fraction, θ is the angle of inclination to the horizontal, P is the tube periphery and A is the cross-sectional area. The three terms on the RHS of equation (2.33) correspond to the frictional, accelerational and gravitational components respectively, i.e.

$$-\frac{dp}{dz} = -\frac{dp_F}{dz} - \frac{dp_A}{dz} - \frac{dp_G}{dz} \tag{2.34}$$

where:

$$-\frac{dp_F}{dz} = \frac{\tau_w P}{A} = \frac{\tau_w (\pi D)}{\frac{\pi D^2}{4}} = \frac{4\tau_w}{D} \tag{2.35}$$

$$-\frac{dp_A}{dz} = \dot{m}^2 \frac{d}{dz}\left\{\frac{(1-x)^2}{\rho_L (1-\varepsilon_G)} + \frac{x^2}{\rho_G \varepsilon_G}\right\} \tag{2.36}$$

$$-\frac{dp_G}{dz} = g\left\{\rho_G \varepsilon_G + \rho_L (1-\varepsilon_G)\right\} \sin\theta \tag{2.37}$$

The gravitational and accelerational components require a knowledge of the void fraction, ε_G. However, in vertical two-phase flow, the normally dominant component is the frictional term and a number of correlations had been proposed to quantify it, usually in the form of a two-phase multipliers which relate the pressure gradient to that of the single-phase flow. Hence, the frictional pressure gradient term can be written as :

$$-\frac{dp_F}{dz} = \frac{\tau_w P}{A} = \phi_{LO}^2 \left(\frac{dp_F}{dz}\right)_{LO} = \phi_G^2 \left(\frac{dp_F}{dz}\right)_G = \phi_L^2 \left(\frac{dp_F}{dz}\right)_L \tag{2.38}$$

where frictional multipliers ϕ_G and ϕ_L relate the frictional pressure gradient to that of gas or liquid phase flowing alone in the channel and are defined as follows:

$$\phi_G^2 = \frac{dp_F/dz}{(dp_F/dz)_G} \tag{2.39}$$

$$\phi_L^2 = \frac{dp_F/dz}{(dp_F/dz)_L} \tag{2.40}$$

while ϕ_{LO} relates the two-phase frictional pressure gradient to that of a single-phase flow at the total mass velocity with the physical properties of the liquid phase and is defined as:

$$\phi_{LO}^2 = \frac{dp_F/dz}{(dp_F/dz)_{LO}} \tag{2.41}$$

The most well known and widely used correlations for frictional pressure gradient prediction are those by Lockhart and Martinelli (1949), Martinelli and Nelson (1948), Thom (1964), Baroczy (1966), Chisholm (1973) and Friedel (1979). These correlations are widely discussed in many standard textbooks (e.g. Butterworth (1977), Hewitt (1982), Whalley (1990) and Collier and Thome (1994)) and only the essence of each correlation will be discussed here.

Historically, the Lockhart-Martinelli (1949) model is the most widely used, even though it is not very accurate and is based on only a small fraction of the now available two-phase pressure drop data (see Hewitt, 1982). It is, in essence an empirical fit to a series of experiments performed by Martinelli and co-workers in the period 1944-49. The key features of the Lockhart-Martinelli model are:

- The pressure drop multipliers ϕ_L^2 and ϕ_G^2 are a function of the Martinelli parameter X^2 defined as follows:

$$X^2 = \frac{(dp_F/dz)_L}{(dp_F/dz)_G} \tag{2.42}$$

  where $(dp_F/dz)_L$ and $(dp_F/dz)_G$ are the frictional pressure gradients for the liquid and gas phase flowing alone in the channel. Lockhart and Martinelli presented this relationship in a graphical form, as shown in Figure 2.13.

- As can be seen in Figure 2.13, they also defined four *flow regions* on the basis of the behaviour of the flow (either viscous or turbulent) for each phase respectively

when they are considered to pass alone through the channel. The void fraction can also be evaluated from the graph.

Chisholm (1967) showed that the Lockhart-Martinelli graphical relationships for the multipliers can be simply and accurately presented as:

$$\phi_L^2 = 1 + \frac{C}{X} + \frac{1}{X^2} \tag{2.43}$$

$$\phi_G^2 = 1 + CX + X^2 \tag{2.44}$$

where C is a dimensionless parameter which is independent of quality, x, but is dependent on the nature of the flow of the single-phase fluids flowing alone in the channel as given in Table 2.1 below,

Liquid	Gas	Subscript	C
Turbulent	Turbulent	tt	20
Viscous	Turbulent	vt	12
Turbulent	Viscous	tv	10
Viscous	Viscous	vv	5

Table 2.1 Values of C to fit the Lockhart-Martinelli curves (adapted from Chisholm (1967)).

Martinelli and Nelson (1948) extended the Lockhart-Martinelli (1949) correlation to enable the prediction for steam-water data from atmospheric to the critical pressure. Martinelli and Nelson noted that the Lockhart-Martinelli correlations did not become asymptotic to the correct value as the pressure tends towards the critical pressure. Consequently, they introduced a revised multiplier correlation as illustrated in Figure 2.14. Although the revised correlation was derived for steam-water data, it has been subsequently used for other fluids with the same pressure, p, to critical pressure, p_c, ratio. This pressure effect seen by Martinelli and Nelson could be attributed to the variation of surface tension of water with pressure, since the surface tension was not

accounted for by the Lockhart-Martinelli correlation. As a result, the use of the Martinelli and Nelson correlation for other fluids may not be strictly valid.

Hewitt (1982) and Hewitt et al. (1994) reported that these traditional Martinelli-type correlations are inadequate in representing a wide range of two-phase flow pressure gradient data and that deviations of up to 100% are not uncommon. Furthermore, these Martinelli-type correlations do not take adequate account of the influence of mass flux and it was shown that there is a systematic effect of mass flux on the pressure drop multipliers (Cicchitti et al. 1960).

Thom (1964) repeated the Martinelli and Nelson exercise and produced an alternative set of values for the pressure drop multipliers. His revised values were derived from an extensive set of experimental data for steam-water pressure drops on heated and unheated horizontal and vertical tubes.

Baroczy (1966) was the first person to attempt to take into account the influence of mass flux on the two-phase frictional multiplier, ϕ_{LO}^2. The method of calculation that he proposed utilises two separate sets of curves. Figure 2.15 shows a plot of ϕ_{LO}^2 as a function of a dimensionless physical property group $\frac{\rho_G}{\rho_L}\left(\frac{\eta_L}{\eta_G}\right)^{0.2}$ with quality x as a parameter. It should be noted that Figure 2.15 is restricted to only the reference mass flux of 1356 kg m^{-2} s^{-1} (1 x 10^6 lb ft^{-2} h^{-1}). In order to use the calculation method for other mass fluxes, Baroczy provided correction factors, also a function of the same physical property group for mass fluxes of 339, 678, 2712 and 4068 kg m^{-2} s^{-1} as illustrated in Figure 2.16. Clearly, the complex graphical nature of Baroczy's method is its key disadvantage, and thankfully, Chisholm (1973) proposed a correlation that fitted Baroczy's curves quite well and further extended the range of data covered.

The correlation proposed by Chisholm (1973) is as follows:

$$\phi_{LO}^2 = 1 + \left(Y^2 - 1\right) B\, x^{(2-n)/2} \left(1 - x\right)^{(2-n)/2} + x^{2-n} \qquad (2.45)$$

where n is the power to which the Re is raised in the friction factor - Reynolds number relationship (0.25 for Blasius) and the parameter B is given by

$$B = 55/\dot{m}^{0.5} \text{ for } 0 < Y < 9.5 \tag{2.46}$$

$$B = 520/\left(Y\,\dot{m}^{0.5}\right) \text{ for } 9.5 < Y < 28 \tag{2.47}$$

$$B = 15000/\left(Y^2\dot{m}^{0.5}\right) \text{ for } 28 < Y \tag{2.48}$$

where $\dot{m}$ is the mass flux while,

$$Y^2 = \frac{\left(dp_F/dz\right)_{GO}}{\left(dp_F/dz\right)_{LO}} \tag{2.49}$$

Friedel (1979) proposed one of the most accurate two-phase pressure drop correlations. He compared his correlation against an extensive data bank of 25 000 experimental data points as well as other correlations. Friedel's correlation can be written as follows,

$$\phi_{LO}^2 = E + \frac{3.24\,F\,H}{Fr^{0.045}\,We^{0.035}} \tag{2.50}$$

where

$$E = (1-x)^2 + x^2\left(\frac{\rho_L\,f_{GO}}{\rho_G\,f_{LO}}\right) \tag{2.51}$$

$$F = x^{0.78}\,(1-x)^{0.24} \tag{2.52}$$

$$H = \left(\frac{\rho_L}{\rho_G}\right)^{0.91}\left(\frac{\eta_G}{\eta_L}\right)^{0.19}\left(1-\frac{\eta_G}{\eta_L}\right)^{0.7} \tag{2.53}$$

$$Fr = \frac{\dot{m}^2}{g\,D\,\rho_{TP}^2} \tag{2.54}$$

$$We = \frac{\dot{m}^2\,D}{\rho_{TP}\,\sigma} \tag{2.55}$$

and f_{GO} and f_{LO} are the single-phase friction factors for the total mass flux flowing with gas and liquid properties, respectively. The two-phase density, ρ_{TP} , for the Friedel's (1979) correlation is given by the following relationship:

$$\rho_{TP} = \left(\frac{x}{\rho_G} + \frac{(1-x)}{\rho_L} \right)^{-1} \tag{2.56}$$

The correlation outlined above is valid only for vertical upwards and horizontal flows. A different variant is available for vertical downflow. Friedel's correlation was reported (e.g. Collier and Thome 1994) to have standard deviations of around 40% which is large when compared to those for single-phase flow, but is probably around the best that can be obtained using purely empirical correlation for two-phase flow. It seems that the best way forward in improving this accuracy is by means of phenomenological modelling and considerable work has been done, for instance in annular flow by Hewitt and co-workers. Details of some of these methods applied in the present author's work are presented in the Chapter 6, the modelling chapter of this thesis.

2.3.2 Void fraction models

The other key hydrodynamic parameter in the design of two-phase gas-liquid flow systems is the void fraction. The primary purpose of this sub-section is to present some of the established prediction methods for void fraction. As defined in the multiphase flow literature, the void fraction is the fraction of the channel volume or cross-sectional area occupied by the gas phase. The void fraction can be related to the velocity ratio, S as follows:

$$\varepsilon_G = \frac{\dot{V}_G}{S\dot{V}_L + \dot{V}_G} \tag{2.57}$$

The prediction methods for void fraction can be categorised in terms of increasing accuracy and sophistication, ranging from the simple homogeneous model to more complex phenomenological models and including the drift flux models and empirical correlations derived from experimental data banks. The salient features of each of these categories will be discussed in turn, except for the phenomenological models which will be discussed in detail and depth in Chapter 6.

For the homogeneous model, the average gas and liquid velocities are identical, hence the velocity ratio S = 1, thus simplifying equation (2.57) to the following,

$$\varepsilon_G = \frac{\dot{V}_G}{\dot{V}_L + \dot{V}_G} \tag{2.58}$$

The homogeneous model was found (see Hewitt (1982)) to be less inaccurate at high pressure and high mass flux but on the whole, it deviates significantly from experimental values of void fraction.

Zuber and Findlay (1965) were the pioneers of the concept of the drift flux model for predicting the void fraction. Their idea was then developed further by Wallis (1969) for one-dimensional flow analysis. The bases for drift flux model can be found in detail in Zuber and Findlay (1965) and Wallis (1969). A full treatment of the drift flux model is not presented in this thesis since it can be easily found in the above references. The key difference between these two works are their respective treatment of radial variations of void fraction and local velocity profile across the channel cross-section. Wallis (1969) assumed that the wall shear stress is negligible and as a result, there is no variation in the void fraction and the gas and liquid mean velocities across the channel cross-section. On the other hand, the Zuber and Findlay (1965) model takes into account of these variations by using the average values and the weighted mean values of these flow parameters to arrive at the following void-quality relationship (assuming that the *drift velocity* of gas phase u_{GU} is constant across the channel):

$$\varepsilon_G = \frac{U_G}{C_0(U_G + U_L) + u_{GU}} \tag{2.59}$$

which contains two empirical parameters C_0 and u_{GU}. C_0 is the distribution parameter which is a measure of the radial variations of void fraction and the local gas and liquid velocities whilst u_{GU} accounts for the relative velocity between the phases. The value of C_0 is a function of the flow regime and has the value of 1.1 - 1.2 for bubbly and slug flow. The values of C_0 can also be evaluated from expressions such as those suggested by Rouhani (1969),

$$C_0 = 1 + 0.2(1 - x)\left(\frac{gD\rho_L^2}{\dot{m}^2}\right)^{0.25} \tag{2.60}$$

and by Fréchou (1986) for slug flow,

$$C_0 = 1.2 + \frac{0.8}{1 + 10^{-8}\, Re^{2.55}} \tag{2.61}$$

where Re is Reynolds number in the liquid region. As for the relative phase velocity, u_{GU}, Zuber and Findlay (1965) proposed the following expression:

$$u_{GU} = 1.18\left(\sigma g \frac{\rho_L - \rho_G}{\rho_L^2}\right)^{0.25} \tag{2.62}$$

and Rouhani (1969),

$$u_{GU} = 1.18(1 - x)\left(\sigma g \frac{\rho_L - \rho_G}{\rho_L^2}\right)^{0.25} \tag{2.63}$$

However, the need for greater accuracy for a larger range of void fraction data has led to the usage of empirical correlations, the most commonly known are those of Lockhart and Martinelli (1949), Martinelli and Nelson (1948) and CISE (Premoli et al. (1971)). Among the more recent correlations is that of the Chexal and Lellouche

(1991). Both the Martinelli correlations relate the void fraction to the Martinelli parameter, X, in graphical forms; a curve-fit to the Lockhart-Martinelli (1949) graphical solution for the turbulent-turbulent region is

$$\varepsilon_G = \frac{\phi_L - 1}{\phi_L} \tag{2.64}$$

where ϕ_L is the frictional pressure gradient multiplier of the liquid phase flowing alone in the channel as defined earlier in equation (2.40).

Premoli et al. (1971) proposed the following correlation taking into account the effects of mass flux. The correlation they proposed involved the determination of the velocity ratio, S where

$$S = 1 + E_1 \left(\frac{y}{1 + y E_2} - y E_2 \right)^{1/2} \tag{2.65}$$

with

$$y = \frac{\beta}{1 - \beta} \tag{2.66}$$

and

$$\beta = \frac{\dot{V}_G}{\dot{V}_L + \dot{V}_G} \tag{2.67}$$

which is the volume flow ratio. The two parameters E_1 and E_2 are both functions of the Reynolds and Weber numbers, together with the phase density ratios and are defined as follows:

$$E_1 = 1.578\, Re^{-0.19} \left(\frac{\rho_L}{\rho_G} \right)^{0.22} \tag{2.68}$$

$$E_2 = 0.0273\, We\, Re^{-0.51} \left(\frac{\rho_L}{\rho_G} \right)^{-0.08} \tag{2.69}$$

Following a series of investigations into void fraction for various type of fluids, pipe diameters and inclinations, combinations of flow directions, pressures (from 1 bar to

180 bars) and also for diabatic and adiabatic conditions, Chexal and Lellouche (1991) proposed an empirical correlation based on the drift flux model. The primary features of the Chexal-Lellouche correlation are:

- It is continuous with pressure and flow direction.
- It covers a very wide range of pipe sizes, pressures and flows.
- It eliminates the need to know the flow regime beforehand.
- It is applicable for a wide range of two-phase/two component mixtures.

The correlation was also designed to enable the prediction of the counter-current flooding limitation. Originally, the correlation was developed for the vertical upward steam-water flow but has been extended and revised to include downflow, horizontal flow, air-water and refrigerant data. The major difference between the Chexal and Lellouche (1991) adaptation of the drift flux model to those of Zuber and Findlay (1965) or Wallis (1969) is in the correlations used for the prediction of distribution parameter C_0 and the drift velocity, u_{GU} for the drift flux formulation shown in equation (2.59).

The next level of sophistication involves the consideration of the flow regimes (phenomenological modelling). This is the main approach adopted in the author's modelling of void fraction for the sub-atmospheric evaporator system described in detail in Chapter 6. In this chapter, it is sufficient to state the type of models used for each flow regime as follows in Table 2.2 below:

Flow regime	Void fraction model
Subcooled boiling	Drift flux
Bubbly flow	Drift flux
Slug flow	Nicklin-Davidson (1962)
Churn flow	*New* "slug-annular" model
Annular flow	Geometrical solution

Table 2.2 Void fraction models used in SAE modelling

This then concludes the first major part of this literature review on hydrodynamics. The second part of the review in the next chapter will focus on heat transfer, starting with an overview of the subject followed by a more detail review on flow boiling.

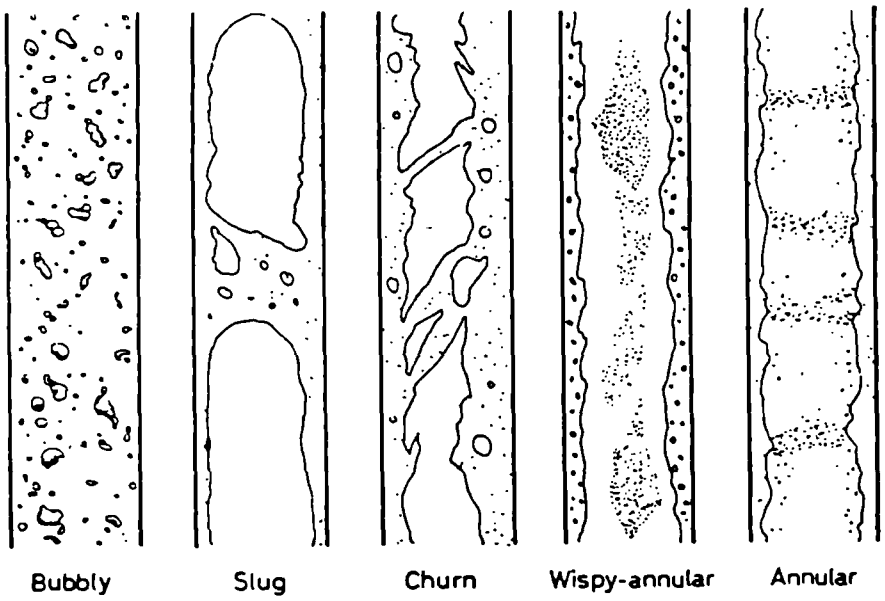

Figure 2.1 Two-phase flow regimes in vertical co-current flow (from Collier and Thome 1994)

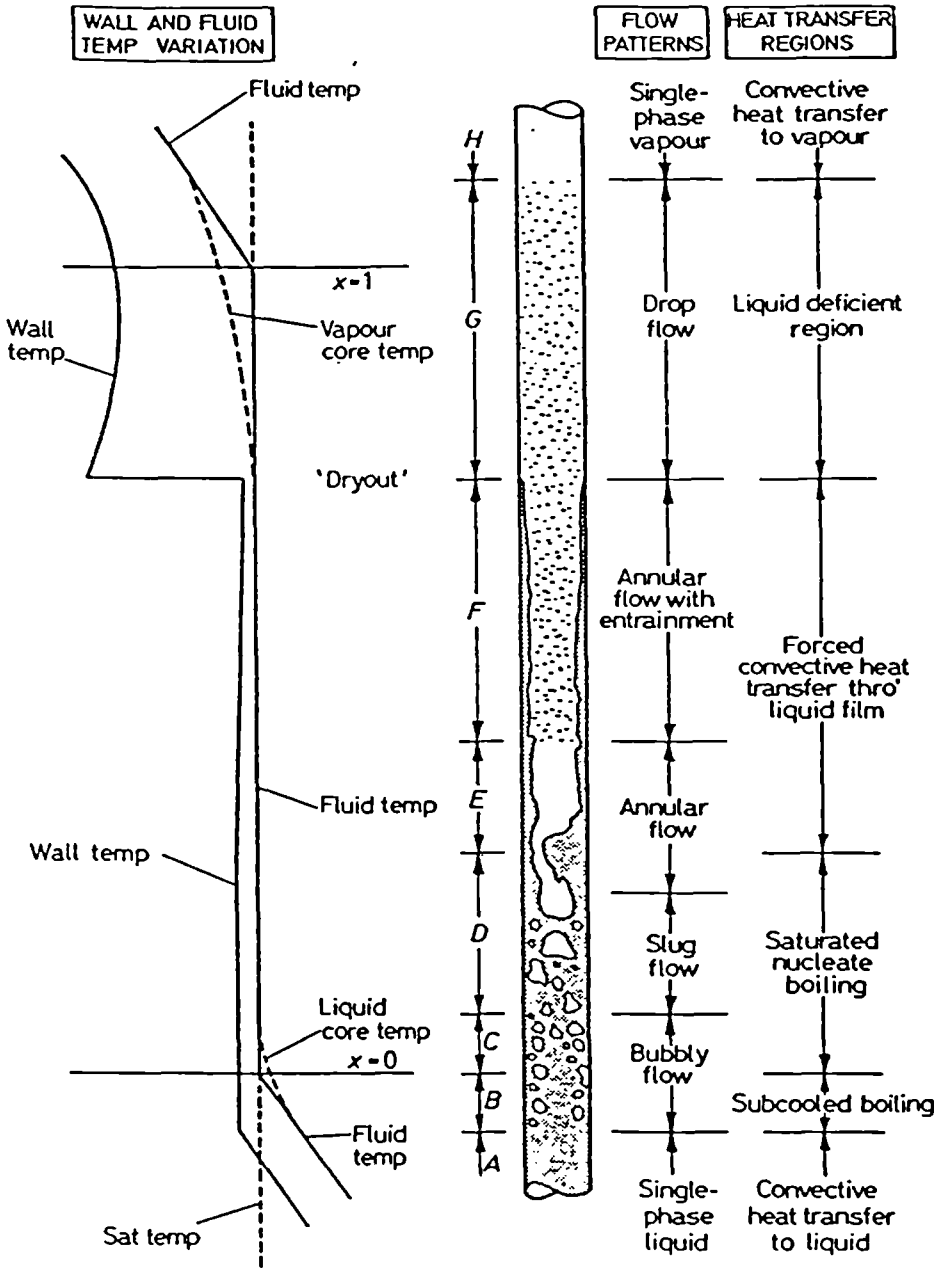

Figure 2.2 Two-phase flow regimes and regions of heat transfer in a vertical heated tube (from Collier and Thome 1994)

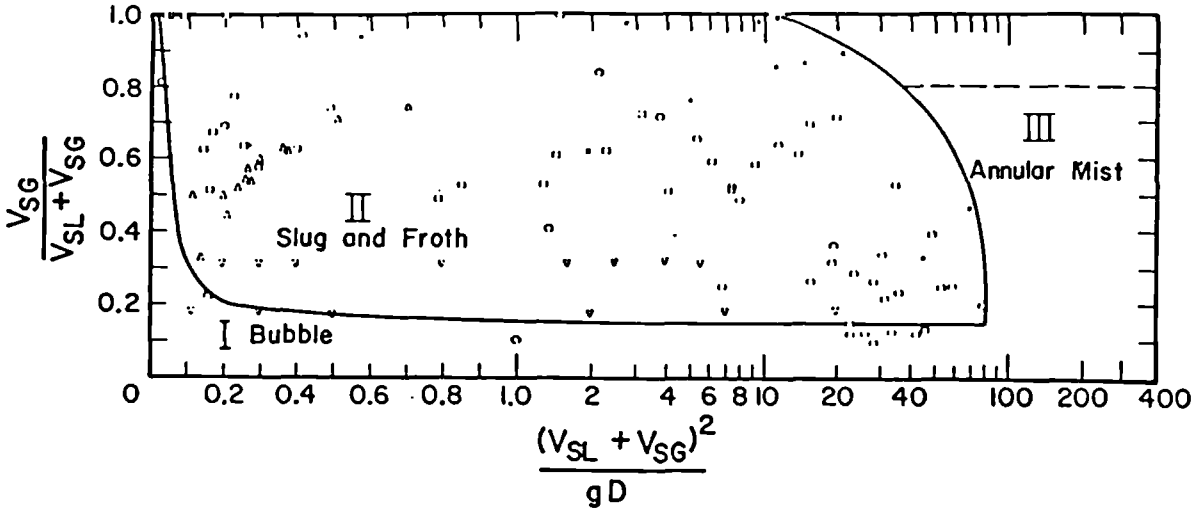

Figure 2.3 Flow regime map by Griffith and Wallis (1961)

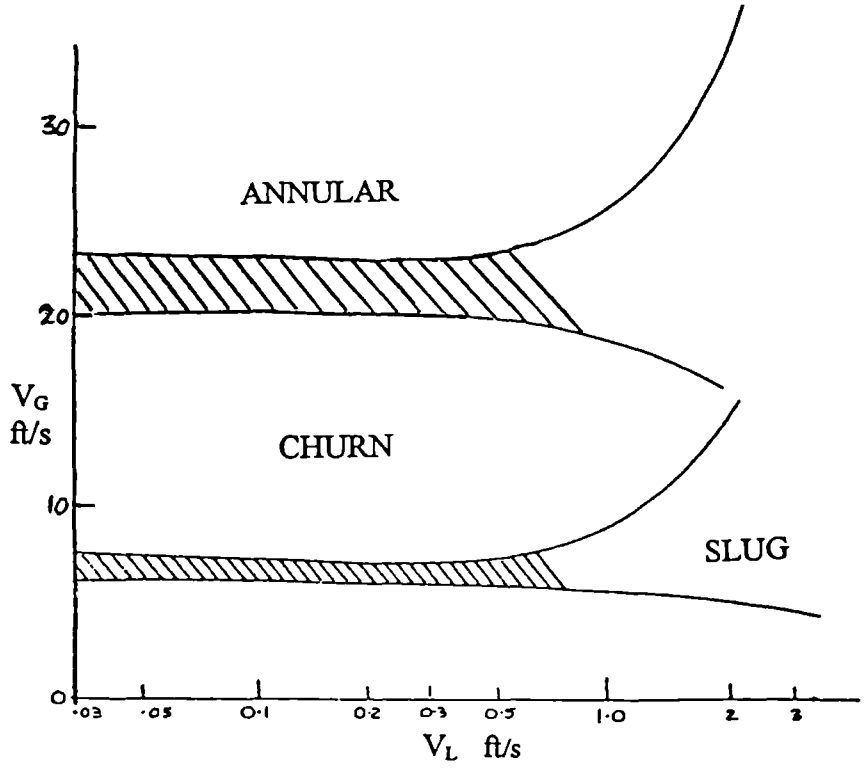

Figure 2.4 Flow regime map by Chaudhry et. al. (1965)

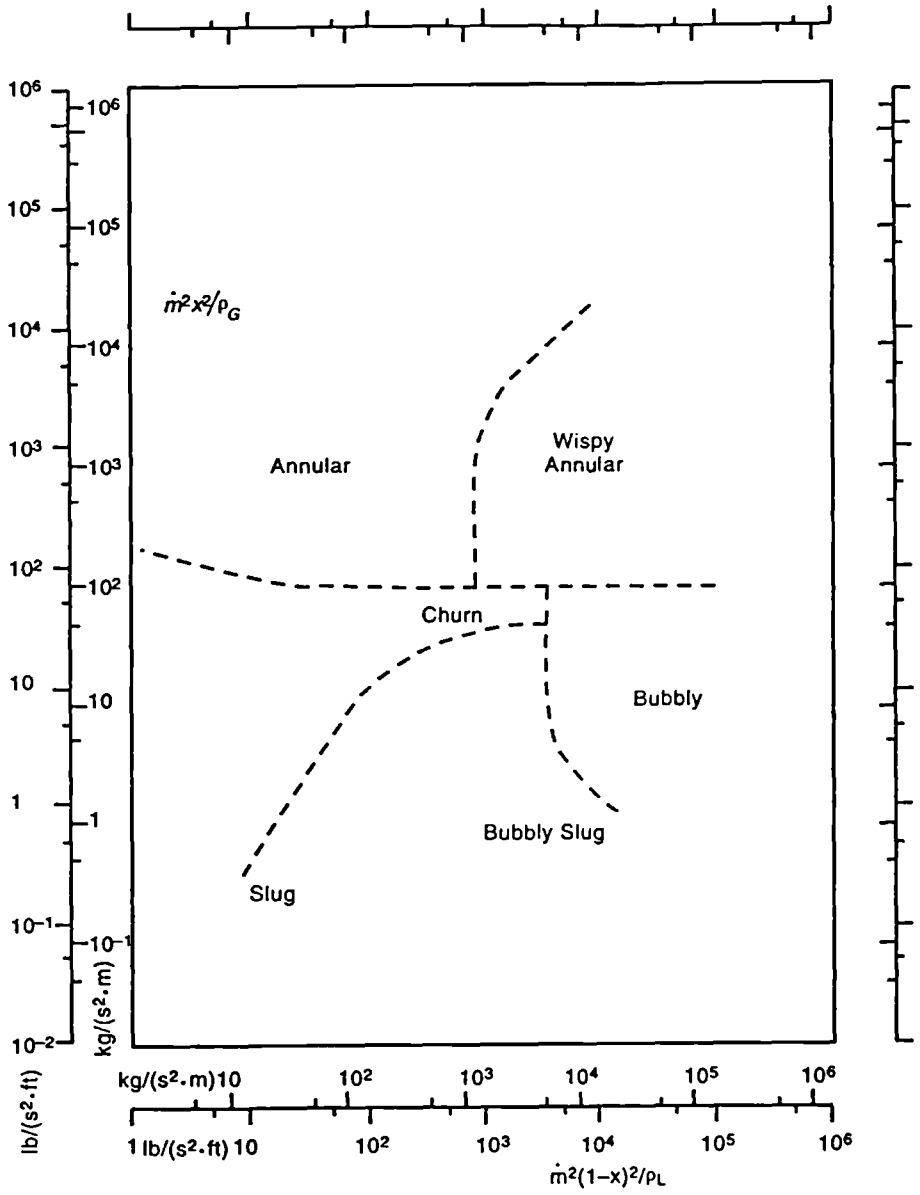

Figure 2.5 Flow regime map by Hewitt and Roberts (1969)

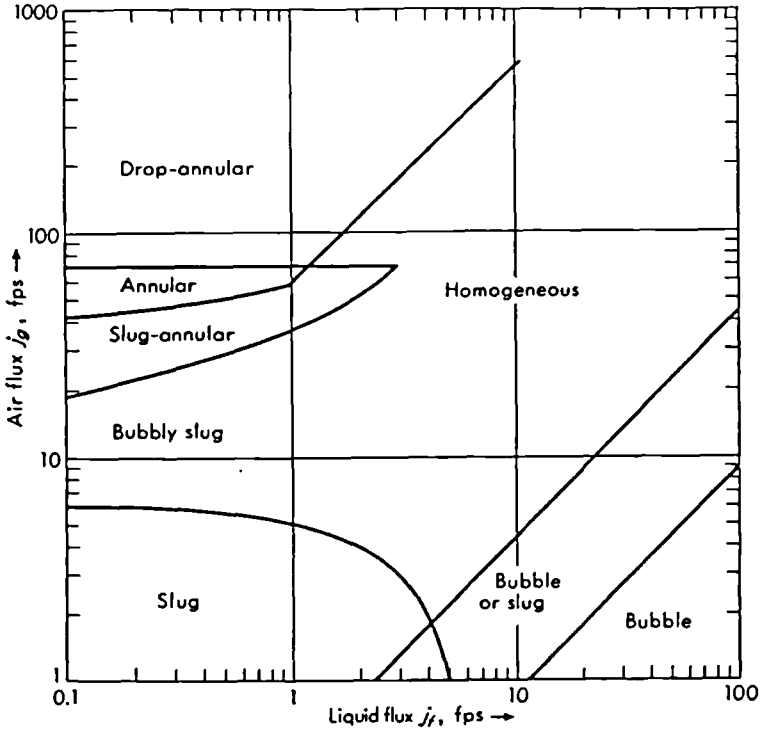

Figure 2.6 Flow regime map by Wallis (1969)

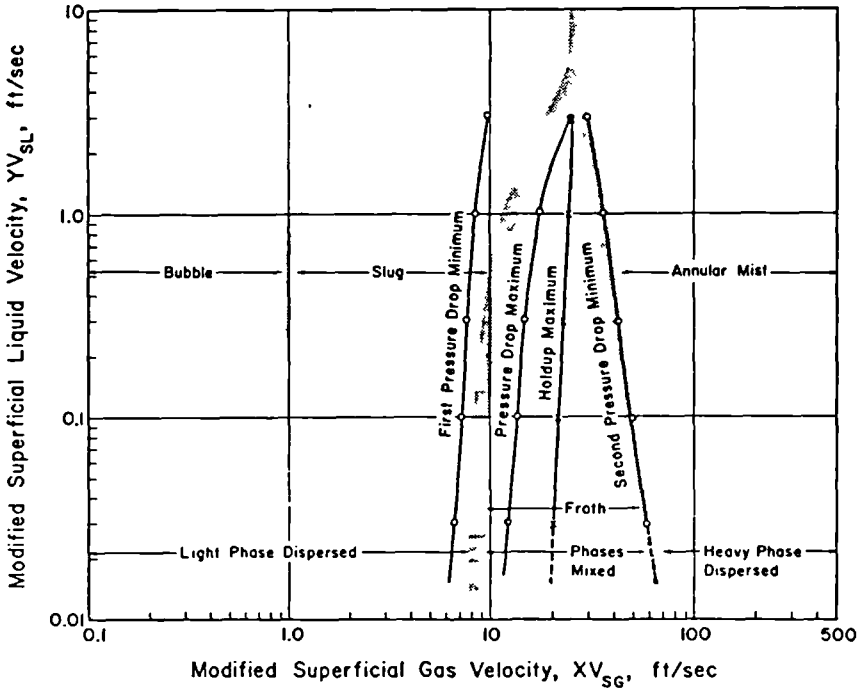

Figure 2.7 Flow regime map by Govier and Aziz (1972)

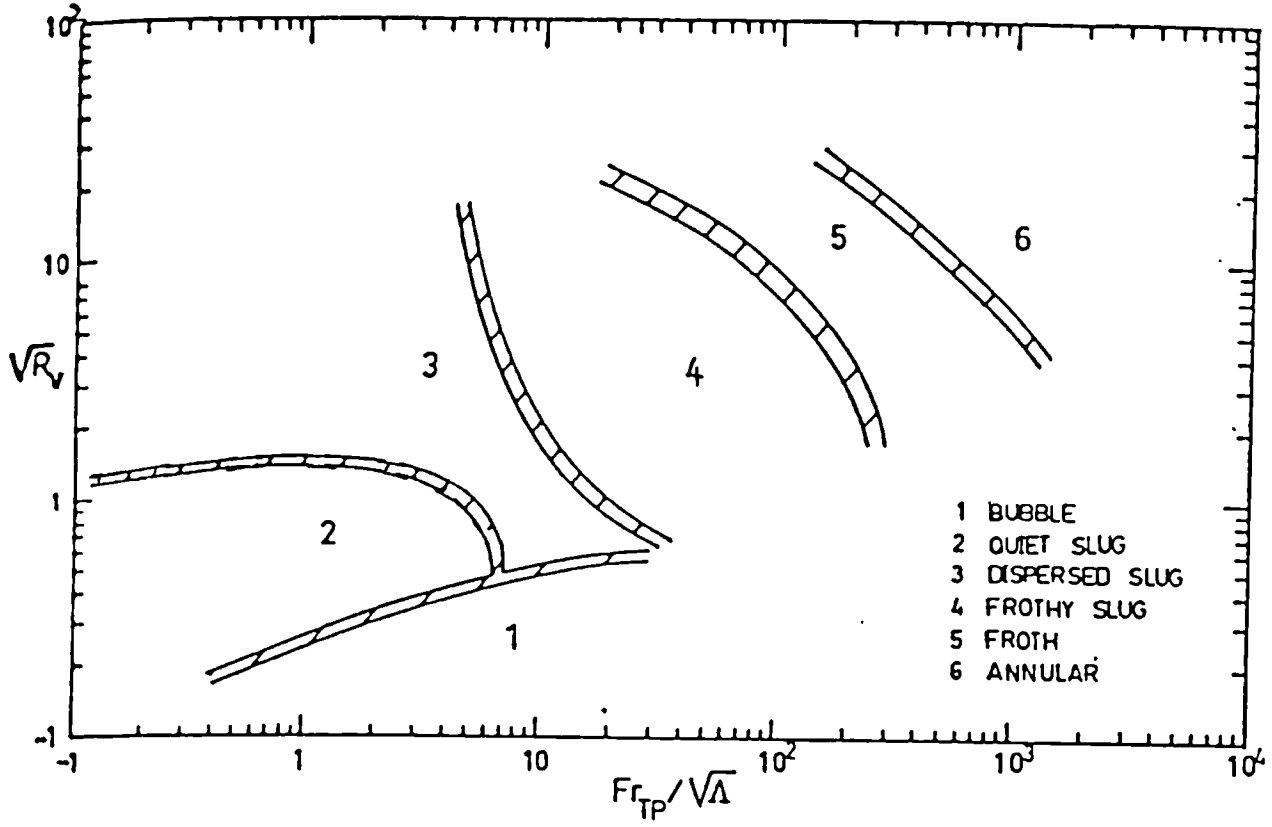

Figure 2.8 Flow regime map by Oshinowo and Charles (1974)

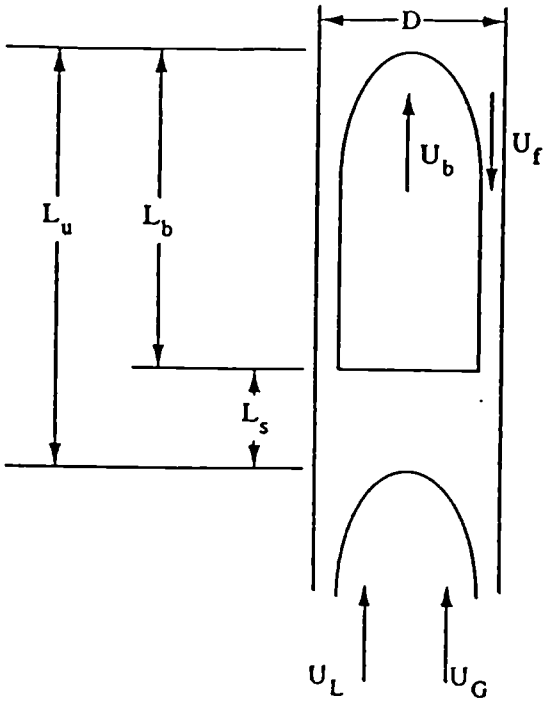

Figure 2.9 Model of slug flow of McQuillan and Whalley (1985)

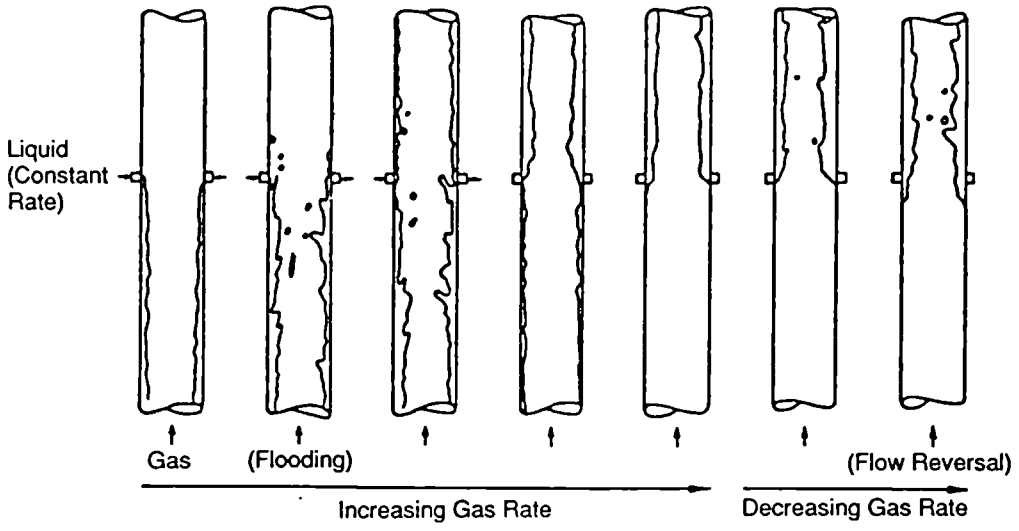

Figure 2.10 Flooding and flow reversal

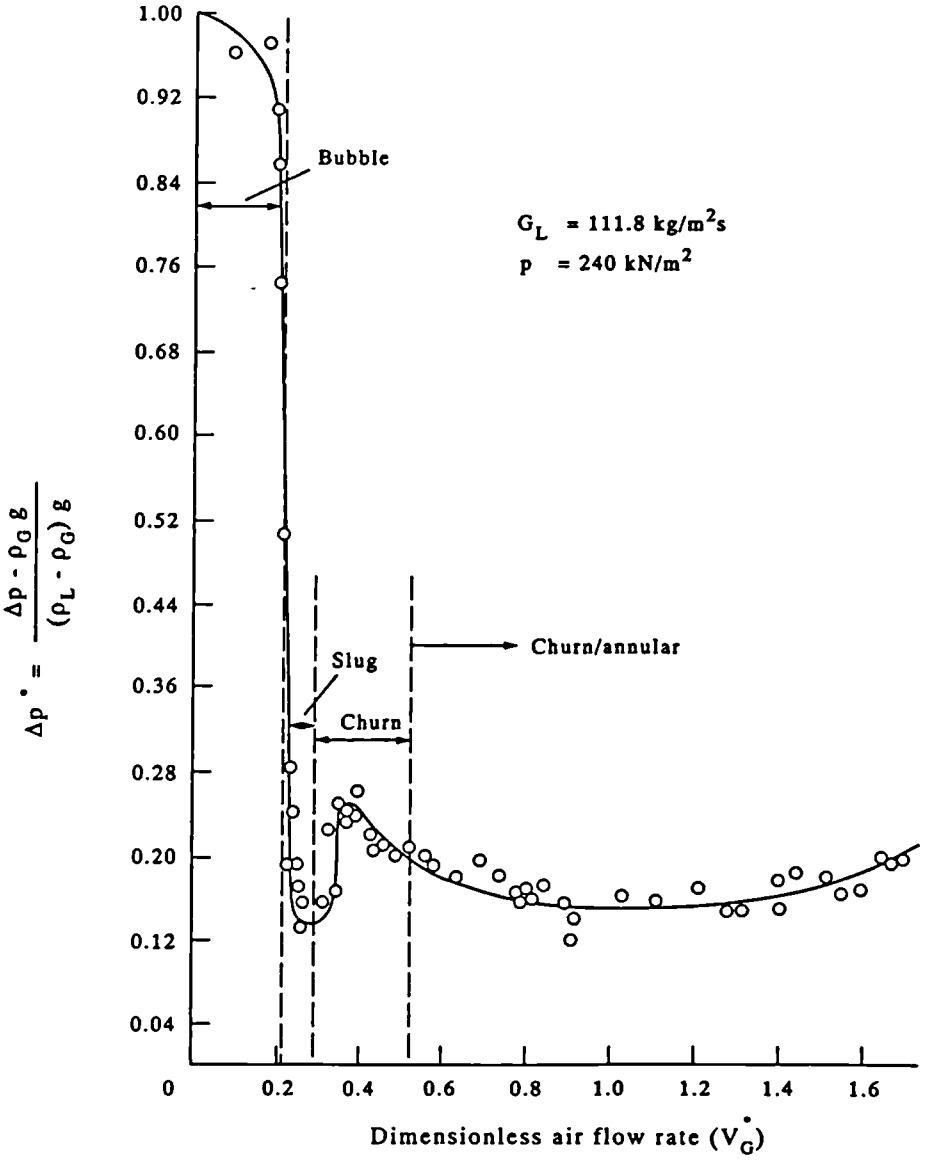

Figure 2.11 Measured pressure gradient as a function of gas flow rate, experimental results of Owen (1986)

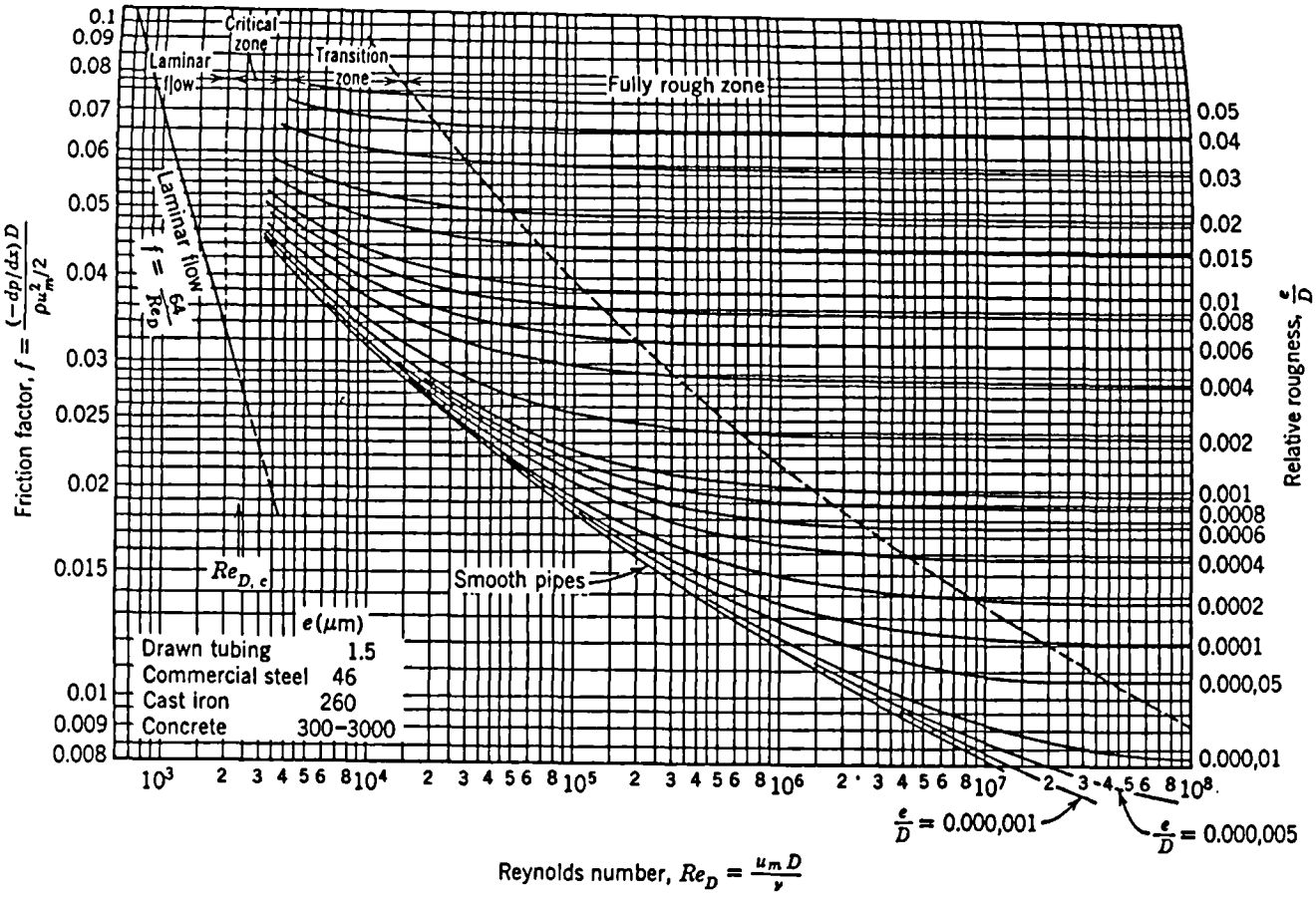

Figure 2.12 Friction factor for fully developed flow in a circular tube - Moody (1944) (from Incropera and DeWitt 1990)

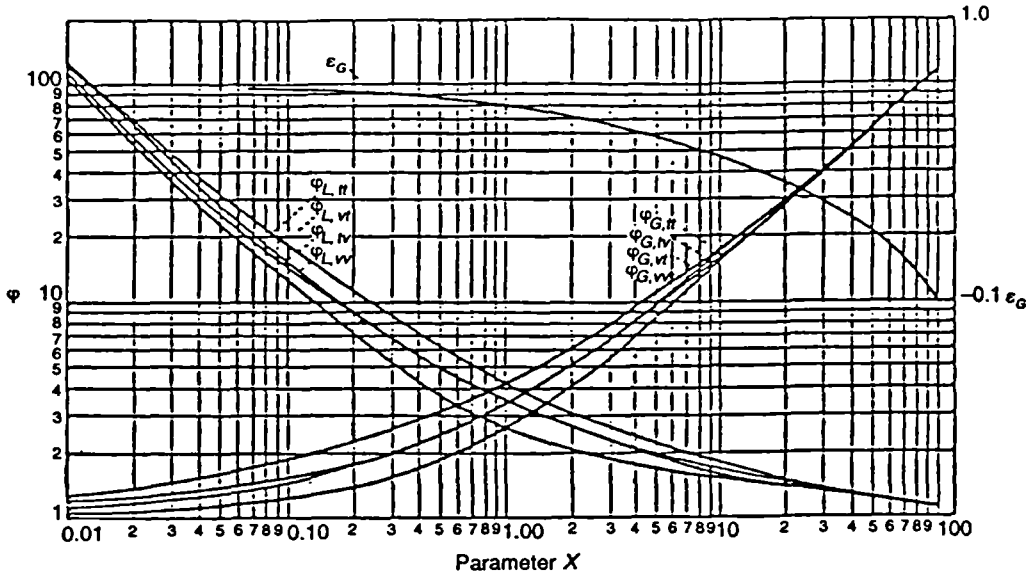

Figure 2.13 Pressure drop multiplier correlation of Lockhart and Martinelli (1949)

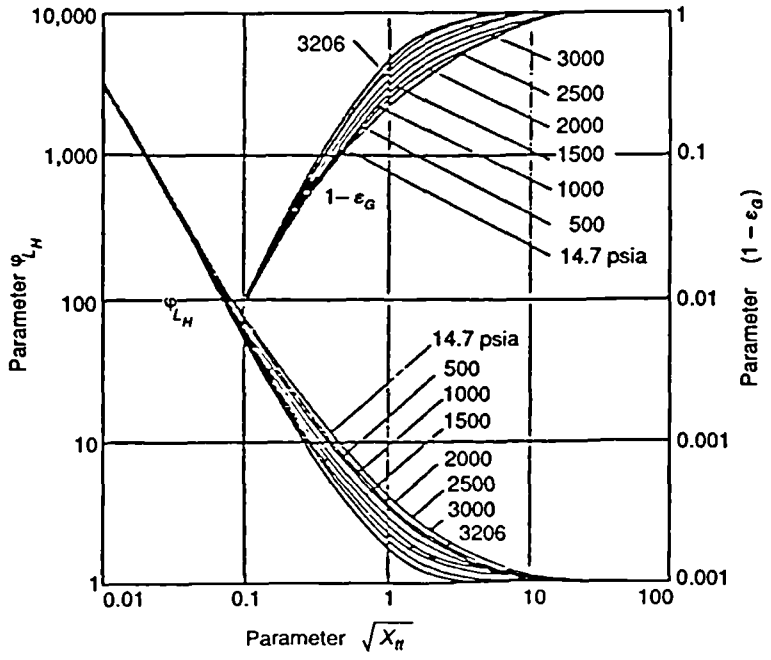

Figure 2.14 Martinelli and Nelson (1948) correction to the Lockhart and Martinelli (1949)

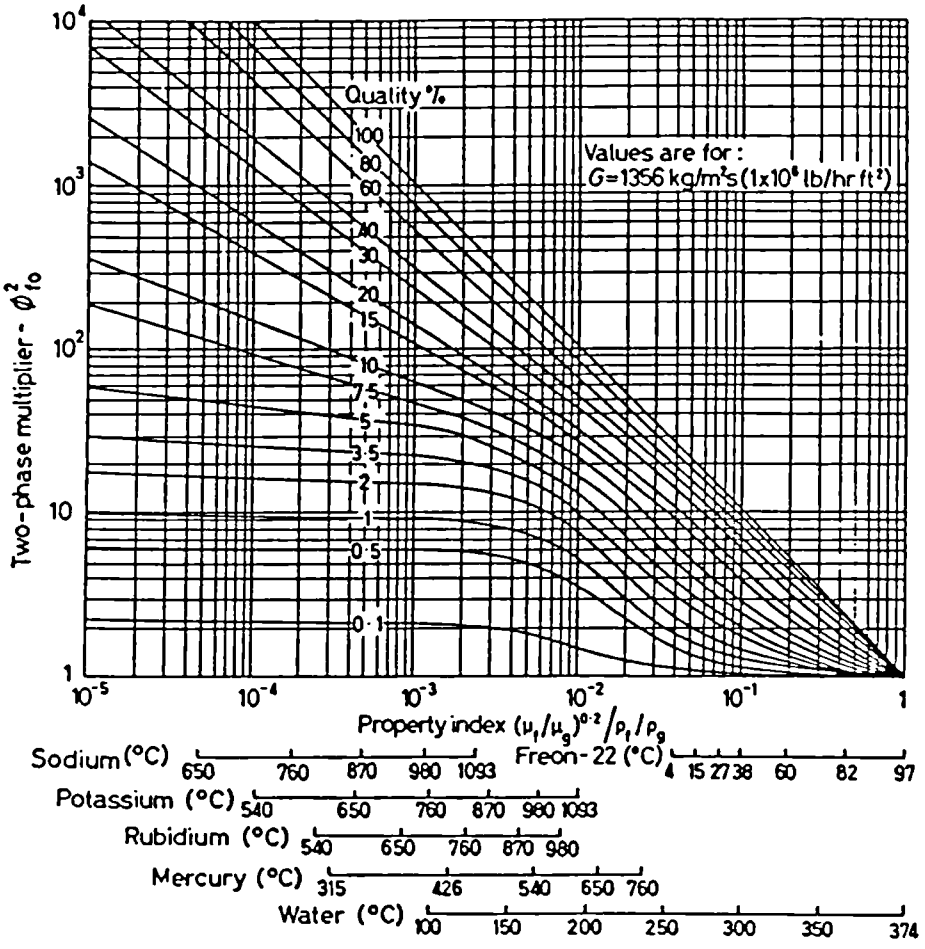

Figure 2.15 Two-phase friction pressure drop correlation of Baroczy (1966)

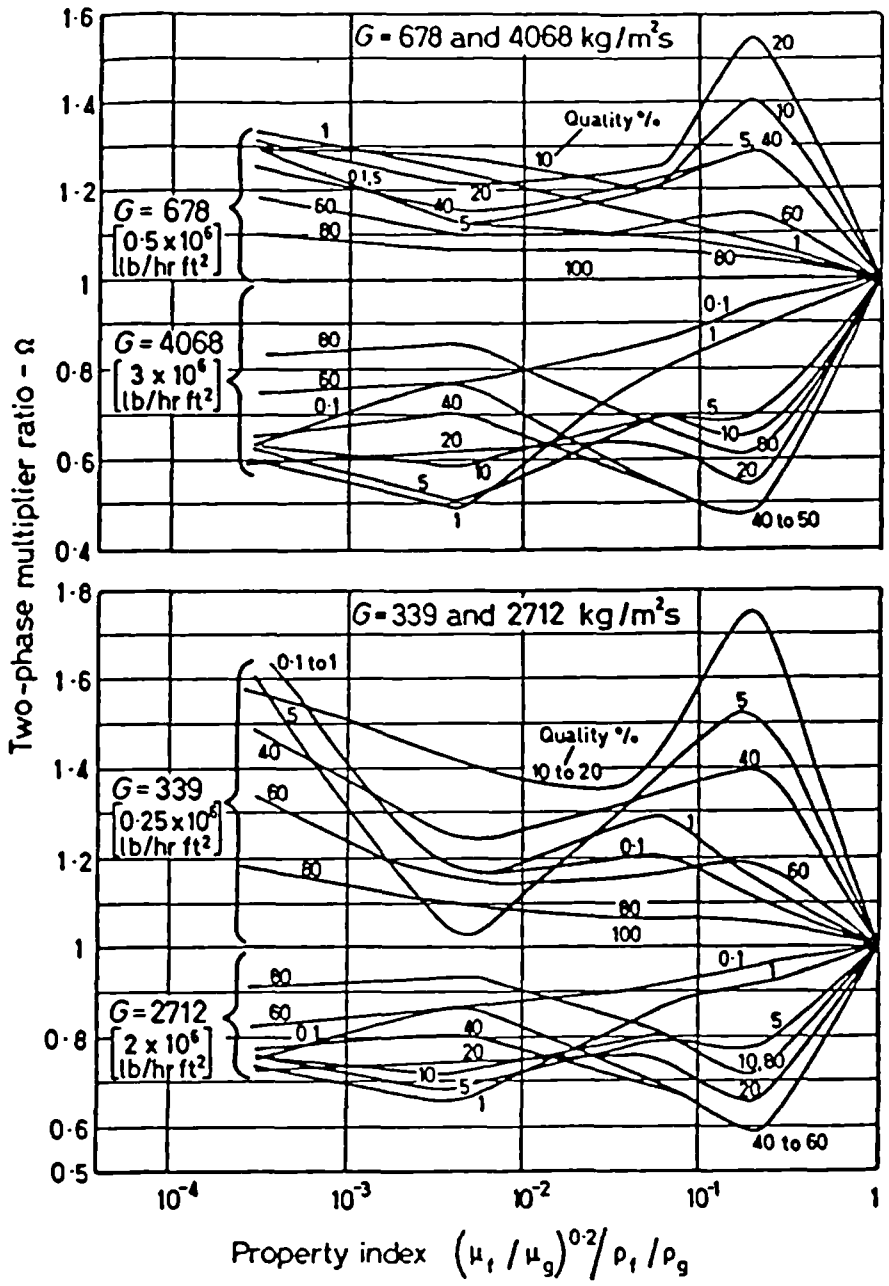

Figure 2.16 Mass velocity correction vs property index of Baroczy (1966)

CHAPTER 3

LITERATURE REVIEW :

HEAT TRANSFER

One of the most complex and fundamental fields in boiling heat transfer is that of flow boiling. The field is extremely large and dispersed. It had been reviewed and presented in many standard reference textbooks on heat transfer, for example Collier and Thome (1994) and Carey (1992) as well as in research papers such as those by Hewitt (1995a), Nishikawa (1995), Spindler (1994) and Butterworth and Shock (1982). As described earlier in section 2.2.1, the flow regimes encountered in a flow boiling system differ from the adiabatic case mainly because of the rate of change in quality. Furthermore, the complexity in flow boiling is increased by the fact that different boiling mechanisms may be encountered as one progresses along the heated tube.

The heat transfer mechanisms encountered in flow boiling may be presented in terms of boiling regime maps. These maps were presented by Collier (1972) and could be found in Collier and Thome (1994) and Carey (1992). They are illustrated in Figures 3.1 (for a constant wall heat flux condition with applied heat flux as the ordinate) and in Figure 3.2 (for an isothermal tube wall condition with the wall superheat as the ordinate). Both boiling regime maps have the bulk fluid enthalpy (and quality) as their abscissas. For Figure 3.1, assuming the scenario of a low constant heat flux, the flow

system would traced a horizontal path across the boiling regime map, passing successively through the following regimes:

1. Single-phase liquid convection
2. Subcooled nucleate boiling
3. Saturated nucleate boiling
4. Two-phase forced convective boiling
5. Mist evaporation (liquid deficient region)
6. Single-phase vapour convection

These heat transfer regimes are also illustrated in Figure 2.2 in Chapter 2, where they are presented alongside the corresponding hydrodynamic flow patterns. In the following sections, the heat transfer regimes from single-phase liquid convection to two-phase forced convective boiling will be reviewed under the 3 main headings of single-phase liquid convection, nucleate boiling and two-phase forced convection. The choice of heading is difficult because of the interactions between the various mechanisms. The second region covers the zone between the onset of nucleate boiling (ONB) and the point at which two-phase forced convection begins to make a significant contribution. Nucleate boiling per se may also contribute in the final (two-phase forced convection) region. Subcooled nucleate boiling and saturated nucleate boiling will be treated together under the heading of fully developed nucleate boiling within the nucleate boiling section, since the transition from subcooled to saturated nucleate boiling is defined purely from a thermodynamic viewpoint, where it is the point when the mean liquid temperature reaches that of the saturation temperature (x=0) which is found from simple energy balances, whilst the nucleate boiling heat transfer mechanism is essentially the same. We shall begin the reviews with the single-phase liquid convection.

3.1 Single-phase liquid convection

In single-phase liquid convection, assuming fully developed conditions both hydrodynamically and thermally, the heat transfer problem is solved differently for laminar and turbulent flows. Laminar flow in a circular tube can be solved theoretically. The full theoretical treatment of laminar single-phase liquid convection is presented in many standard heat transfer textbooks such as Incropera and DeWitt (1990), and is mentioned here in passing for completeness, though the flow conditions in the present studies were turbulent.

The heat transfer coefficient, α ($Wm^{-2}K^{-1}$) is defined from the expression

$$\dot{q} = \alpha \left(T_w - T_{fluid} \right) \tag{3.1}$$

where $\dot{q}$ is the applied heat flux (Wm^{-2}), T_w is the wall temperature and T_{fluid} is the mixed mean temperature of the fluid. For a constant wall heat flux, the heat transfer coefficient in fully developed heat transfer is calculated from:

$$Nu = \frac{\alpha D}{\lambda} = 4.36 \tag{3.2}$$

where λ is the thermal conductivity ($Wm^{-1}K^{-1}$) and D is the tube diameter. For fully developed laminar flow, the local heat transfer coefficient is independent of the Reynolds and Prandtl numbers as well as the axial position.

Turbulent flows cannot be predicted from first principles because of their complexity, greater emphasis had been placed by researchers on empirical correlations. One such correlation is that of Colburn (1933) for smooth pipes which was obtained by considering the Chilton-Colburn analogy and is given as follows.

$$Nu = 0.023\, Re^{4/5}\, Pr^{1/3} \tag{3.3}$$

Dittus and Boelter (1930) proposed a slightly modified version of Colburn (1933) equation after an analysis of a wide range of experimental data,

$$Nu = 0.023\, Re^{0.8} Pr^{n} \tag{3.4}$$

where $n = 0.4$ for heating and $n = 0.3$ for cooling. Both correlations have been tested experimentally and are valid for the range $0.7 \leq Pr \leq 160$, $Re \geq 10\,000$ and $L/D \geq 10$. The Dittus and Boelter (1930) correlation is the preferred version and is generally recommended. However, one should bear in mind that it has an associated overall r.m.s. error of around 13% (see Engineering Sciences Data Unit (ESDU), 1967). Since the Dittus and Boelter (1930) correlation was found to be less accurate for liquids with high Prandtl number in their comparisons, ESDU (1967) proposed and recommend the following correlation

$$Nu = 0.0225\, Re^{0.795} Pr^{0.495} \exp\left[-0.0225 \left(\ln Pr\right)^2\right] \tag{3.5}$$

with an overall r.m.s. error of around 10.2% and valid for the range of $0.3 < Pr \leq 300$, $4 \times 10^3 \leq Re \leq 10^6$ and $L/D \geq 10$

There are a few other correlations (e.g. see Incropera and DeWitt (1990)) for various kind of flow conditions such as that of Sieder and Tate (1936) for flow with large physical property variations, Gnielinski (1976) [see equation (3.85)] for smaller Reynolds number with a valid range of $0.5 < Pr < 2000$ and $2300 < Re < 5 \times 10^6$ and that of Pethukov (1970) given below

$$Nu = \frac{(f/2)\, Re\, Pr}{1.07 + 12.7\,(f/2)^{1/2}\left(Pr^{2/3} - 1\right)} \tag{3.6}$$

where f is the Fanning friction factor. Although the Pethukov (1970) correlation was reported to provide errors of less than 10%, it is a much more complex correlation to use when compared with the Dittus and Boelter (1930) or ESDU (1967) correlations.

Single-phase liquid convection will continue as the wall and fluid temperature rise (under constant heat flux), raising the wall superheat until the point when the first active nucleation sites are first observed. This point is known as the *onset of nucleate boiling* (ONB). It marks the transition from single-phase liquid convection to combined convection and nucleate boiling and corresponds to the threshold value of wall superheat that must be attained before any nucleation sites will become active. ONB marks the end of the single-phase forced convective region and the beginning of the nucleate boiling region.

3.2 Nucleate boiling

The *subcooled flow boiling* region is ~~known~~ defined as that region between ONB and saturated flow boiling. Its significance lies in the fact that it is, in essence a major transitional region for both heat transfer and fluid dynamics. Within the subcooled boiling region can be further sub-divided into two distinct sub-regions, namely the *partial subcooled boiling* and *fully developed nucleate boiling* as shown in Figure 3.3. To fully understand these sub-regions, it is simpler to trace the sequence of events that occur, starting from ONB until saturated flow boiling (see also Butterworth and Shock (1982) and Spindler (1994)).

Subcooled flow boiling starts at ONB. However, in many situations and conditions, ONB is not necessarily accompanied by a significant increase in void fraction. What this means is that bubbles merely grow and then collapse (condense) at, or very close to the wall. However, due to the simultaneous evaporation (growth) and condensation (collapse) of these bubbles and the agitation caused by these processes, there is an

increase in the heat transfer coefficient. As the flow progresses downstream, the fluid heats up and bubbles can now survive longer and start to slide along the wall but are still unable to penetrate into the core of the subcooled bulk liquid flow. At a point further downstream, known as the *net vapour generation* (NVG) point, bubbles will now grow, depart from the wall and survive for a significant time in the bulk liquid. From this point onwards, the void fraction due to subcooled boiling becomes significant and this also marks the beginning of the bubbly flow regime, from a hydrodynamic point of view. The void fraction rises very rapidly after NVG sometimes giving a void fraction (even in flow with net subcooling) which exceeds the 30% required for the bubbly to slug flow regime transition. This effect is computed in the modelling of the sub-atmospheric evaporator (SAE) system to be described in Chapter 6.

Thus, the partial subcooled boiling region is the region from ONB to NVG. This is a transitional region in which both the single-phase forced convective and nucleate boiling effects are important, with the nucleate boiling effects growing more dominant as the flow proceeds downstream. With an increasingly more favourable condition for nucleation, the nucleation site density will increase until it reaches the point when it is so high that the nucleate boiling component of the heat transfer is essentially equivalent to that of saturated nucleate pool boiling. The flow has now entered into its fully developed nucleate boiling phase, which lies between the NVG point and saturated flow boiling.

Hence, to predict the subcooled boiling region, the key requirements are the estimation of the ONB and NVG points and the prediction of heat transfer in the partial subcooled boiling and the fully developed nucleate boiling regions respectively.

3.2.1 Onset of Nucleate Boiling (ONB) and Net Vapour Generation (NVG)

Since ONB is of crucial importance in the study and prediction of subcooled boiling, a fair amount of effort had been expended by many researchers over the years in the quest to predict its position. In the present review, the focus will be on those models developed for water, in particular those proposed by Hsu (1962), Bergles and Rohsenow (1964), Sato and Matsumura (1964) and Davis and Anderson (1966). For refrigerants and organic fluids, (i.e. well-wetting fluids), the investigations are typified by those of Hino and Ueda (1985) and Hahne et al. (1990) and the literature in this area is reviewed by Spindler (1994).

Hsu's (1962) model for pool boiling can be seen as the forerunner for later models for ONB. Hsu postulated that a bubble will begin to grow only when the surrounding liquid is sufficiently superheated. This meant that there is a time period known as the *waiting period* for the liquid to achieve the desired superheat. A nucleation site is only considered active when this waiting period is finite, therefore imposing a criterion which in turns sets the limits to the sizes of possible effective nucleation sites. Hsu (1962) also assumed a transient conduction process as the mode of heat transfer from the wall to the liquid, calculating the liquid temperature gradient in the transient conduction following the departure of a bubble. Hsu's (1962) model, although for pool boiling and superseded by later models, is important because of the insight that it provides into the mechanisms and factors that affect nucleation such as subcooling, fluid physical properties and the thickness of the superheated liquid layer.

Building on Hsu's (1962) model, other investigators developed their own prediction methods and models for ONB based on similar lines. Among these investigators were Bergles and Rohsenow (1964). The key difference in Bergles and Rohsenow (1964) approach lies in the fact that they treated the forced convection case and were thus able to assume a linear temperature profile in the vicinity of (the assumed) hemispherical bubble. Bergles and Rohsenow (1964) postulated that a bubble will

grow when the temperature at its outer limit reaches the critical value for growth at the given bubble radius. This assumes that the velocity field is not disturbed by the bubble; a more realistic model was proposed by Kenning and Cooper (1965) who considered the dividing streamline for the flow over the bubble. Bergles and Rohsenow (1964) produced a graphical technique to solve these governing equations to predict ONB and found their calculations to be in good agreement with their measured data for water in forced convection flow in stainless steel and nickel tubes. Based on their graphical results, Bergles and Rohsenow (1964) recommended the following relation to predict the ONB for water in a heated tube as :

$$\dot{q}_{ONB} = 5.30\, p^{1.156} \left[1.80 \left(T_w - T_{sat}\right)_{ONB}\right]^{2.41/p^{0.0234}} \tag{3.7}$$

The above dimensional relation has been modified from the original relation given in Bergles and Rohsenow (1964) such that the units for the pressure, temperature and heat flux are respectively kPa, °C and Wm^{-2}. Bergles and Rohsenow (1964) stressed that their proposed model, like Hsu's (1962), is only applicable to boiling surfaces that have a wide spectrum of cavity sizes, a condition that they suggested should be easily satisfied by many commercially produced surfaces.

Sato and Matsumura (1964) also developed an analytical treatment for the ONB problem in a similar vein to that of Bergles and Rohsenow (1964). They compared their analysis with their own experimental data for water at atmospheric pressure flowing in a rectangular stainless steel duct and with data from other researchers at higher pressures. Sato and Matsumura (1964) found agreement with their proposed equation for ONB which was as follows,

$$\dot{q}_{ONB} = \frac{\lambda_L\, h_{LG}\, \rho_G}{8\, \sigma\, T_{sat}} \left(T_w - T_{sat}\right)^2 \tag{3.8}$$

Davis and Anderson (1966) modified and extended the Bergles and Rohsenow (1964) analytical treatment to arrive at the following equations:

$$(T_w - T_{sat})_{ONB} = \frac{(RT_{sat}^2/h_{LG})\ln(1+\xi')}{1-(RT_{sat}/h_{LG})\ln(1+\xi')} + \frac{\dot{q}\, y'}{\lambda_L} \tag{3.9}$$

where

$$y' = \frac{C_1\,\sigma}{p} + \sqrt{\left(\frac{C_1\,\sigma}{p}\right)^2 + \frac{2\,C_1\,\lambda_L\,\sigma\,T_{sat}}{\dot{q}\,h_{LG}\,\rho_G}} \tag{3.10}$$

$$\xi' = \frac{2C_1\,\sigma}{py'} \tag{3.11}$$

and

$$C_1 = 1+\cos\theta \tag{3.12}$$

In these equations, θ is the contact angle of the liquid-vapour interface on the solid surface. For systems at higher pressures or for low surface tension, using a hemispherical bubble model with $\theta = 90^\circ$ and therefore C_1=1, Davis and Anderson (1966) argued that their proposed equation (3.9) can be simplified and reduced to that of Sato and Matsumura (1964), see equation (3.8). The model proposed by Davis and Anderson (1966) is used as part of the modelling code for the present research and will be discussed in further details in Chapter 6.

At this point, it is well worth noting that the above mentioned ONB equations and models are only able to predict the point of ONB accurately if there exists a sufficiently wide range of potential nucleation sites on the wall surface. Consequently, one should exercise caution when using these equations for specific surfaces.

As with the study of ONB, a number of relationships and models have also been proposed for the position and conditions of net vapour generation (NVG). A survey of some of these models can be found in Lahey and Moody (1977) and Zeitoun (1994). The models proposed by Levy (1967), Saha and Zuber (1974) and more recently, Zeitoun and Shoukri (1995) will be reviewed in depth in the modelling chapter of this thesis, i.e. Chapter 6. Briefly, Levy (1967) predicted the position of NVG from a bubble force balance and using a single-phase liquid turbulent temperature distribution. Saha and Zuber (1974) suggested that NVG could be governed either thermally or hydrodynamically depending on the local Stanton (*St*) and Peclet (*Pe*) numbers; Zeitoun and Shoukri (1995) from their experimental investigation, proposed a model

based on the balance between vapour generation and condensation rates at the NVG point and found that their proposed model and experimental data is consistent with the Saha and Zuber (1974) model for the thermally controlled net vapour generation.

3.2.2 Partial subcooled boiling

In the partial subcooled boiling regime, the methods that have been developed to predict the heat transfer rate, are based on the concept of a combined contribution from both the single-phase liquid convection and the nucleate boiling mechanisms. The degree of contribution by each mechanism varies as the boiling process progresses. Immediately after the initiation of nucleate boiling, only a relatively small number of nucleation sites are active so that a proportion of the heat will still be transferred by single-phase liquid convection between the bubbles. However, as the wall temperature is increased, more bubble sites will become active until the whole surface is covered and the boiling is now said to be fully developed and the single-phase component is therefore reduced to zero. Hence, any form of interpolation and prediction method must take into account of this limiting behaviour of the heat transfer coefficient where, when one mechanism is activated, the other is deactivated.

Kutateladze (1961) proposed that both these mechanisms interact in an asymptotical (power law) manner, as given in equation (3.13).

$$\alpha = \left(\alpha_{spl}^2 + \alpha_{nb}^2\right)^{1/2} \tag{3.13}$$

Kutateladze's (1961) equation is consistent in predicting the limiting behaviour outlined above.

Other investigators, such as Bowring (1962) and Rohsenow (1953) utilised a different interpolation method based on the sum of the single-phase liquid heat flux and the nucleate boiling heat flux. Both the Bowring (1962) and Rohsenow (1953) methods

for predicting partial subcooled boiling heat transfer can be found in detail in standard heat transfer textbooks such as Collier and Thome (1994) or Carey (1992). They differ from one another in the manner in which they sought to determine the heat flux for both the single-phase liquid convection and nucleate boiling components.

Bowring (1962) proposed that if the wall temperature is greater than (or equal to) the saturation temperature but less than (or equal to) the wall temperature required for fully developed nucleate boiling, the single phase liquid convection heat flux can be evaluated from

$$\dot{q}_{spl} = \alpha_{spl} \left(T_{sat} - T_L (z) \right) \quad \text{for} \quad T_{sat} \leq T_w \leq T_{w.fdb} \tag{3.14}$$

and if the wall temperature is greater than (or equal to) the wall temperature required for fully developed nucleate boiling, then the single phase liquid convection heat flux contribution is zero.

$$\dot{q}_{spl} = 0 \quad \text{for} \quad T_{w.fdb} \leq T_w \tag{3.15}$$

It is clear that the point where the fully developed boiling begins is crucial, in order to evaluate its temperature. Bowring (1962) noted that Engelberg-Forester and Grief (1959) , based on their experimental data, concluded that the heat flux where fully developed boiling begins is approximately by

$$\dot{q}_{fdb} = 1.4 \, \dot{q}_1 \tag{3.16}$$

where $\dot{q}_1$ corresponds to the heat flux at the point of intersection between single phase liquid convection and the fully developed nucleate boiling curves. Bowring (1962) assumed that this point corresponded to that of the onset of nucleate boiling.

On the other hand, Rohsenow (1953) suggested the use of a conventional single-phase liquid convection equation (i.e. equation (3.14)), for predicting the single-phase

contribution while for the nucleate boiling contribution, he suggested the use of his saturated nucleate pool boiling correlation (Rohsenow (1952)).

$$\frac{C_{pL}\,\Delta T_{sat}}{h_{LG}} = C_{SF}\left[\frac{\dot{q}_{nb}}{\eta_L\, h_{LG}}\sqrt{\frac{\sigma}{g(\rho_L-\rho_G)}}\right]^{0.33}\left(\frac{C_{pL}\,\eta_L}{\lambda_L}\right)^{s} \qquad (3.17)$$

where C_{SF} is an experimentally determined constant for different liquid-surface combinations while s is the fluid index, taken as 1.0 for water and 1.7 for other fluids. A C_{SF} value of 0.020 for the boiling of water on a stainless steel surface has been determined by Bergles and Rohsenow (1964).

Bergles and Rohsenow (1964) also proposed a method for predicting the heat transfer for partial subcooled boiling in the form of the following equation:

$$\dot{q} = \dot{q}_{spl}\left\{1+\left[\frac{\dot{q}_{nb}}{\dot{q}_{spl}}\left(1-\frac{\dot{q}_{Bi}}{\dot{q}_{nb}}\right)\right]^{2}\right\}^{1/2} \quad for \quad \dot{q} \geq \dot{q}_{ONB} \qquad (3.18)$$

where $\dot{q}_{Bi}$ is the fully developed pool boiling heat flux at a wall temperature corresponding to the point of ONB. Another method to be reviewed is that proposed by Butterworth (1970) (see Collier and Thome, 1994) which is an extension to subcooled boiling of the Chen (1966) correlation for the quality region as follows:

$$\dot{q} = \alpha_{nb}\left(T_w - T_{sat}\right) + \alpha_{spl}\left(T_w - T_B\,(z)\right) \qquad (3.19)$$

Chen's (1966) parameter F was set at unity. A fuller discussion of Chen's (1966) correlation and the Butterworth's (1970) extension will be discussed in detail later.

3.2.3 Fully developed nucleate boiling

As the flow progresses downstream, it enters into the fully developed nucleate boiling phase which spans across the subcooled and saturated flow boiling conditions. The transition from subcooled to saturated nucleate boiling is defined purely from a thermodynamic viewpoint, where it is the point when the mean liquid temperature reaches the saturation temperature (i.e. when the quality, x=0). This point can be found from simple energy balances; however, the nucleate boiling heat transfer mechanism remains essentially the same. Since nucleate boiling is one of the major heat transfer mechanisms it is hardly surprising to find a vast number of correlations proposed to predict it. Nevertheless, a fundamental difficulty in correlating nucleate boiling still remains in that the heat transfer coefficient varies greatly from one heating surface to another. Also, for a given surface, the coefficient may vary with time and due to the fouling of the heat transfer surface.

As discussed in the previous section, Rohsenow (1952) proposed a correlation taking into account the surface effects in the form of the experimentally determined fluid-surface combination constant C_{SF} and is given below in equation (3.20) (see also equation(3.17)).

$$\frac{C_{pL}\,\Delta T_{sat}}{h_{LG}} = C_{SF}\left[\frac{\dot{q}_{nb}}{\eta_L\, h_{LG}}\sqrt{\frac{\sigma}{g(\rho_L-\rho_G)}}\right]^{0.33}\left(\frac{C_{pL}\,\eta_L}{\lambda_L}\right)^{s} \qquad (3.20)$$

Although Rohsenow (1952) correlation acknowledges the importance of surface effects, in practice, the values of C_{SF} are rarely known and often have to be guessed. Rohsenow (1952) recommended a value of C_{SF} of 0.013 as a first approximation for cases where C_{SF} is not known and s = 1.0 for water.

Another widely used correlation, although it does not take into account surface effects, is that of Forster and Zuber (1955) which is given as follows

$$\alpha_{FZ} = \frac{0.00122\,\Delta T_{sat}^{0.24}\,\Delta p_{sat}^{0.75}\,C_{pL}^{0.45}\,\rho_L^{0.49}\,\lambda_L^{0.79}}{\sigma^{0.5}\,h_{LG}^{0.24}\,\eta_L^{0.29}\,\rho_G^{0.24}} \tag{3.21}$$

where Δp_{sat} is the difference in saturation pressure corresponding to the saturation temperature difference ΔT_{sat} . Forster and Zuber (1955) derived their correlation from their analytical treatment for bubble growth. They showed that the product of the bubble radius and its growth rate is constant for a specific superheat. The Forster and Zuber (1955) correlation is also commonly encountered as the nucleate boiling component of the Chen (1963, 1966) correlation for saturated convective flow boiling.

Stephan and Abdelsalam (1980) proposed several fluid specific correlations for different classes of fluids, covering water, organics, refrigerants and cryogens by using statistical regression techniques. Stephan and Abdelsalam (1980) also proposed a general expression applicable to all the classes of fluids given below, equation (3.22), but with reduced accuracy relative to the fluid specific correlation.

$$\frac{\alpha_{nb}\,D}{\lambda_L} = 0.23\left(\frac{\dot{q}\,D_d}{h_{LG}\,T_{sat}}\right)^{0.674}\left(\frac{\rho_L}{\rho_G}\right)^{0.297}\left(\frac{h_{LG}\,D_d^{\,2}}{\kappa_L^2}\right)^{0.371}\left(\frac{\rho_L}{\rho_L-\rho_G}\right)^{1.73}\left(\frac{\kappa_L^2\,\rho_L}{\sigma\,D_d}\right)^{0.35} \tag{3.22}$$

where κ is the thermal diffusivity and D_d is the bubble departure diameter obtained from

$$D_d = 0.0208\,\theta\left[\frac{\sigma}{g\,(\rho_L-\rho_G)}\right]^{1/2} \tag{3.23}$$

The contact angle, θ was fixed at a value of 35° irrespective of the fluid. All the nucleate boiling correlations mentioned above can be categorised as being based on physical properties.

Another important category of nucleate boiling correlations are those based on reduced pressure p_r (i.e. $p_r = {}^{p}/_{p_c}$ where p_c is the fluid critical pressure). The Mostinski (1963) correlation of the form

$$\alpha = A^* \, \dot{q}^{0.7} \, F(p) \tag{3.24}$$

is one of the most commonly used correlation of this class. In this correlation, A^* is given by

$$A^* = 3.596 \times 10^{-5} \, p_c^{0.69} \tag{3.25}$$

while the pressure function, $F(p)$ is given by

$$F(p) = 1.8 \, p_r^{0.17} + 4 \, p_r^{1.2} + 10 \, p_r^{10} \tag{3.26}$$

The Mostinski (1963) correlation is less complex and easier to use; it dispenses with the need for extensive physical property data and was found to be just as accurate (see Collier and Thome (1994)) as the physical property based correlations.

Cooper (1982, 1984) developed a more accurate form of the reduced pressure correlation after analysing a wide range of boiling data. Cooper (1984) showed that for a given fluid, the physical properties can be represented as

$$property = p_r^{k} \left(-\log_{10} p_r\right)^{n} \times constant \tag{3.27}$$

Consequently, a correlation for heat transfer coefficient that includes physical properties can also be written as

$$\alpha = \frac{\dot{q}}{\Delta T_{sat}} = \dot{q}^{m} \, p_r^{q} \left(-\log_{10} p_r\right)^{r} \times constant \tag{3.28}$$

where k, n, m, q and r are indices which are determined from correlating the data set. From his analysis of his data set, Cooper (1984) proposed the following correlation for nucleate boiling,

$$\alpha = C\,\dot{q}^{0.67}\; p_r^{\left(0.12-0.2\log_{10} R_p\right)}\left(-\log_{10} p_r\right)^{-0.55}\; M^{-0.5} \qquad (3.29)$$

where R_p is the surface roughness parameter (Glättungstiefe, based on the German DIN 4762) in terms of micrometers, M is the molecular weight and the constant C was given by Cooper (1984) as 55 although some authors (e.g. Wadekar (1995)) have adjusted it to better fit specific data sets. For an unspecified surface, R_p is set to equal to 1 micrometer. Cooper (1984) also recommended that a factor of 1.7 should be applied to the value of the heat transfer coefficient in the case of boiling on horizontal copper cylinder. The Cooper (1984) correlation covers reduced pressures from 0.001 to 0.9 and molecular weights from 2 to 200.

Another alternative approach for predicting the nucleate pool boiling heat transfer coefficients is that of Gorenflo (1993). The procedure proposed is based on the calculation from a reference heat transfer coefficient $\alpha_{nb,o}$ which is evaluated at the normalised conditions of reduced pressure, $p_{r,o} = 0.1$, surface roughness, $R_{p,o} = 0.4$ μm and $\dot{q}_o = 20\,000$ W/m^2 for all fluids. Gorenflo (1993) provided reference values of $\alpha_{nb,o}$ for a selection of fluids (e.g. for water, $\alpha_{nb,o} = 5600$ W/m^{2}K). The nucleate pool boiling coefficient, α_{nb} at other pressure, heat flux and wall roughness can be evaluated from

$$\alpha_{nb} = \alpha_{nb,o}\, F_{PF} \left(\frac{\dot{q}}{\dot{q}_o}\right)^{nf} \left(\frac{R_p}{R_{p,o}}\right)^{0.133} \qquad (3.30)$$

The terms F_{PF} and nf are the pressure correction factor and the heat flux correction. Gorenflo (1993) provided the following expressions to evaluate the two correction factors for all fluids

$$F_{PF} = 1.2\, p_r^{0.27} + \left(2.5 + \frac{1}{1-p_r}\right) p_r \tag{3.31}$$

$$nf = 0.9 - 0.3\, p_r^{0.3} \tag{3.32}$$

except for water which he suggested using the following expressions

$$F_{PF} = 1.37\, p_r^{0.27} + \left(6.1 + \frac{0.68}{1-p_r}\right) p_r^2 \tag{3.33}$$

$$nf = 0.9 - 0.3\, p_r^{0.15} \tag{3.34}$$

The wall roughness term, R_p is set to be equal to 0.4 μm for an unknown surface. The Gorenflo (1993) method is a later version of the 1988 method and was used by Steiner and Taborek (1992) in their saturated flow boiling model.

Recently, Yagov (1995) introduced a new correlation based on a mechanistic approach. The boiling process was considered to be influenced by the heat transfer through a *macro-film* beneath large vapour bubbles and by local heat transfer around the individual vapour stems within this macro-film. The final equation proposed by Yagov (1995) is written as follows:

$$\alpha_{nb} = 0.07\left[\frac{\lambda_L^2\, \dot{q}^2}{\nu_L\, \sigma\, T_{sat}}\left(1 + \frac{h_{LG}\, \Delta T_{sat}}{2\, R\, T_{sat}^2}\right)\left(1 + \sqrt{1 + 800\, B} + 400\, B\right)\right]^{1/3} \tag{3.35}$$

where ν_L is the liquid kinematic viscosity, R is the gas constant and B is given by:

$$B = \frac{h_{LG}\left(\nu_L\, \rho_G\right)}{\sigma\left(\lambda_L\, T_{sat}\right)^{1/2}} \tag{3.36}$$

Yagov (1995) recommended that the single-phase liquid heat transfer coefficient, α_L is to be calculated using the correlation by Pethukov et al. (1986) which is as follows:

$$Nu = \frac{Re_L \, Pr_L \, (f/8)}{\left(1 + 900/Re_L\right) + 12.7\sqrt{f/8}\left(\mathrm{Pr}_L^{2/3} - 1\right)} \tag{3.37}$$

where f is the friction factor to be calculated from:

$$f = \frac{1}{\left[1.82 \log_{10}\left(Re_L\right) - 1.64\right]^2} \tag{3.38}$$

It is fairly obvious that there is an abundance of correlations available of which only a few key ones are mentioned here. In general, the accuracy is rather poor due to the surface effects. Cooper (1984) has been recommended (see Hewitt, Shires and Bott (1994)) for its simplicity and improved accuracy, but more importantly for its dispensation with extensive physical properties data which are not readily available for many fluids.

3.2.4 Subcooled boiling heat transfer correlations

Another category of heat transfer correlations are those which were specially formulated for the subcooled flow boiling based on the usage of dimensionless groups. These group of correlations were obtained from dimensional analysis and regression analysis of experimental data. Typical correlations in this category are those by Papell (1963), Badiuzzaman (1967) and Moles and Shaw (1972). The constants used in the following correlations were obtained for water; different constants may be required for refrigerants and hydrocarbons.

Papell (1963):

$$\frac{\alpha_{scb}}{\alpha_{FC}} = 90\left[\left(\frac{\dot{q}}{h_{LG}\,\rho_G\,u}\right)\left(\frac{h_{LG}}{C_{pL}\,\Delta T_{sub}}\right)^{1.2}\left(\frac{\rho_G}{\rho_L}\right)^{1.08}\right]^{0.7} \qquad (3.39)$$

Badiuzzaman (1967):

$$\frac{\alpha_{scb}}{\alpha_{FC}} = 178\left[\left(\frac{\dot{q}}{h_{LG}\,\rho_G\,u}\right)\left(\frac{h_{LG}}{C_{pL}\,\Delta T_{sub}}\right)^{1.2}\left(\frac{\rho_G}{\rho_L}\right)^{1.08}\left(\frac{\Delta T_{sub}}{T_{sat}}\right)^{0.6}\right]^{0.75} \qquad (3.40)$$

Moles and Shaw (1972)

$$\frac{\alpha_{scb}}{\alpha_{FC}} = 78.5\,Pr_L^{0.46}\left(\frac{\dot{q}}{h_{LG}\,\rho_G\,u}\right)^{0.67}\left(\frac{h_{LG}}{C_{pL}\,\Delta T_{sub}}\right)^{0.5}\left(\frac{\rho_G}{\rho_L}\right)^{0.70} \qquad (3.41)$$

where u is the fluid flow velocity.

3.3 Two-phase forced convection

At higher qualities, both the nucleate boiling and two-phase forced convective heat transfer mechanisms may be significant. The relative importance of one mechanism over the other varies along the length of the heated tube. In the region immediately after the saturation point, where the wall of the tube is covered with a large number of active nucleation sites, and both the vapour void fraction and quality are still relatively low, the nucleate boiling mechanism is much more dominant than the forced convective mechanism. As the flow continues downstream, more and more liquid is vaporised and the void fraction increases rapidly. Consequently, the flow velocity is higher and this tends to enhance the forced convective transport of energy from the heated wall.

Furthermore, as described in Chapter 2, the rapid increase in void fraction and change in vapour velocity also induces changes in the flow patterns. For fluids where there is a significant difference between liquid and vapour densities, the changes in flow patterns from bubbly to slug, churn and annular flow may occur in a very short period of time and over a very short length of tube. Once the annular flow pattern is established, evaporation from the liquid-vapour interface becomes increasingly important. As the liquid film on the wall thins, the process of heat transfer from the wall, convective heat transfer across the liquid film to the liquid-vapour interface becomes so efficient that the temperature at the wall drops below that required for nucleate boiling, causing it to be suppressed. The heat transfer mechanism is then dominated by the two-phase forced convection.

Several investigators have found that for convective heat transfer across a liquid film, the heat transfer coefficient can be correlated in terms of the turbulent-turbulent Martinelli parameter, X_{tt}. Based on this concept, Dengler and Addoms (1956) proposed a correlation, equation (3.42),for their predominantly convective heat transfer data for water in a vertical tube.

$$\frac{\alpha_{FC}}{\alpha_L} = 3.5\left(\frac{1}{X_{tt}}\right)^{0.5} \tag{3.42}$$

where α_{FC} is the heat transfer coefficient in two-phase flow

α_L is the heat transfer coefficient for the liquid phase flowing alone in the pipe

X_{tt} is the Martinelli parameter (see Chapter 2) defined as

$$X_{tt} = \sqrt{\frac{(dp_F/dz)_L}{(dp_F/dz)_G}} \tag{3.43}$$

where $(dp_F/dz)_L$ and $(dp_F/dz)_G$ are the frictional pressure gradients for the liquid and gas phase flowing alone in the pipe. α_L can be calculated from the Dittus and

Boelter (1930) type of equation [see equation (3.4)]. By using a Blasius (1913) type friction factor relation with $n = 0.2$, the Martinelli parameter can be rewritten as

$$X_{tt} = \left(\frac{1-x}{x}\right)^{0.9} \left(\frac{\rho_G}{\rho_L}\right)^{0.5} \left(\frac{\eta_L}{\eta_G}\right)^{0.1} \tag{3.44}$$

Based on a data fit to convective heat transfer data of organic fluids, Guerrieri and Talty (1956) proposed a similar form of correlation given as follows

$$\frac{\alpha_{FC}}{\alpha_L} = 3.4 \left(\frac{1}{X_{tt}}\right)^{0.45} \tag{3.45}$$

These two correlations above are valid only for cases where there are no significant nucleate boiling effects. Similar concepts were used by a number of other investigators; the two correlations presented above are given to exemplify the approach.

For saturated flow boiling at lower qualities and conditions where an interaction between nucleate boiling and forced convective heat transfer mechanisms are important, there exist a large number of different methodologies and correlations. The very existence of such a diverse range simply reflects the basic uncertainty in the field on these fundamental heat transfer mechanisms, in particular their interactions with each other. To quote Steiner and Taborek (1992): "In flow boiling, the nucleate and convective components are superimposed by a very complex mechanism which so far is not well understood."

In order to facilitate the review of these combined heat transfer correlations, Webb and Gupte (1992) divided them into three classes based on the concepts used to combine the nucleate boiling and forced convection contributions. These classes were called *superposition*, *enhancement* and *asymptotic* models. There is also another category which is based on *simple correction factors* (see Chan (1990)). Therefore, the

following sections reviewing the different saturated flow boiling correlations will be arranged according to these classifications, in the following order:

- Simple correction factor correlations
- Superposition correlations
- Enhancement correlations
- Asymptotic correlations

3.3.1 Simple correction factor correlations

To account for the contribution of nucleate boiling, Dengler and Addoms (1956) empirically developed a multiplying factor to their convective heat transfer correlation as follows

$$F_{NB} = 0.67\left[\left(\Delta T_{sat} - \Delta T_{ONB}\right)\left(\left(\frac{dp}{dT}\right)_{sat}\frac{D}{\sigma}\right)\right]^{0.1} \tag{3.46}$$

where $\left(\frac{dp}{dT}\right)_{sat}$ is the gradient of the saturation pressure versus saturation temperature curve, all properties were calculated at the wall temperature. Dengler and Addoms (1956) suggested that F_{NB} is only used when its value exceeds unity. The implication of this criterion is that the nucleate boiling component is only relevant when the wall superheat ΔT_{sat}, is larger than that for the onset of nucleate boiling. Dengler and Addoms (1956) included term $\left(\Delta T_{sat} - \Delta T_{ONB}\right)$ to account for the diminishing influence of nucleate boiling as the velocities increase. Based on a best fit of their data, Dengler and Addoms (1956) also suggested that the temperature difference required for ONB be calculated from

$$\Delta T_{ONB} = 10\, U_{TP}^{0.3} \tag{3.47}$$

where U_{TP} is the average two-phase mixture velocity.

Guerrieri and Talty (1956) also proposed a nucleate boiling correction factor to be applied to the convective heat transfer coefficient calculated from equation (3.45); this correction factor is correlated from their data as

$$F_{NB} = 0.187\left(\frac{r^*}{\delta}\right)^{-5/9} \tag{3.48}$$

where r^* is the radius of an equilibrium bubble corresponding to the wall superheat and δ is the thickness of the laminar sublayer given by

$$\delta = \frac{10\,\eta_L}{\rho_L}\sqrt{\frac{4\,\rho_L}{(dp/dz)_{TP}\,D}} \tag{3.49}$$

where $(dp/dz)_{TP}$ is the two-phase pressure gradient. Guerrieri and Talty (1956) also made a proviso that the value of the nucleate boiling correction factor cannot be less than unity, and if it is, then its value should be set to equal unity. According to Guerrieri and Talty (1956), this limit occurs when r^*/δ is equal to 0.049. Therefore, a value of r^*/δ greater than 0.049 was physically interpreted as a result of the liquid in the laminar film moving swiftly enough to prevent bubble nucleation at the wall cavities for the existing film temperature difference. It should be noted that apart from being limited to the data and conditions from which they were derived, these simple correction factor correlations are deficient in their lack of attempt to clearly distinguish between the nucleate boiling and convective heat transfer components.

3.3.2 Superposition correlations

The idea of a superposition model was initially mooted and utilised by Rohsenow (1952) in his evaluation of subcooled flow boiling. Bowring (1962) and Bergles and Rohsenow (1964) also utilised the same concept in their proposed prediction methods for subcooled flow boiling. However, the popularity and usage of the model only took off significantly when Chen (1963) employed it in his saturated flow boiling correlation. Since then, there have been several variants of the model proposed, most notably the correlations by Gungor and Winterton (1986, 1987). Both the Chen (1963, 1966) and Gungor and Winterton (1986, 1987) correlations can also be classified (see Hewitt (1995a)) as superposition models with *nucleation suppression* while Wadekar (1995) proposed a superposition model with a *forced convection suppression*. All three models will be discussed in this section.

Chen (1963, 1966) correlation

In a research work done for the United States Atomic Energy Commission, Chen (1963) compared the correlations of Dengler and Addoms (1956), Guerrieri and Talty (1956), Bennett et al. (1961) and Shrock and Grossman (1962) against an experimental database of 594 points of water and hydrocarbons compiled from the work of Dengler and Addoms (1956), Guerrieri and Talty (1956), Sani (1960), Wright (1961) and Shrock and Grossman (1962). Noting the discrepancies between these correlations and the data, Chen (1963) proposed a new form of correlation which recognised both the suppression of nucleate boiling and the enhancement of forced convection. In 1966, Chen improved on his original 1963 correlation by providing a theoretical basis for the enhancement in forced convection using an analysis based on the Reynolds analogy.

Chen (1963, 1966) reported that Dengler and Addoms (1956) correlation predicted their own data fairly well but it predicted coefficients which are too high when compared with the data from other sources. On the other hand, though the Guerrieri

and Talty (1956) correlation also correlates their own data well, it underpredicts the coefficients measured by Dengler and Addoms (1956) and Sani (1960) whilst giving reasonable agreement with the data of Shrock and Grossman (1962). The correlation by Bennett et al. (1961) was reported to predict reasonable values for the majority of the water data, albeit with wide scatter, it was found to underpredict the hydrocarbon data by as much as 50%. Chen (1966) found that the Schrock and Grossman (1962) correlation underpredicts the hydrocarbon data by as much as 30% and it appears to bisect the water data with a scatter range from -50% to +30%. Chen (1963, 1966) concluded that none of the correlations he compared is satisfactory and therefore, set about to develop a new correlation which gave an average deviation of ± 12%.

In deriving his correlation, Chen (1963, 1966) postulated that two basic mechanisms occur in saturated flow boiling which he termed the *macro-convective* heat transfer mechanism and the *micro-convective* mechanism normally associated with bubble nucleation and growth. He further postulated, following Rohsenow (1952), that both these mechanisms are additive in their contributions to the heat transfer in the following form

$$\alpha_{TP} = \alpha_{\text{macro}} + \alpha_{\text{micro}} \tag{3.50}$$

For the micro-convective or nucleate boiling component, Chen (1966) proposed the following expression:

$$\alpha_{\text{micro}} \left(\text{or } \alpha_{NB}\right) = S\, \alpha_{FZ} \tag{3.51}$$

where α_{FZ} is coefficient calculated from the Forster and Zuber (1955) pool boiling correlation (equation (3.21)) and S is a suppression factor to account for the reduction in the nucleate boiling contribution due to the suppression of nucleation sites. This reduction in nucleation sites can be attributed to the lower mean liquid superheat available in forced convection compared to pool boiling because of the thinner boundary layer. The suppression factor, S, is therefore a dimensionless ratio of the mean liquid superheat to the wall superheat.

For the macro-convective or forced convective component, Chen (1966) used a modified Dittus-Boelter equation in the form

$$\alpha_{macro}\left(\text{or } \alpha_{FC}\right) = 0.023\left(Re_{TP}\right)^{0.8}\left(Pr_{TP}\right)^{0.4}\left(\frac{\lambda_{TP}}{D}\right)F \qquad (3.52)$$

where F is sometimes known as the enhancement factor or two-phase convective multiplier, and is the ratio of the two-phase Reynolds number to the liquid Reynolds number, based on the liquid fraction of the flow, i.e.

$$F = \left(\frac{Re_{TP}}{Re_L}\right)^{0.8} \quad \text{or re-written as} \quad Re_{TP} = Re_L\, F^{1.25} \qquad (3.53)$$

where Re_L is the Reynolds number for the liquid phase flowing alone in the pipe. The enhancement factor, F, reflects the much higher velocities and therefore, higher forced convective heat transfer in the two-phase flow compared to the single-phase liquid flow. Chen (1966) has also shown from an analysis of the Reynolds momentum-analogy with some simplifying assumptions, F can be shown to be a function of the Martinelli parameter, X_{tt}. Chen (1966) also argued that since most of the heat is transferred through an annular film of liquid adhering to the wall, the liquid properties would have the dominant effect and are used in his modified Dittus-Boelter (see equation (3.52)). Similarly, the values of the Prandtl numbers for liquid and vapour are of the same magnitude, therefore resulting in a two-phase Prandtl number value close to that for the liquid phase. Thus, $\lambda_{TP} = \lambda_L$ and $Pr_{TP} = Pr_L$.

Chen (1966) presented both the enhancement factor and suppression factor in the form of graphical correlations as illustrated Figures 3.4 and 3.5 respectively. Butterworth (1979) presented curve-fits to both the Chen (1966) functions as:

$$F = 2.35\left(\frac{1}{X_{tt}} + 0.213\right)^{0.736} \tag{3.54}$$

$$S = \frac{1}{1 + 2.53 \times 10^{-6}\ Re_{TP}^{1.17}} \tag{3.55}$$

For $\frac{1}{X_{tt}} < 0.1$, the F takes a value of unity (F=1). For the saturated flow boiling region ($x > 0$), the heat flux is given simply by:

$$\dot{q} = \alpha\ \Delta T_{sat} \tag{3.56}$$

whilst for the subcooled boiling region ($x < 0$), the heat flux can be calculated from Butterworth (1970) recommendation is follows:

$$\dot{q} = \alpha_L\left(T_w - T_B\right) + \alpha_{NB}\left(T_w - T_{sat}\right) \tag{3.57}$$

where α_L is calculated for the single-phase liquid flow from the Dittus-Boelter correlation, T_w is the wall temperature and T_B is the bulk mixed mean liquid temperature. Following Butterworth's (1970) recommendation for the subcooled flow boiling region, the suppression factor, S, may be calculated by setting the two-phase Reynolds number equal to that of the single-phase liquid. In order to extend the applicability of the Chen (1963, 1966) correlation to other fluids, Bennett and Chen (1980) proposed several Prandtl number expressions for the enhancement factor. Recently, Chen and Tuzla (1995) reported on experiments which attempt to delineate between the contributions of forced convection and nucleate boiling for saturated convective flow boiling. Their findings were consistent with the Chen (1963, 1966) postulations, is that two-phase flow enhances convective heat transfer (beyond that for single-phase liquid convection) and suppresses the nucleate boiling contribution (below that of pool boiling).

Gungor and Winterton (1986) correlation

By applying the same approach and basic form of correlation as Chen (1966), Gungor and Winterton (1986) developed a new general correlation for flow boiling from a database of 3693 saturated boiling data points which they had amassed from published literature. Their so-called 'Birmingham Data Bank', at that time covered both the subcooled and saturated flow boiling regimes for water, refrigerants (R11, R12, R22, R113 and R114) and ethylene glycol in upward and downward vertical flows, horizontal flows and in annuli.

Although the basic form of the Gungor and Winterton (1986) correlation is similar to Chen (1966), i.e.

$$\alpha_{TP} = E\,\alpha_{FC} + S\,\alpha_{NB} \tag{3.58}$$

the two correlations differ in the method in which the various terms in the above equation (3.58) are calculated. While the forced convective heat transfer component is still calculated from the Dittus-Boelter equation, the enhancement factor, in this case, E, was given by

$$E = 1 + 24\,000\,Bo^{1.16} + 1.37\left(\frac{1}{X_{tt}}\right)^{0.86} \tag{3.59}$$

According to Gungor and Winterton (1986), the introduction of the dimensionless boiling number, Bo, in addition to the Lockhart -Martinelli parameter, merely reflects and accounts for the additional and significant disturbance to the boundary layer (and hence improved heat transfer) caused by the generation of vapour in the boiling process. The dimensionless boiling number, Bo is defined as

$$Bo = \frac{\dot{q}}{\dot{m}\,h_{LG}} \tag{3.60}$$

and was first introduced by Davidson (1943) as a measure of the nucleate boiling contribution.

Gungor and Winterton (1986) obtained their enhancement factor, E, from iterative empirical curve-fitting of their experimental data bank. Similarly, they obtained an expression for the suppression factor, S, which is a function of the two-phase Reynolds number as

$$S = \frac{1}{1 + 1.15 \times 10^{-6} \, E^2 \, Re_L^{1.17}} \tag{3.61}$$

For the nucleate pool boiling heat transfer coefficient, Gungor and Winterton (1986) recommended the use of Cooper (1984) reduced pressure correlation [see also equation (3.29)] with the surface roughness parameter set to its default value of 1 micrometer for an unspecified surface, thereby simplifying the Cooper (1984) correlation to:

$$\alpha_{NB} = 55 \, \dot{q}^{0.67} \, p_r^{0.12} \left(-\log_{10} p_r\right)^{-0.55} M^{-0.5} \tag{3.62}$$

Gungor and Winterton (1986) also recommended the following modifications:

- If the tube is *horizontal* and the Froude number is less than 0.05, stratified flow occurs and the tube wall is only partially wetted; to take into account of this occurrence, the enhancement factor, E, should be multiplied by:

$$E_2 = Fr^{(0.1 - 2\,Fr)} \tag{3.63}$$

and the suppression factor, S, should be multiplied by:

$$S_2 = \sqrt{Fr} \tag{3.64}$$

- For *subcooled boiling*, the basic form of the correlation should be replaced by:

$$\dot{q} = \alpha_L (T_w - T_B) + S\, \alpha_{NB} (T_w - T_{sat}) \qquad (3.65)$$

where α_L is the single-phase liquid flow Dittus-Boelter heat transfer correlation, T_w is the wall temperature and T_B is the bulk mixed mean liquid temperature. S is calculated from equation (3.61) with E=1. There is no enhancement factor since there is no net vapour generation, but the suppression factor is still effective. Gungor and Winterton (1986) argued that there may still be enhancement factor caused by *local* vapour generation, but this assumption gave their correlation a worse fit to the data bank, so it was not included.

It should be noted here that Gungor and Winterton's (1986) recommended modification for subcooled boiling is similar to that of Butterworth (1970) to the Chen (1963, 1966) correlation; the only major difference is the use of a more updated nucleate pool boiling correlation, i.e. Cooper (1984). Subsequently, in a later paper, Gungor and Winterton (1987) compared their 1986 modified subcooled boiling correlation [equation (3.65)] and the Butterworth (1970) modified Chen correlation [equation (3.57)] against the subcooled boiling specific correlations such as Papell (1963), Badiuzzaman (1967) and Moles and Shaw (1972); they found that their correlation and the Butterworth (1970) method gave about the same deviations but that both fared better than the subcooled boiling specific correlations.

- Gungor and Winterton (1986) also recommended the use of a *heated equivalent diameter* for flow in an annulus, where this is defined as the ratio of (4 x flow area) to the heated perimeter.

Gungor and Winterton (1987) correlation

Gungor and Winterton (1987) developed another more simplified general correlation for saturated flow boiling. They argued that because of the difficulty of obtaining vapour viscosity values (required in the Martinelli parameter) and that since they had

not found any work which reported conclusively that the viscosity ratio plays a significant role in the flow boiling process, they set out to developed a new correlation for the enhancement factor E as a function only of the boiling number, quality and density ratio.

Gungor and Winterton (1987) noted, from their analysis of the 'Birmingham Data Bank', that, for most cases, the nucleate boiling contribution is relatively small compared to the forced convection contribution. They also noted that the values of the suppression factor, S calculated from the data showed a large scatter, thus making the correlation to the two-phase Reynolds number poorer. They, therefore, proposed to replace the nucleate boiling term with a simpler expression. Gungor and Winterton (1987) tested the variations of the nucleate boiling term against the boiling number, total heat flux and single-phase heat transfer coefficient. They claimed a very clear relationship between the nucleate boiling term with the single-phase heat transfer coefficient and proceeded to correlate them. They also noted that the variation is quite narrow and hence suggested its inclusion into their already modified enhancement factor, E, resulting in a new basic form of their correlation [compared to equation (3.58)] as follows:

$$\frac{\alpha_{TP}}{\alpha_L} = E = 1 + C_1\, Bo^m + C_2 \left(\frac{x}{1-x}\right)^n \left(\frac{\rho_L}{\rho_G}\right)^z \qquad (3.66)$$

where the constants C_1, C_2, m, n and z were obtained by fitting the data in the data bank through an iterative procedure. Gungor and Winterton (1987) suggested the following values of the constants: $C_1 = 3000$, $C_2 = 1.12$, $m = 0.86$, $n = 0.75$ and $z = 0.41$, therefore making their new, improved and simplified general correlation for saturated flow boiling:

$$\frac{\alpha_{TP}}{\alpha_L} = E = 1 + 3000\, Bo^{0.86} + 1.12 \left(\frac{x}{1-x}\right)^{0.75} \left(\frac{\rho_L}{\rho_G}\right)^{0.41} \qquad (3.67)$$

While Gungor and Winterton (1987) still made the same recommendations for horizontal flow, flow with a Froude number of less than 0.05 and for flow in an annulus as those given above for Gungor and Winterton (1986) correlation, they found that their attempt to extend their new correlation into the subcooled boiling region was less successful. However, they did made some comparisons for subcooled boiling, most notably the Butterworth (1970) modification of Chen's (1966) correlation into subcooled boiling against both the data bank as well as against the Gungor and Winterton (1986), Papell (1963), Badiuzzaman (1967), Moles and Shaw (1972) and Shah (1984) correlations. They found and concluded that the Butterworth (1970) modified Chen correlation appeared to be the most accurate (mean deviation of 12.4%), although its database is marginally smaller (830 instead of the 936 subcooled boiling data points, i.e. 88.68% of the total database available then), and Gungor and Winterton (1987) advised caution in that these excluded data points may cause the good agreement to worsen. Their own correlation came second best with a mean deviation of 20.6%.

It is interesting to note that Gungor and Winterton did not directly compared their 1986 against their 1987 correlations, as one would normally expect ! Bearing in mind that the 'Birmingham Data Bank' had grown during the time period between the two Gungor and Winterton correlations, comparing the results presented in both their papers indicated that the 1987 correlation is more accurate, but only by a mean deviation of 0.6% in the value of the heat transfer coefficient from the 1986 correlation. It therefore seems that a better recommendation would be to use the Gungor and Winterton (1986) correlation with its added advantage of better applicability in the subcooled boiling region.

In spite of their improved accuracy, later work by Liu and Winterton (1991) and the review by Steiner and Taborek (1992) revealed some flaws in both the Gungor and Winterton's correlations. Steiner and Taborek (1992) highlighted the fact that the combinations of parameters in the Gungor and Winterton's enhancement and suppression factors were not derived from a mechanistic modelling approach but rather from repeated regression analysis of all the possible parameters. Liu and Winterton

(1991) highlighted the doubts on the use of the boiling number in the enhancement factor calculation which reduced its applicability in the subcooled boiling region.

Wadekar (1995)

Recently, Wadekar (1995) introduced an alternative superposition saturated flow boiling model. His proposed model is based on the concept of the suppression of convective heat transfer due to the presence of nucleate boiling. Wadekar's (1995) model can be expressed as:

$$\alpha_{TP} = \left(1 - A_{nb}\right) \alpha_{FC} + \alpha_{nb} \tag{3.68}$$

where A_{nb} is defined as the time averaged fraction of the total heat transfer area over which nucleate boiling is effective. Wadekar (1995) stipulated that the nucleate boiling component is not multiplied by A_{nb} because the pool boiling correlations used were based on the overall area rather than the effective area. Wadekar (1992) proposed that A_{nb} is calculated from

$$A_{nb} = 1 - \exp\left(-\theta\right) \tag{3.69}$$

where

$$\theta = \frac{k\, \Delta T_{sat}^{2.5}\, p_r}{Re_{TP}} \tag{3.70}$$

and k is an empirical constant related to the constant C from Cooper (1984) [see equation (3.29)] in the following expression:

$$k = 177\, C \tag{3.71}$$

Wadekar (1995) suggested that the nucleate boiling component should be calculated from the Cooper (1984) correlation. He treated the constant C as a fluid dependent variable with C = 35 for water, 48 for ethanol and 57 for refrigerants. For the two-

phase convective flow, the correlation for the enhancement factor, F, proposed by Kenning and Cooper (1989) was used and is given as follows:

$$\alpha_{FC} = \alpha_L F \tag{3.72}$$

$$F = 1.8\left(\frac{1}{X_{tt}}\right)^{0.87} + 1 \tag{3.73}$$

while the single-phase heat transfer coefficient α_L was obtained from the Dittus-Boelter equation.

However, Hewitt (1995a) argued against the plausibility of the suppression of the forced convective component by stating the following arguments:

(1) Visual observations by Hewitt et al. (1965) and Kenning and Hewitt (1986) had shown the suppression of nucleation in annular flow. Hewitt et al. (1965) found that the heat flux required for nucleation increases with increasing quality and mass flux.

(2) Recent experiments by Kandlikar (1995) showed that the wall superheat required to nucleate from a given cavity increases with increasing velocity.

Other correlations which apply the superposition concept in combining the forced convection and nucleate boiling heat transfer mechanisms for two-phase flow include those by Bjorge, Hall and Rohsenow (1982), Polley et al. (1980) and Jensen and Hsu (1987).

3.3.3 Enhancement correlations

The term *enhancement* models were used by Webb and Gupte (1992) to describe and classify the Boiling Number based correlations developed from that initially proposed by Shah (1976). Shah (1976) presented his proposed correlation in a graphical form called CHART and this is illustrated in Figure 3.6. The CHART correlation uses 4 dimensionless parameters given by the following equations:

$$\psi = \frac{\alpha_{TP}}{\alpha_L} \tag{3.74}$$

where

$$Co = \left(\frac{1}{x} - 1\right)^{0.8} \left(\frac{\rho_G}{\rho_L}\right)^{0.5} \tag{3.75}$$

$$Bo = \frac{\dot{q}}{\dot{m}\, h_{LG}} \tag{3.76}$$

$$Fr_L = \frac{\dot{m}^2}{\rho_L^2\, g\, D} \tag{3.77}$$

The single-phase heat transfer coefficient, α_L is calculated from the Dittus-Boelter equation. The dimensionless convective number, *Co*, was introduced to represent the convective boiling component and can also be regarded as a modified Martinelli parameter without the viscosity term. For vertical pipes, ψ is expressed as a function of *Co* with *Bo* as a parameter. For horizontal pipes, ψ is expressed as a function of *Co* with Fr_L as a parameter where $Fr_L \leq 40$. For $Fr_L > 40$, then ψ is expressed as a function of *Co* with *Bo* as a parameter.

Later, Shah (1982) curve-fitted his graphical CHART correlation (modified to include an increased experimental database).. Full details of the Shah (1982) equations representing his CHART correlation can be found in standard textbooks such as Carey (1992) and Collier and Thome (1994). The key points to be noted from the Shah (1982) equations are:

- Alternative equations for ψ are given for convective and nucleate boiling respectively. The larger of these values is chosen for calculation of the heat transfer coefficient.

- According to Shah (1982), the equations fit the CHART curves to within ±6% over most part of the curves with the following two exceptions:
  1) Near $Co = 0.004$ and $Bo = 50 \times 10^{-4}$.
  2) For horizontal tubes at $Fr_L < 0.04$ and $Bo < 1 \times 10^{-4}$

In the first case, Shah (1982) noted that his proposed equations over-predict by about 11%, but he concluded that it is of little consequence because these conditions normally fall into the post-dryout region of the evaporator. In the second case, Shah (1982) found that for some cases, the equations under-predict by as much as 20% for Co between 0.3 and 1.0. Shah (1982) decided against providing more accurate equations in this region since low Bo are rarely encountered.

In 1990, Kandlikar proposed his version of the enhancement model which he derived from large database of 5246 data points for water, refrigerants, neon and helium for saturated flow boiling inside vertical and horizontal tubes. Kandlikar's (1990) proposed model, which is essentially a modified form of the Shah (1982) correlation, is presented in the following form:

$$\alpha_{TP} = \alpha_L \left(C_1 \, Co^{C_2} \left[25 \, Fr_L \right]^{C_5} + C_3 \, Bo^{C_4} \, F_{fl} \right) \qquad (3.78)$$

The constants C_1 to C_5 are given Table 3.1 while the fluid dependent parameter F_{fl} for the fluids tested by Kandlikar (1990) are given in Table 3.2 below. Kandlikar (1990) recommends that for other fluids not listed in the Table 3.2, the fluid dependent parameter, F_{fl} can be estimated as the multiplier that must be applied to the Forster and Zuber (1955) correlation to correlate the pool boiling data of the fluid of interest. The

boiling number, convective number and Froude number are calculated using the same equations proposed by Shah (1982).

In using the same criterion as Shah (1982), Kandlikar (1990) suggested that the heat transfer coefficient at any given condition is evaluated using both sets of constants for the two regions. Since the transition from one region to the other occurs at the intersection of the respective correlations, the *larger* of the two heat transfer coefficient values represents the predicted value from his correlation. Kandlikar (1990) stated that this approach will provide a continuity between the convective and nucleate boiling regions.

Constant	Convective Region	Nucleate Boiling Region
C_1	1.1360	0.6683
C_2	- 0.9	- 0.2
C_3	667.2	1058.0
C_4	0.7	0.7
C_5^*	0.3	0.3

$C_5^* = 0$ for vertical tubes and for horizontal tubes with $Fr_L > 0.04$.

Table 3.1 Kandlikar (1990) constants C_1 to C_5

Fluid	F_{fl}
Water	1.00
R-11	1.30
R-12	1.50
R-13 B 1	1.31
R-22	2.20
R-113	1.30
R-114	1.24
R-152 a	1.10
Nitrogen	4.70
Neon	3.50

Table 3.2 Kandlikar (1990) fluid dependent parameter F_{fl}

3.3.4 Asymptotic correlations

The general asymptotic model can be mathematically expressed as

$$\alpha_{TP} = \left[(\alpha_{nb})^n + (\alpha_{FC})^n \right]^{1/n} \tag{3.79}$$

This model provides a smooth transition as the boiling mechanism changes from one which is predominantly nucleate boiling to that of forced convection, as observed in many flow boiling experiments. Equation (3.79) is general, with the exponent n laying between the range, $1 \leq n < \infty$. If $n = 1$, the equation becomes that of the superposition model and for $n \rightarrow \infty$, the equation becomes that of the larger of the two values as in the Shah (1982) and Kandlikar (1990) correlation. The asymptotic modelling approach has been formalised and promoted by Churchill and Usagi (1972) in their

modelling of forced and natural convection heat transfer regimes where each regime is dominated by different limiting thermal mechanisms.

In 1961, Kutateladze proposed his asymptotic 'power law' model for subcooled boiling heat transfer as given in equation (3.13). Kutateladze (1961) used the exponent $n = 2$ but there is no theoretical basis for his selection of n except that it gives a best fit to his data.

Liu and Winterton (1991) developed a new approach based on the asymptotic model after they had noted the deficiencies in the earlier Gungor and Winterton (1986, 1987) correlations. One of the key features of their approach is the adoption of Chen's (1966) basic postulations on two-phase flow enhancement and nucleate boiling suppression factors. However, they questioned Chen's (1966) use of the superposition method and chose to use the model proposed by Kutateladze (1961) instead. Their proposed model can be written as

$$\alpha_{TP} = \left[(E\,\alpha_L)^2 + (S\,\alpha_{nb})^2 \right]^{1/2} \tag{3.80}$$

$$E = \left[1 + x\,Pr_L \left(\frac{\rho_L}{\rho_G} - 1 \right) \right]^{0.35} \tag{3.81}$$

$$S = \frac{1}{\left(1 + 0.055\,E^{0.1}\,Re_L^{0.16} \right)} \tag{3.82}$$

where E and S are the enhancement and suppression factors and Re_L is the Reynolds number for liquid flowing alone in the tube.

The nucleate boiling α_{nb} and forced convective α_L components are calculated from the Cooper (1984) and Dittus and Boelter (1930) correlations respectively. Liu and Winterton (1991) derived their enhancement and suppression factors by performing iterative regression analysis on a data bank of 5193 data points from the Birmingham data bank. They also recommended the same modifications as Gungor and Winterton

(1986) for horizontal flows, flows with Froude number less than 0.05 and for flows in annuli. For subcooled flow boiling, they recommend the following equation,

$$\dot{q} = \left[\left(E\, \alpha_L \left(T_w - T_B \right) \right)^2 + \left(S\, \alpha_{nb}\, \Delta T_{sat} \right)^2 \right]^{1/2} \tag{3.83}$$

Another more recent variant of the asymptotic model for flow boiling heat transfer is that of Steiner and Taborek (1992). Instead of following the trend of previous works towards statistical development of flow boiling correlations, they aimed to develop their correlation based on *mechanistic* modelling that obeys the established principles and observations of nucleate pool boiling and forced convective heat transfer. They chose the asymptotic model as their correlation's foundation on the basis that they can develop the nucleate boiling and forced convective components independently from each other. Furthermore, it inherently reflects the components interaction with each other.

Details of Steiner and Taborek's (1992) procedures can be found in their paper, as well as in Collier and Thome (1994). The salient features of their correlation are outlined below. The correlation proposed by Steiner and Taborek (1992) can be written as follows,

$$\alpha_{TP} = \left[\left(\alpha_{nb,o}\, F_{nbf} \right)^3 + \left(\alpha_{LO}\, F_{tp} \right)^3 \right]^{1/3} \tag{3.84}$$

where

$\alpha_{nb,o}$ is the local 'normalised' nucleate pool boiling coefficient at a standard condition of heat flux and reduced pressure. Steiner and Taborek (1992) chose the normalised parameters at reduced pressure $p_{r,o} = 0.1$; wall roughness $R_{p,o} = 1$ μm and the normalised heat flux (for water) $\dot{q}_o = 150\,000\ \mathrm{W/m^2}$. The normalised nucleate pool boiling coefficient can also be calculated from experimental data or pool boiling correlations, provided they are normalised. The normalisation procedures presented by Gorenflo (1993) was recommended.

F_{nbf} is the nucleate boiling correction factor that accounts for the differences between pool and flow boiling conditions. It takes into account the effects of pressure, heat flux, tube diameter, surface roughness and a blanket residual correction, expressed as a function of the molecular weight.

α_{LO} is the local single-phase forced convection coefficient based on total flow as liquid. Steiner and Taborek recommended the Gnielinski (1976) correlation (equation (3.85) below) but stated that the simpler Dittus-Boelter equation may also be used in the case of turbulent flow.

$$Nu = \frac{(f/8)(Re_{LO} - 1000)\,Pr}{1 + 12.7\,(f/8)^{1/2}\left(\mathrm{Pr}_L^{2/3} - 1\right)} \tag{3.85}$$

with the Fanning friction factor calculated from

$$f = \left[0.7904 \ln\left(Re_{LO}\right) - 1.64\right]^{-2} \tag{3.86}$$

F_{tp} is the two-phase multiplier to account for the enhancement of convection in two-phase flow. It is a function of the quality, x and the liquid/vapour density ratio and is given as

$$F_{tp} = \left[(1-x)^{1.5} + 1.9\,x^{0.6}\left(\frac{\rho_L}{\rho_G}\right)^{0.35}\right]^{1.1} \tag{3.87}$$

This expression is valid only for quality less than that for the dryout condition.

The correlation was validated using the University of Karlsruhe databank of 13 000 data points covering 15 fluids from 34 sources. Steiner and Taborek (1992) compared their correlation against those of Chen (1966), Shah (1982) and Gungor and Winterton (1986, 1987) for ethanol, ammonia and R-12 but they did not make any comparisons

for water. As expected, Steiner and Taborek (1992) showed their correlation to be better than all the others, as is *de rigueur* for new correlations.

3.3.5 Additional discussions on correlations

Apart from the work referenced above and aimed at producing flow boiling correlations, other related research work is reviewed below, particularly where it is relevant to making judgements on prediction methods.

Aounallah et al. (1982) and Kenning and Hewitt (1986)

Aounallah et al. (1982) conducted experiments in the annular flow regime with the specific aim of distinguishing between the conventional explanation of pure convective mechanism at high qualities and the alternative hypothesis of Mesler (1973) on enhanced nucleate boiling due to thinning films in annular flow. From their experiments, they concluded that over the range of heat fluxes that they had used, the relationship between the heat flux and wall superheat is closely linear indicating a forced convective mechanism. Kenning and Hewitt (1986) confirmed Aounallah et al. (1982) findings by noting the effects and existence of nucleate boiling suppression in annular flow. In both papers, the Chen (1966) correlation was tested and found to be in good agreement with the experimental results. Ross and Radermacher (1987), in experiments on pure and mixed refrigerants (R152a and R13 B1), also showed the existence of nucleate boiling suppression in annular flow.

Cooper (1989) and Kenning and Cooper (1989)

Cooper (1989) conducted a re-examination of Chen (1966) nucleate boiling term and compared it against his own 1984 reduced properties correlation. The re-examination employed all the then available published data for water together with the additional data from Kenning and Cooper (1989) which were regarded as highly accurate and which was able to distinguish the 'apparently nucleate' regime with some confidence. However, Cooper (1989) concluded that in view of the extremely wide scatter present in the data points, there is no strong case for replacing the Forster and Zuber (1955) nucleate boiling term in Chen's (1966) correlation. However, he did recommend the use of the reduced properties based nucleate boiling correlation on the grounds of its simplicity.

Kenning and Cooper (1989) conducted experiments on saturated flow boiling of water at 160 to 600 kPa in vertical 9.6 and 14.4 mm bore thin-walled cupronickel tubes. They concluded that the heat transfer coefficient is equal to the larger of the convective coefficient or the nucleate boiling coefficient and are not additive (within experimental error). They also suggested modifications to the Chen's (1966) enhancement factor, F for annular flow and as for plug/churn flow, the inclusion of the a multiplication factor based on the dimensionless superficial gas velocity, U_G^* (defined in equation (2.22)).

Webb and Gupte (1992) and Steiner and Taborek (1992)

Both Webb and Gupte (1992) and Steiner and Taborek (1992) conducted critical reviews and comparisons of some of the most commonly used and referenced flow boiling correlations at that time, including Chen (1966), Shah (1976, 1982), Gungor and Winterton (1986, 1987) and Kandlikar (1990). Both papers highlighted the shortcomings of the correlations of Winterton and co-workers criticising in particular the extensive use of iterative regression analysis to arrive at the expressions for the two-phase flow enhancement and suppression factors. Webb and Gupte (1992) even raised serious doubts on the procedures that Winterton and co-workers adopted in their regression analysis for the enhancement factors. They concluded that Winterton and co-workers had erroneously done so by calculating the nucleate boiling heat transfer coefficient at the total heat flux rather than at the nucleate boiling heat flux. This resulted in a smaller value of the enhancement factor than the correct value.

Chen and Tuzla (1995)

From their experiments and using a combination of two-phase convection (no boiling) and saturated convective boiling results, Chen and Tuzla (1995) delineated the relative contributions of the forced convective and nucleate boiling heat transfer mechanisms. Their results showed that in comparison to single-phase convection and pool boiling, two-phase flow significantly enhances the convective heat transfer mechanism but suppresses the contribution of the nucleate boiling component even more than originally suggested by Chen (1966).

Hewitt (1995a, 1995b)

Hewitt (1995b) presented (at the Convective Flow Boiling Conference at Banff, Canada) a survey of the phenomenological background to forced convective evaporation. He reported results obtained by Chan (1990) which showed some indications of the influence of secondary nucleation in what had been assumed to be pure forced convective heat transfer. The Chan experiments appeared to show large differences between evaporation and condensation at identical flow conditions. These experiments were subject to large uncertainty and are currently being repeated by G. Sun at Imperial College. Although the initial results (Hewitt, 1995b) appeared to confirm the original findings by Chan, improvements in the experimental techniques have led to the conclusion that the coefficients for forced convective condensation and evaporation are identical (Hewitt, 1995a). This indicated that the secondary nucleation mechanism as proposed by Mesler (1973) is not likely to be significant in two-phase forced convective systems.

3.4 Sub-atmospheric heat transfer literature

Only a limited amount of work has been done for flow boiling of water at sub-atmospheric pressure. To the present author's knowledge, only the research work done by Stone (1971) is closely related to the work described in this thesis. Stone (1971) conducted a series of experiments on subcooled and saturated flow boiling of water in a vertical test section at sub-atmospheric pressures. The test sections and experimental parameters used by Stone (1971) are as follows:

Stone (1971) test sections details:

- Material of construction : **Inconel X**
- Inside tube diameters : 0.584 and 1.219 cm.
- Wall thickness : 0.25 mm.
- Tube length : 14.6, 29.2, 61.0 121.9 cm.

- Maximum surface roughness (from surface analyser) : 5 nm.

The experimental parameters and range of Stone (1971) experiments were:

- Mass flux : 0.67 to 141 kg/m^2 s
- Heat flux : 43.8 to 11 400 kW/m^2
- Exit pressure : 24 to 690 kN/m^2
- Exit quality : up to 0.65
- Liquid subcooling : up to 151 K.

The results and conclusions from Stone (1971) can be summarised as follows:

Large subcooling (~ 83 K)

At low heat fluxes, there was no boiling with the heat transfer coefficient decreasing initially with distance in the thermal entrance region and then increases slightly as a result of the effect of increasing temperature on the physical properties.

At intermediate heat fluxes, onset of nucleate boiling and subcooled flow boiling were encountered. Stone noted the continual rise of the heat transfer coefficient with distance, as one would expect as the boiling mechanism changes from single-phase liquid convection to nucleate boiling. Higher heat fluxes caused the position of ONB to shift towards the inlet as expected and the value of the heat transfer coefficient was noted to be higher than the intermediate heat flux case.

Stone remarked that for the subcooled boiling runs, the inside wall temperature was found to increase with distance but is of small magnitude. Nevertheless, this effect was not predicted by the subcooled boiling correlations that he tested. He used the Rohsenow (1952), Forster and Zuber (1955), Engelberg-Forster and Greif (1959) and Papell (1963) subcooled boiling correlations. Stone found that Papell (1963) subcooled boiling correlation fitted his data best but he noted an increasing deviation as $x \rightarrow 0$.

Small subcooling (~ 22 K)

Once again, Stone (1971) found that as the heat flux increases, the point of ONB moves nearer to the inlet of the test section. He also noted that inside wall temperature increases with distance for the subcooled boiling runs. This time, however, the agreement with Papell (1963) correlation was poorer, especially at the lowest heat flux, indicating that the limits of the range of applicability of Papell (1963) correlation to subcoolings greater than around 20 K.

Other conclusions and observations from the Stone (1971) experiments

Stone showed that heat transfer coefficients, based on a wall-to-liquid temperature difference corrected for non-equilibrium, vary less with quality and showed more consistent trend than heat transfer coefficients based on either wall-to-bulk or wall-to-saturation temperature differences. The Stone experimental data has been a regular source for data banks such as the Birmingham data bank and has been correlated by flow boiling correlations described in the previous section. Stone also noted the following from his data:

- For constant heat flux, mass flux and quality, the heat transfer coefficient was found to increase with increasing pressure. This was contrary to the correlations that he tested which predicted the opposite trend.

- If the heat transfer coefficient was calculated based on the difference between the wall and the saturation temperature, rather complex results were obtained as illustrated in Figure 3.7. From the point of view of the present study, the most important feature of the results shown in Figure 3.7 is the existence of peaks ("overshoots") in the heat transfer coefficient at qualities near zero. This is particularly pronounced at high heat fluxes.

This then concludes the literature review on heat transfer. The next chapter will focus on the SAE experiments.

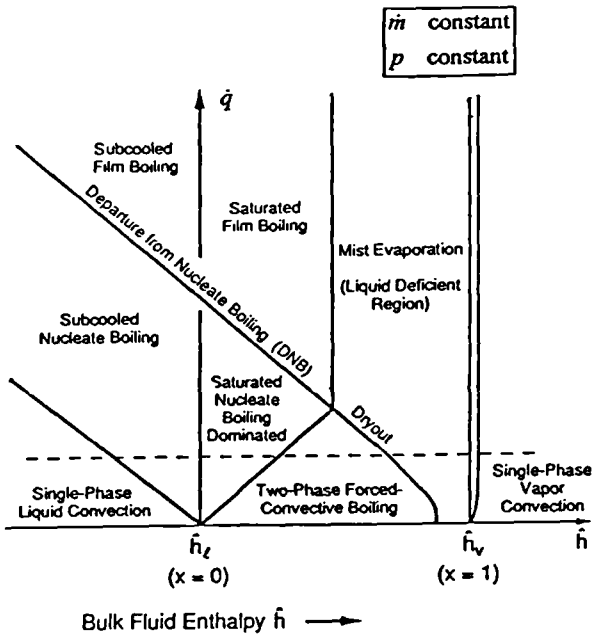

Figure 3.1 Collier's boiling regimes for a constant wall heat flux condition (adapted from Carey 1992)

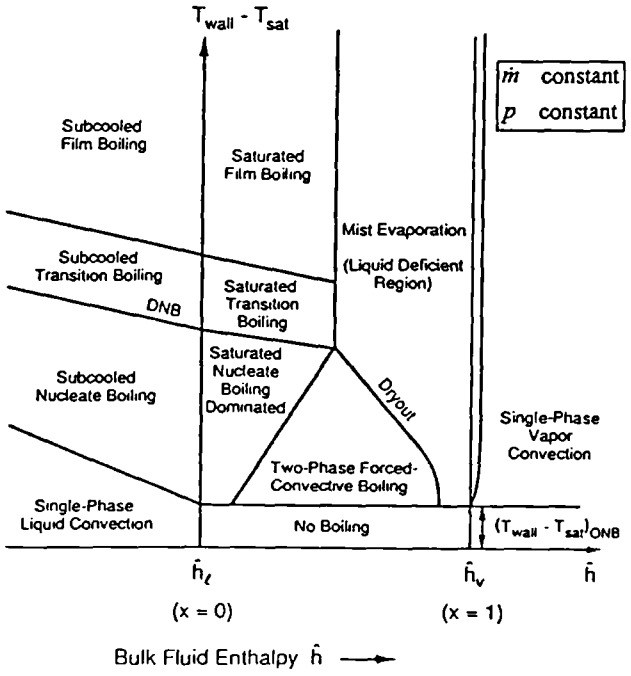

Figure 3.2 Collier's boiling regimes for an isothermal tube wall condition (adapted from Carey 1992)

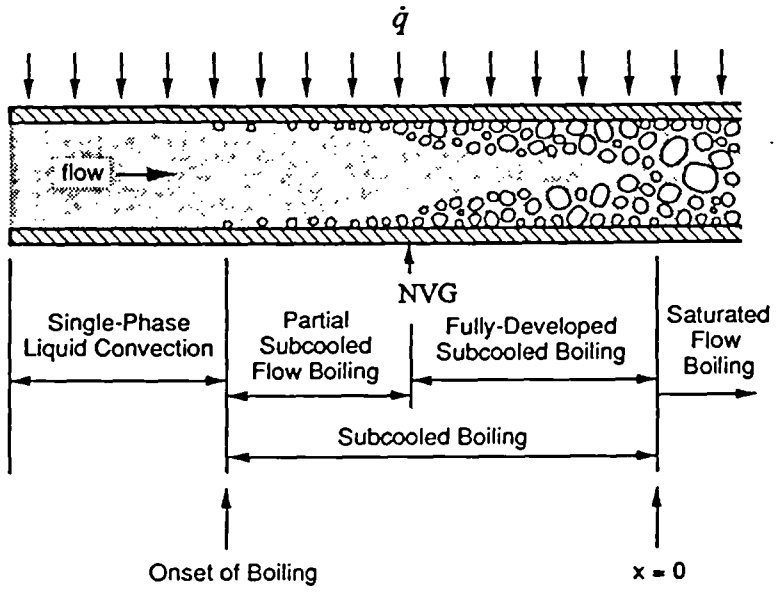

Figures 3.3 Subcooled flow boiling regimes (adapted from Carey 1992)

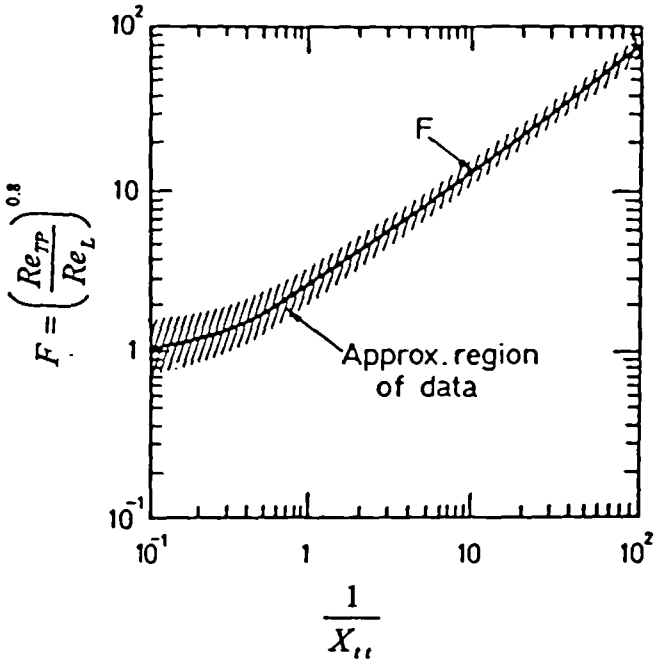

Figure 3.4 Two-phase flow enhancement factor, F (Chen 1966)

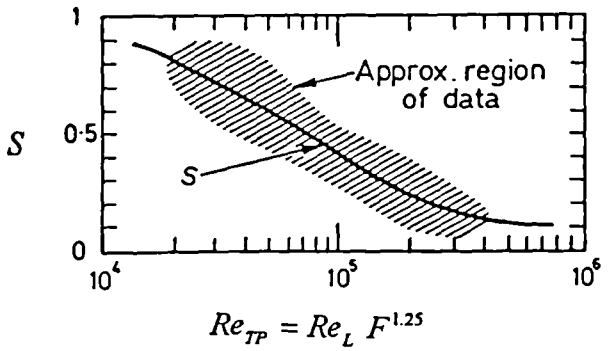

Figure 3.5 Suppression factor, S (Chen 1966)

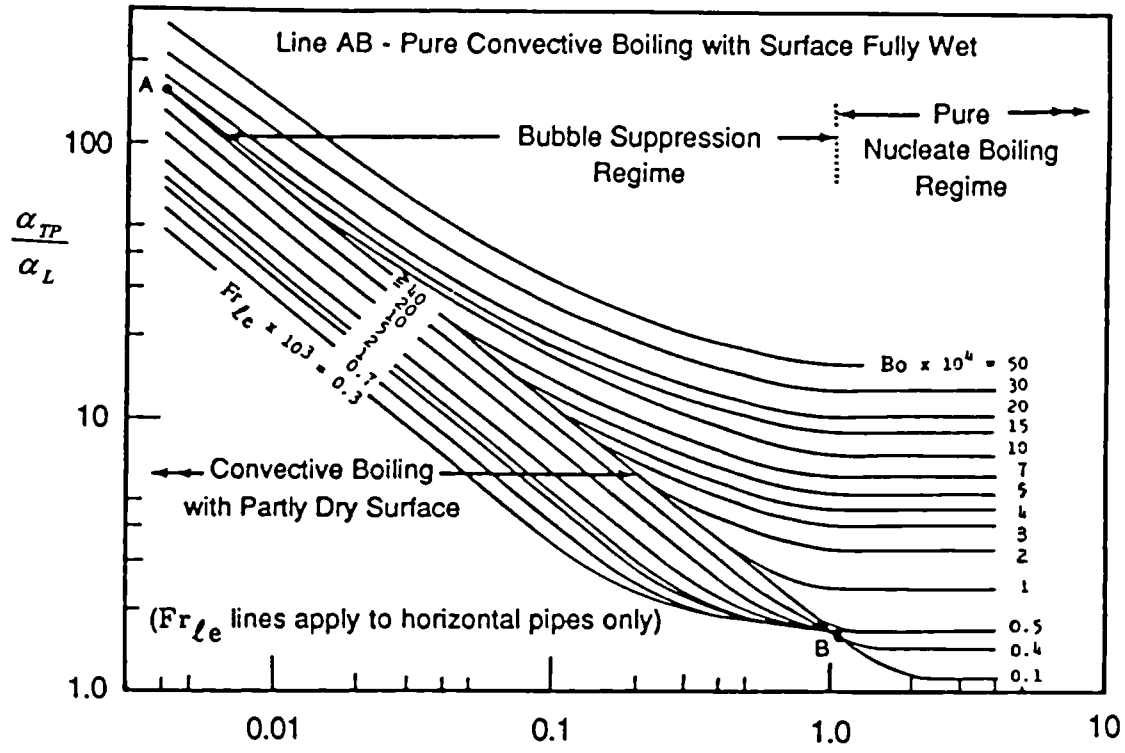

$$Co = \left(\frac{1}{x} - 1\right)^{0.8} \left(\frac{\rho_G}{\rho_L}\right)^{0.5}$$

Figure 3.6 Shah (1976) CHART graphical correlation

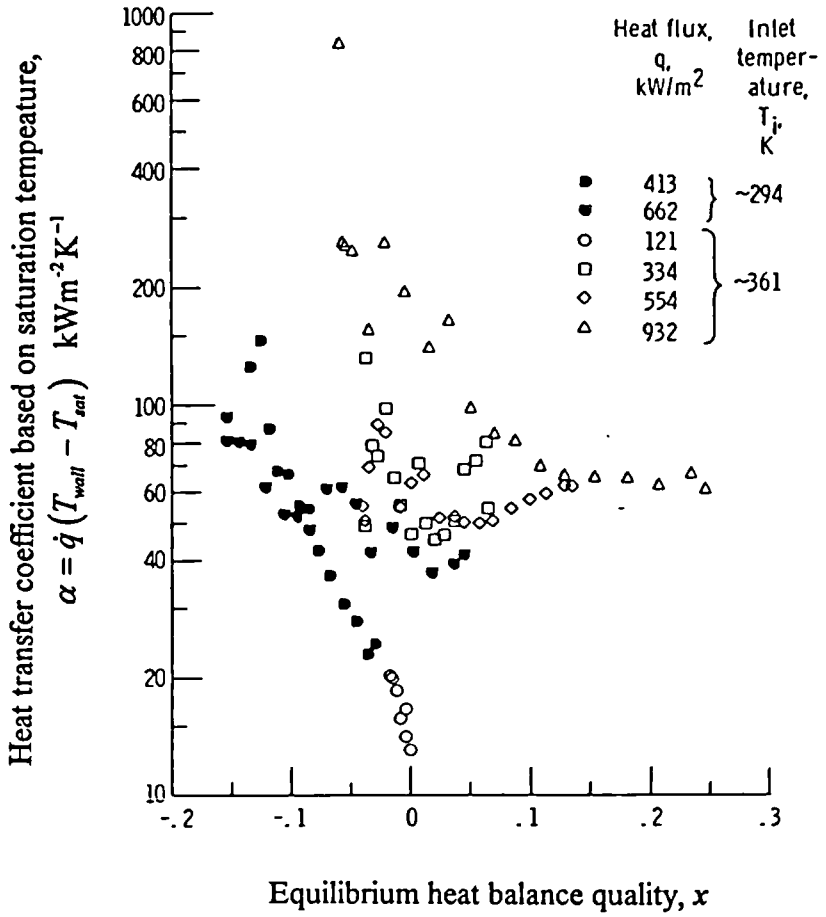

Figure 3.7 Stone's (1971) results with heat transfer coefficient *overshoot*

$\dot{m} = 5.9$ kgm^{-2}s^{-1}

$p_{exit} = 119$ *to* 146 kNm^{-2} abs

CHAPTER 4

SUB-ATMOSPHERIC PRESSURE VAPORISATION EXPERIMENTS

4.1 Introduction

The key component of this research was to design, construct, commission and operate an industrial scale sub-atmospheric evaporator (SAE) experimental rig. The core infrastructure and design of this rig, i.e. its direct-joule electrical heating facilities and data acquisition system were based and salvaged from a decommissioned United Kingdom Atomic Energy Authority (UKAEA) Harwell boiling test rig. These components were fully checked and tested before they were integrated with the new equipment and electrical components which made up the sub-atmospheric rig.

The two major features of this rig which set it apart from the other boiling facilities cited in the literature surveyed by the author are the capability of the rig to be operated at sub-atmospheric pressures, as low as 0.2 bar (20 kPa) and its industrial scale test section (approximately 4 metres in height), which makes the data and results obtained directly relevant to an actual industrial reboiler.

The SAE rig was constructed and commissioned in collaboration with Dr. P.F. Pickering and is also described in his Ph.D. thesis (Pickering, 1994). The rig had a

dual purpose, namely the observation of the onset and nature of density wave instabilities and, secondly, the generation of data for heat transfer coefficient and pressure drop in steady state flow. Dr. Pickering's work was on instabilities and the present work was concerned with steady state measurements. Hence, the rig has an added feature in its ability to be easily converted by means of re-routing the fluid flows into two different types of experiments.

The subsequent sections in this chapter will describe the design and construction of the SAE rig, the safety mechanisms installed, the general operating procedures for the forced convective experiments, the instrumentation used and their calibrations, the data acquisition programs used and finally, the experimental matrix conducted. The results and analysis of these experiments are discussed in the next chapter, Chapter 5.

4.2 Sub-atmospheric Evaporator (SAE) Rig

4.2.1 Design and construction of SAE

A full schematic diagram highlighting the key components of the dual-purpose low pressure boiling test facility incorporating both the steady state sub-atmospheric forced convective vaporisation (SAE) and the stability experiments is given in Figure 4.1 with photographs given in Figures 4.2. For the instability experiments, a header column was used which kept a constant pressure difference across the heated test section whilst allowing the test section flow rate to oscillate due to density wave instability, thus simulating a thermosyphon loop. In the present experiment, the header column was valved out of the circuit and steady flow to the test section was maintained. In the present experiments, the valves V6, V7, V8, V10 and V17 were closed thereby isolating and closing the thermosyphon loop. The operation of the thermosyphon loop was given in detail by Pickering (1994). A simplified flowsheet showing just the SAE mode of operation is given in Figure 4.3.

The SAE experimental loop can be sub-divided further into two distinct fluid flow circuits as shown in Figure 4.3. The primary circuit consists of the actual experimental test section and the electrical heating system, while the secondary circuit focuses on the pressure control of the whole SAE rig and the mains cooling water supply system to the reflux condenser. It should be noted at this point that the present configuration of the SAE rig was a revised setup of the original design which included the placement of a pre-condenser between the test section and the primary tank as shown in Figure 4.4. The pre-condenser was removed after the commissioning stage of the rig as it was found to cause large instabilities to both the pressure and flow rate readings.

In the primary circuit of the SAE rig, the test fluid, which was distilled water, was stored in the large primary tank. This primary tank was designed as a stainless steel pressure vessel with a fluid capacity of about 400 litres, although it was always filled to only 3/4 of this capacity during the running of the SAE rig. The primary tank was situated about 3 metres above the ground and had a 3/4 inch nominal bore, schedule 10, ASTM 316 grade stainless steel pipe connecting the bottom of the tank to a screw type pump. The pump was manufactured by MONOPUMPS Ltd. was driven by a 1-phase 0.37 kW electric motor and was used to pump the distilled water around the primary SAE circuit. The flow rate was measured with a Fisher and Porter Model 2000 rotameter and controlled using two ball valves before and after the rotameter. More details on the flow rate measurements will be given in a later section.

The liquid was then preheated by passing it through an electrical preheater (manufactured by ELTRON Ltd) which included two electrical cartridge heaters with a maximum power rating of 1 kW each. The preheater was operated thermostatically by pre-setting the desired water outlet temperature at the heating control panel (see Figure 4.5). The preheated liquid then flowed through the feed pipe which was welded into a short cylinder of stainless steel. This cylinder had a radial hole which was coaxial with the feed pipe, which led to another radial axial hole in the cylinder which was coaxial with the test section. Both these holes in the cylinder formed a 90 degrees bend connecting the feed pipe to the test section. This cylinder also had 4 bolt holes

drilled to match the bottom flange of the test section, thereby making it a flange as well as a bend. These flanges were grooved to house ordinary nitrile 'O'- ring seals.

The test section was manufactured from a seamless high grade ASTM 316 stainless steel tube. This particular grade of stainless steel was used throughout the construction of the SAE test section and its associated pipework because of its highly uniform material properties and also because of its high corrosion tolerance, especially to acidic solutions such as nitric acid. In other words, there is the scope for using the SAE rig for a large variety of test fluids besides distilled water and including nitric acid solutions. The wall thickness of the test section was also measured. This was done by the Non-destructive Testing Centre (NDT) at the UKAEA Harwell Research Establishment using ultrasonic instruments. The measurements were made in 4 positions around the circumference of test section for 93 axial position, every 50 mm along its length. The results from these measurements showed that the test section had a very uniform internal diameter of 22.98 mm with an average wall thickness of 1.76 ± 0.02 mm. The consistency and uniformity of the wall thickness and material properties of the test section ensured that the heat flux generated along the test section was effectively constant.

The heat flux was supplied ohmically to the test section. This was achieved by fitting large power clamps to each end of the test section. Each power clamp was fabricated from two thick copper plates (1 inch thickness) which, when bolted together, formed a cylindrical hole through which the test section passed. It was vital that good electrical contact was made between the surfaces of the test section and the power clamps, so as to avoid the occurrence of "hot spots" (i.e. high resistance zones) which could both damage the test section and distort the heat distribution. Since the power clamps had very low electrical resistance, only minute and negligible amount of heat were produced in the power clamps or in the wall of the test-section in contact with the power clamps, resulting in the majority of the conversion/dissipation of electrical energy into heat occurring in the wall of the test section between the power clamps. Hence, the actual heated length of the test section is taken to be that length between the upper and lower power clamps. The amount of AC electric current that passed

through the test section was controlled by means of two manually controlled variacs (with a coil ratio of 500 to 1, and manufactured by Brentford Transformers Ltd.) which fed a large fixed transformer from which the test section current was derived. The electrical system will provide, a maximum current of 1 kA (or a power rating of 20 kW) which approximated to a maximum heat flux of around 60 kWm^{-2}. It was necessary to insulate the test section electrically from the rest of the SAE rig. This was done by fitting a Delrin PTFE spacer between the two flanges at the bottom of the test section and a QVF glass visualisation section at the top end of the test section. Initially, whole test section was lagged with ARMAFLEX rubber insulation (manufactured by Armstrong World Industries Ltd.) to minimise heat losses as well as an added safety measure. After the commissioning phase of the rig and from heat balances performed, it was decided that the whole SAE rig should be lagged to minimise heat loss, and this was also done using the ARMAFLEX insulation.

The QVF glass visualisation section was specially chosen because of its insulating property and its high temperature tolerance, up to 400 ° C. The QVF glass is 15 cm in length and have a bore of approximately 23 mm. This QVF glass visualisation section was used extensively to provide a visual check on the flow regime leaving the heated test section.

Beyond the QVF glass visualisation section, the test fluid enters into another short cylinder of stainless steel which was similarly fashioned (as the one below and before the test section) into an upper flange as well as a 90 degrees bend, thereby diverting the path of the flow from the vertical to the horizontal direction once again. This short upper cylinder was welded to a return line, which returns the two-phase steam and water mixture leaving the test section back to the primary tank. This test fluid return line was made from 1 inch nominal bore, schedule 10, ASTM 316 stainless steel pipe. Once the two phase steam and water mixture entered the primary tank, they were separated by natural convection and the steam was condensed back into saturated water in a reflux condenser which is part of the secondary flow circuit of the SAE.

The secondary flow circuit of the SAE rig is essentially the pressure control system and the cooling water supply to the reflux condenser. The reflux condenser was connected vertically on top of the primary tank. This reflux condenser was a shell and tube heat exchanger. It was ~~made~~ custom made to specification by Johnson-Hunt Ltd. and it contained 48 straight tubes with each tube having an internal diameter of 19.25 mm and a length of 886 mm. The total heat transfer area was 2.6 m^2 and this was more than sufficient for the maximum possible steam flow rate encountered during the course of the experiments conducted. As the SAE rig was mainly operated at sub-atmospheric pressures, the reflux condenser was specially customised and manufactured in order for it to be able to cope with flooding since at these low pressures, the amount of vapour generated and its volumetric flow rate is often too large for a standard commercial condenser.

On the shell side, water from the mains water supply was used. The amount of water supplied was regulated by two KDG 2000 Rotameters.

To control the system pressure, the top header of the reflux condenser was connected to a liquid ring seal vacuum pump (manufactured by CHEMVAC Ltd.) with a 2.2 kW single-phase electric motor. By using this vacuum pump, the whole SAE rig could be evacuated to sub-atmospheric pressures. A small 'bleed' line (valve V18 in Figure 4.1) with a small orifice ball valve was introduced to this vacuum line and was used to regulate the system pressures, therefore allowing experiments to be performed at different test section exit pressures. A liquid ring seal vacuum pump was used because of its ability to withstand damage caused by entrained droplets which might enter the pump should an unintentional flooding of the reflux condenser occur.

As can be seen from above description, the whole SAE rig was built to simulate as closely as possible actual industrial scale operations. The next section will briefly focused on the safety designs and measures that were implemented on the SAE rig.

4.2.2 Safety system of the SAE rig

During the design phase of the SAE rig, a simple safety study (based on the Hazard and Operability (HAZOP) methodology) was carried out. In this study, the following possible hazards associated with the operation of the SAE rig were identified and the necessary precautions and safety measures implemented.

Electrical Hazards

The electrical power for the SAE rig comes directly from the main public electrical supply at 240 V and 50 Hz. It is then converted (through the variacs and the transformer) to lower voltages and higher currents. This power is used to directly heat the wall of the test section. The maximum voltage across the test section is 20 V and the maximum current through the test section is 1 kA. At these maximum settings, the outside of the test section may reach temperatures of around 120°C and to prevent accidental burning, the whole test section is lagged with ARMAFLEX thermal and electrical insulation. Furthermore, the test section is placed at the back of the SAE rig (see Figure 4.2) and is not easily accessible, being protected by the whole SAE rig structure.

Vacuum System

The steady state forced convective vaporisation experiments were carried out at sub-atmospheric pressures. Under these conditions, there was no danger of over-pressurisation. However, for additional safety, two safety relief valves V20 and V21, see Figure 4.1 (set to vent at 1.3 and 1.5 bar abs. respectively) were introduced as well as electrical pressure switches, which sense the system pressure at the same location as the safety relief valves. The orifice size of the safety relief valves was calculated to enable the complete discharge of the maximum possible flow rate through the flow

loop. As a precaution against rust, the components of the valves are made from brass, bronze and gunmetal. The electrical pressure switches will switch off the power to the test section and the preheater if they sense a pressure of greater than 1.3 bar abs. The whole safety system was fully tested during the commissioning stage and routinely inspected and tested.

Steam Generation

The SAE rig does not use any external steam utilities for heating but it does produce low grade steam during the course of the SAE experiments. This low grade steam was not classified as a hazard, and in any case, its pressure is fully controlled and monitored by the electrical pressure switches and safety relief valves mentioned above.

In order to ensure safe and reliable operation of the SAE rig, operating procedures covering the start up and shut down instructions as well as the actual experimental procedures were drawn up and are given in the next section.

4.2.3 Operating procedures of the SAE rig

The sub-atmospheric evaporator (SAE) rig was designed to be able to run in two modes of operation i.e. a steady state forced convective mode or a dynamic natural circulation (thermosyphon) mode. As mentioned earlier, these two modes can be easily switched by changing the positions of the various valves installed on the rig (see Figure 4.1). This thesis will only describe the steady state forced convective mode of operation; the dynamic natural circulation (thermosyphon) mode was described in detail by Pickering (1994) in his Ph.D. thesis. The next sub-section will described the experimental procedures adopted during the steady state forced convective

experiments. This was followed by another sub-section on start-up, shut-down and emergency procedures for safe and reliable running of the SAE rig.

4.2.3.1 Experimental procedures

Before running the SAE rig, part of the routine adopted is to check that the liquid level is sufficient in the primary tank (by observing the liquid level viewing tube); normally about 3/4 tank full of distilled water is desired. This is then followed by a check on all the valves and connections to ensure that the valves were in the correct position for the steady state forced convective mode of operation, as well as to ensure that there were no leaks in the circuit. For the sub-atmospheric steady state force convective vaporisation experiments, the valves V6, V7, V8, V10 and V17 (see Figure 4.1) were closed thereby isolating and closing the thermosyphon loop. After completing these inspections, the cold water used for providing the liquid ring seal for the vacuum pump was replaced with a new charge. The SAE rig was now ready to run and the start-up was commenced.

Test fluid (distilled water) from the primary tank flowed into the primary pump and was pumped around the primary flow circuit. The flow rate was measured and regulated by a rotameter and the valve V4. The valve V4, was also used to throttle the flow thereby stabilising the flow over a wider range of mass fluxes. The test fluid then passed through an electrical preheater that was used to thermostatically control the inlet liquid temperature. After the preheater, the test fluid entered the test section which was ohmically heated by passing high electrical AC current through its wall, and the heat generated was transferred into the test fluid causing it to heat up and boil. Measurements of pressure, fluid temperatures and wall temperatures at pre-designated positions were taken. The two-phase steam-water mixture then passed through the QVF glass viewing section (where the exit flow pattern was noted) before returning to the primary tank via valve V9. Inside the primary tank, the steam and water were separated. The steam passed into the reflux condenser and was condensed. The

condensate then flowed down back into the primary tank. The exit pressure of the test section was controlled by using the 'bleed' valve, V18 which permitted air to be bled into the system at a constant rate, thereby fixing the exit pressure of the test section. This continuous evacuation of the SAE rig was made possible by the aid of a liquid ring seal vacuum pump, described in the previous section.

After starting up the SAE rig, the test fluid was heated up by operating the rig at atmospheric conditions until it reached the desired temperature. When the desired inlet temperature was obtained, the experimental parameters relevant for that day's runs were set up (i.e. setting the correct exit pressure, heat and mass fluxes) and the rig was then left to settle down and reach steady state. During this period, continuous scans of experimental measurements were made and monitored. Only when, after 5 successive scans, were the changes in the temperature readings (both fluid and wall temperatures), the mass flow rate and pressure readings minimal, was the decisive set of experimental measurements logged as an experimental data run. Even then, the scanning would continue for at least 2 more scans, to ensure data reliability before altering the experimental parameters for the next set of conditions. Some of these experimental conditions (in Section 4.4) were repeated by raising and decreasing the heat fluxes and conducted on different days as a check for both hysteresis and data reproducibility. It was found that there was no hysteresis and the experimental runs were reproducible. The results from these experiments will be discussed in detail in Chapter 5.

The measurements made in the experiments were the axial fluid temperature (measured in the centre-line of the test section), outside wall temperature and pressure distributions along the length of the test section. The measurements made were used to provide information about the hydrodynamic behaviour (pressure drop) of the flow and the local heat transfer coefficient distribution and variation along the test section.

Upon completion of experiments for a particular day, the SAE rig was then systematically shut-down following the procedures drawn up in the next sub-section.

4.2.3.2 Start-up and shut-down procedures

The following start-up, shut-down and emergency procedures for the safe and reliable operation of the SAE rig were drawn up as part of the safety requirements for SAE boiling facility at Imperial College. The final version (see also Pickering (1994)) was drawn up after the installation and commissioning phase of the dynamic natural circulation (thermosyphon) loop facility was added to the original steady state forced convective loop. The procedures used are listed below and are **valid only** for the current configuration of the SAE rig. Future researchers using the same facility should draw up their own procedures bearing in mind the addition/subtraction of the safety facilities and process equipment.

SAE rig Start-up Procedures

(1) Switch on the power to the rig at the mains electricity riser.

(2) Turn on the cooling water to the reflux condenser.

(3) Open valves V1, V2, V3, V4, V5, V9 and V18.

(4) Close valves V6, V7, V8, V10 and V17.

(5) Start the primary liquid pump.

(6) Close V2 and adjust V4 so as to have a high flow rate of liquid through the test-section.

(7) Switch on the electrical preheater and the power to the test-section.

(8) When the desired system temperature is reached, switch on the vacuum pump and close valve V18 until the desired system pressure is attained.

(9) Set the power to the test-section and the flow rate to the values required for the experiment and allow the system to come to a steady state.

SAE rig Shut-down Procedures

(1) Switch off the power to the test-section and the electrical preheater.

(2) Open valve V18 to re-pressurise the rig.

(3) Switch off the vacuum pump.

(4) Increase the flow rate to the test-section by opening valve V4. Run with an increased flow rate for approximately 1 minute (during actual steady state forced convective experiments, at least 10 minutes were allowed) to cool the test-section wall.

(5) Open valves V2, V4, V6, V7, V8, V10 and V17.

(6) Switch off the primary liquid pump.

(7) Turn off the cooling water to the reflux condenser.

(8) Isolate the SAE rig from the mains electricity supply at the riser.

In case of *emergency*, there were 2 emergency buttons that immediately switch off all the power to the SAE rig when pressed. They were located on the SAE rig and on the control panel. After the emergency shut-down of power, the subsequent procedures are identical to those for the normal shut-down (step 5 onwards), and only when these were completed should any inspections and analysis of the emergency be carried out.

4.3 Instrumentation and measurement techniques

This section will discuss ~~about~~ the instrumentation and measurement techniques used during the course of the steady state forced convective experiments.

4.3.1 Power measurements

The amount of electrical power dissipated in the test section during the steady state forced convective experiments was measured using an AC Watt-meter (manufactured by H.W. Sullivan). The total power was determined by measurements of the current and potential difference across the test section. The AC current was measured using a 500 to 1 inductance coil whilst the potential difference was measured from copper wires connected to the copper power clamps at both ends of the test section. The watt-meter had been calibrated at the UKAEA Research Establishment at Harwell. Since the power measurements were read off from the watt-meter visually, care was taken to avoid any parallax misreading, therefore, the readings can be read to an accuracy of ±1 W. This reading is then scaled up by a factor of 125 (calculated from the watt-meter scale factor and inductance coil) and then divided by the total surface area of the test section to give the heat flux. The following table 4.1 relates the power readings from the watt-meter to its associated heat flux values in kWm^{-2}.

Watt-meter Power Reading (W)	Heat Flux to the test section (kWm^{-2})
26	10
52	20
78	30
104	40
130	50

Table 4.1 Watt-meter power readings (W) to heat flux (kWm^{-2})

4.3.2 Temperature measurements

The temperatures measured for the steady state forced convective experiments were those of the outside surface wall temperatures and the bulk test fluid temperatures along the axial length of the test section.

The bulk test fluid temperatures were measured by using 9 minerally insulated stainless steel sheathed Nickel-Chromium/Nickel-Aluminium (K-type) thermocouples at prescribed intervals along the test section, as shown in Figure 4.6. These thermocouples were 1.5 mm in diameter and 100 mm in length with endings with standard miniature male plugs. The fluid temperature thermocouples were passed through holes (attached with stainless steel "union" fittings) in the test section wall so as to bring their tips to the centre of the tube. The thermocouples were then sealed to the tube wall by tightening the fittings.

For the outside surface wall temperatures, they were measured using 62 welded-tip PTFE-insulated exposed junction K-type thermocouples. These thermocouples were 0.6 mm in diameter and 1 m in length, ending again with standard miniature male plugs. The method of mounting needed to ensure good thermal contact and full electrical insulation at the test section wall. A few options were available from published literature, e.g. see Hewitt (1978) and the final method of mounting adopted was shown in Figure 4.7.

The mounting method adopted used an unfractured anodised aluminium strip (about 0.5 mm thick) sandwiched between two layers of thermal conducting paste (heat sink compound RS 554-311)). The exposed thermocouple tip was then embedded into one of the thermal conducting paste layers and the whole setup was thoroughly wrapped with polyimide (Kapton™ film) tape. Anodised aluminium strips were used because they provided excellent thermal conduction but more importantly, they were good electrical insulators. However, this electrical insulating property was only effective if the surface was not *cracked* or *fractured.* This is because a fractured surface will

enable electrical contact between the thermocouple and the test section, and since a high voltage (relative to the EMF induced by the temperature difference, e.g. a typical voltage applied across the test section was of the order 5-20 V while the EMF generated by the temperature difference sensed by the thermocouples were of the order 2-4 mV) was applied across the test section, this would vitiate the readings of the thermocouples. Prior to utilising this particular method of mounting, a short and simple experimental trial was conducted to test its effectiveness.

In this short experimental test, as shown in Figure 4.8, a copper plate of comparable thickness (1.5 mm) to the test section (1.76 mm) was used. Bolted onto this copper plate were two power resistors (Arco/87.04 HS50/22R ± 5% Ω), which were used to heat the plate. Two identical thermocouples were mounted on either side of the plate. On one side, the thermocouple was soldered directly onto the plate to provide intimate contact while, on the other side, the other thermocouple was mounted and taped as it would have been done so for the actual test section. The two thermocouples were then connected to a switchbox which in turn was connected to a Keithley digital multimeter. This test showed that the EMF (potential difference) registered by both these thermocouples were identical. Therefore, one could conclude that the measurement from a thermocouple mounted in this fashion is identical to one that was directly soldered, with the added benefit that the anodised aluminium strip (surface unfractured) provided a highly cost-effective electrically insulation.

Although the outside surface wall temperature was measured, it is the difference in temperature between the **inside surface wall** and the boiling fluid temperatures that is of use in the heat transfer coefficient calculations and analysis. Therefore, it is necessary to calculate the temperature difference across the test section wall. The equation need to estimate this wall temperature difference is given in Appendix A and is as follows:

$$T_{wi} = T_{wo} + \left\{ \frac{-\dot{q}_i r_i}{\lambda} \left[\frac{1}{2} - \frac{r_o^2}{\left(r_o^2 - r_i^2\right)} \ln\left(\frac{r_o}{r_i}\right) \right] \right\} \qquad (4.1)$$

where T_{wi} is the ~~inlet~~ inside wall temperature, T_{wo} is the ~~outlet~~ outside wall temperature, $\dot{q}_i$ is the heat flux based on the inner surface area, λ is the thermal conductivity of the test section wall, r_i is the inner wall radius of the test section and r_o is the outside wall radius of the test section.

During the course of the experiments, some of the thermocouples were found to have lost their electrical isolation and consequently were not taken into account in the analysis. The thermocouple performance before and after the experiments was checked by ensuring that for an unheated flow system, they gave similar EMF's. Since there was a large number (71) of thermocouples involved, a suitable reference junction was needed which could be used for all the thermocouples simultaneously and the idea of using an *isothermal box* was mooted and applied. The use and construction of the isothermal box will be presented in the next sub-section.

4.3.2.1 Isothermal box (Reference Junction)

It must be appreciated that a thermocouple does not measure the temperature at the measuring point (junction), but it is a differential measurement between the measuring junction and reference junction. It follows then that for any form of accurate temperature measurement, the reference junction must either be held at a fixed known temperature (such as an ice-point) or accurate compensation be used for any temperature variations of the junction.

For the steady state forced convective experiments, it had been decided on the grounds of the number of thermocouples involved and the difficulty in using the fixed reference junction (ice-point) due to the non-availability of a regular supply of ice and an ice-crusher, the compensation method was chosen instead in the form of an **isothermal box**.

In such a box, the all thermocouple reference junctions were connected to 4 electrical terminal blocks which were bolted down to an aluminium block (since aluminium is an excellent conductor). The blocks were then heavily thermally insulated from the environment using polystyrene sheets and enclosed in an electrical steel wall box. These reference junctions were then allowed to follow the mean ambient temperature inside the box, which varied very slowly. This variation of temperature was accurately sensed and measured by a highly sensitive and accurate Platinum probe which was taped onto the aluminium block among the reference junctions' terminal blocks. The signal was then relayed to a Keithley multimeter (Model 195A Digital Multimeter, manufactured by Keithley Instruments Inc.) where the voltage was converted to temperature readings (accurate to ±0.001 °C) based on the polynomial fit conforming to the DIN 43760 standard.

4.3.2.2 Thermocouple calibrations

The whole temperature measurement system (i.e. thermocouples, compensating cables and leads, data logging computer and software) was calibrated using a constant temperature hot water bath (as heat source for the hot junction) and the prepared isothermal box (reference junction). For an accurate and sensitive independent reference temperature measurement of the hot water bath, a Platinum probe connected to a Fluke Multimeter (tested and accurate to ± 0.001 °C, and was calibrated by the Electronics Section of the Chemical Engineering Department) was used. A schematic block diagram of the calibration arrangement is given in Figure 4.9.

The EMF for each thermocouple at different temperature settings were logged and plotted. The temperature settings were staggered by first raising the temperature settings (i.e. measurements at 10, 30, 50, 70 and 90°C) and then followed by a gradual decrease (i.e. measurements at 80, 60, 40 and 20°C). This procedure was followed to detect any possible hysteresis in the data-logging system; which fortunately, there wasn't any. Each plot for each thermocouple was then curve-fitted using linear

regression and an almost perfect linear regression (R^2 value $\cong$ 1) was obtained for each of the thermocouples, confirming the linear response expected of the K-type thermocouples. The values obtained were also compared with those of the polynomial fit from BS 4937 : Part 4 : 1973 and were found to be in excellent agreement (within ± 0.05 °C). The results of the thermocouple calibrations and the location of each thermocouple relative to the first point of measurement are given in Appendix B.

4.3.3 Pressure drop and flow rate measurements

Pressure measurements

The pressure along the length of the test section were measured using pressure transducers that were designed for measuring absolute pressures. These pressure transducers were supplied by Maywood Instruments Ltd (Micro Gage Type P102). These transducers were also designed to withstand pressure cycling with a low static error band (i.e. high stability) and have in-built passive thermal compensation rendering the transducers immuned to thermal gradients. Each of these transducers was connected to a digital indicator (Series D-2000), also supplied by Maywood Instruments Ltd. The pressure transducers and their respective digital indicators had been calibrated and certified in the range of 100-1000 mbar by Maywood Instruments Ltd. These calibrations were checked at atmospheric pressure against that of a highly accurate mercury barometer and ~~was~~ were found to be in good agreement by Pickering (1994). It was found that the transducers' response was very repeatable and linear with an estimated accuracy of ± 3 mbar. The calibrations were checked *in situ* before and after each set of runs based on hydrostatic head calculations and vacuum checks for calibration drifts, where with no fluid flow, all the transducers will show the same readings. Fortunately, no drifts were detected due to the high stability of the transducers used.

The transducers were connected to the test section via pressure tappings at 6 locations (see Figure 4.6 and Table 4.2). The whole arrangement is shown schematically in Figure 4.10. As can be seen from Figure 4.10, the pressure tapping lines were filled with distilled water (by sucking in the water from a reservoir controlled using a 'flip' valve by slightly depressurising the test section) before each experiment, so as to *flush out* any trapped air bubbles in the lines that may interfere with the accuracy of the pressure readings. During the commissioning phase of the SAE rig, pressure transducer No. 4 failed and was promptly replaced with a new replacement transducer and digital indicator (with its associated calibration) for the subsequent experimental series.

Pressure Transducer No:	Position relative to the first point of measurement (m)
1	0.0
2	0.34
3	1.09
4	2.09
5	3.09
6	4.09

Table 4.2 Pressure transducer measurement positions

Flow rate measurements

The flow rate was measured with a Fisher and Porter Model 2000 rotameter (with a stainless steel float metric type S, size 24 and a metric series tube, size 24) and controlled using two ball valves before and after the rotameter. The rotameter was calibrated by measuring the time taken to collect 20 kg ± 50 gm of water at each rotameter graduation and the values obtained were in agreement with those provided by the manufacturer's calibration chart. The minimum and maximum stable flow rates obtainable from this rotameter were 0.018 and 0.16 kg/s respectively.

During the course of the earlier experiments, there was a small but regular flow oscillations (less than ± 10% of desired setting) was observed. Although the magnitude involved was small, the flow oscillations were further damped by using more inlet throttling until a state of nominal steady state can be said to have been achieved.

4.3.4 Flow regime observation

The flow regime of the stream leaving the test section was observed in the QVF glass visualisation section immediately after the exit of the test section. Though this visualisation is obviously limited, it had proved to be invaluable in the sense that it allowed monitoring of the progress of the flow during the experiments as well as the determination of the exit flow regime.

4.3.5 Data acquisition system

In order to provide a consistent, regular and less tedious method of measurement recordings, a data acquisition system was set up. In the initial data acquisition system, both the pressure and temperature measurements were data logged, but at later stages, the pressure measurements were brought off-line because there was a small oscillation in the readings (about ±10 mbar maximum). This meant that the mean pressures were difficult to assess using the low-speed data logger used in the present experiments. It was decided that it would be more accurate to note down the maximum and minimum values of the oscillation and then to average them. The accuracy of this procedure was verified by recording the pressures on a small test using the high speed data logger used for the thermosyphon experiments (see Pickering, 1994). For the temperature measurements, there ~~was~~ were no oscillations but a small drift upwards of around 0.2 °C were recorded approximately every 5 minutes (i.e. 5 scans on the data logger). This

was to be expected as the fluid was continually heated up as it flowed round the SAE rig.

The key components of the data acquisition system were an IEEE 488 data acquisition card (fitted inside an IBM PC) which was connected to a Datron Model 1051 Multi-function Multimeter. The multimeter was fed with input signals gathered from the EMF generated by the temperature difference between the thermocouples and the reference junction (isothermal box). These signals were gathered by a Datron Model 1200 Signal Scanner and a Model 1210 Extension Scanner. It took approximately 1 second for each channel (thermocouple) to be scanned and the total time for a complete scan through all the channels was about 1.5 minutes.

A controlling software (program) called PROGRAM ACQUIRE was written in **BASIC A** to coordinate all the switching from one channel to the next and also to set/trigger the automatic sequence of operations between the scanners, multimeter and data acquisition card. The results of each scan were displayed on the IBM PC screen and upon completion of a whole cycle, it prompted the experimenter to either save the scans in a data file or to discard them and start on a new scan cycle. The saved data files (in ASCII format) were then converted to more functional and meaningful data/results in analysis programs written by the author. All the final analysis were performed on spreadsheets and this is the final format of all the saved data. The results and conclusions from these analyses will be discussed in the next chapter.

The final section for this experimental chapter will focus on the experimental matrix used.

4.4 Experimental matrix

Two major sets of experiments were performed, i.e. for annular flow regimes and sub-annular flow regimes at the test section outlet respectively. The calculations performed to determine the operating conditions that would cause annular flow to occur near the exit of the test section are given in Appendix D. The main focus of the work reported in this thesis is for the annular flow outlet conditions. The remainder of this section highlights the range of operating conditions that were used for both sets of experiments.

Range of mass flux

For annular flow : 50.17 and 62.3 $kgm^{-2}s^{-1}$

For sub-annular flow: 150, 200, 250,300 and 350 $kgm^{-2}s^{-1}$

Range of heat flux

For annular flow : 40 and 50 kWm^{-2}

For sub-annular flow: 10, 20, 30,40 and 50 kWm^{-2}

Range of outlet pressure

For annular flow : 250, 500 and 1000 mbar abs.

For sub-annular flow : 250, 300, 400, 500,750 and 1000 mbar abs.

Range of inlet subcooling

For annular flow : $\approx$ 15 °C and $\approx$ 40 °C

For sub-annular flow : from 20°C to 70°C.

Altogether 226 experimental runs were conducted, of which the first 200 of them were in the sub-annular flow regimes whilst the final 26 runs were in the churn to annular flow regime. It is these final 26 experimental runs that will be analysed and scrutinised in detail for they represent more closely the type of flow conditions that one would normally expects in an industrial sub-atmospheric vertical evaporator system. The initial 200 sub-annular runs are more appropriately classified and regarded as *extended* commissioning runs for the SAE rig and the fine-tuning of the operational procedures and instrumentation. Furthermore, to verify some of the results obtained, a further 16 selected repeat runs were conducted and repeatability had been established.

A listing of the final 26 experimental runs performed, together with the 16 repeat runs are given in Appendix E showing the key flow parameters. A detailed account of the analysis and conclusions from these experimental runs is presented in the next chapter.

Figure 4.1 Complete Final Flowsheet of Sub-atmospheric Evaporator (SAE) Rig

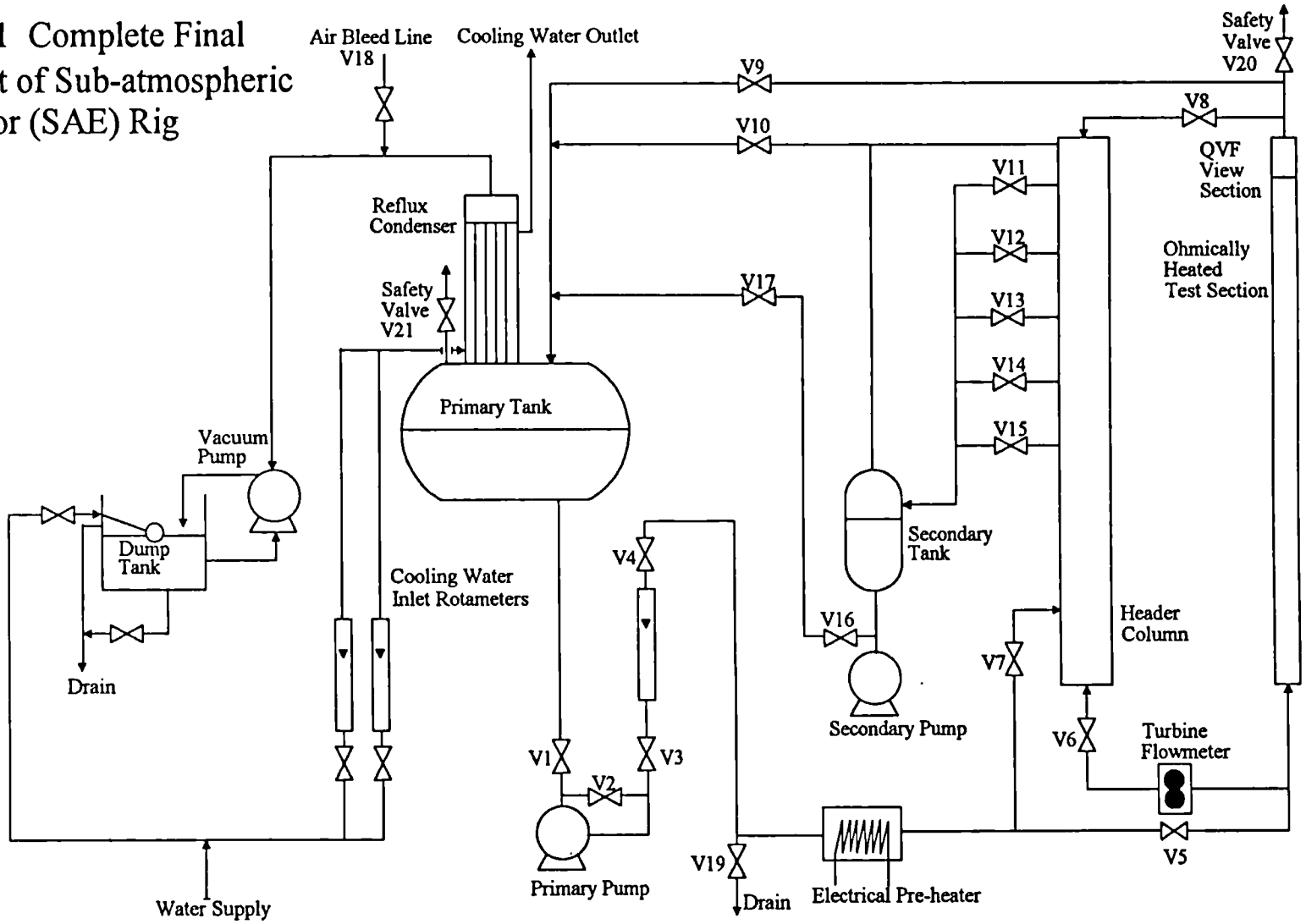

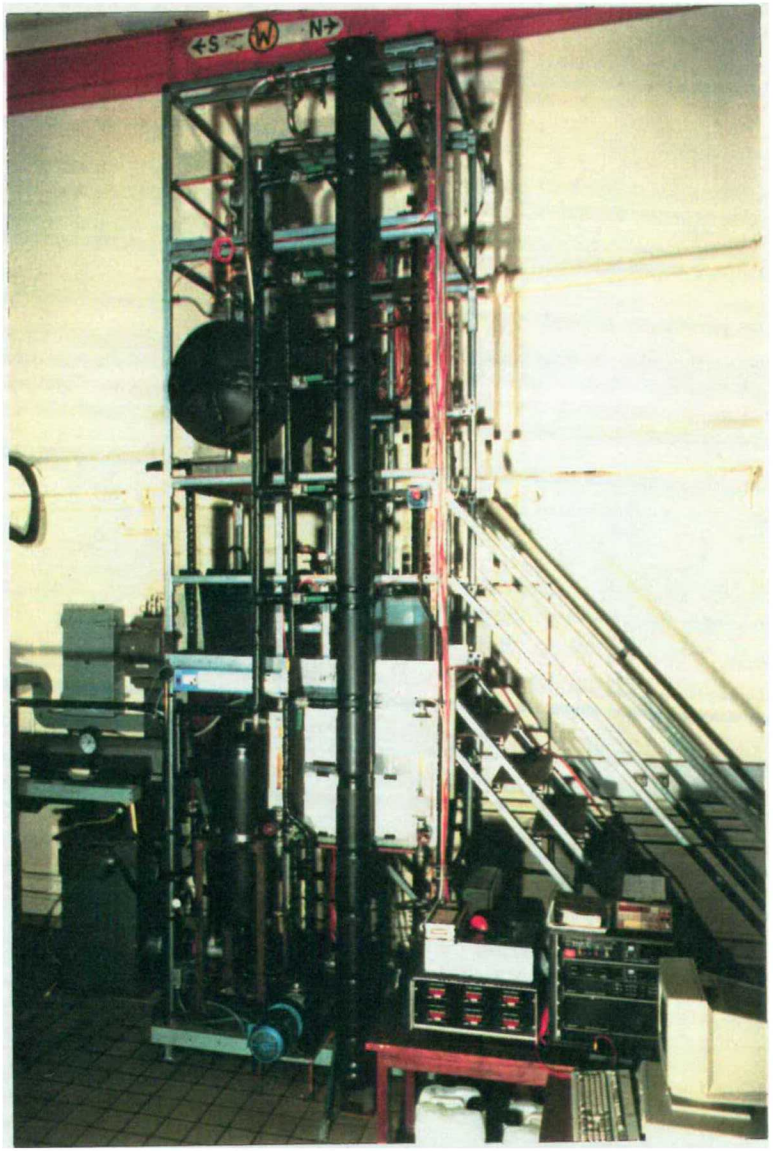

Figure 4.2a Photograph of SAE rig (front view)

4.2b (side view)

Figure 4.3 Simplified Final flowsheet of SAE Rig Highlighting the Forced Convective Mode

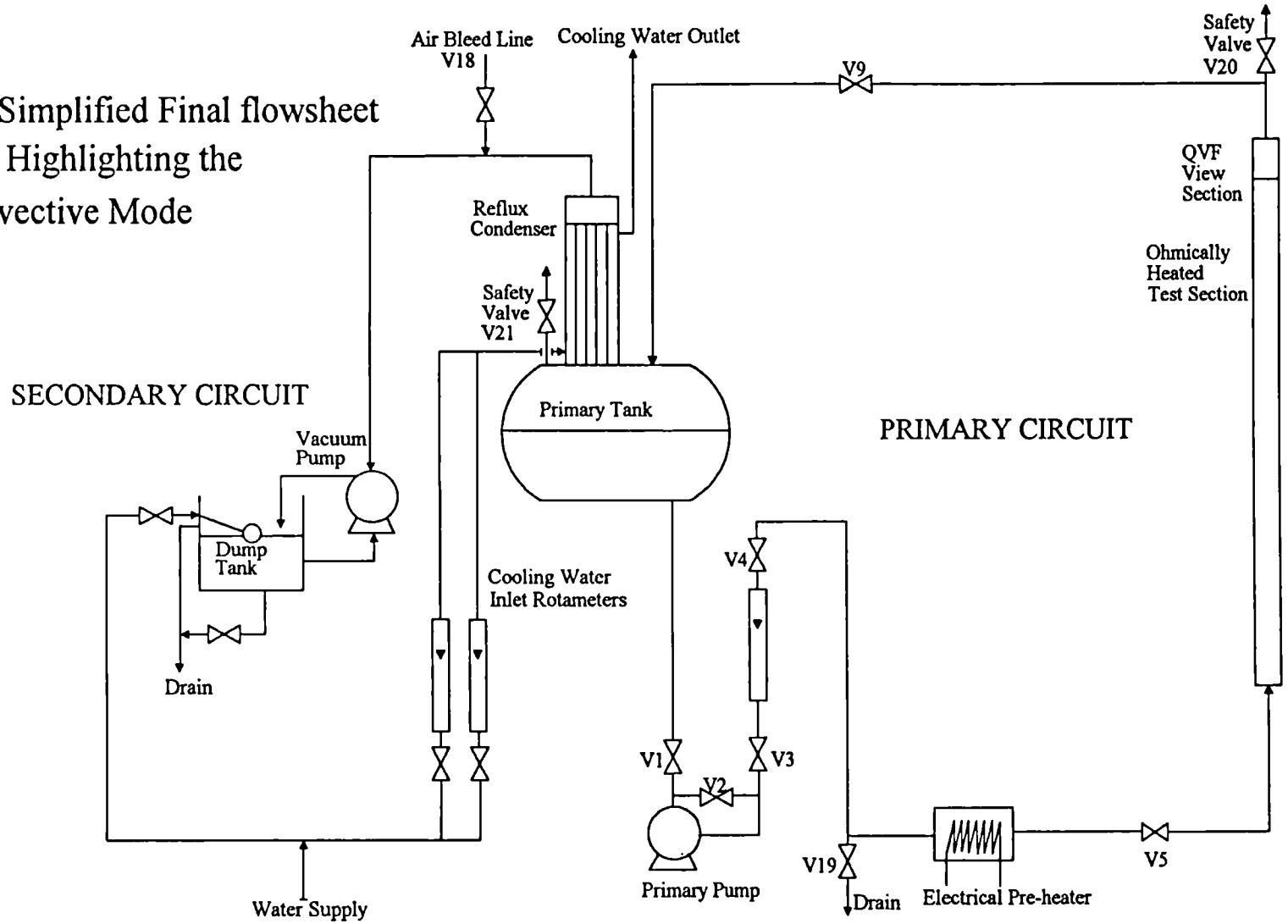

Figure 4.4 Original flowsheet of SAE Rig Highlighting the Forced Convective Mode with Precondenser (until June 1992)

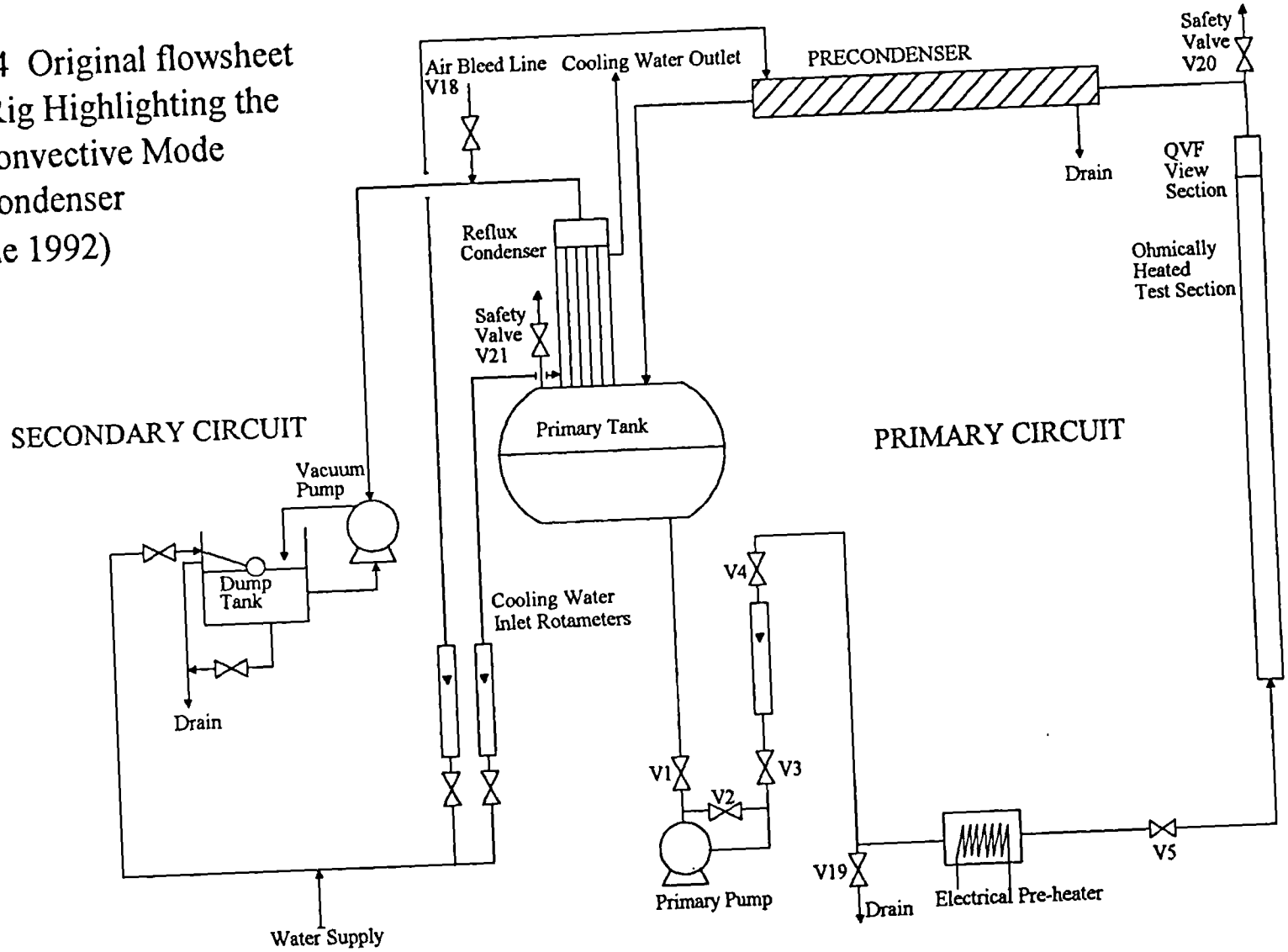

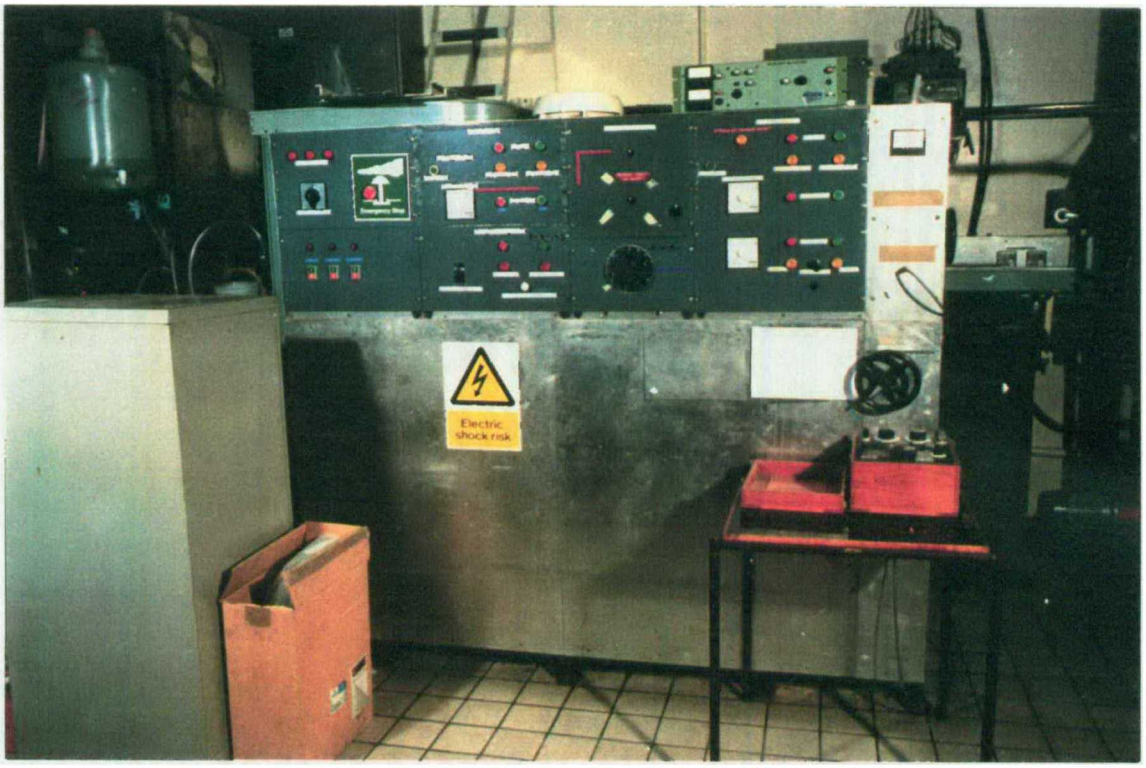

Figure 4.5a Heating control panel

Figure 4.5b Data acquisition system

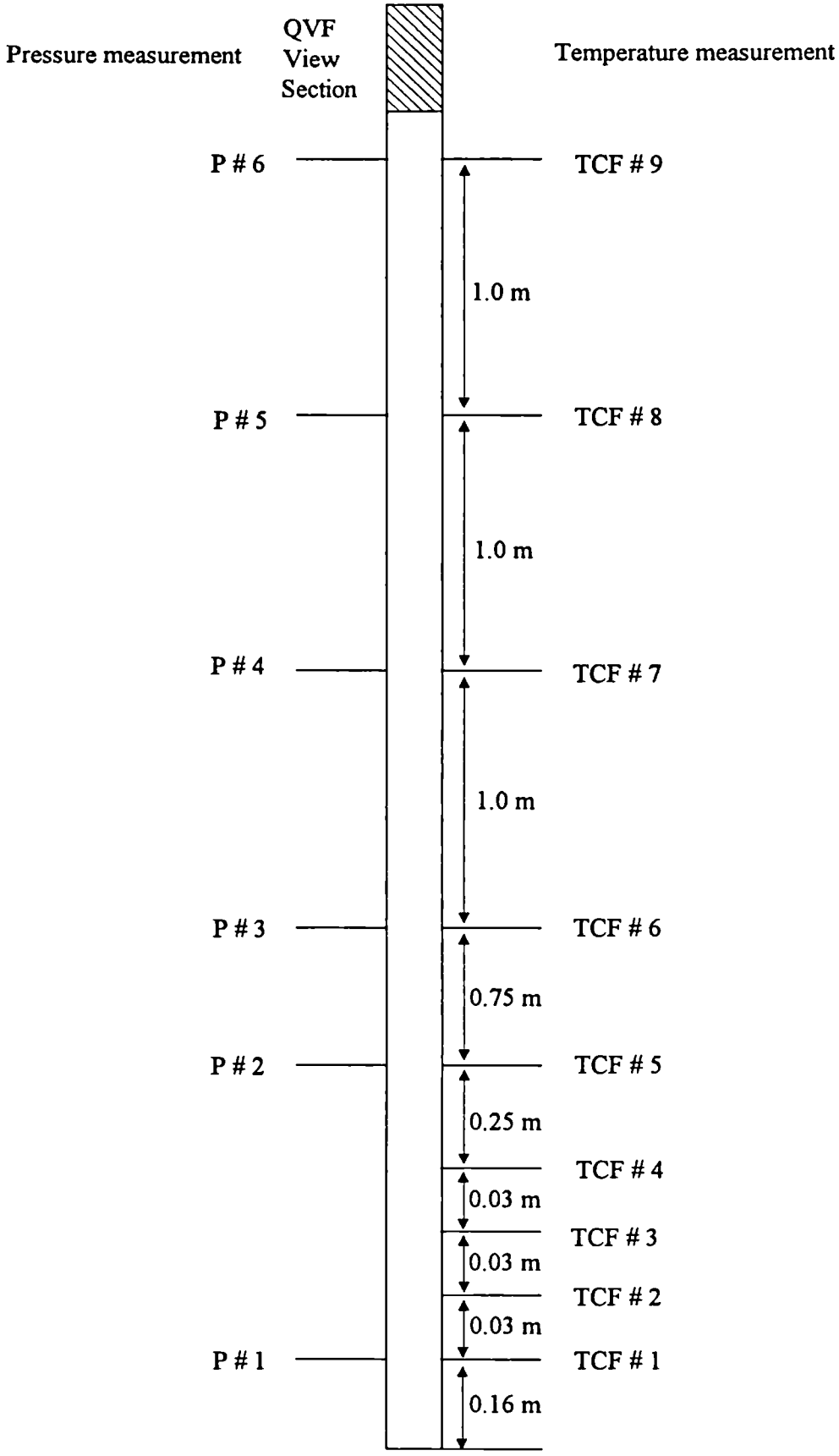

Figure 4.6 Position of fluid temperature and pressure measurement points on the test section.

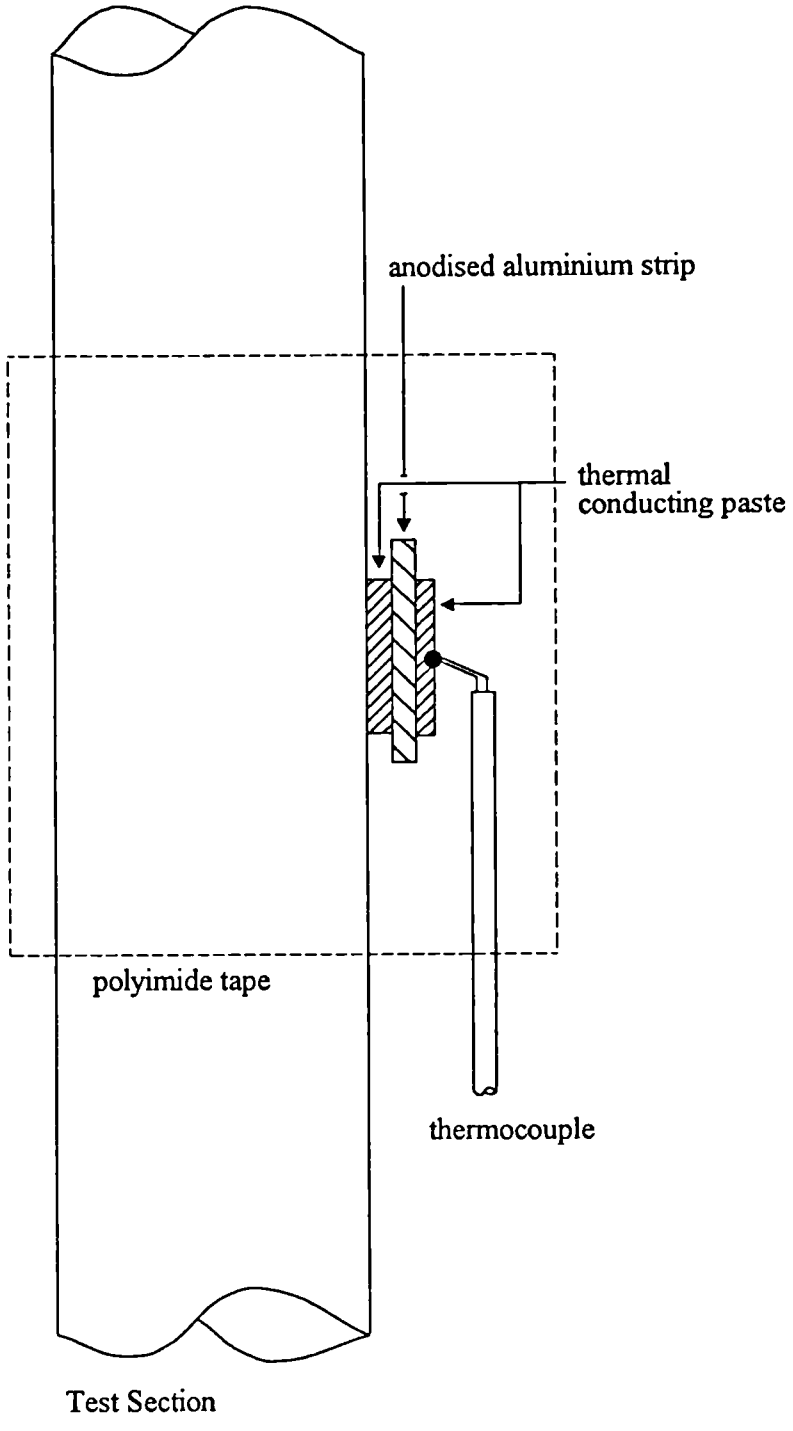

Figure 4.7 Wall temperature measurement setup.

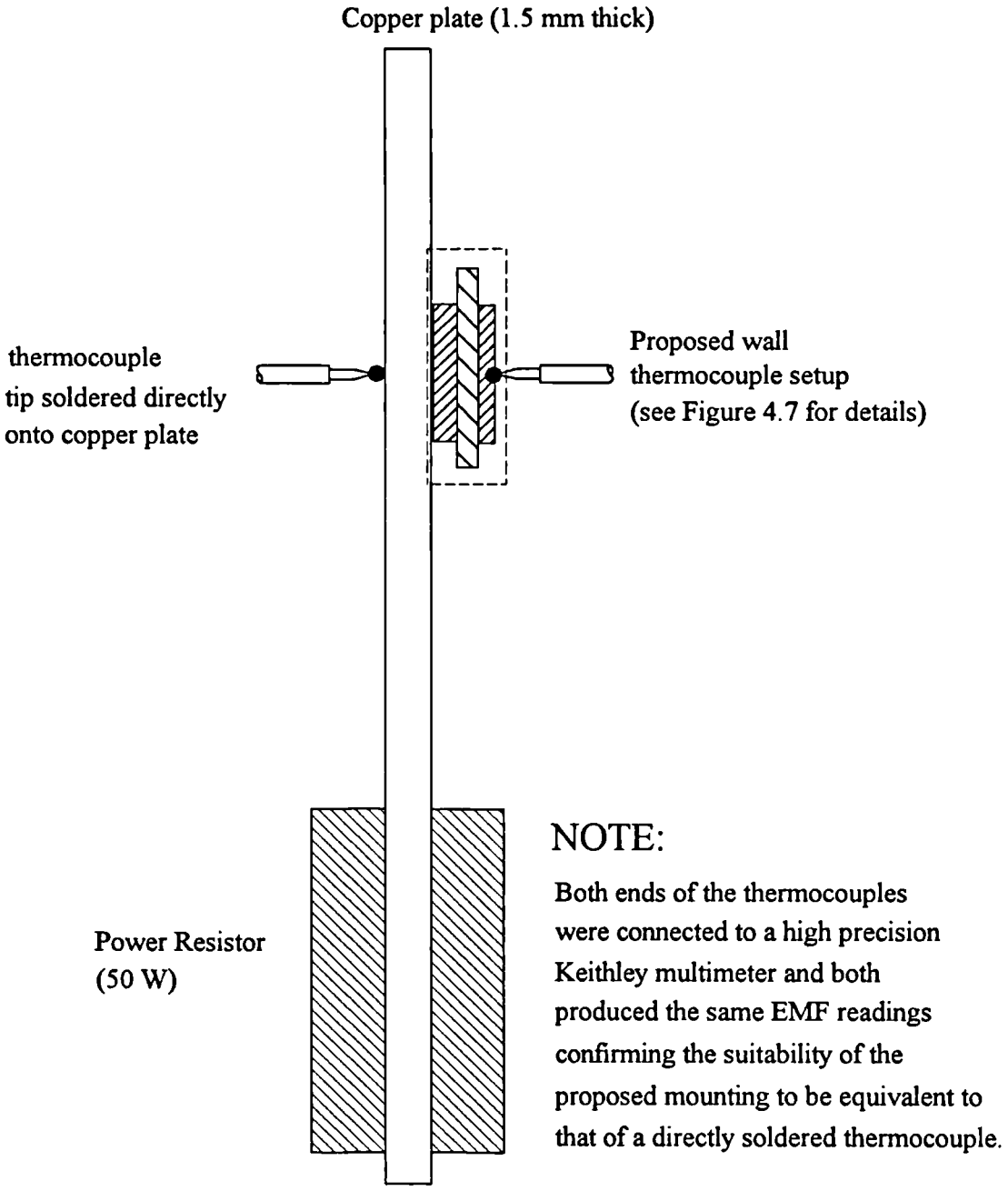

Figure 4.8 Wall temperature measurement test setup.

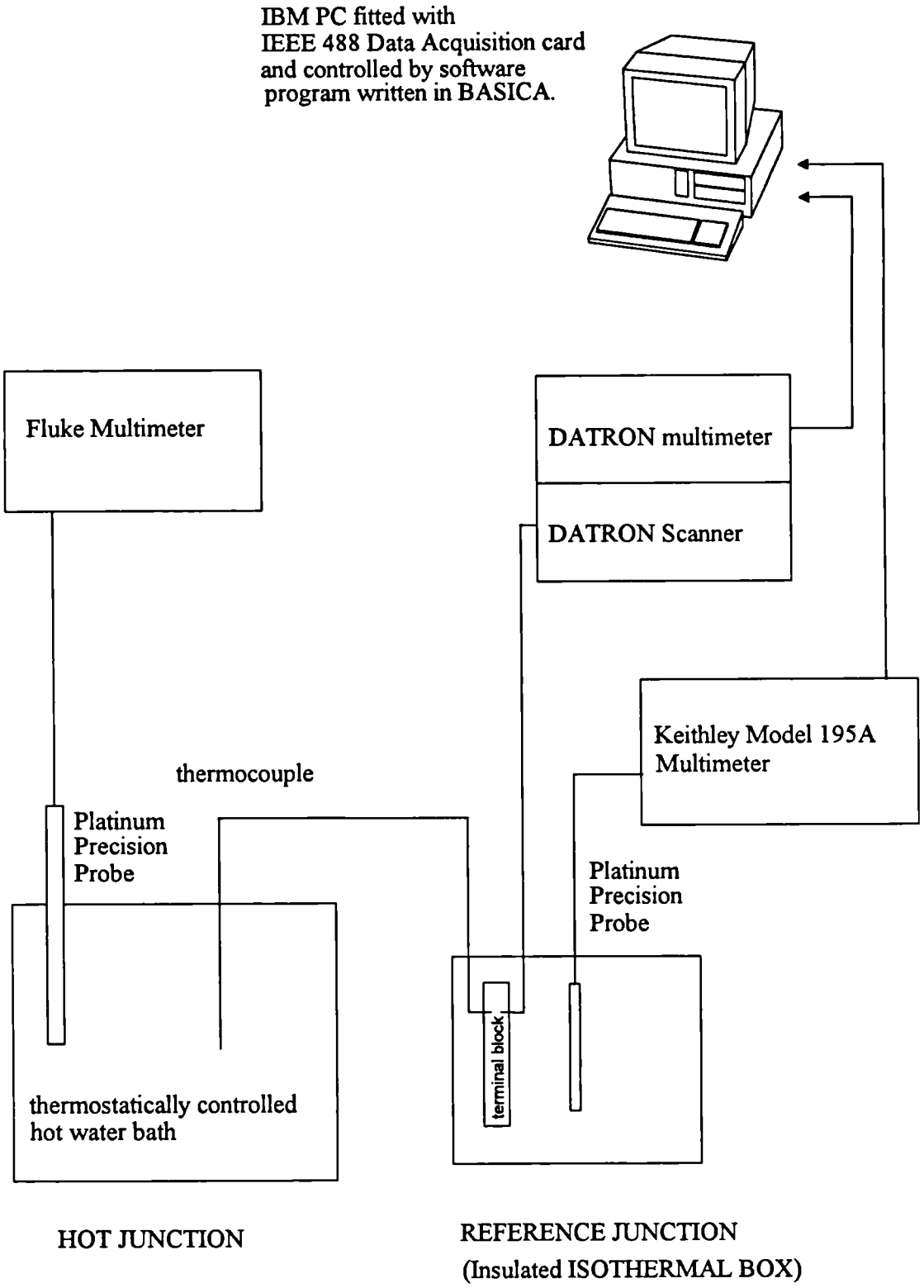

Figure 4.9 Thermocouple calibration block diagram.

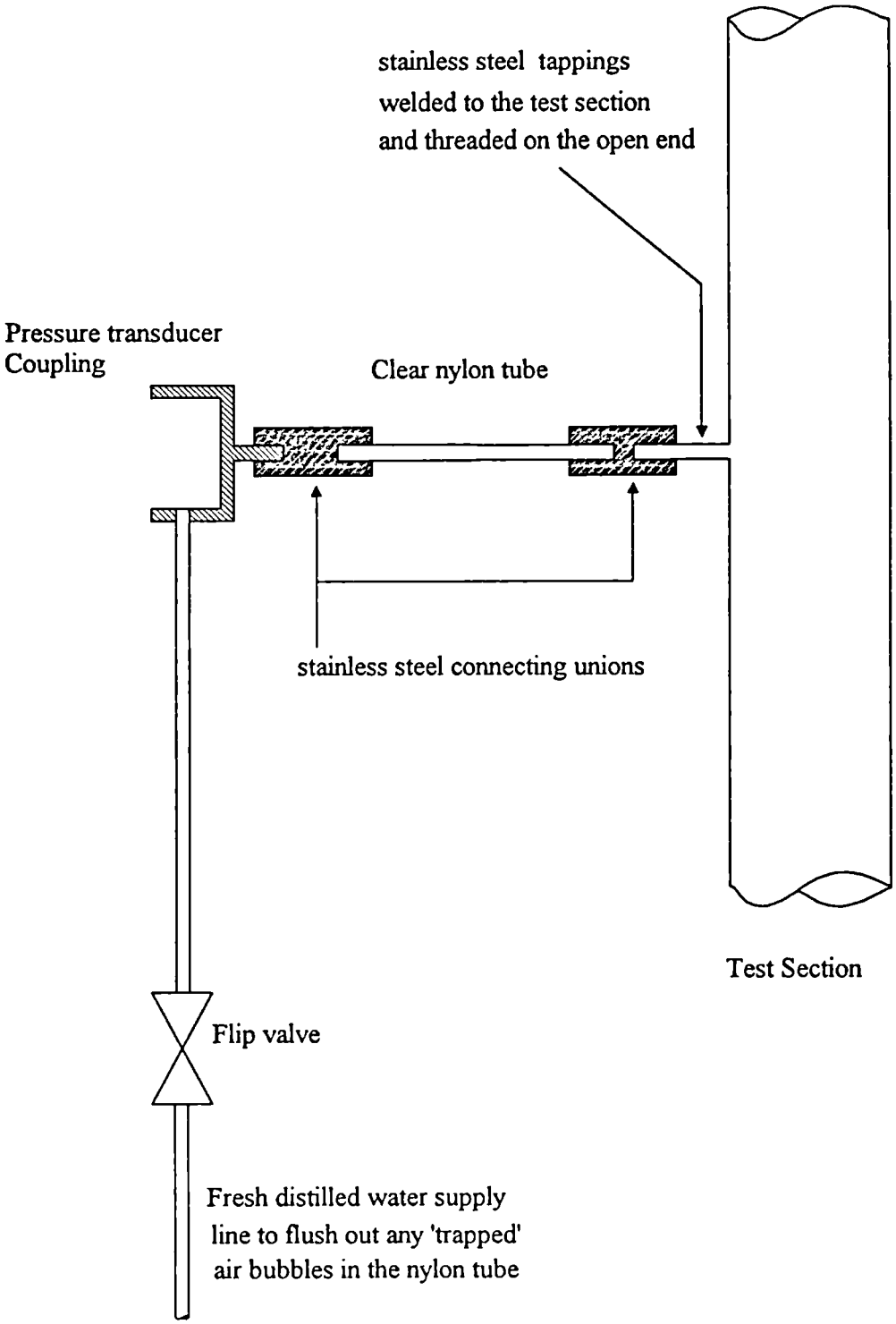

Figure 4.10 Typical pressure transducer setup.

CHAPTER 5

EXPERIMENTAL RESULTS AND ANALYSES

5.1 Introduction

After the successful commissioning of the SAE rig and the finalisation of the operational and experimental procedures, two series of experimental runs were conducted. The first series of 26 runs formed the main experimental database while a second series of 16 selected repeat runs were performed in order to establish the repeatability of the trends observed in the main experimental database.

The following sections will discuss the pressure drop and heat transfer results and the effects on them of the key flow parameters; namely mass flux, heat flux, outlet pressure and inlet subcooling.

5.2 Pressure drop results

Small pressure oscillations were observed (about ±10 mbar, excluding the estimated accuracy of ±3 mbar) during the course of the experiments. This represents a total fluctuation of pressure measurements of around ±2.95 % in relation to the average

outlet pressure of 441.357 mbar abs. over the whole experimental database (see Appendix C for full error analysis and estimation). The pressure measurements were made visually by averaging between the maximum and minimum values of the oscillation without any additional loss in accuracy when compared to the case where the pressure readings were recorded at high frequency as explained in the previous chapter. In order to ensure that the measurements collected were relatively steady, the pressure were monitored both before and after the actual data set as outlined in the experimental procedure section of the previous chapter.

Figures 5.1 showed some typical pressure measurements from the experimental runs at 250, 500 and 1000 mbar abs outlet pressure. One of the intriguing feature of the pressure readings was the manner in which pressure fell in a linear manner with quality (or distance, since, at constant heat flux, the quality varies linearly with distance), implying an almost constant pressure gradient. From these observations, one can conclude that the *sum* of the individual pressure drop components, namely frictional, gravitational and accelerational pressure drops was approximately constant along the channel with the frictional pressure gradient increasing to compensate for a reduction in the gravitational component.

As it was not possible to experimentally measure each of these individual pressure drop components in the current SAE rig configuration, a calculated pressure drop profile based on the present author's modelling computer code is given in Figure 5.2 to illustrate this point. It should be noted that the modelling code is able to predict all the overall experimental pressure drops to within a mean deviation of 20.64%. However, as can be seen in Figure 5.2, although the overall pressure drop shows good agreement, the *predicted profile* is not closely matched. When analysing the three components of pressure drop obtained from the model, a rapid drop in the gravitational component was calculated where the flow changes from single to two-phase flow but this was not seen experimentally. The possibility of a pressure reading error was ruled out on the basis of the transducers' high stability.

Since the pressure varied nearly linearly with distance, an average pressure gradient, $(dp/dz)_{avg}$ can be assigned as being representative of the whole channel. Although the average pressure gradients for the experimental runs conducted were relatively similar in value, nevertheless, one can see the emergence of possible trends when one varies the mass fluxes, heat fluxes, outlet pressures and inlet subcoolings. To illustrate these trends, the results are tabulated in the following sections and, for comparisons, the calculated overall pressure drop components are given in Figures 5.3 to 5.8. In each of the following tables, the parameter that was varied is highlighted in **bold**. Note that the run numbers are indicative of the pressures; for example, Run 1000-4 is test No. 4 at 1000 mbar abs. exit pressure.

5.2.1 Variations with mass flux

Tables 5.1, 5.2 and 5.3 present the experimental runs in groups that highlight the variation to the pressure gradient as a result of changing mass fluxes.

Outlet Pressure : 250 mbar abs.				
Run	$\dot{m}\,(\mathrm{kgm^{-2}s^{-1}})$	$\dot{q}\,(\mathrm{kWm^{-2}})$	$\Delta T_{subcool}\,(^{\circ}\mathrm{C})$	$(dp/dz)_{avg}$ $(\mathrm{Nm^{-3}})$
250-1	**50.17**	50	16.28	3227.4
250-3	**62.3**	50	16.21	3227.4
250-2	**50.17**	40	16.49	3178.5
250-4	**62.3**	40	14.95	3202.9
250-5	**50.17**	50	39.89	3912.0
250-6	**62.3**	50	39.07	4425.4
250-7A	**50.17**	40	39.66	4425.4
250-8A	**62.3**	40	38.73	4645.5
250-7B	**50.17**	40	29.70	3912.0
250-8B	**62.3**	40	29.99	4278.7

Table 5.1 Mass flux variation for pressure gradient

(Outlet pressure =250 mbar abs.)

Outlet Pressure : 500 mbar abs.				
Run	$\dot{m}\left(\mathrm{kgm^{-2}s^{-1}}\right)$	$\dot{q}\left(\mathrm{kWm^{-2}}\right)$	$\Delta T_{subcool}\left(^{\circ}\mathrm{C}\right)$	$(dp/dz)_{avg}$ $\left(\mathrm{Nm^{-3}}\right)$
500-1	**50.17**	50	12.34	2934.0
500-3	**62.3**	50	12.23	3031.8
500-2	**50.17**	40	12.19	2934.0
500-4	**62.3**	40	11.99	2982.9
500-5	**50.17**	50	40.28	3912.0
500-6	**62.3**	50	39.88	4229.8
500-7	**50.17**	40	39.38	4107.6
500-8	**62.3**	40	39.13	4743.3

Table 5.2 Mass flux variation for pressure gradient

(Outlet pressure =500 mbar abs.)

Outlet Pressure : 1000 mbar abs.				
Run	$\dot{m}\left(\mathrm{kgm^{-2}s^{-1}}\right)$	$\dot{q}\left(\mathrm{kWm^{-2}}\right)$	$\Delta T_{subcool}\left(^{\circ}\mathrm{C}\right)$	$(dp/dz)_{avg}$ $\left(\mathrm{Nm^{-3}}\right)$
1000-1	**50.17**	50	13.76	2909.5
1000-3	**62.3**	50	15.56	2909.5
1000-2	**50.17**	40	12.49	2885.1
1000-4	**62.3**	40	13.16	2909.5
1000-5	**50.17**	50	44.71	3912.0
1000-6	**62.3**	50	44.15	4376.5
1000-7	**50.17**	40	42.11	4449.9
1000-8	**62.3**	40	40.98	4914.4

Table 5.3 Mass flux variation for pressure gradient
(Outlet pressure =1000 mbar abs.)

From all the results presented above, it can be clearly seen that a distinct trend of increasing pressure gradient (within experimental error) with increasing mass fluxes. This is in agreement with other researchers' experimental observations that an increase in the flow rate at the same constant heat flux will cause a rise in the gravitational pressure drop term due to a larger liquid hydrostatic head, while those of frictional and accelerational terms will increase as a result of higher mass velocity; this is consistent with the predictions as illustrated in Figure 5.3 for a typical run.

5.2.2 Variations with heat flux

The following tables 5.4, 5.5 and 5.6 present the experimental runs in groups that highlight the variation to the pressure gradient as a result of changing heat fluxes.

Outlet Pressure : 250 mbar abs.				
Run	$\dot{m}\left(\mathrm{kgm^{-2}s^{-1}}\right)$	$\dot{q}\left(\mathrm{kWm^{-2}}\right)$	$\Delta T_{subcool}\left(^{\circ}\mathrm{C}\right)$	$(dp/dz)_{avg}$ $\left(\mathrm{Nm^{-3}}\right)$
250-1	50.17	50	16.28	3227.4
250-2	50.17	40	16.49	3178.5
250-3	62.3	50	16.21	3227.4
250-4	62.3	40	14.95	3202.9
250-5	50.17	50	39.89	3912.0
250-7A	50.17	40	39.66	4425.4
250-7B	50.17	40	29.70	3912.0
250-6	62.3	50	39.07	4425.4
250-8A	62.3	40	38.73	4645.5
250-8B	62.3	40	29.99	4278.7

Table 5.4 Heat flux variation for pressure gradient

(Outlet pressure =250 mbar abs.)

Outlet Pressure : 500 mbar abs.				
Run	$\dot{m}\left(\mathrm{kgm^{-2}s^{-1}}\right)$	$\dot{q}\left(\mathrm{kWm^{-2}}\right)$	$\Delta T_{subcool}\left(^{\circ}\mathrm{C}\right)$	$(dp/dz)_{avg}$ $\left(\mathrm{Nm^{-3}}\right)$
500-1	50.17	**50**	12.34	2934.0
500-2	50.17	**40**	12.19	2934.0
500-3	62.3	**50**	12.23	3031.8
500-4	62.3	**40**	11.99	2982.9
500-5	50.17	**50**	40.28	3912.0
500-7	50.17	**40**	39.38	4107.6
500-6	62.3	**50**	39.88	4229.8
500-8	62.3	**40**	39.13	4743.3

Table 5.5 Heat flux variation for pressure gradient

(Outlet pressure =500 mbar abs.)

Outlet Pressure : 1000 mbar abs.				
Run	$\dot{m}\left(\mathrm{kgm^{-2}s^{-1}}\right)$	$\dot{q}\left(\mathrm{kWm^{-2}}\right)$	$\Delta T_{subcool}\left(^{\circ}\mathrm{C}\right)$	$(dp/dz)_{avg}$ $\left(\mathrm{Nm^{-3}}\right)$
1000-1	50.17	**50**	13.76	2909.5
1000-2	50.17	**40**	12.49	2885.1
1000-3	62.3	**50**	15.56	2909.5
1000-4	62.3	**40**	13.16	2909.5
1000-5	50.17	**50**	44.71	3912.0
1000-7	50.17	**40**	42.11	4449.9
1000-6	62.3	**50**	44.15	4376.5
1000-8	62.3	**40**	40.98	4914.4

Table 5.6 Heat flux variation for pressure gradient

(Outlet pressure =1000 mbar abs.)

There are 2 features consistently displayed by the results tabulated above:

- For the **lower subcoolings** (~ 15 °C), the results showed a **decrease** (or no variation) in the pressure gradient as the heat flux is decreased for all the different outlet pressures.
- For the **higher subcoolings** (~ 40 °C), the results showed an **increase** in pressure gradient as the heat flux is decreased for all the different outlet pressures.

These findings clearly illustrate the complex interactions between the three pressure drop components. In the first instance, at the lower subcoolings (high mass qualities), the reduction in heat flux will reduce the frictional and accelerational components whose effects are greater at higher qualities, but the gravitational component had not increased as much to compensate for these reductions. Hence a drop in the pressure gradient was observed, consistent with the calculations as illustrated in Figure 5.4. On the other hand, for the higher subcooling cases (low mass qualities), while the frictional and accelerational components will drop as the heat flux is reduced, their magnitudes and effects are less, and with the gravitational component being larger at these low qualities, an increase in pressure gradient was observed again consistent with the calculations as shown in Figure 5.5.

5.2.3 Variations with outlet pressure

Table 5.7 given below highlights the effects on the SAE experimental pressure gradients as a result of varying the outlet pressures. Once again, one can elicit 2 distinguishing trends caused by the different inlet subcoolings as well as the varying outlet pressures.

- For the **lower subcoolings** (~ 15 °C), the results showed a **decrease** in the pressure gradient as the outlet pressure is increased.
- For the **higher subcoolings** (~ 40 °C), the results showed a small **increase** (or no variation) and some scatter in the pressure gradient as the outlet pressure is increased.

Run	$\dot{m}\left(\mathrm{kgm^{-2}s^{-1}}\right)$	$\dot{q}\left(\mathrm{kWm^{-2}}\right)$	$\Delta T_{subcool}\left(^{\circ}\mathrm{C}\right)$	$(dp/dz)_{avg}$ $\left(\mathrm{Nm^{-3}}\right)$
250-1	50.17	50	16.28	3227.4
500-1	50.17	50	12.34	2934.0
1000-1	50.17	50	13.76	2909.5
250-2	50.17	40	16.49	3178.5
500-2	50.17	40	12.19	2934.0
1000-2	50.17	40	12.49	2885.1
250-3	62.3	50	16.21	3227.4
500-3	62.3	50	12.23	3031.8
1000-3	62.3	50	15.56	2909.5
250-4	62.3	40	14.95	3202.9
500-4	62.3	40	11.99	2982.9
1000-4	62.3	40	13.16	2909.5
250-5	50.17	50	39.89	3912.0
500-5	50.17	50	40.28	3912.0
1000-5	50.17	50	44.71	3912.0
250-6	62.3	50	39.07	4425.4

500-6	62.3	50	39.88	4229.8
1000-6	62.3	50	44.15	4376.5
250-7A	50.17	40	39.66	4425.4
250-7B	50.17	40	29.70	3912.0
500-7	50.17	40	39.38	4107.6
1000-7	50.17	40	42.11	4449.9
250-8A	62.3	40	38.73	4645.5
250-8B	62.3	40	29.99	4278.7
500-8	62.3	40	39.13	4743.3
1000-8	62.3	40	40.98	4914.4

Table 5.7 Outlet pressure variation for pressure gradient (the number in the run name prior to the hyphen denotes the outlet pressure in mbar abs).

In a similar vein to the trends displayed when one varies the heat flux, for the cases of low subcoolings (high mass qualities), as one decreases the outlet pressure (and hence the system pressure), the boiling point is lowered. Consequently, more vapour is formed and the frictional and accelerational components of the pressure drop increase as the gravitational component drops. However, in high quality two phase flow, both the frictional and accelerational components' contributions are more significant than at low quality. Consequently, the overall total pressure drop increases with decreasing outlet pressure as illustrated by the calculations shown in Figure 5.6. For the higher subcooling runs (low mass qualities), although both the frictional and accelerational components are still influential on the two phase pressure drop, the degree and magnitude of their influence has receded while that of the gravitational component has increase. This reduction may reduce or even shift the trend of the overall total pressure drop, hence the scattering and the small increases in the results (see Figure 5.7).

5.2.4 Variations with inlet subcooling

The following tables, Table 5.8, 5.9 and 5.10 highlight the effect on the pressure gradient as a result of varying the inlet subcooling.

Outlet Pressure : 250 mbar abs.				
Run	$\dot{m}\left(\mathrm{kgm^{-2}s^{-1}}\right)$	$\dot{q}\left(\mathrm{kWm^{-2}}\right)$	$\Delta T_{subcool}\left(^{\circ}\mathrm{C}\right)$	$(dp/dz)_{avg}$ $\left(\mathrm{Nm^{-3}}\right)$
250-1	50.17	50	**16.28**	3227.4
250-5	50.17	50	**39.89**	3912.0
250-2	50.17	40	**16.49**	3178.5
250-7A	50.17	40	**39.66**	4425.4
250-7B	50.17	40	**29.70**	3912.0
250-3	62.3	50	**16.21**	3227.4
250-6	62.3	50	**39.07**	4425.4
250-4	62.3	40	**14.95**	3202.9
250-8A	62.3	40	**38.73**	4645.5
250-8B	62.3	40	**29.99**	4278.7

Table 5.8 Inlet subcooling variation for pressure gradient (Outlet pressure =250 mbar abs.)

Outlet Pressure : 500 mbar abs.				
Run	$\dot{m}\left(\mathrm{kgm^{-2}s^{-1}}\right)$	$\dot{q}\left(\mathrm{kWm^{-2}}\right)$	$\Delta T_{subcool}\left(^{\circ}\mathrm{C}\right)$	$(dp/dz)_{avg}$ $\left(\mathrm{Nm^{-3}}\right)$
500-1	50.17	50	**12.34**	2934.0
500-5	50.17	50	**40.28**	3912.0
500-2	50.17	40	**12.19**	2934.0
500-7	50.17	40	**39.38**	4107.6
500-3	62.3	50	**12.23**	3031.8

500-6	62.3	50	**39.88**	4229.8
500-4	62.3	40	**11.99**	2982.9
500-8	62.3	40	**39.13**	4743.3

Table 5.9 Inlet subcooling variation for pressure gradient (Outlet pressure =500 mbar abs.)

Outlet Pressure : 1000 mbar abs.				
Run	$\dot{m}\left(\mathrm{kgm^{-2}s^{-1}}\right)$	$\dot{q}\left(\mathrm{kWm^{-2}}\right)$	$\Delta T_{subcool}\left(^{\circ}\mathrm{C}\right)$	$\left(dp/dz\right)_{avg}$ $\left(\mathrm{Nm^{-3}}\right)$
1000-1	50.17	50	**13.76**	2909.5
1000-5	50.17	50	**44.71**	3912.0
1000-2	50.17	40	**12.49**	2885.1
1000-7	50.17	40	**42.11**	4449.9
1000-3	62.3	50	**15.56**	2909.5
1000-6	62.3	50	**44.15**	4376.5
1000-4	62.3	40	**13.16**	2909.5
1000-8	62.3	40	**40.98**	4914.4

Table 5.10 Inlet subcooling variation for pressure gradient (Outlet pressure =1000 mbar abs.)

All the tabulated results above clearly showed a distinct trend of increasing pressure gradient with increasing inlet subcooling. Once again, the reasoning behind this trend is that of the shifting balance of influence between the pressure drop components and for the case of higher subcoolings, the reduction of frictional and accelerational components influence was offset by the larger increase in gravitational component as demonstrated by Figure 5.8.

5.3 Heat transfer coefficient results

The measurement of heat transfer coefficient in the SAE experiments is one of the three main thrusts of the research work reported in this thesis, the others being the design, construction and commissioning of the SAE rig reported in Chapter 4, and the SAE modelling computer code reported in Chapter 6. The uniqueness of these results is derived mainly from the dearth of experimental data presently available for sub-atmospheric flow boiling. In brief, some rather unusual features of sub-atmospheric flow boiling were observed and possible explanations as to their occurrences were presented. Before the results of the analysis on the effects of the various operating parameters on the heat transfer coefficients are presented, the methods adopted in processing and analysing the experimental data are first discussed.

5.3.1 Heat transfer data analysis

In order to ensure that the data processing and analysis procedures adopted were consistent throughout the whole research work, the following equations were used in calculating the experimental heat transfer coefficients. The key variables used are:

(I) Fluid temperature.
(II) Inside wall temperature.
(III) Pressure measurements (as discussed in an earlier section 5.2).
(IV) Heat flux.

We will now look at each of these variables in turn, starting with the fluid temperature.

(I) **Fluid temperature**

Single-phase liquid flow ($x \leq 0$)

Although there were fluid thermocouples available for measuring the bulk fluid centre-line temperatures, their primary function is to check on the consistency and agreement with temperatures derived from the heat balance as follows:

$$T_{fluid} = T_{inlet} + \frac{4\,\dot{q}\,z}{\dot{m}\,D\,C_{pL}} \tag{5.1}$$

Good agreement between the measured and calculated fluid temperatures were observed, as the examples of some typical runs shown in Figure 5.9 to 5.11. The calibrations and accuracy of the bulk fluid thermocouples are given in detail in Appendix B and C.

Two-phase flow ($x > 0$)

As in the case for single-phase liquid flow, the bulk fluid temperatures measured using the centre-line fluid thermocouples in two-phase flow region were used to compare and check against the fluid saturation temperature obtained from the empirical saturated pressure and temperature correlation given below as,

$$T_{sat} = \frac{3842.56}{23.2189 - \ln p} - 228.6 \tag{5.2}$$

This empirical correlation was taken from a steam-water thermodynamic and transport properties subroutine made available through HTFS (Heat Transfer Fluid Flow Service, at National Engineering Laboratory (NEL) at East Kilbride, UK). The applicability and accuracy of this correlation and the whole subroutine in general had been verified when compared against the UK Steam Tables (1970). The agreement was found to be excellent in the range of interest, i.e. 0°C to 100°C.

From the 6 pressure measurements, where they were found to exhibit a linear profile (as discussed in the previous section 5.2), linear regression curves were fitted. From

these curves, the local pressure and its corresponding saturated temperature can be calculated for the two-phase flow region.

(II) Inside wall temperature

The inside wall temperature is calculated by estimating the heat conduction across the thin tube wall from the measured outside wall temperature, see Appendix A. The two temperatures are related by the following equation,

$$T_{wi} = T_{wo} + \left\{ \frac{-\dot{q}_i r_i}{\lambda} \left[\frac{1}{2} - \frac{r_o^2}{\left(r_o^2 - r_i^2\right)} \ln\left(\frac{r_o}{r_i}\right) \right] \right\} \tag{5.3}$$

where T_{wi} is the ~~inlet~~ inside wall temperature, T_{wo} is the ~~outlet~~ outside wall temperature, $\dot{q}_i$ is the heat flux based on the inner surface area, λ is the thermal conductivity of the test section wall, r_i is the inner wall radius of the test section and r_o is the outside wall radius of the test section, as derived in Appendix A. The calibrations and error estimations associated with the wall temperatures are given and analysed in Appendix B and C.

(III) Pressure measurements

The accuracy and methodology adopted was discussed in the previous section 5.2 and its errors are estimated in Appendix C.

(IV) Heat flux

The heat flux is calculated from the ratio of the total power supplied for direct joule heating to the inner surface area of the test section. It was assumed that the power

supplied was dissipated evenly both radially and axially along the whole test section. This assumption is justifiable on the basis of the uniformity of the wall thickness and material of construction of the test section. As with the other variables, the error estimation and analysis is presented in Appendix C.

(V) Heat transfer coefficient

From all the key variables mentioned above, the heat transfer coefficient is calculated from:

$$\alpha = \frac{\dot{q}}{T_{w1} - T_{fluid}} \tag{5.4}$$

where $T_{fluid} = T_{spl}$ for $x \leq 0$

$T_{fluid} = T_{sat}$ for $x > 0$

The error estimated for a typical averaged experimental run (see Appendix C) was found to be:

$$\left(\frac{d\alpha}{\alpha}\right) = \pm 0.132 \tag{5.5}$$

which is around the same degree and range of accuracy reported for and expected of other accurate experiments such as those of Kenning and Cooper (1989), who reported an experimental accuracy of approximately 10%.

The results from the experiments were repeatable as illustrated in Figures 5.12 to 5.15 which show the results for heat transfer coefficient as a function of local quality for the selected 16 repeat experimental runs of the second series of experiments plotted together with the original runs. It should be noted here that during this second series of runs, difficulties were encountered in lowering the inlet subcooling to be the same value as in the original runs except for experimental run 250-1A, see Figure 5.12. Consequently, the runs were repeated at a higher subcooling than the original, thus full reproducibility were not achieved. Nevertheless, the key point of the second series of experiments was to re-confirm the trends observed in the original runs, and in this

respect, it was a success. One should also bear in mind of the difficulty in controlling flow boiling experiments especially where nucleate boiling is the dominant mechanism due to a variety of effects, in particular the surface roughness and ageing, which in turn affect the nucleation site density.

In order to highlight the different features noted in the SAE experimental results, a structured analysis was performed based on the systematic variation of each operating parameter while holding the others constant. The following sections will focus on the effects on the heat transfer coefficient as one varies the mass flux, heat flux, outlet pressure and inlet subcooling respectively. The chapter will then close with a summary of the key results and conclusions.

5.3.2 Variations with mass flux

The effects caused by the variation of mass flux were analysed and presented below. This section will first present all the observations and analyses at each exit pressure. It will then be followed by a section of further analysis and discussion to elucidate on some of the more unusual features observed.

5.3.2.1 Experimental observations and analyses

The following observations and analyses were made from the experimental results obtained at the test section exit pressures at 250, 500 and 1000 mbar abs.

Exit pressure at 250 mbar abs.

(I) All the main experimental results at the 250 mbar abs. exit pressure are presented in Figures 5.16 to 5.20 (and with the additional analyses on the repeated runs given in Figures 5.29 to 5.32). It can be concluded from all the

comparisons made, that the effect on the value of the heat transfer coefficient as a result of varying the mass flux from 50.17 to 62.3 $kgm^{-2}s^{-1}$ was small in the subcooled boiling region ($x < 0$).

(II) From all the results shown in Figures 5.16 to 5.20, the low mass flux runs (50.17 $kgm^{-2}s^{-1}$) consistently showed that they entered into the saturated two-phase flow boiling region before the higher mass flux runs (62.3 $kgm^{-2}s^{-1}$). This fact is clearly reflected by the higher vapour qualities achieved by the low mass flux runs. This is a logical conclusion since there is less liquid mass to be heated up.

(III) From all the results shown in Figures 5.16 to 5.20, some data scatter were observed especially in Figure 5.17. From these results, there appears to be a mass flux influence on heat transfer coefficient in the quality region, albeit very small. However, when the data is more closely scrutinised in terms of its error analysis as shown in Figure 5.33, and based on the trends shown by all the runs when the vapour quality increases beyond 5% (where the magnitude of the heat transfer coefficients are virtually the same), one can safely conclude that the implied mass flux effects as a result of data scatter are within the scope of experimental errors detailed in Appendix C.

Hence, the actual underlying trend is one where there is relatively little dependency of the heat transfer coefficient on mass flux and vapour quality. These are the classical features of a *nucleate boiling dominant* heat transfer mechanism, as supported by results obtained at higher exit pressures. Nevertheless, the data scatter seen should be properly addressed and accounted for and this will be discussed later.

(IV) Another mystifying feature exhibited prominently in the high inlet subcooling runs, see Figures 5.18 to 5.20, is the existence of a maxima in the value of the heat transfer coefficient at very low vapour qualities. Although this feature is no longer brand new, its existence had recently been reported by Thome (1995)

in reference to the work of Kattan et al. (1995), the difference in this case is its occurrence for water at sub-atmospheric pressure as opposed to refrigerants as observed by Kattan et al. (1995). Interestingly, a maxima at low vapour qualities can also be seen in Stone (1971) sub-atmospheric studies (refer to Figure 3.7 in Chapter 3) but he did not explicitly analyse its existence.

The maxima observed in these experiments at 250 mbar abs. was estimated to be as high as 4 times the value obtained in the latter part of the test section where the heat transfer coefficient has settled down to a fairly constant value in the predominantly nucleate boiling region as discussed earlier. This feature will be analysed and discussed in more detail below.

(V) The heat transfer coefficient estimated in the latter part of the test section where nucleate boiling is dominant, ranged from 6 000 to 9 000 $Wm^{-2}K^{-1}$.

Exit pressure at 500 mbar abs.

(I) All the experimental results at the 500 mbar abs. exit pressure are presented in Figures 5.21 to 5.24. As for the 250 mbar abs. experiments, it can be concluded that there is no significant effect on the value of the heat transfer coefficient as a result of varying the mass fluxes (at 50.17 and 62.3 $kgm^{-2}s^{-1}$) in the subcooled region ($x < 0$).

(II) Similar to the results at 250 mbar abs., the low mass flux runs (50.17 $kgm^{-2}s^{-1}$) at 500 mbar abs. consistently showed that they reached the saturated two-phase flow boiling region before the higher mass flux runs (62.3 $kgm^{-2}s^{-1}$) as seen by the higher vapour qualities that they had achieved.

(III) For vapour qualities, $x > 0.05$, all the experimental runs conducted at 500 mbar abs. also showed the heat transfer coefficient to be relatively independent of

mass flux and x, indicating the presence of a nucleate boiling dominated heat transfer mechanism.

(IV) The maxima previously observed at the 250 mbar abs. experiments is also present for the high inlet subcooling (~ 40°C) experimental runs at 500 mbar abs., see Figures 5.23 and 5.24. However, at this higher exit pressure, the magnitude of the maxima had been greatly reduced, to approximately 2 times the value obtained in the latter part of the test section where the heat transfer coefficient had relatively settled down to a roughly constant value in the predominantly nucleate boiling region as discussed earlier.

(V) The heat transfer coefficient estimated in the predominantly nucleate boiling region at the latter part of the test section ranged from approximately 7 000 to 9 000 $Wm^{-2}K^{-1}$.

Exit pressure at 1000 mbar abs.

(I) All the experimental results at the 1000 mbar abs. exit pressure are presented in Figures 5.25 to 5.28. As seen in the previous experiments at 250 and 500 mbar abs., the subcooled region heat transfer coefficient was found to be independent of mass flux.

(II) From Figures 5.25 to 5.28, and in accordance with the previous observations at 250 and 500 mbar abs., the low mass flux runs was found to have entered into the saturated two-phase flow boiling region before the high mass flux runs and gave higher outlet qualities.

(III) As illustrated in all the runs depicted in Figures 5.25 to 5.28, in the saturated two-phase flow boiling region, $x > 0$, the dominant heat transfer mechanism is that of nucleate boiling. This conclusion is borne out by the results which

showed that the heat transfer coefficient to be relatively independent of mass flux and vapour quality, x.

(IV) The maxima in heat transfer coefficient at low qualities previously observed at the 250 and 500 mbar abs. experiments is no longer distinct or prominent for the high inlet subcooling (~ 40 - 44°C) experimental runs at 1000 mbar abs. From Figures 5.27 and 5.28, when one takes into account of the data scatter, there is no clear cut distinction between the low and high vapour quality heat transfer coefficient values.

(V) The heat transfer coefficient estimated in the predominantly nucleate boiling region at the latter part of the test section ranged from approximately 6 000 to 8 000 $Wm^{-2}K^{-1}$.

5.3.2.2 Further analysis and discussion

There are 2 key features noted in the earlier analyses on the effect of varying mass flux at 250, 500 and 1000 mbar abs. exit pressures that warranted further analysis and discussion.

- **Data scatter**

  The data scatter shown prominently in Figures 5.17 and 5.23, highlights the difficulty associated with the measurement of mean superheat during nucleate boiling. Kenning (1990, 1992) investigated the variation in wall temperature patterns using a thin stainless steel heated plate during nucleate pool boiling of water; the observations were made by observing the response of a layer of thermochromic liquid crystal deposited on the outer surface of the plate. Kenning (1992) concluded that spatial variations in wall temperatures may cause errors in the measurement of wall superheats, resulting in errors in calculated heat transfer coefficients. This conclusion seems superficially to be consistent with the scatter

revealed in the repeat of the experiments (see for instance Figures 5.29 and 5.30). However, as shown in Figure 5.33, the scatter in measurements were found to be well within the limits of experimental accuracy of ±13.2% as estimated in the error analysis in Appendix C.

The data scatter observed were not confined only to Run 250-4 or the 250 mbar abs. experiments, but can also be seen in other runs at different exit pressures, see Figure 5.34 for error analysis on Run 500-5 against Run 500-6.

- **Heat transfer coefficient maxima at low qualities ($x \cong 0.0$)**

  As was mentioned above, the heat transfer coefficient may show a sharp maximum at around zero quality. This phenomenon is particularly pronounced at 250 mbar abs. outlet pressure, less so at 500 mbar abs. and is only just apparent at 1000 mbar abs. (see Figures 5.19, 5.24 and 5.26). Following from a series of deductions and eliminations of the clues offered by the trends and experimental observations noted during these runs, it is postulated that the most probable explanation of this intriguing phenomenon is the existence of localised thermal non-equilibrium instability as proposed and described by Jeglic and Grace (1965) and Ishii (1982).

  Jeglic and Grace (1965) conducted a study on the onset of flow oscillations occurring when subcooled water at sub-atmospheric pressures undergoes a phase change under forced-flow conditions in an electrically heated Inconel X tube. They concluded that the instabilities and oscillations they observed were apparently due to thermodynamic non-equilibrium. Jeglic and Grace (1965) found that, in order for flow oscillations to occur, the rate of change in void fraction has to be high and abrupt in subcooled boiling, and their visual studies showed this abrupt transition to be in the form of an emerging slug.

  Ishii (1982) elaborated on the Jeglic and Grace (1965) findings by stating that from the operating conditions Jeglic and Grace had employed and because of poor nucleation and heat transfer, the liquid can become highly superheated. However,

once a bubble is nucleated, it grows explosively (because of the high liquid superheat). The consequences of this explosive like growth are a very rapid increase in void fraction, a sudden release of thermal energy stored in the superheated liquid into the bubble growth and the removal of heat from the wall, causing a drop in wall temperature. Compounded together, these effects will cause the sudden rise in the value of heat transfer coefficient as observed in Figures 5.18 to 5.20, 5.23 and 5.24.

It should be noted here that one may argue that a drop in wall temperature is to be expected in all flow boiling experiments at the inception of nucleate boiling. The author does not dispute this fact, but in the present study, the key difference is that because of the higher specific volume of the steam at low pressures, a given amount of heat released from the superheated liquid and the wall would create a much larger volume of vapour.

Although the findings of Jeglic and Grace (1965) cannot be quantitatively linked to the findings of the SAE experiments stated here, one can relate them qualitatively and hence support the explanation and discussion presented in this section, through the following points and trends:

(1) From the SAE experimental results, the heat transfer coefficient maxima at low qualities, was found to be dependent on inlet subcooling. Its value is lower at low inlet subcooling. Jeglic and Grace (1965) argued that in their experimental results, when the inlet subcooling is small, the heat flux required for net vapour generation is lower than that for larger subcooling. Consequently, the rate of change of void fraction was expected to be less, resulting in a smoother transition from bubbly to annular flow. They suggest that for flow oscillations to occur, the transition must be abrupt, so that high inlet subcooling makes the system more susceptible to the instability. In the present experiments, however, subcooling is changed independently of heat flux. A possible explanation of the influence of subcooling is that, with low subcooling, nucleate boiling at the wall is initiated early in the test section and prevents excessive superheats in the liquid. At higher

inlet subcoolings, on the other hand, nucleate boiling does not occur immediately and its eventual occurrence may be associated with the instability phenomenon described above.

(2) The heat transfer coefficient maxima in the SAE experiments were found to be dependent on exit pressure (i.e. system pressure). The higher the system pressure, the lower the value of heat transfer coefficient. In their study, Jeglic and Grace (1965) argued that for higher pressure systems, flow oscillations could not be obtained in the subcooled boiling region. They argued that the decrease in latent heat of vaporisation with increasing pressure is much less than the corresponding decrease in liquid-vapour density ratio, see Table 5.11 below. Thus, according to them, the net effect of pressure increase would be a lower rate of change of void fraction, which in their studies is unfavourable for flow oscillations, while the same arguments applied here would imply that the rapid heat removal associated with the rapid vaporisation and void growth is reduced.

p (mbar abs.)	ρ_L (kgm^{-3})	ρ_G (kgm^{-3})	ρ_L/ρ_G ratio	h_{LG} (J/kg)	λ_L ($Wm^{-1}K^{-1}$)
250	980.490	0.161	6090	2.346×10^6	0.658
500	970.780	0.309	3142	2.306×10^6	0.670
1000	958.405	0.590	1624	2.259×10^6	0.678

Table 5.11 Some key saturated water/steam physical properties at different pressures (extracted from UK Steam Tables, 1970)

(3) As can be seen from Table 5.11, the tendency for the liquid to superheat is much greater as the pressure decreases, since the latent heat of vaporisation rises while the liquid thermal conductivity decreases. Both factors may account for a less efficient single-phase heat transfer across liquid layer next to the heated wall into the bulk fluid core, resulting in a more superheated layer of liquid. This effect may explain the existence (even at higher pressures) of the heat transfer coefficient maximum in refrigerant system as reported by Thome (1995). The thermal

conductivity of refrigerants is much less than that of water. The physical properties of a typical refrigerant are shown in Table 5.12.

ρ_L (kgm^{-3})	ρ_G (kgm^{-3})	ρ_L/ρ_G ratio	h_{LG} (J/kg)	λ_L ($Wm^{-1}K^{-1}$)
1467.0	5.86	250.341	0.180×10^6	0.0865

Table 5.12 Some key Freon 11 (R-11) physical properties (extracted from CRC Handbook of Chemistry and Physics)

(4) During the SAE experimental runs, it was found that the amount of throttling required to stabilise the flow was greater at lower pressure. Small pressure fluctuations were also observed and both these observations support the hypothesis (consistent with the suggestion of Jeglic and Grace (1965)) that localised thermally induced instabilities may have been taking place.

Based on the observations above, the existence of localised thermally induced instabilities seems to be an explanation for the heat transfer coefficient maxima at high inlet subcoolings, low qualities and low pressures as noted in the SAE experiments. It is noteworthy that visual manifestations of the instability were not observed in the viewing section at the end of the test section. However, the heat transfer coefficient maxima, happened within the first 1m (44 diameters) of the test section, and with another 3m (130 diameters) of heated test section to go, any small flow instability may have been damped out as the flow moves into the churn and annular flow regimes, as observed in the visualisation section.

5.3.3 Variations with heat flux

The effects caused by the variation of heat flux are analysed and presented in this section. This section will first present the key observations and analyses at each exit pressure. This will then be followed by a section of further analysis and discussion to elucidate on some of the more unusual features observed.

5.3.3.1 Experimental observations and analyses

Exit pressure at 250 mbar abs.

The results highlighting the effects of variation of heat flux on the heat transfer coefficient at 250 mbar exit pressure are presented in Figures 5.35 to 5.38. As can be seen from the graphs, there are 3 distinguishing effects.

(I) At low inlet subcoolings (~15 °C), Figures 5.35 and 5.36, the lower heat flux runs returned higher values of heat transfer coefficients in the saturated flow boiling region. This is not expected and a possible explanation to this anomalous result is that of a hysteresis similar to that reported by Abdelmessih et al. (1973, 1974). This hysteresis will be discussed in further detail later.

(II) At high inlet subcoolings (~ 40°C), Figures 5.37 and 5.38, there were no clear difference in the value of the heat transfer coefficient for the different heat flux runs except near quality, x = 0. The heat transfer coefficient maxima as discussed earlier was observed.

(III) In all cases, the overall trend as the vapour quality increases is one of convergence of the heat transfer coefficient towards independence on heat flux.

Exit pressure at 500 mbar abs.

The results highlighting the effects of variation of heat flux on the heat transfer coefficient at 500 mbar exit pressure are presented in Figures 5.39 to 5.42. As can be seen from the graphs, there are 3 notable effects.

(I) At low inlet subcoolings, Figures 5.39 and 5.40, there were no major difference in the heat transfer coefficient between the higher and lower heat flux runs. The distinguishing effect as seen in the 250 mbar abs. exit pressure runs is no longer present.

(II) The heat transfer coefficient maxima is still present for the higher inlet subcooling runs but there was no clear effect as a result of varying the heat flux, unlike the runs conducted at 250 mbar abs.

(III) In all cases, as for the 250 mbar abs., the overall trend as the vapour quality increases is one of convergence of the heat transfer coefficient towards a constant value independent of heat flux.

Exit pressure at 1000 mbar abs.

The results highlighting the effects of variation of heat flux on the heat transfer coefficient at 1000 mbar abs. exit pressure are presented in Figures 5.43 to 5.46. As can be seen from the graphs, 3 key observations in relation to the earlier runs performed at lower pressures can be made.

(I) At low inlet subcoolings, Figures 5.43 and 5.44, there is no distinct effect as a result of varying the heat flux.

(II) At high inlet subcoolings, Figures 5.45 and 5.46, the presence of the heat transfer coefficient maxima as discussed earlier in Section 5.3.2.2 can still be seen but is no longer as prominent as in the lower pressure runs.

(III) As observed before at 250 and 500 mbar abs. exit pressures, the heat transfer coefficients at 1000 mbar abs. also tend towards a value which is independent of heat flux as the quality increases.

5.3.3.2 Further analysis and discussion

The key feature that merited additional scrutiny and analysis is the anomalous results illustrated in Figures 5.35 and 5.36, for the 250 mbar abs. runs at low inlet subcooling. In these figures, the lower heat flux runs produced higher values of heat transfer coefficient relative to the higher heat flux cases. This trend would not normally be expected for nucleate boiling where, conventionally, the heat transfer coefficient would be expected to increase with heat flux. One of the key driving forces behind the second series of repeated runs was to check on this anomaly. The results from the second series of runs are given in Figures 5.53 to 5.58 and confirm the results from the first series. Investigations of the possible causes of this anomaly led to the idea that it could be a manifestation of the effects of hysteresis in the activation of nucleation sites. Some indications of effects of this type is given in work reported by Abdelmessih et al. (1973, 1974).

Abdelmessih et al. (1973, 1974) conducted an experimental investigation to study the temperature profile and hysteresis effects in incipient flow boiling of Freon 11 (Refrigerant - 11) at atmospheric pressure, in an electrically heated test section, made from 304 stainless steel tubing with 0.0109m inner diameter and 0.914m in length. They conducted their experiments by initially increasing the heat flux and then progressively decreasing the heat flux. Their results are shown in Figures 5.59 and 5.60.

From their incremental heat flux results, they found that when the level of superheat needed for incipient of boiling is attained, any further small increment in heat flux will result in vigorous boiling which is accompanied by a sharp drop in wall temperature. They noted that while the level of superheat did not change, the position of the incipient of boiling shifted closer towards their test section inlet, as expected.

However, when they began reducing the heat flux, they observed two distinct effects. The first effect is that there was no shift in the position of the onset of boiling and secondly, the superheat required to sustain boiling decreased with progressive decrement in the heat flux. They showed in their plots that a hysteresis had clearly occurred. They hypothesised that the hysteresis effect is caused by the *continued activation of cavities* as the heat flux decreases which had been inactive at the given heat flux when heat flux was initially increased.

Figures 5.35, 5.36 as well as the repeated runs results of Figures 5.53, 5.54 and 5.57, consistently showed that the heat transfer coefficient for the lower heat flux SAE runs are higher than for the higher heat flux runs. These results can be explained in the following manner, in light of Abdelmessih et al. (1973, 1974) results:

- **Wall temperature** The wall temperature profiles for the 250 mbar abs. tests are shown in Figures 5.47, 5.48, 5.55, 5.56 and 5.58. In most cases, the wall temperature falls rapidly and then more slowly with distance reflecting the trends shown in the heat transfer coefficient. However, if we examine Figure 5.58, we see an initial rise in wall temperature (corresponding to single-phase heat transfer) followed by a fall following the inception of nucleate boiling. The point of inception seems to be the same for both the 50 and 40 kWm^{-2} heat fluxes and this is qualitatively in accord with the findings of Abdelmessih et al. (1973, 1974) for *a reducing heat flux* (see Figure 5.60).

- **Wall superheat** The wall superheat values were lower for the lower heat flux runs. However, for the case of the runs at low subcooling and with an outlet

pressure of 250 mbar abs., the ratio of the heat flux to the wall superheat (i.e. the heat transfer coefficient) is less at the lower heat flux. A similar trend is observed in the results of Abdelmessih et al. as will be seen from examination of Figure 5.60.

From these results and explanations, it seems probable that hysteresis had occurred during the 250 mbar abs. experiments. Having made a case for hysteresis, the following questions need to be answered:

1. Why is the hysteresis effect only seen at low inlet subcooling?
2. Why does the hysteresis effect show itself prominently only at 250 mbar abs. and not at 500 or 1000 mbar abs. exit pressures?
3. How did it happen during the SAE experiments?

The most probable answer to the first question is that in the case of the higher inlet subcoolings, this effect may be overridden or overshadowed by the local thermal non-equilibrium flow instability effects discussed earlier.

The second question may have an answer in the possible changes in the availability of active nucleation sites. At low pressure, the gas content of the liquid will be less since gas is extracted via the reflux condenser and vacuum system. Thus, the circulating liquid may dissolve the gas in the incipient nucleation centres, making the activation of a given site more difficult. However, once a site is activated at higher heat fluxes, then it could remain active when the heat flux is reduced. In the refrigerant system used by Abdelmessih et al. (1973, 1974), the fluid may also have a tendency to dissolve gases from active sites; in addition, the different wetting properties of the refrigerants may make it more difficult to trap gas in potential sites when the system is initially filled with liquid. Both these factors would make the refrigerant system also susceptible to the hysteresis effect.

In order to answer the third question as to how the hysteresis occurred during the SAE experiments, reference may be made to the operational procedures described in Chapter 4, section 4.2.3.2 (see Steps 7 to 9 of the start-up procedures). Following the

procedures outlined, during the start-up of the SAE rig, in order to achieve the desired inlet subcooling and to remove air from the primary tank, the maximum heat flux (around 57 kWm^{-2}) was applied to heat up and boil the test fluid under vacuum. The application of this high heat flux took place in Steps 7 and 8, before the actual adjustments to the mass flux and heat flux to the desired experimental settings, as outlined in Step 9. The consequence of this heat overloading may be the activation of the nucleation sites which may not be active at lower heat fluxes. Once activated, however, these sites may have remained active, even when the heat flux was lowered. It was beyond the time availability of the present experiments to conduct systematic investigations of the hysteresis effects as was done by Abdelmessih et al. (1973, 1974) for their system. Clearly, this could be a subject for future investigations in the SAE rig.

5.3.4 Variations with outlet pressure

The effects caused by the variation of outlet pressure were analysed and presented below. The results showing the effects on the heat transfer coefficient as a result of varying the outlet pressures are illustrated in Figures 5.61 to 5.68.

The boiling heat transfer coefficient would be expected to increase with pressure in the case of pure nucleate boiling. Assuming that this pressure effect can be calculated from pool boiling relationships, one can use the relationships given in Chapter 3, section 3.2.3 to calculate the expected change. The Mostinski (1963) correlation (equation (3.26)) would predict an increase of 13% with an increase in pressure from 250 mbar abs. to 500 mbar abs. and an increase of 27% with an increase in pressure from 250 mbar abs. to 1000 mbar abs. The corresponding figures for the Cooper (1984) correlation (equation (3.29)) are 16% and 34% respectively. It should be borne in mind, however, that these relationships have been developed from data taken at higher pressure than in the present tests. Also, the present tests are for forced

convection rather than for pool boiling. The following points may be made about the effects of pressure seen in the present tests:

It is convenient to discuss the results in two groups, namely those at low subcooling and those at high subcooling. The low subcooling data are presented in Figures 5.61 to 5.64 and one may note the following:

(1) The data for 500 mbar abs. pressure are consistently higher than those at 1000 mbar abs. whereas, from the pool boiling correlations, one would have expected them to be around 15% lower.

(2) The data for 250 mbar abs. are lower (as expected) than those for higher pressures and high heat flux but the heat transfer coefficient is much higher (and can even be the highest) at the lower heat flux. This is clearly a manifestation of the hysteresis effect mentioned above.

For higher subcooling (Figures 5.65 to 5.68), the situation is complicated by the existence of the local thermal instability mechanism discussed above. The following observations may be made:

(1) There is a peak in heat transfer coefficient at around zero quality, this peak being due to the local thermal instability and is more pronounced at the lowest pressure.

(2) For higher qualities, there seems to be no systematic effects of pressure on the data.

5.3.5 Variations with inlet subcooling

The results showing the effect of inlet subcooling are given in Figures 5.69 to 5.80. Most of the effects caused by inlet subcooling have been discussed and detailed indirectly when considering the other flow and heat transfer parameters in the earlier sections 5.3.2 to 5.3.4. The most distinctive feature is the peak in heat transfer coefficient at near zero quality with higher inlet subcooling. This effect being more pronounced as the pressure decreases

5.3.6 Summary of key SAE heat transfer results

From all the observations and analyses conducted on the effect on heat transfer coefficient as a result of varying each of the key flow and heat transfer parameters, the four most important results can be summarised as follows:

- **Nucleate boiling dominant heat transfer at $x \geq 0.05$**

  All the results showed that at higher vapour qualities, $x \geq 0.05$, the heat transfer coefficients were fairly constant with respect to vapour quality and mass flux. Furthermore, all the runs showed consistently that they converged towards a similar value of heat transfer coefficient as the vapour quality increases. These are classical features of a nucleate boiling dominated heat transfer mechanism though there are some unexpected features, particularly with respect to the effect of pressure.

- **Heat transfer coefficient maxima**

  Heat transfer coefficient maxima were observed at around zero quality for the results at high inlet subcooling. The localised thermal instability hypothesis presented by Jeglic and Grace (1965) and referred also by Ishii (1982), provided the best explanation for these maxima. The key factors that influenced flow stability in the SAE experiments were found to be system pressure and inlet subcooling. This is in agreement with the conclusions of Jeglic and Grace (1965).

- **Flow boiling hysteresis**

  The heat transfer coefficient may increase (at the lowest pressure studied) with decreasing heat flux, against the expected trend for nucleate boiling. The hysteresis hypothesis and results presented by Abdelmessih et al. (1973, 1974) provides an explanation of these results and should be investigated further in future work.

- **Contributions of system pressure and inlet subcooling**

  The effects of system/exit pressure and inlet subcooling were shown to be significant as they influenced the flow stability, see Jeglic and Grace (1965). The effect of inlet subcooling was found to be dependent on system pressure, i.e. as the pressure decreases, the effect of inlet subcooling increases. This effect was found to be promoting heat transfer, and the most plausible reasoning is its effect on liquid superheat and flow stability.

5.4 Conclusion

The new results presented in this chapter clearly highlight the complexities and intricacies of the interactions between the flow and heat transfer parameters in sub-atmospheric flow boiling. Though there are links to phenomena observed previously at higher pressures, the sub-atmospheric regime has special features, the most important of which is the large volumetric vapour generation rate for a given heat flux and the changed influence of dissolved gases. Although the present data set is already rather large, there is a clear need to extend the studies of this interesting region to more detailed experiments, particularly on the effects of hysteresis, thermal instabilities and dissolved gases.

Figure 5.1 Typical Pressure Readings For Experimental Runs Against Quality

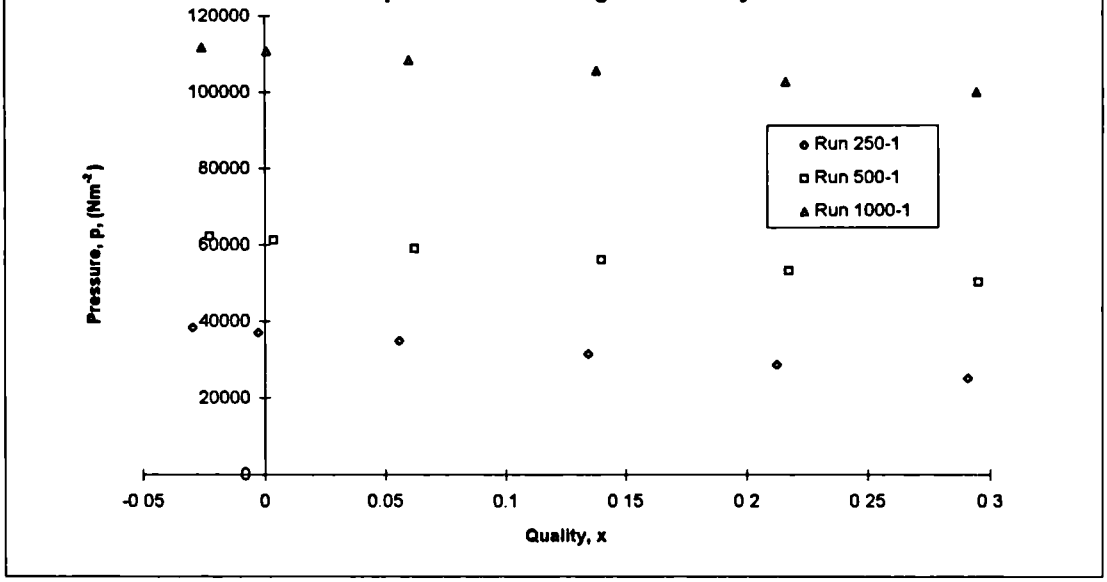

Figure 5.2a Comparison of the SAE modelling with experimentally measured pressure profiles for Run 250-2 (Maximum deviation)

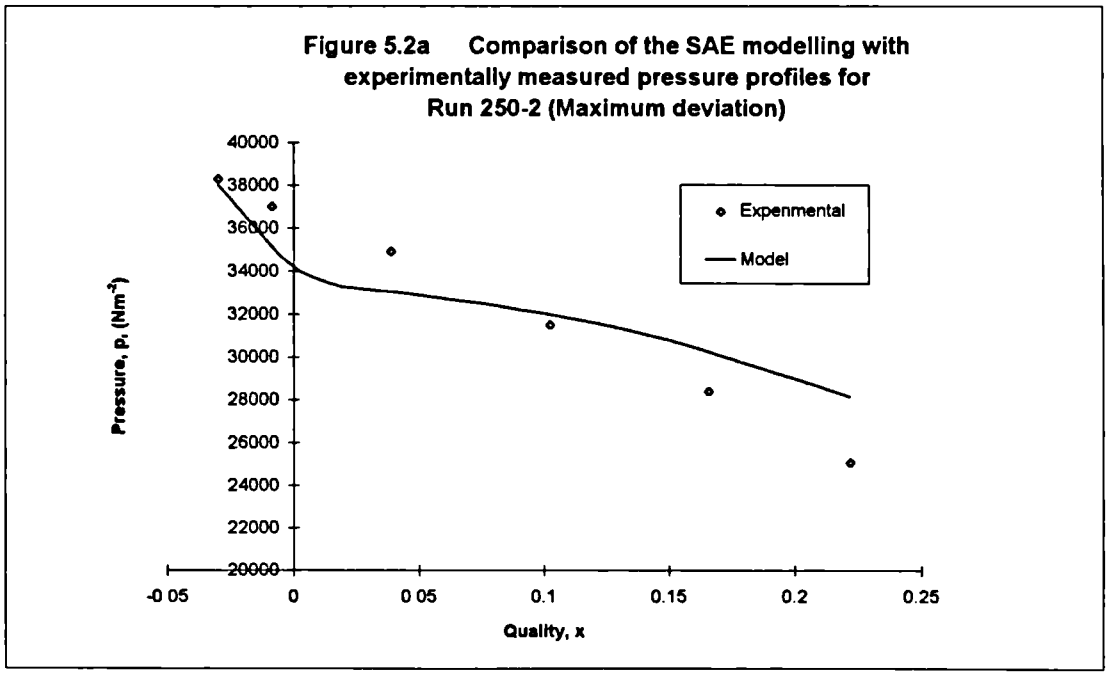

Figure 5.2b Comparison of the SAE modelling with experimentally measured pressure profiles for Run 500-2 (Maximum deviation)

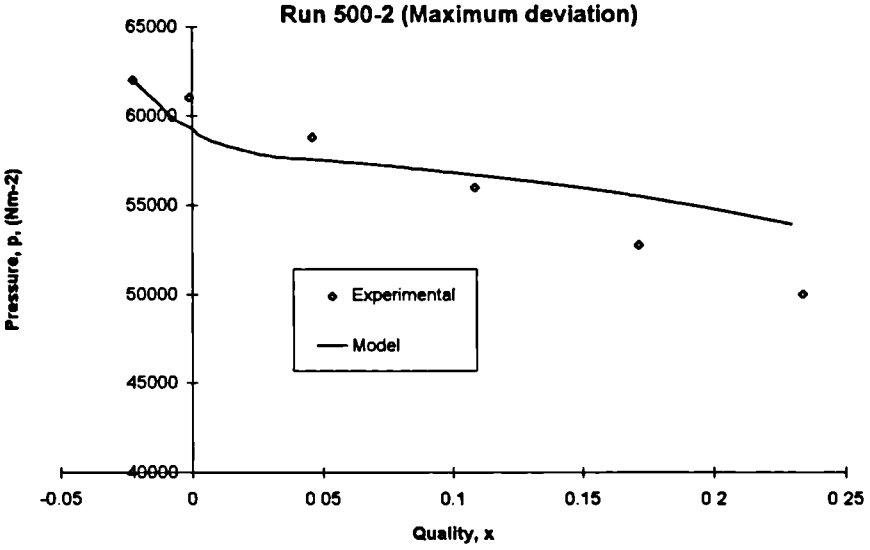

Figure 5.2c Comparison of the SAE modelling with experimentally measured pressure profiles for Run 1000-1 (Maximum deviation)

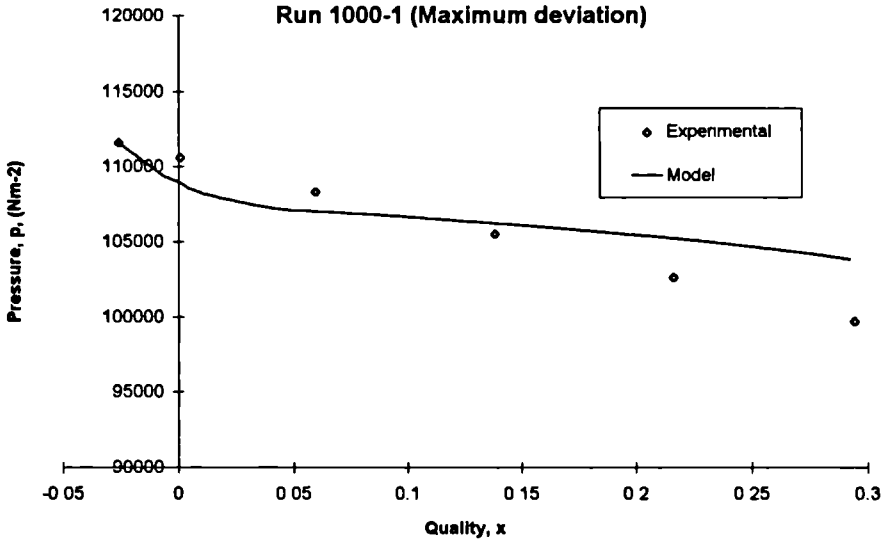

Figure 5.3 Typical experimental runs illustrating the changes in pressure gradient components as a result of increasing the mass flux

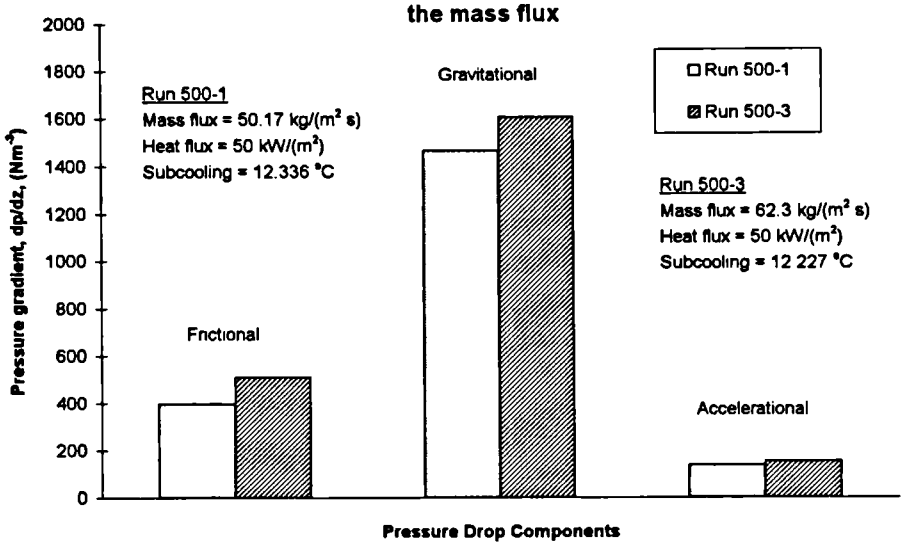

Figure 5.4 Typical experimental runs illustrating the changes in pressure gradient components as a result of decreasing the heat flux at low inlet subcoolings

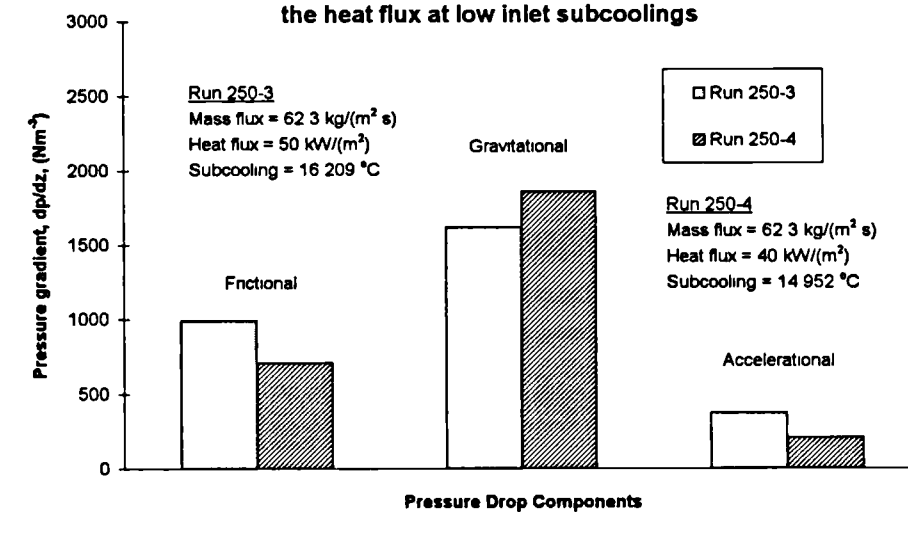

Figure 5.5 Typical experimental runs illustrating the changes in pressure gradient components as a result of decreasing the heat flux at high inlet subcoolings

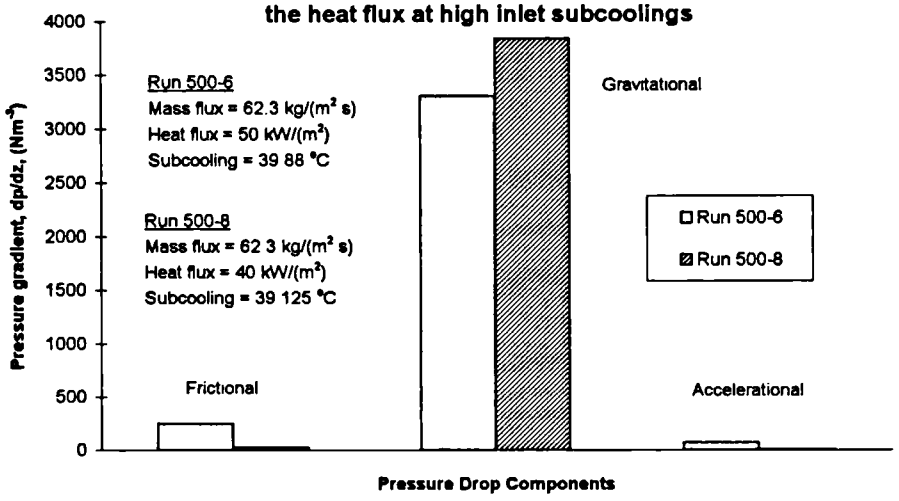

Figure 5.6 Typical experimental runs illustrating the changes in pressure gradient components as a result of increasing the outlet pressure at low inlet subcoolings

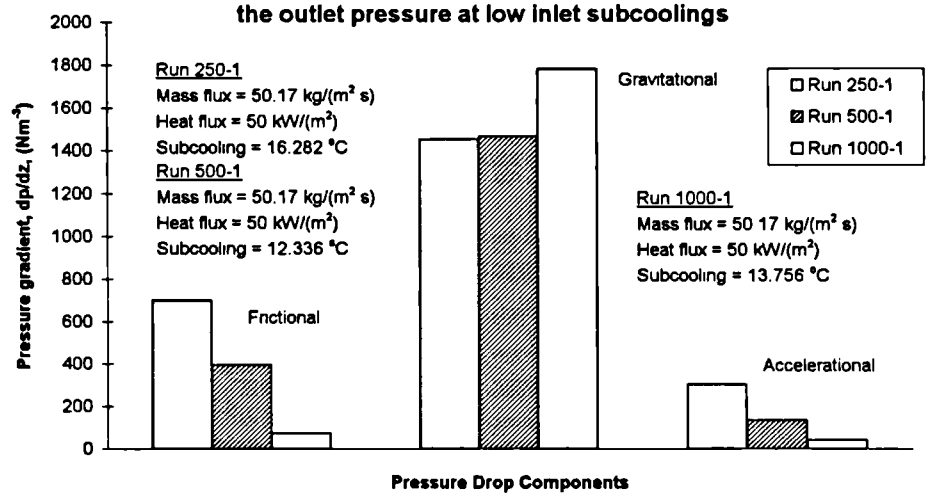

Figure 5.7 Typical experimental runs illustrating the changes in pressure gradient components as a result of increasing the outlet pressure at high inlet subcoolings

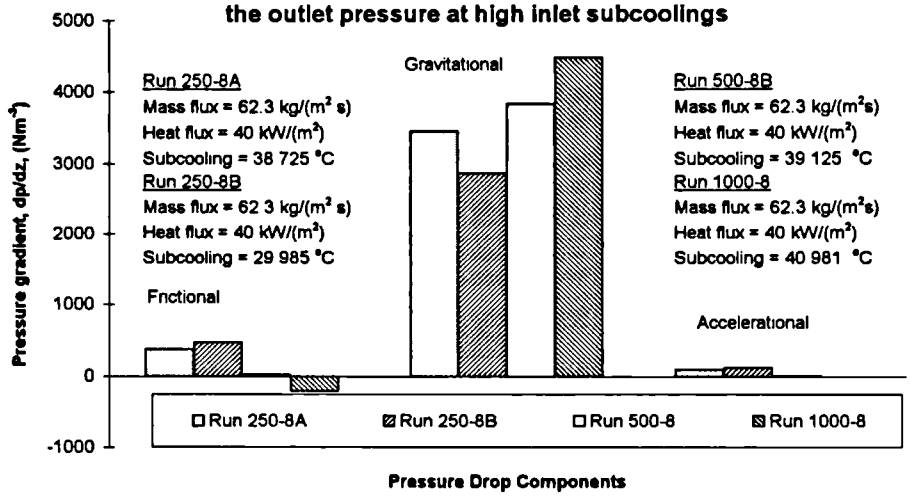

Figure 5.8 Typical experimental runs illustrating the changes in pressure gradient components as a result of increasing the inlet subcoolings

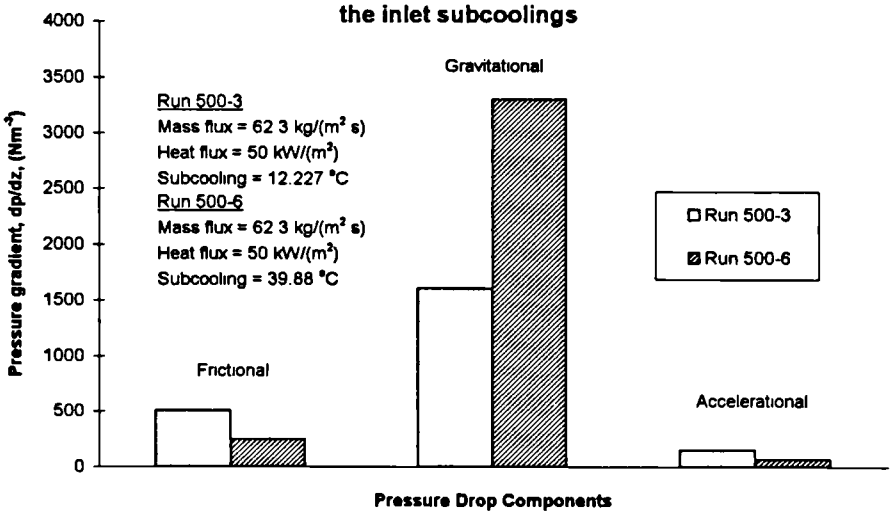

Figure 5.9 Comparison of measured and calculated fluid temperature profiles for a typical run at 250 mbar abs exit pressure (Run 250-1)

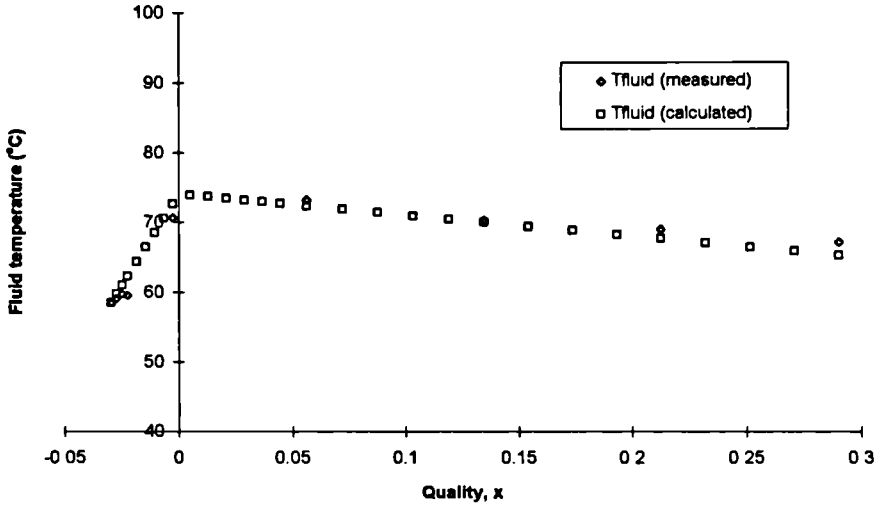

Figure 5.10 Comparison of measured and calculated fluid temperature profiles for a typical run at 500 mbar abs exit pressure (Run 500-1)

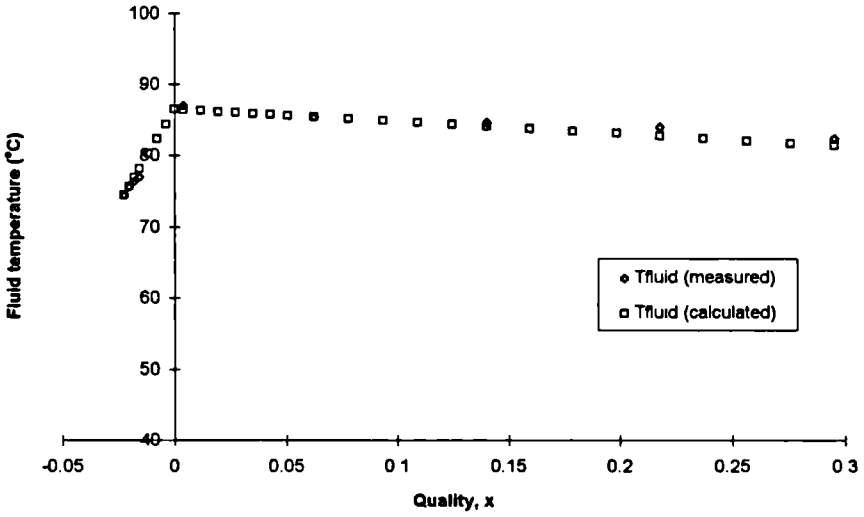

Figure 5.11 Comparison of measured and calculated fluid temperature profiles for a typical run at 1000 mbar abs exit pressure (Run 1000-1)

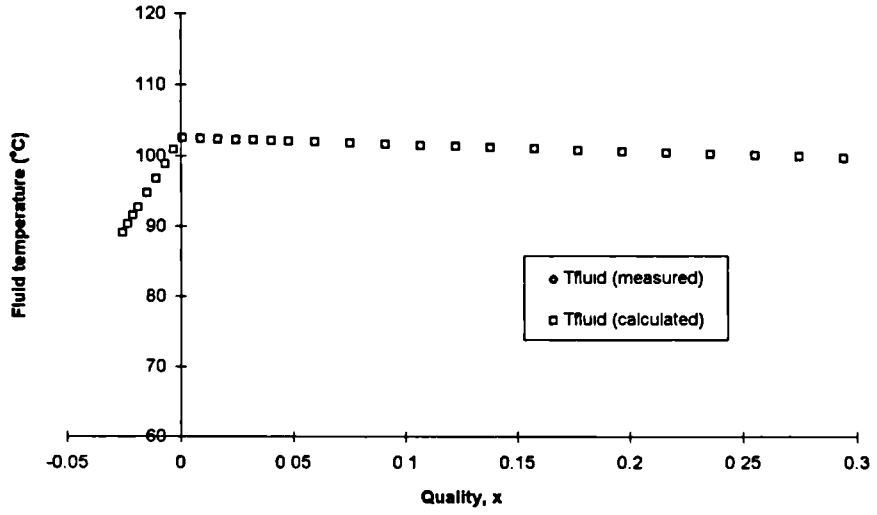

Figure 5.12 Repeated experimental runs for 250-1

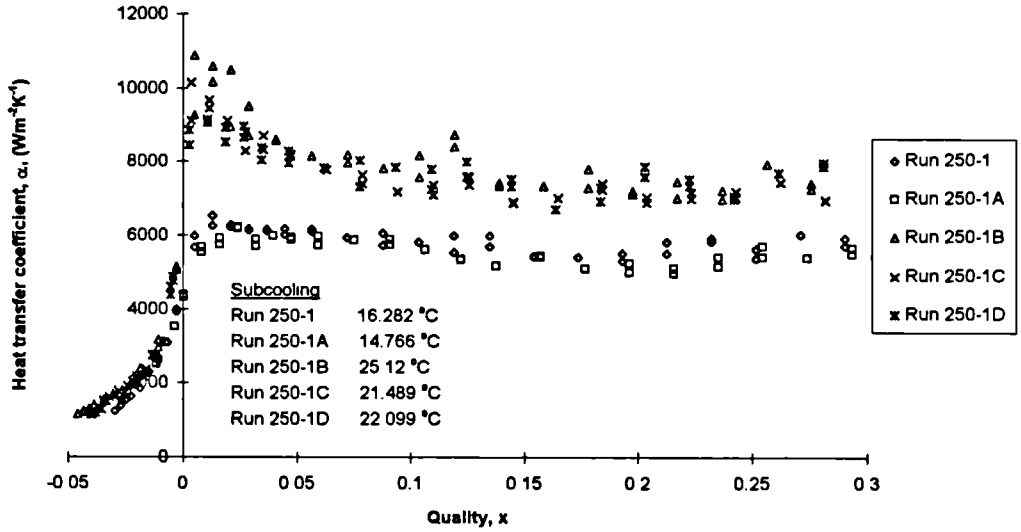

Figure 5.13 Repeated experimental runs for 250-2

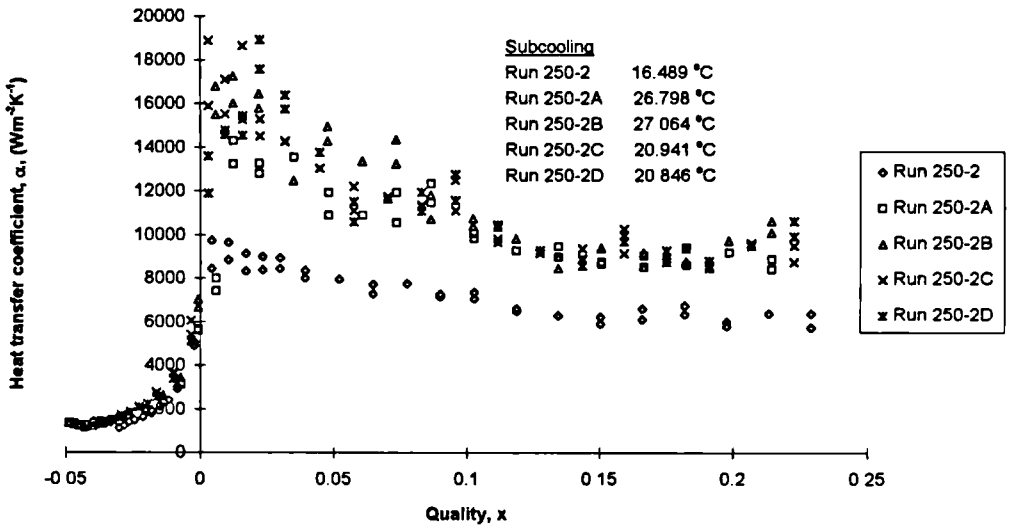

Figure 5.14 Repeated experimental runs for 250-3

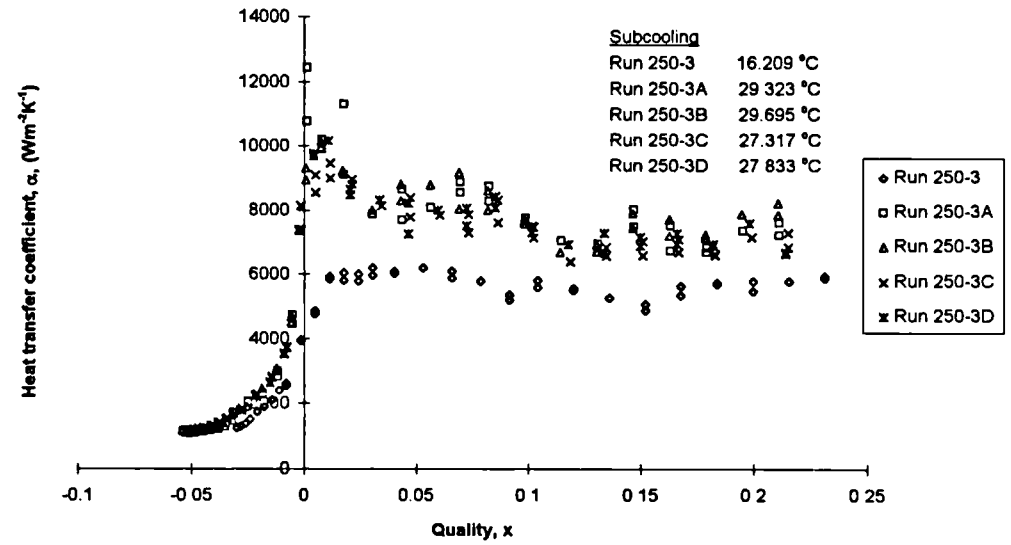

Figure 5.15 Repeated experimental runs for 250-4

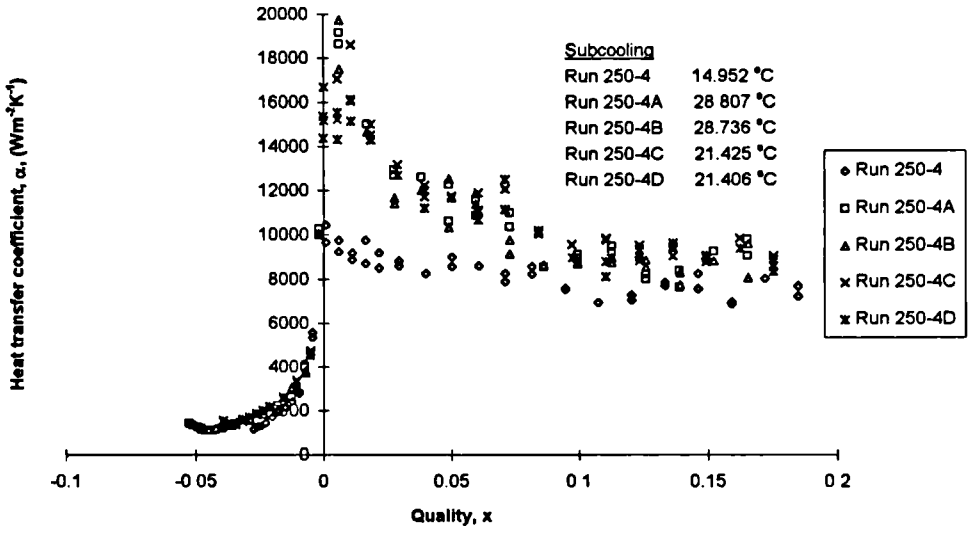

Figure 5.16 Comparison of mass flux variation for Runs 250-1 and 250-3

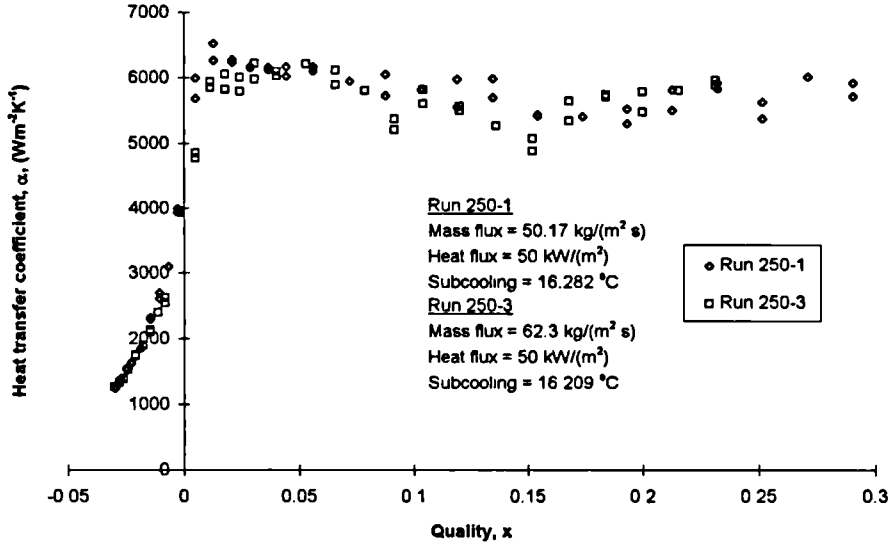

Figure 5.17 Comparison of mass flux variation for Runs 250-2 and 250-4

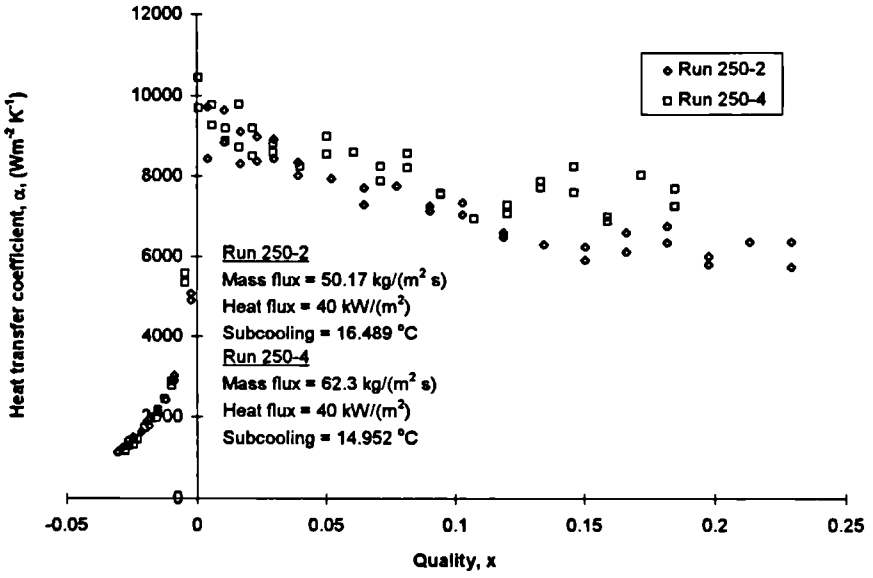

Figure 5.18 Comparison of mass flux variation for Runs 250-5 and 250-6

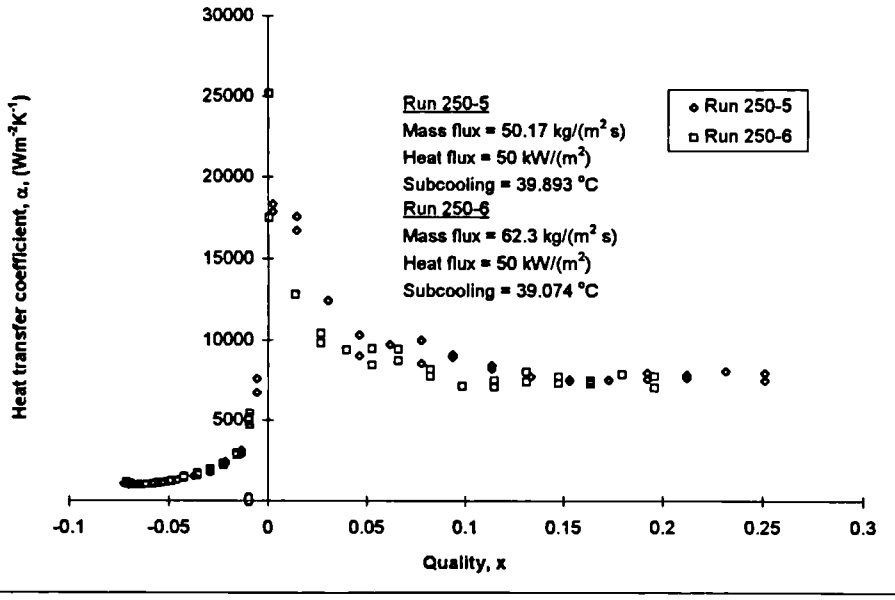

Figure 5.19 Comparison of mass flux variation for Runs 250-7A and 250-8A

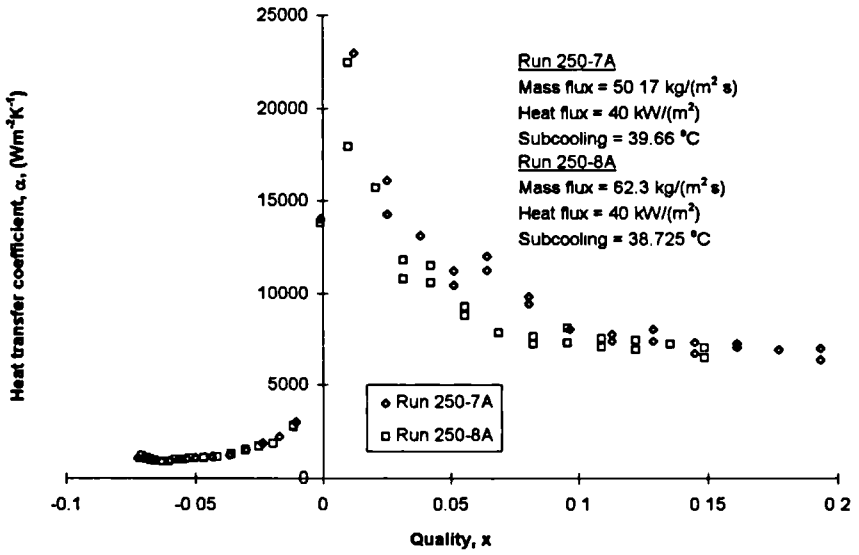

Figure 5.20 Comparison of mass flux variation for Runs 250-7B and 250-8B

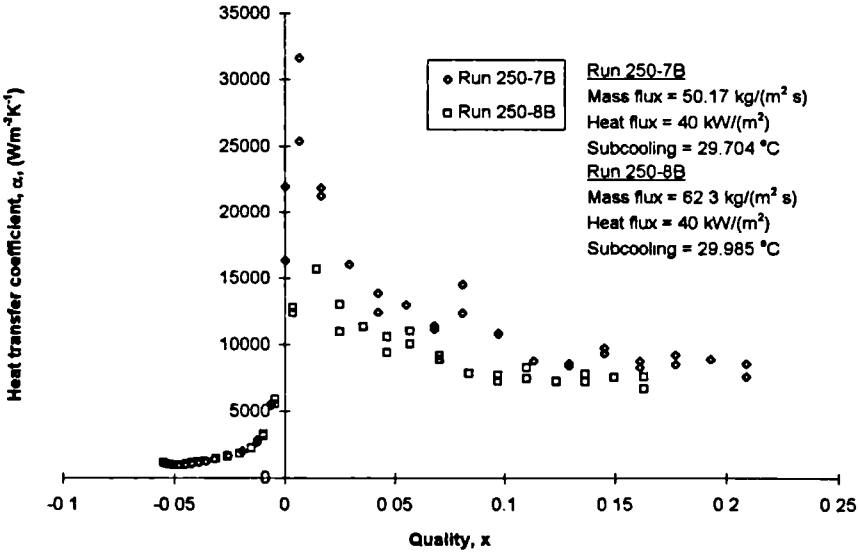

Figure 5.21 Comparison of mass flux variation for Runs 500-1 and 500-3

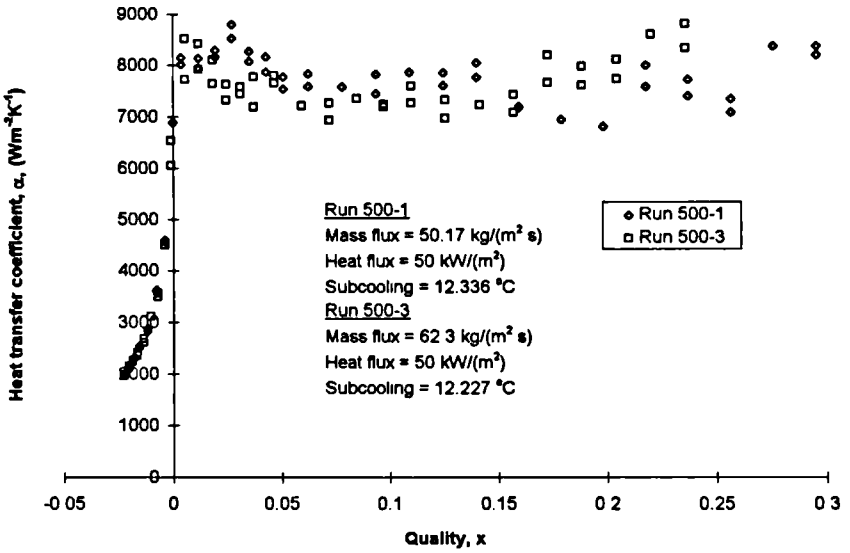

Figure 5.22 Comparison of mass flux variation for Runs 500-2 and 500-4

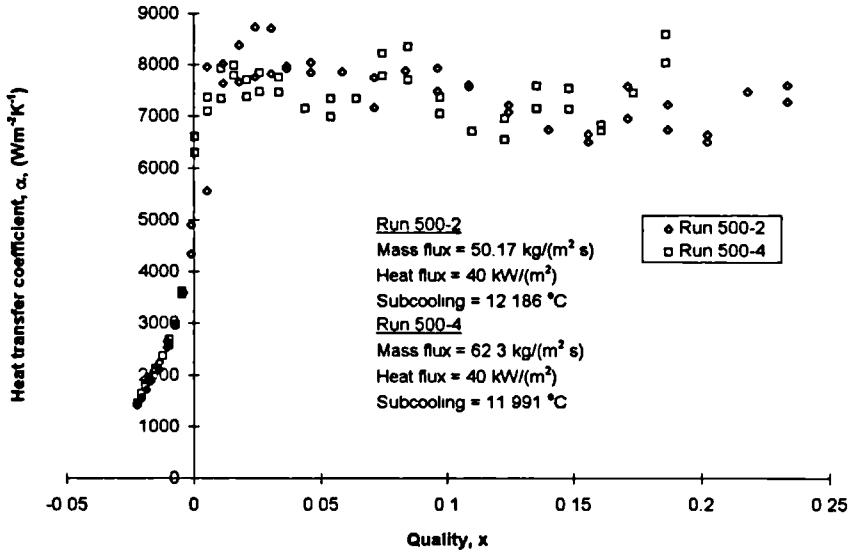

Figure 5.23 Comparison of mass flux variation for Runs 500-5 and 500-6

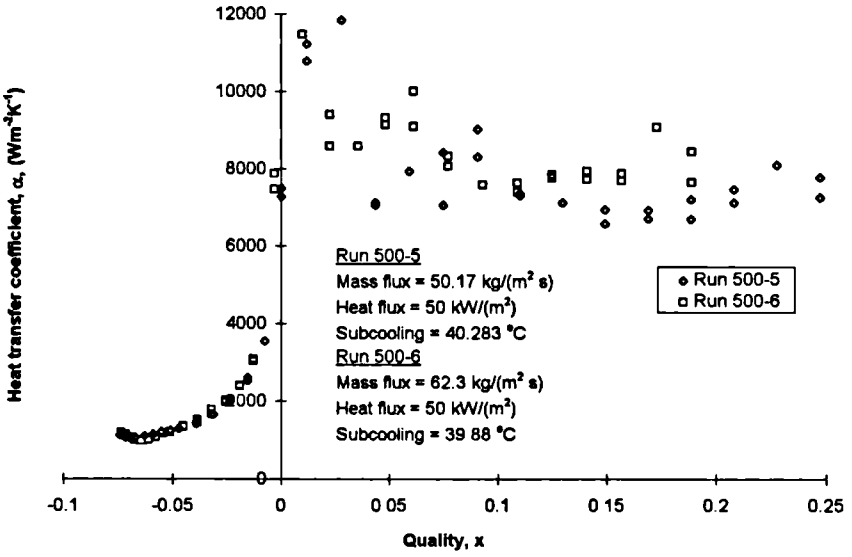

Figure 5.24 Comparison of mass flux variation for Runs 500-7 and 500-8

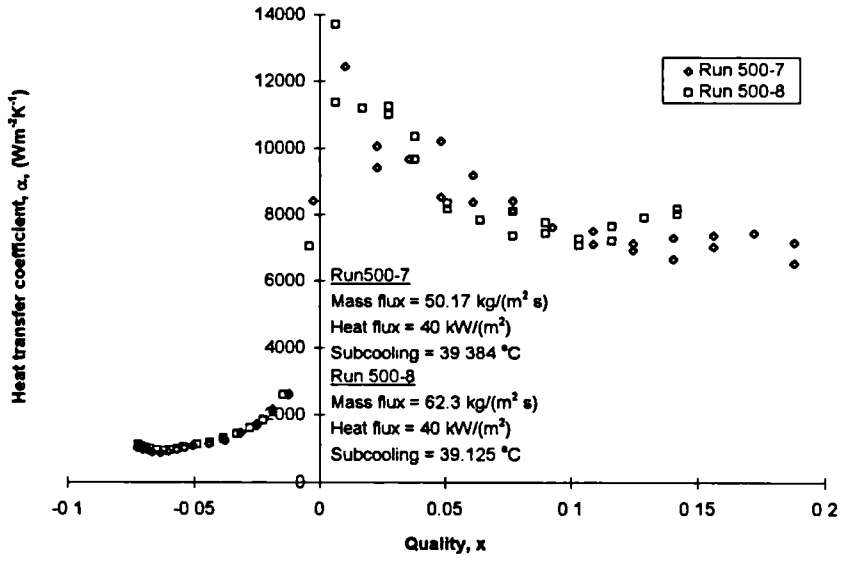

Figure 5.25 Comparison of mass flux variation for Runs 1000-1 and 1000-3

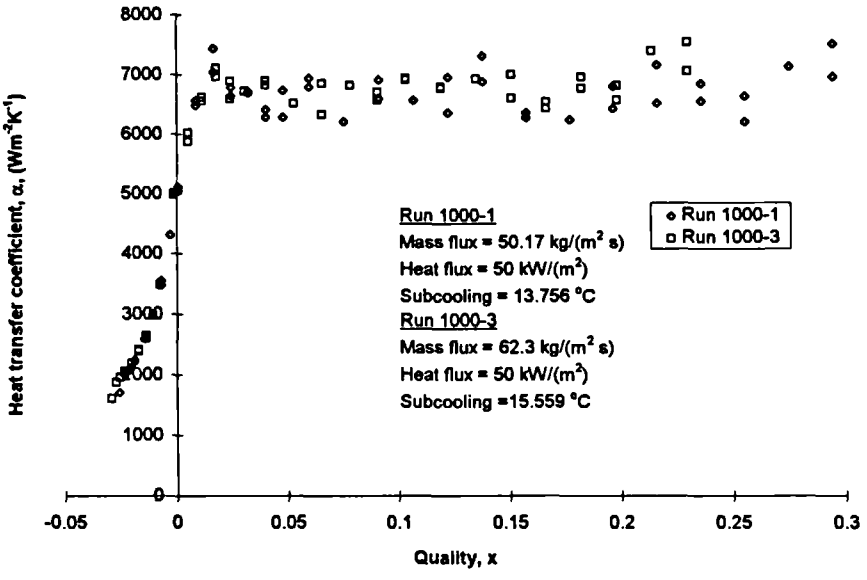

Figure 5.26 Comparison of mass flux variation for Runs 1000-2 and 1000-4

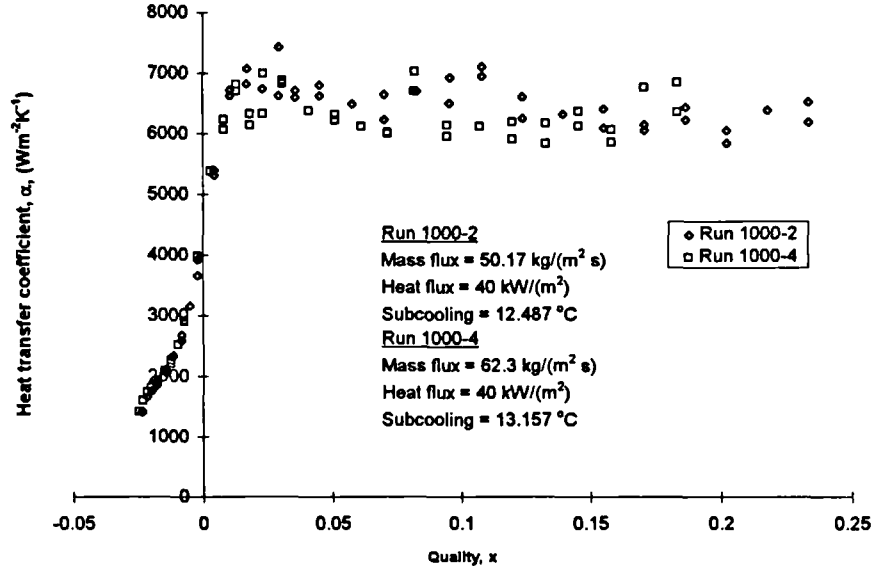

Figure 5.27 Comparison of mass flux variation for Runs 1000-5 and 1000-6

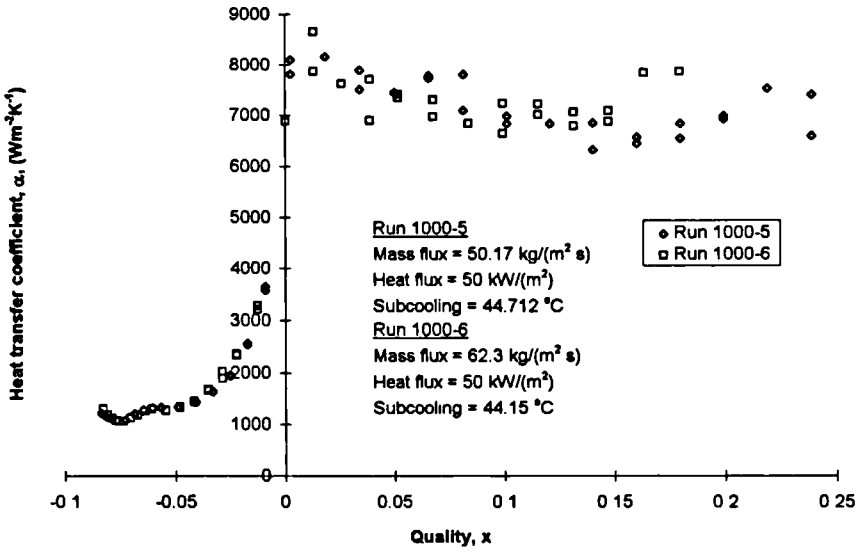

Figure 5.28 Comparison of mass flux variation for Runs 1000-7 and 1000-8

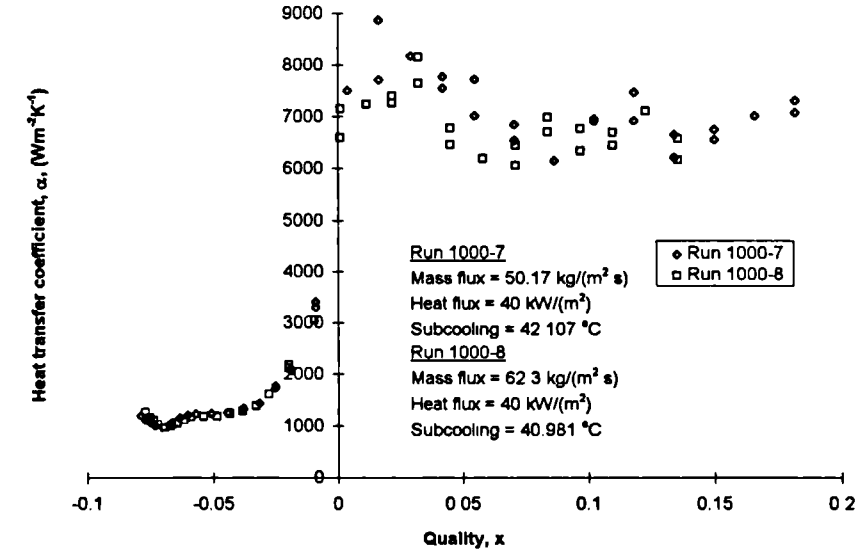

Figure 5.29 Comparison of Repeated Runs 250-2A and 2B against Runs 250-4A and 4B

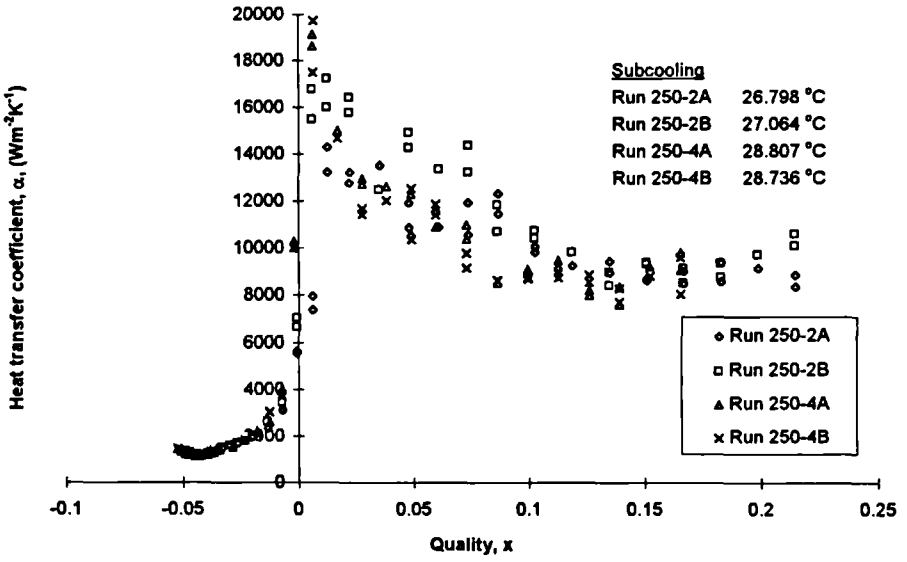

Figure 5.30 Comparison of Repeated Runs 250-2C and 2D against Runs 250-4C and 4D

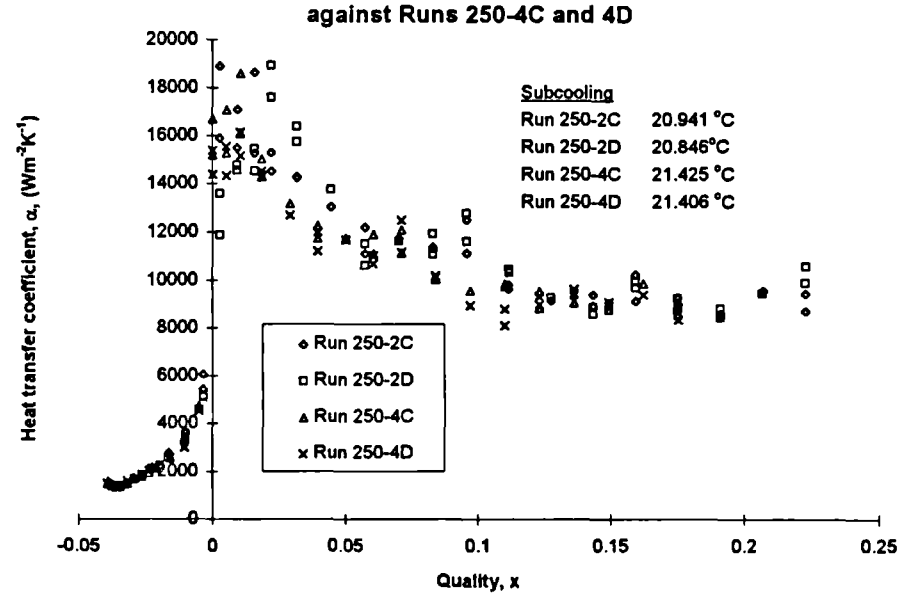

Figure 5.31 Comparison of Repeated Run 250-1A against Run 250-3

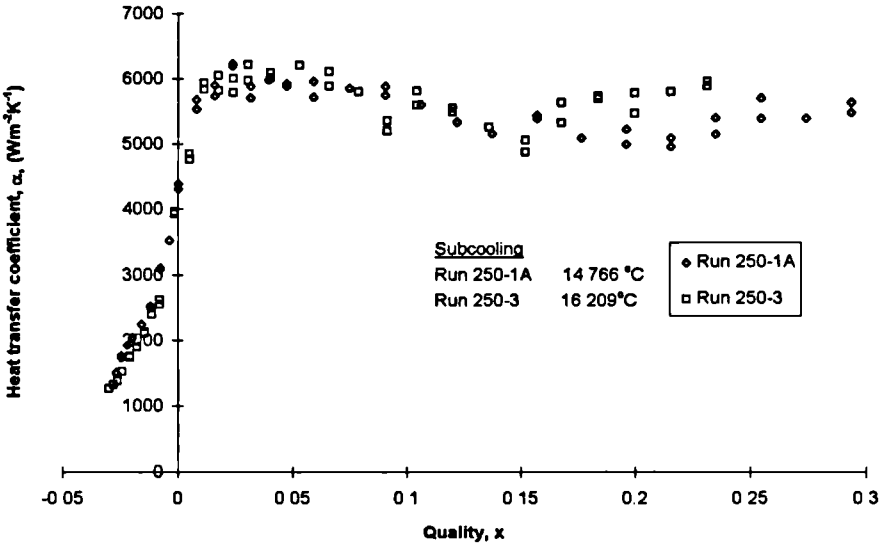

Figure 5.32 Comparison of Repeated Run 250-1B against Runs 250-3C and 3D

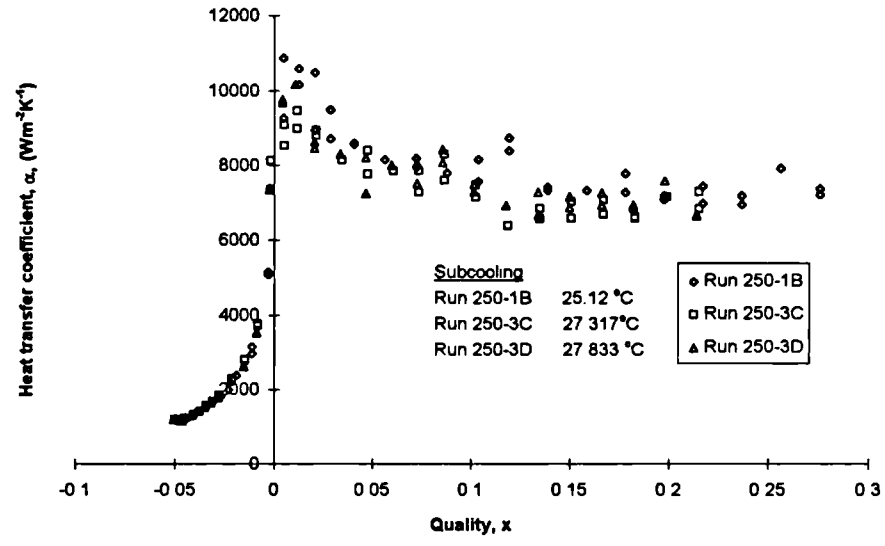

Figure 5.33 Comparison of mass flux variation for Runs 250-2 and 250-4 with error analysis

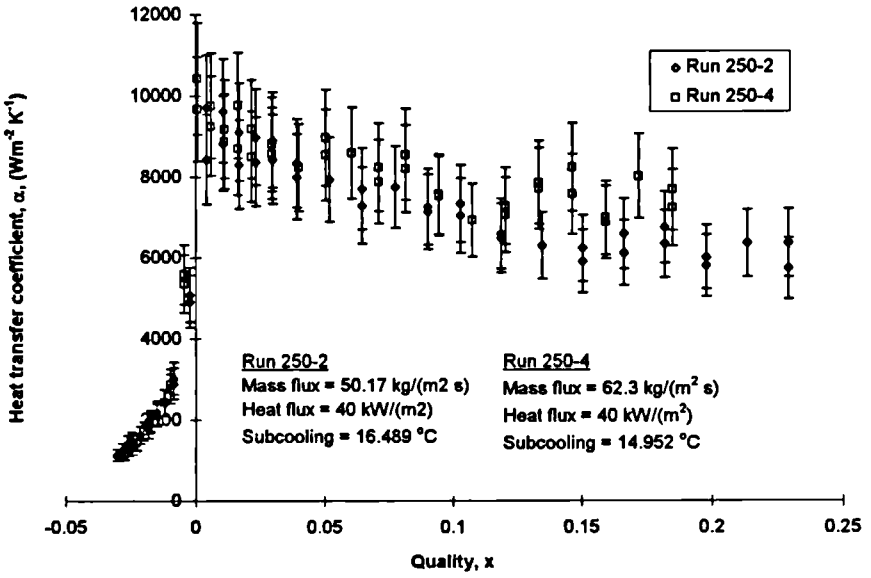

Figure 5.34 Comparison of mass flux variation for Runs 500-5 and 500-6 with error analysis

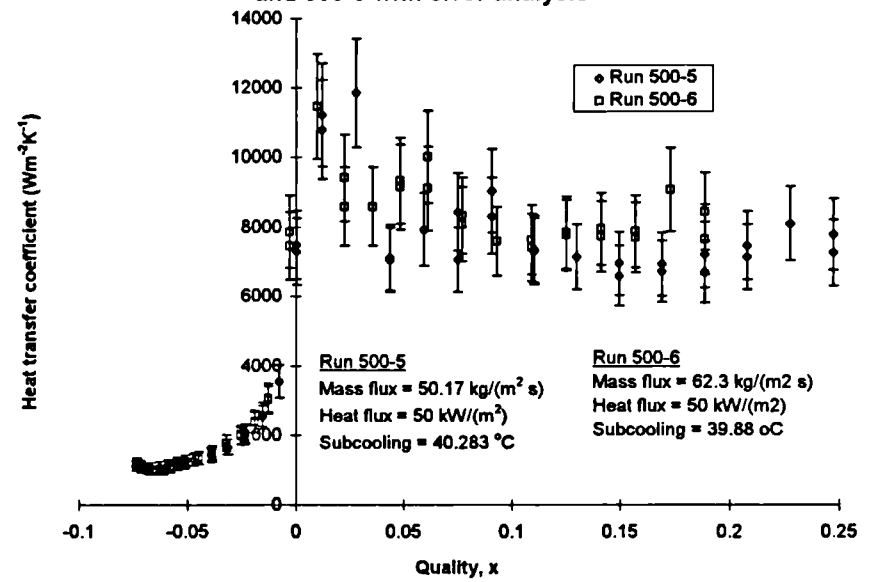

Figure 5.35 Comparison of heat flux variation for Runs 250-1 and 250-2

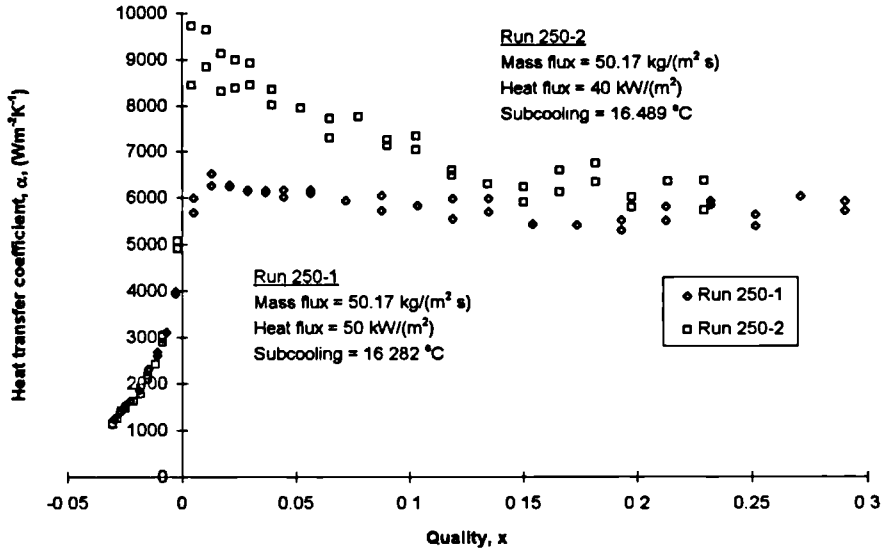

Figure 5.36 Comparison of heat flux variation for Runs 250-3 and 250-4

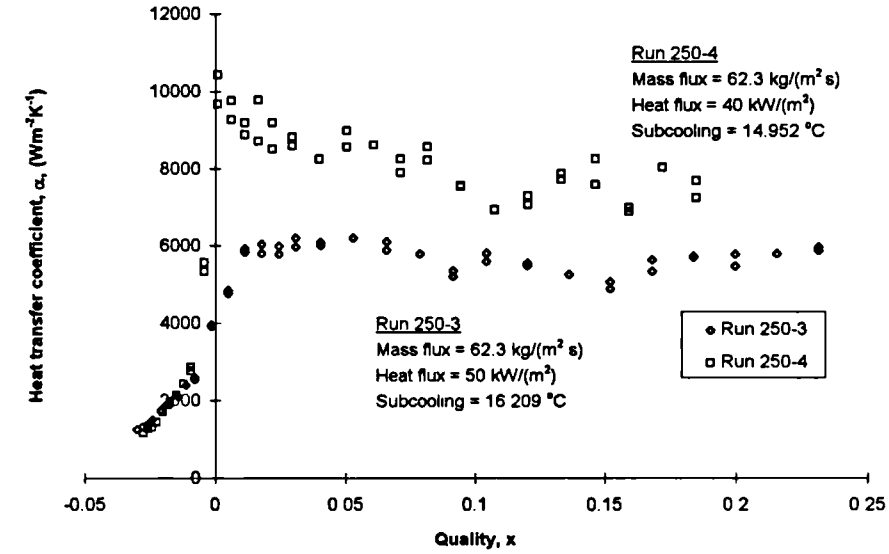

Figure 5.37 Comparison of heat flux variation for Runs 250-5 and 250-7A

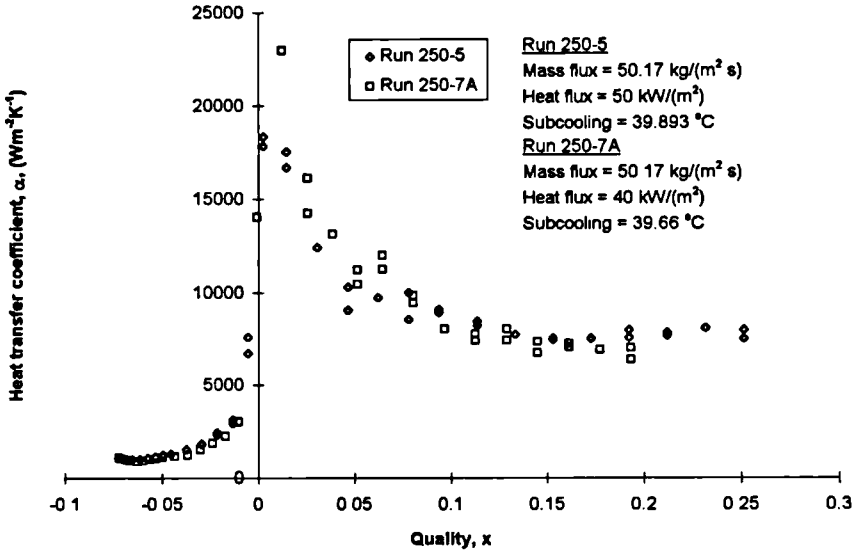

Figure 5.38 Comparison of heat flux variation for Runs 250-6 and 250-8A

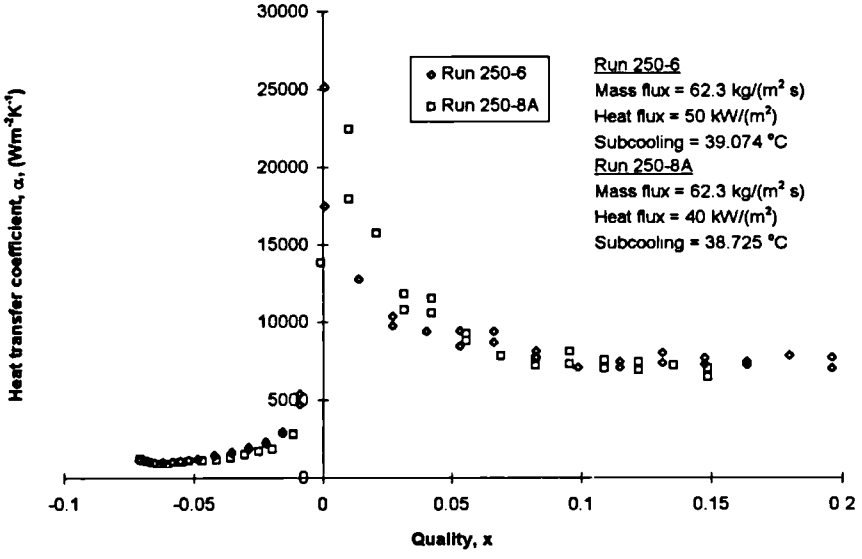

Figure 5.39 Comparison of heat flux variation for Runs 500-1 and 500-2

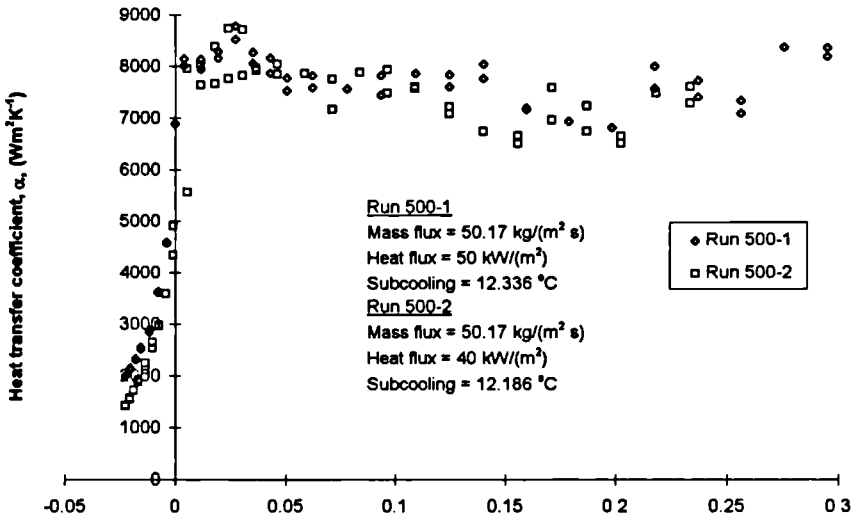

Figure 5.40 Comparison of heat flux variation for Runs 500-3 and 500-4

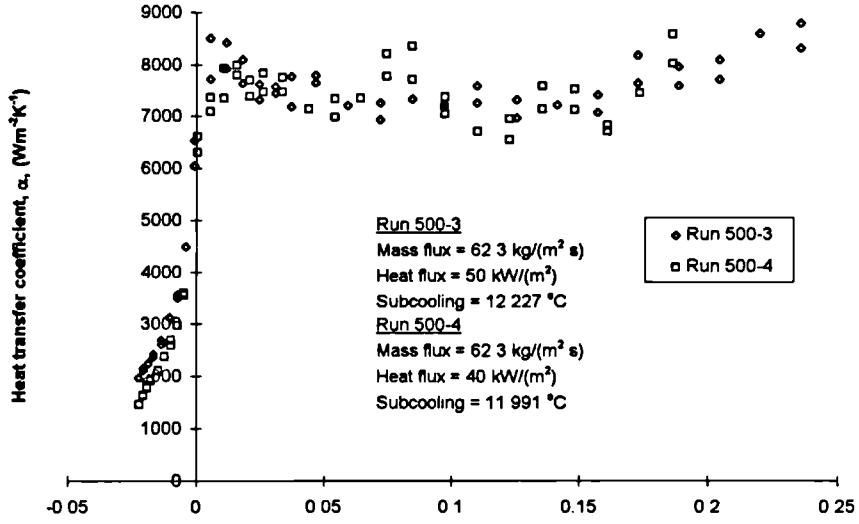

Figure 5.41 Comparison of heat flux variation for Runs 500-5 and 500-7

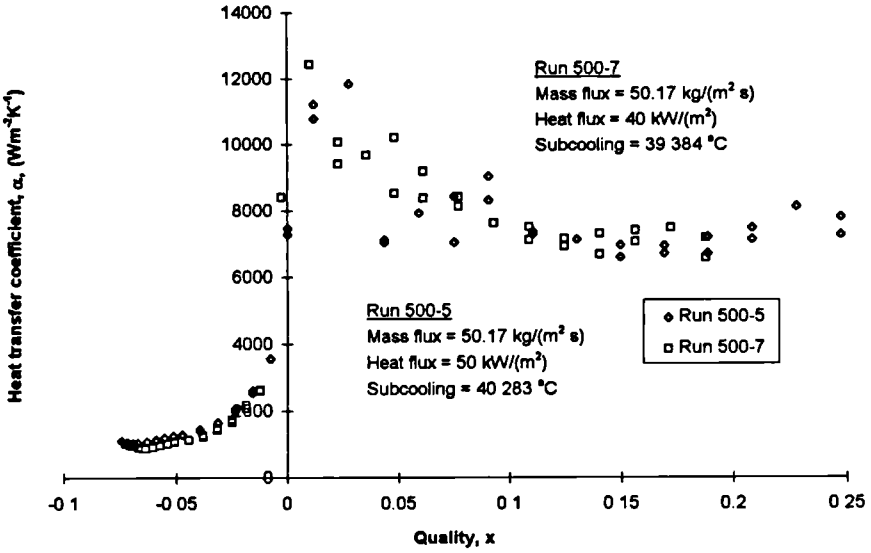

Figure 5.42 Comparison of heat flux variation for Runs 500-6 and 500-8

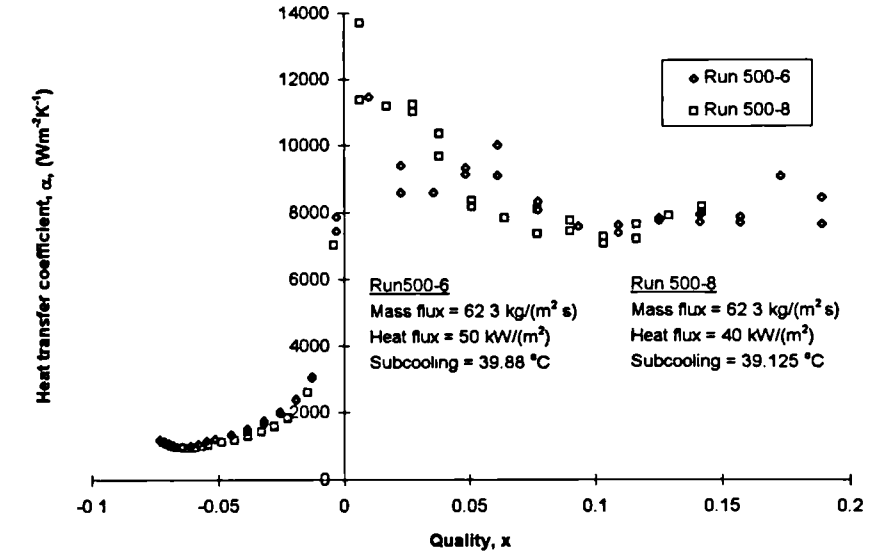

Figure 5.43 Comparison of heat flux variation for Runs 1000-1 and 1000-2

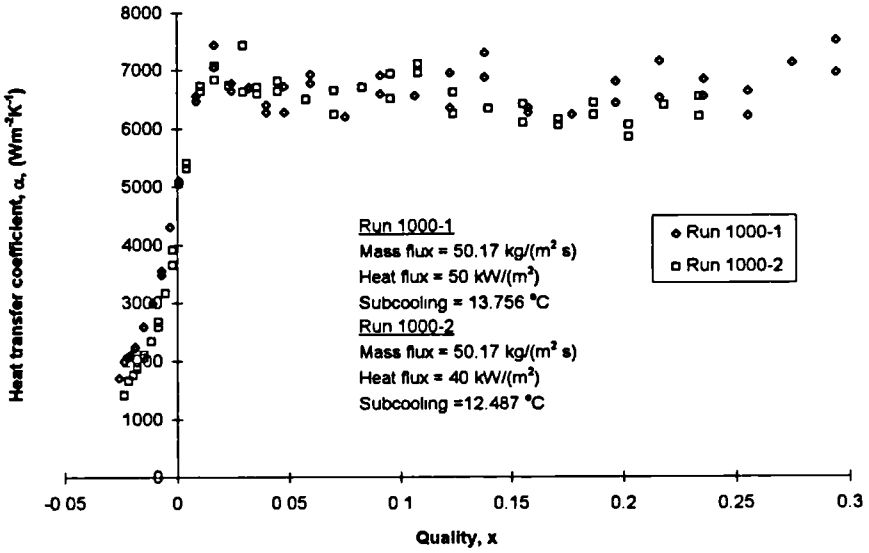

Figure 5.44 Comparison of heat flux variation for Runs 1000-3 and 1000-4

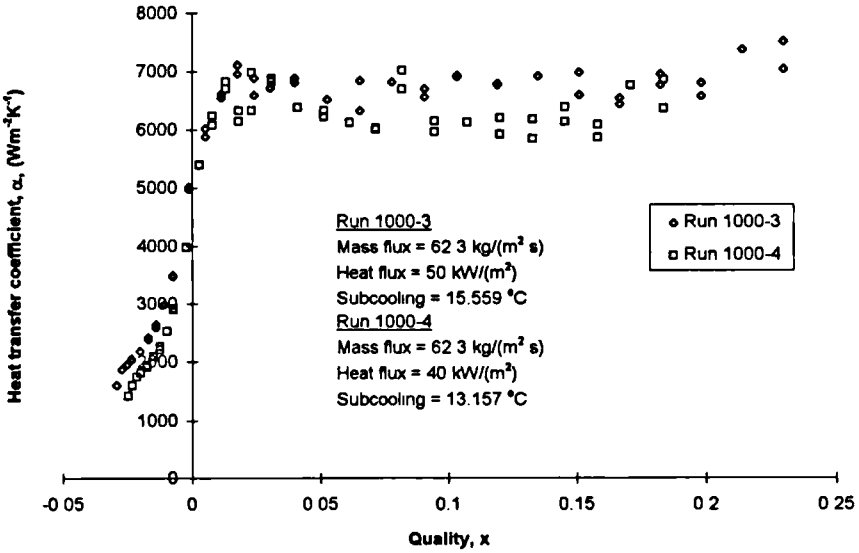

Figure 5.45 Comparison of heat flux variation for Runs 1000-5 and 1000-7

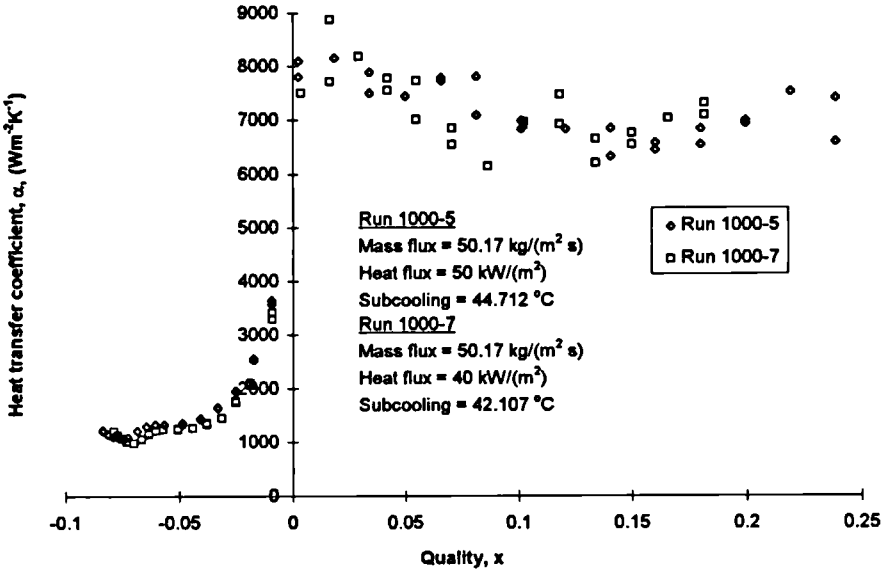

Figure 5.46 Comparison of heat flux variation for Runs 1000-6 and 1000-8

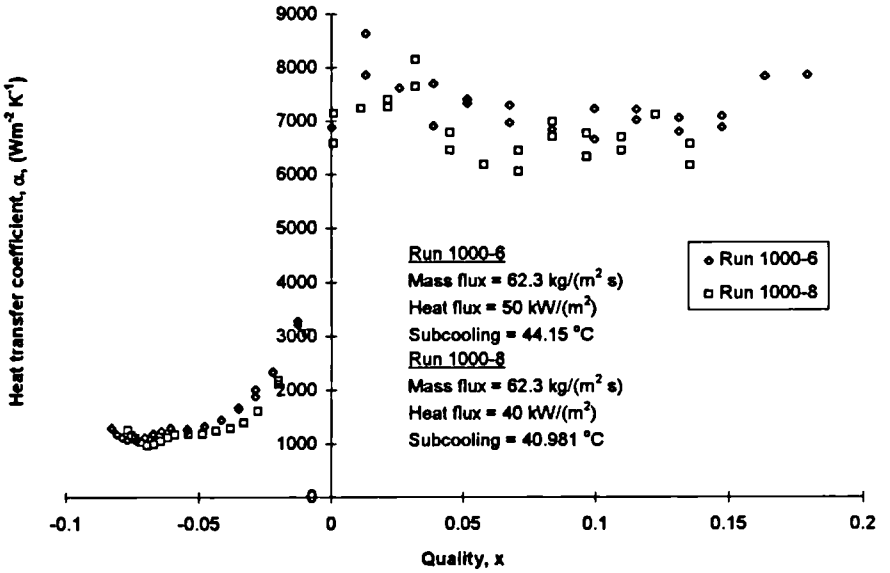

Figure 5.47 Wall temperature profiles along the test section for Runs 250-1 and 250-2

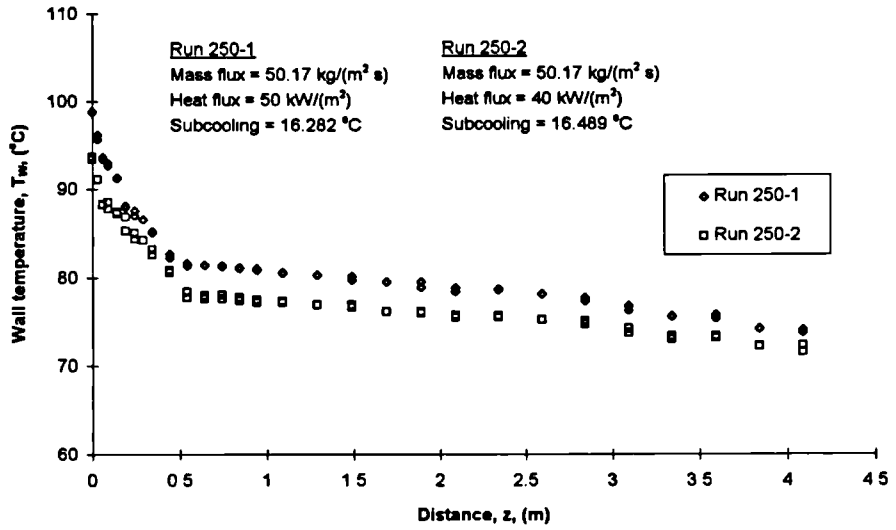

Figure 5.48 Wall temperature profiles along the test section for Runs 250-3 and 250-4

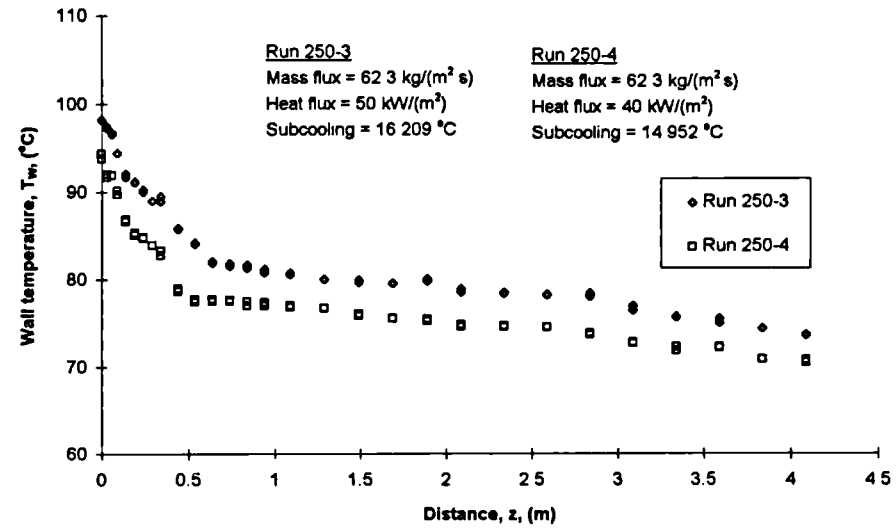

Figure 5.49 Wall temperature profiles along the test section for Runs 500-1 and 500-2

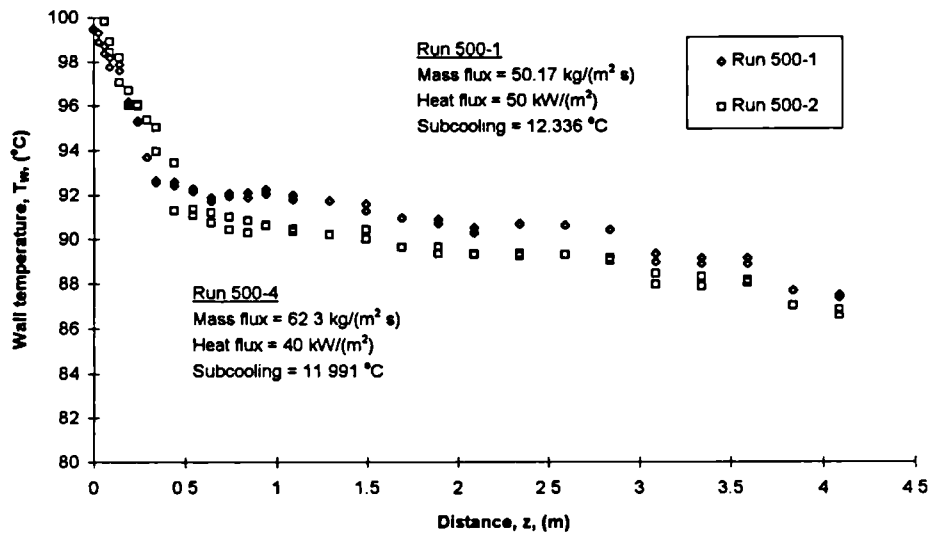

Figure 5.50 Wall temperature profiles along the test section for Runs 500-3 and 500-4

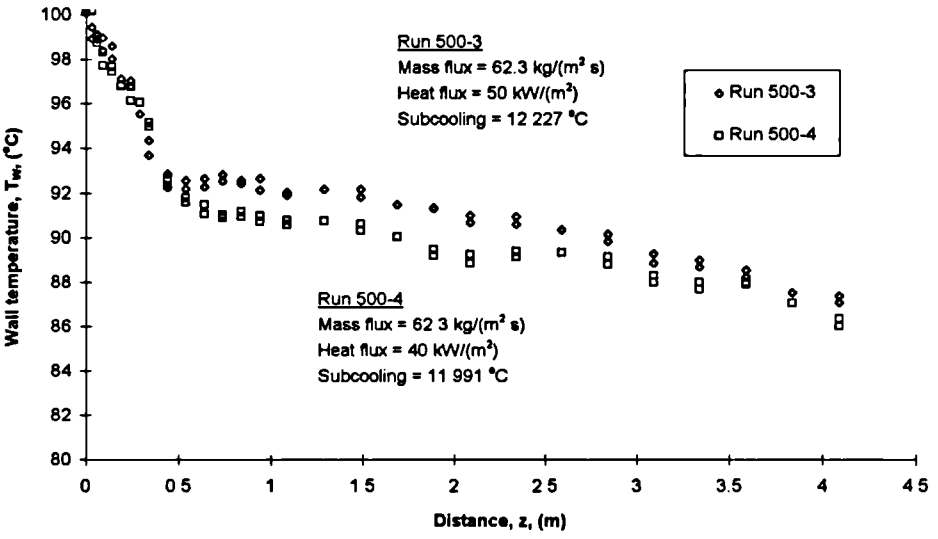

Figure 5.51 Wall temperature profiles along the test section for Runs 1000-1 and 1000-2

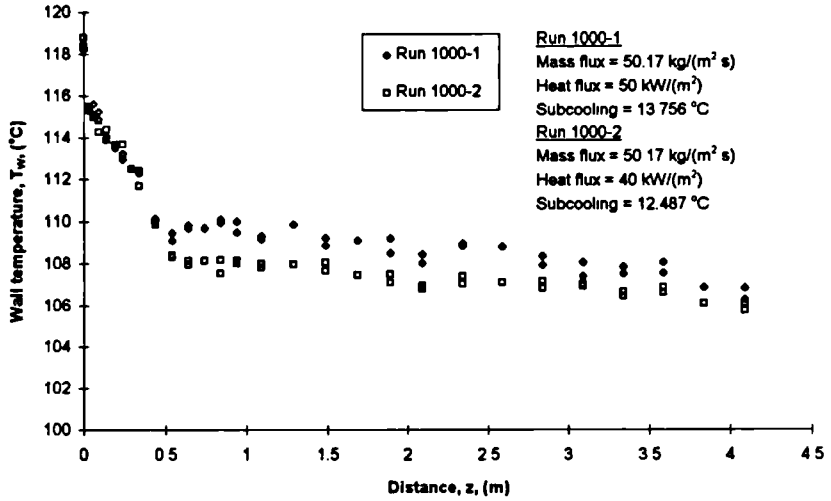

Figure 5.52 Wall temperature profiles along the test section for Runs 1000-3 and 1000-4

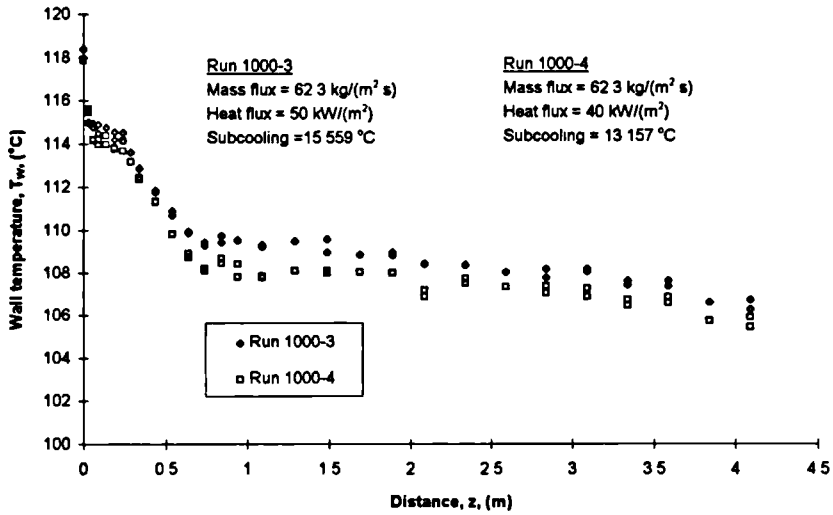

Figure 5.53 Comparison of heat flux variation for repeated runs 250-1B, 250-2A and 250-2B

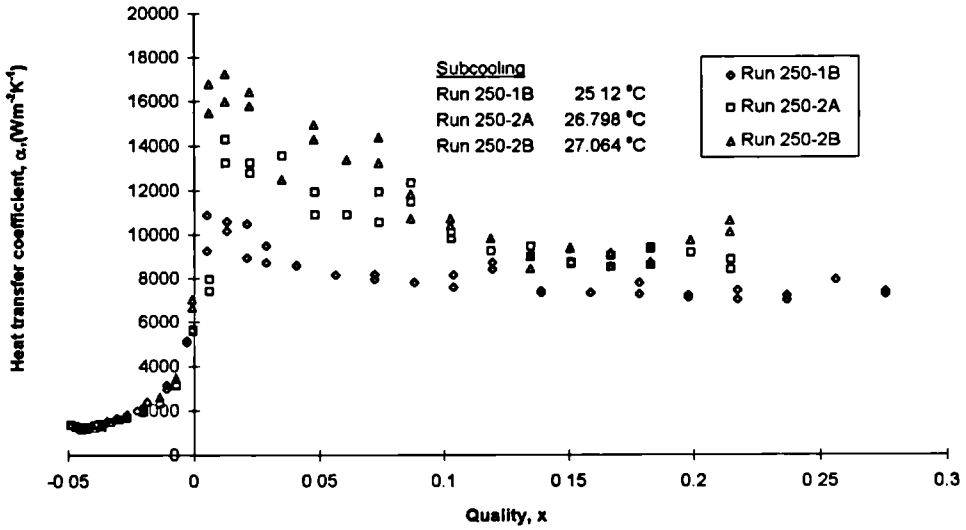

Figure 5.54 Comparison of heat flux variation for repeated runs 250-1C, 250-1D, 250-2C and 250-2D

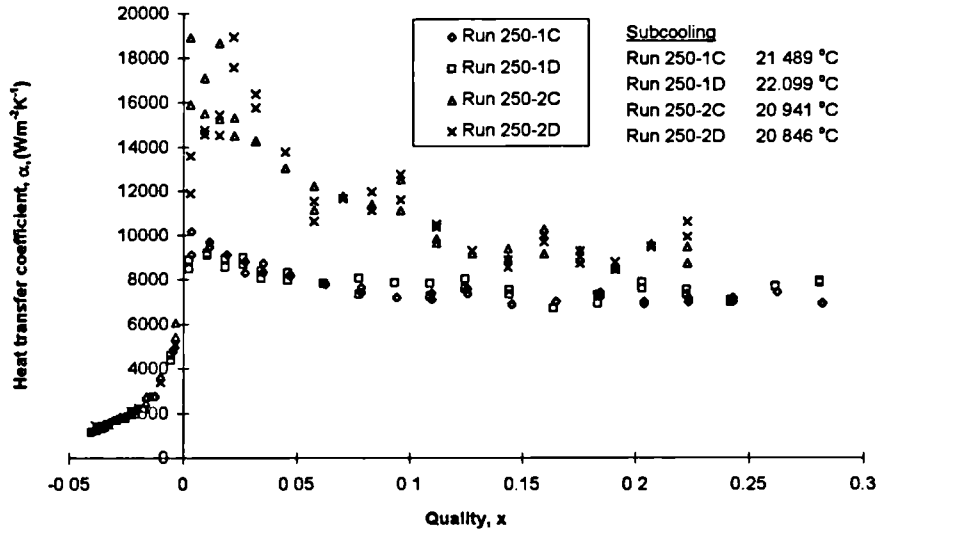

Figure 5.55 Wall temperature profiles for repeated runs 250-1B, 250-2A and 250-2B

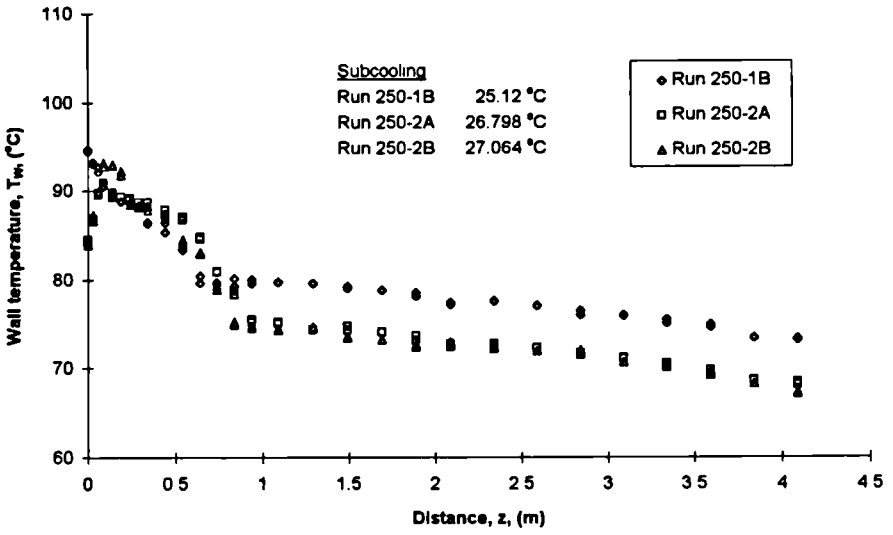

Figure 5.56 Wall temperature profiles for repeated runs 250-1C, 250-1D, 250-2C and 250-2D

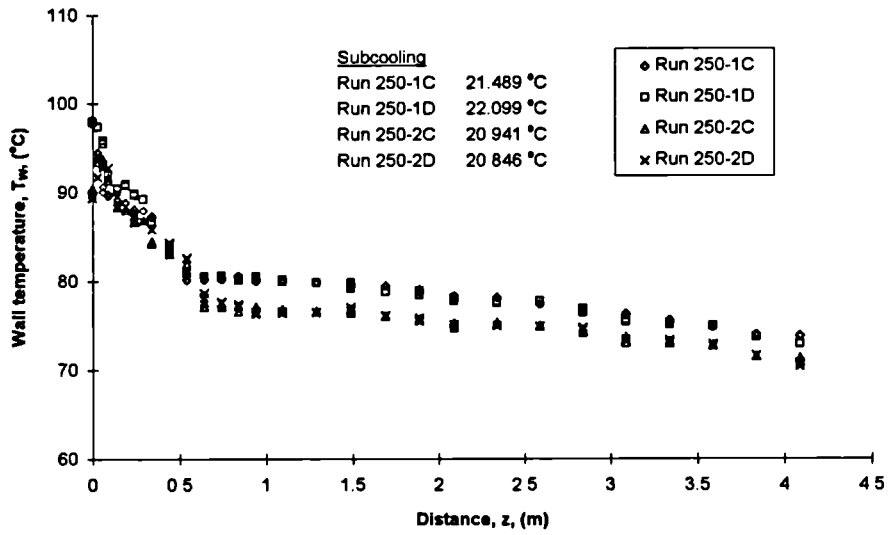

Figure 5.57 Comparison of heat flux variation for repeated runs 250-3A-D, 250-4A and 250-4B

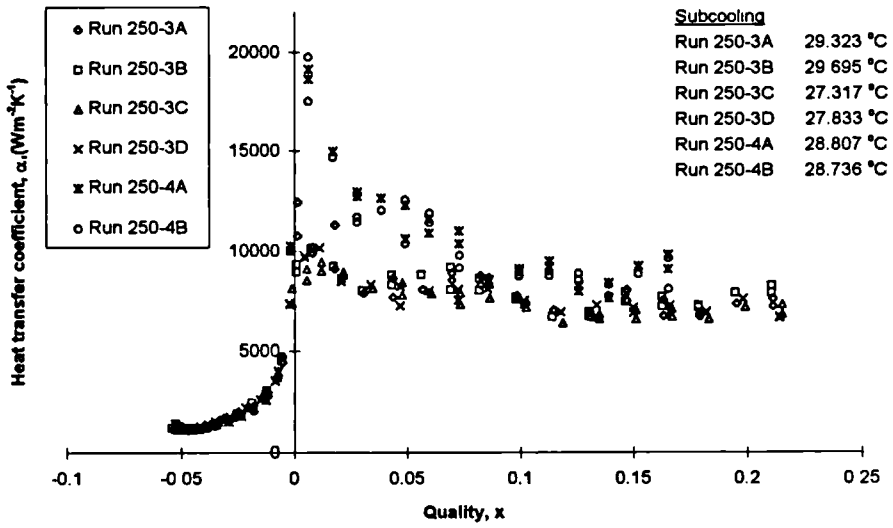

Figure 5.58 Wall temperature profiles for repeated runs 250-3A-D, 250-4A and 250-4B

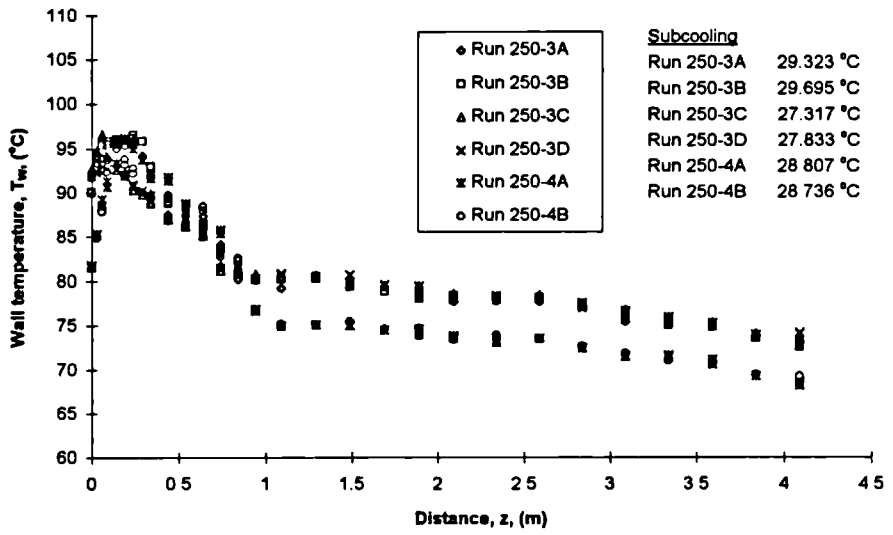

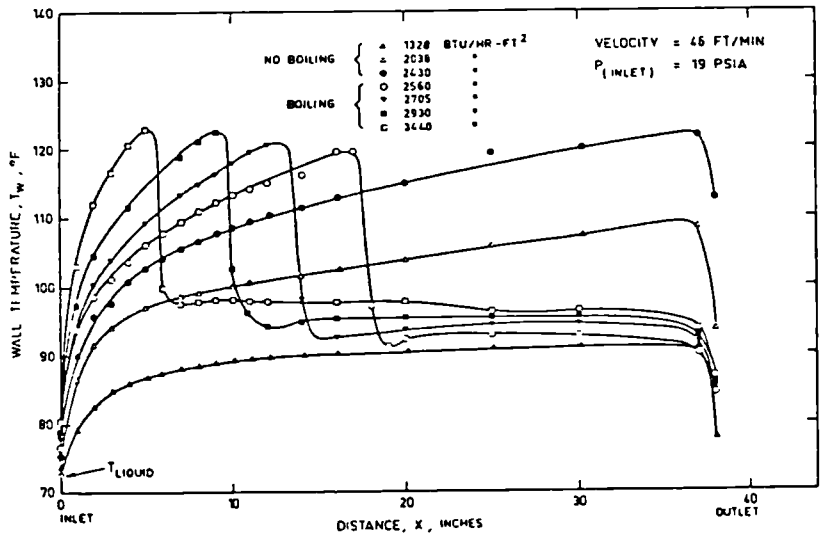

Figure 5.59 Temperature profiles along the test section for increasing heat flux (Abdelmessih et al., 1974)

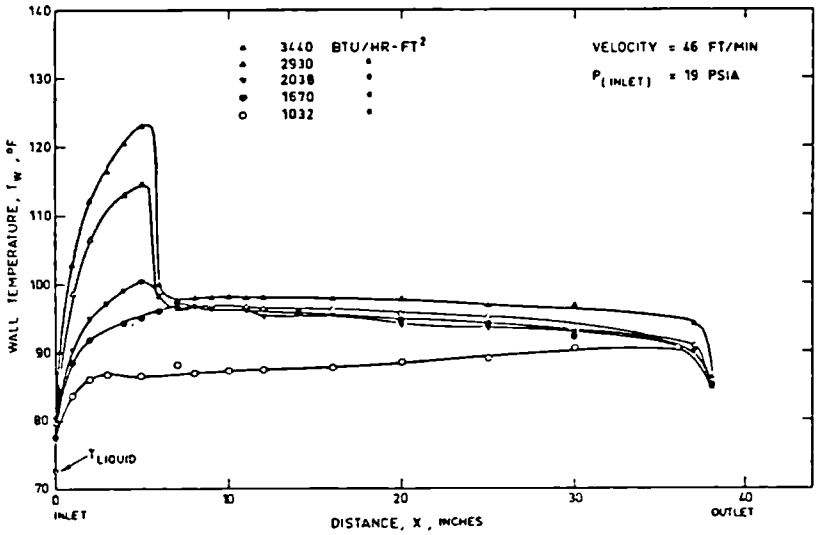

Figure 5.60 Temperature profiles along the test section for decreasing heat flux (Abdelmessih et al., 1974)

Figure 5.61 Comparison of outlet pressure variation for Runs 250-1, 500-1 and 1000-1

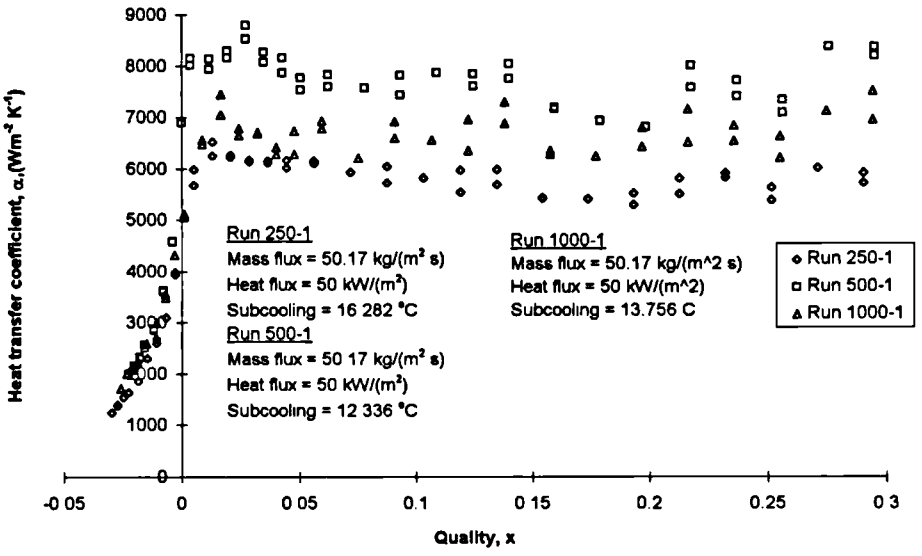

Figure 5.62 Comparison of outlet pressure variation for Runs 250-2, 500-2 and 1000-2

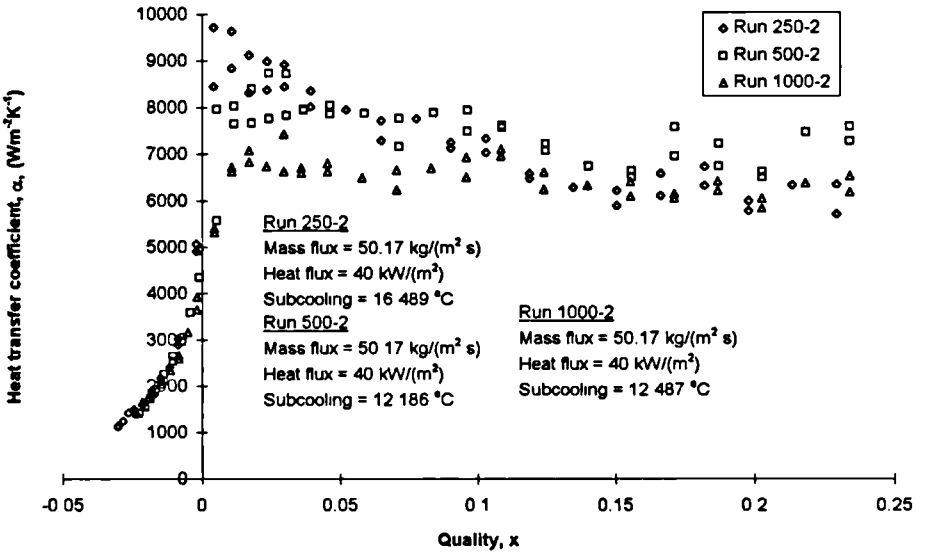

Figure 5.63 Comparison of outlet pressure variation for Runs 250-3, 500-3 and 1000-3

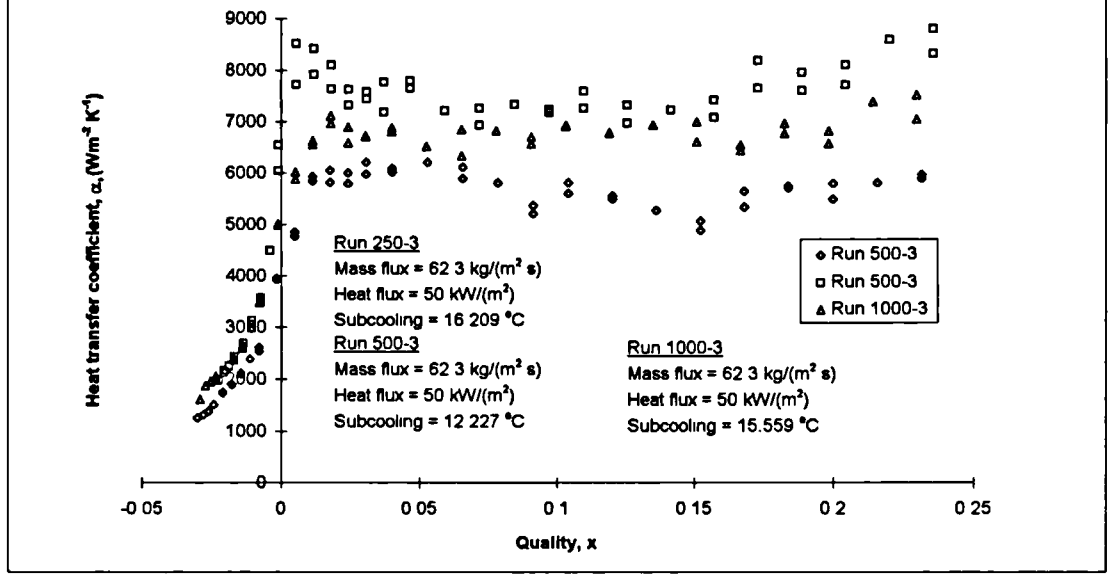

Figure 5.64 Comparison of outlet pressure variation for Runs 250-4, 500-4 and 1000-4

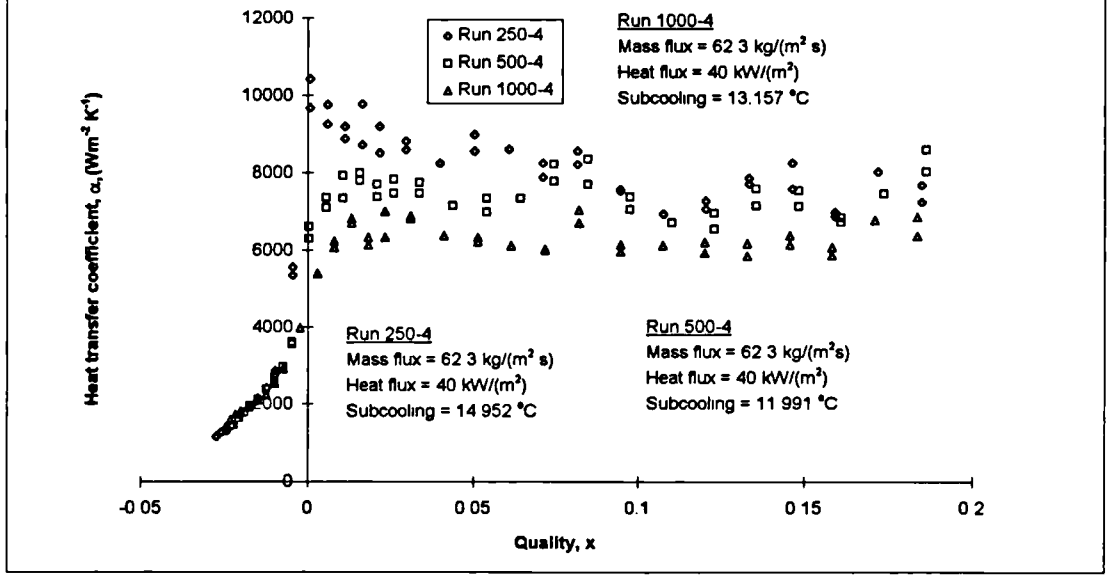

Figure 5.65 Comparison of outlet pressure variation for Runs 250-5, 500-5 and 1000-5

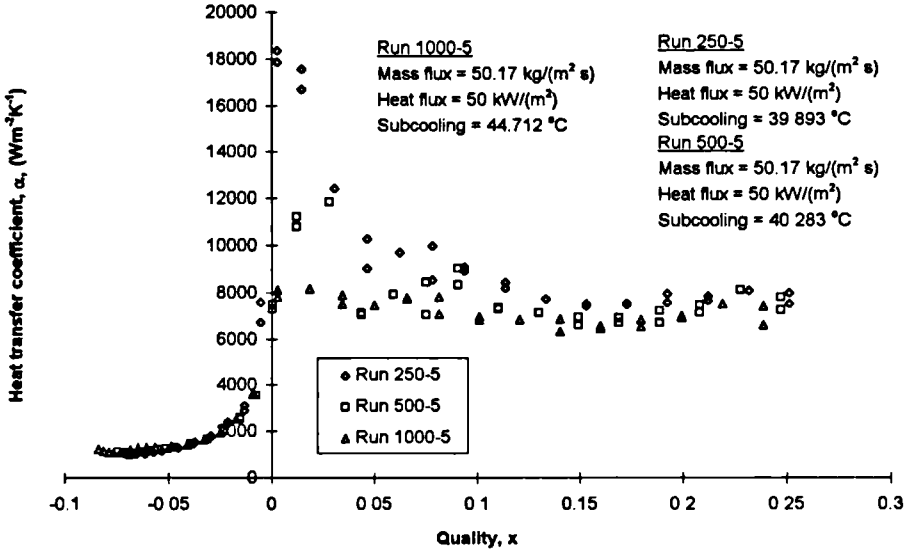

Figure 5.66 Comparison of outlet pressure variation for Runs 250-6, 500-6 and 1000-6

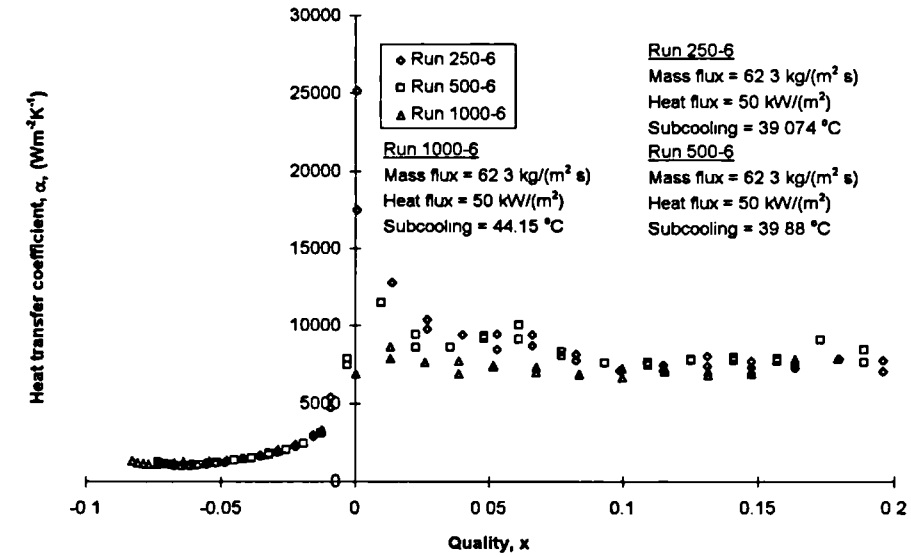

Figure 5.67 Comparison of outlet pressure variation for Runs 250-7A, 500-7 and 1000-7

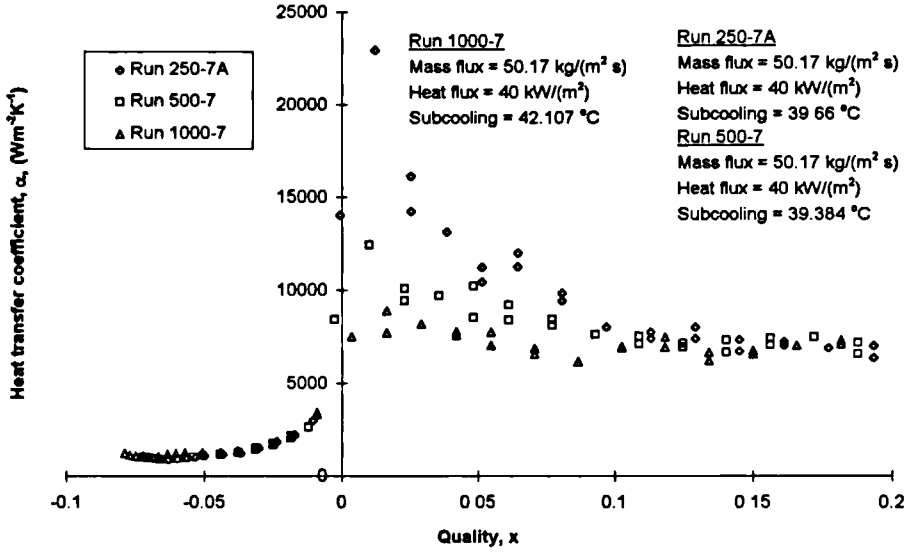

Figure 5.68 Comparison of outlet pressure variation for Runs 250-8A, 500-8 and 1000-8

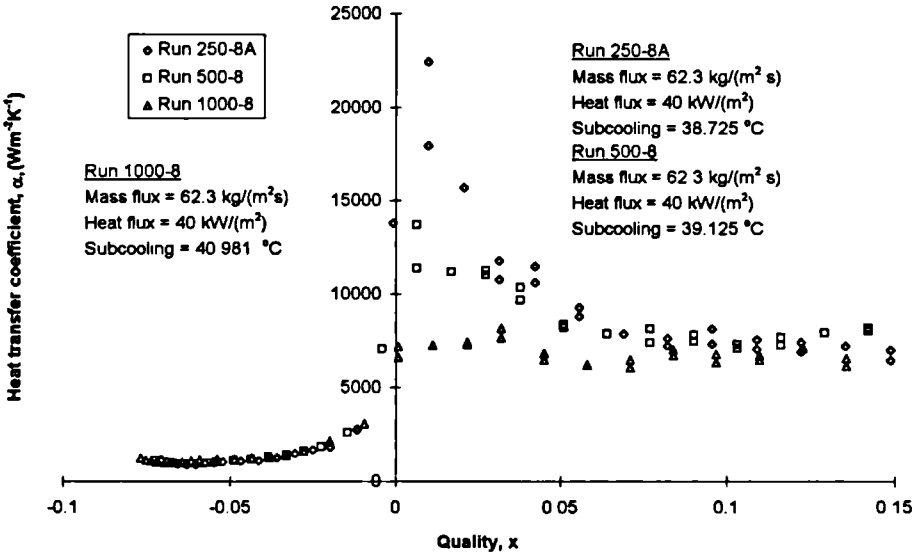

Figure 5.69 Comparison of inlet subcooling variation for Runs 250-1 and 250-5

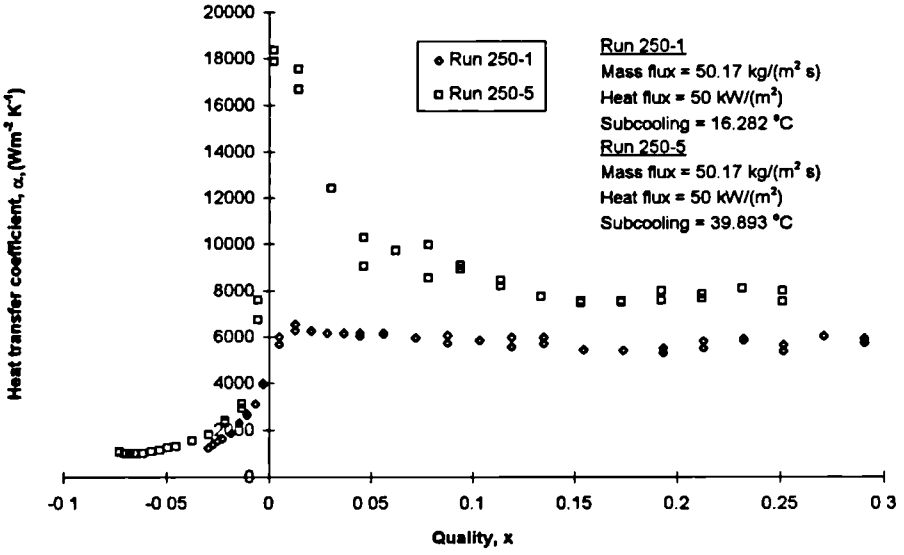

Figure 5.70 Comparison of inlet subcooling variation for Runs 250-2, 250-7A and 250-7B

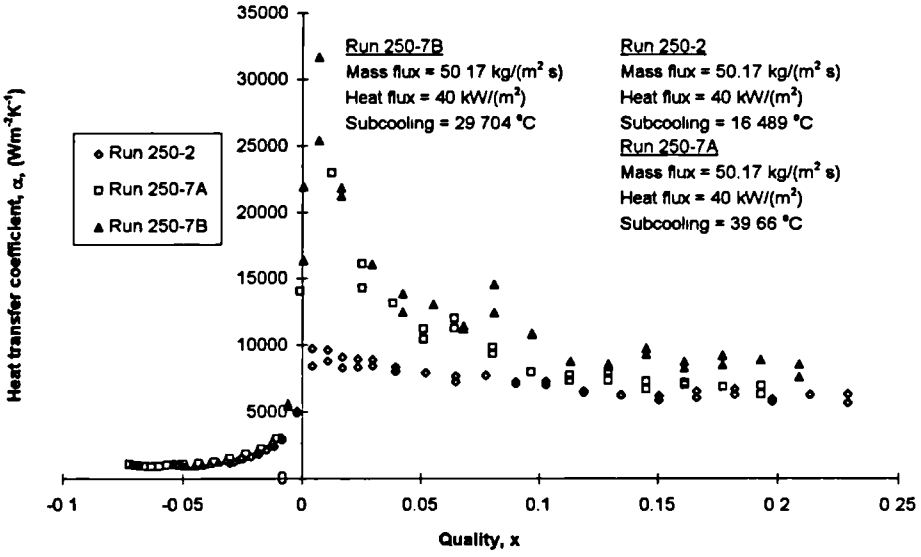

Figure 5.71 Comparison of inlet subcooling variation for Runs 250-3 and 250-6

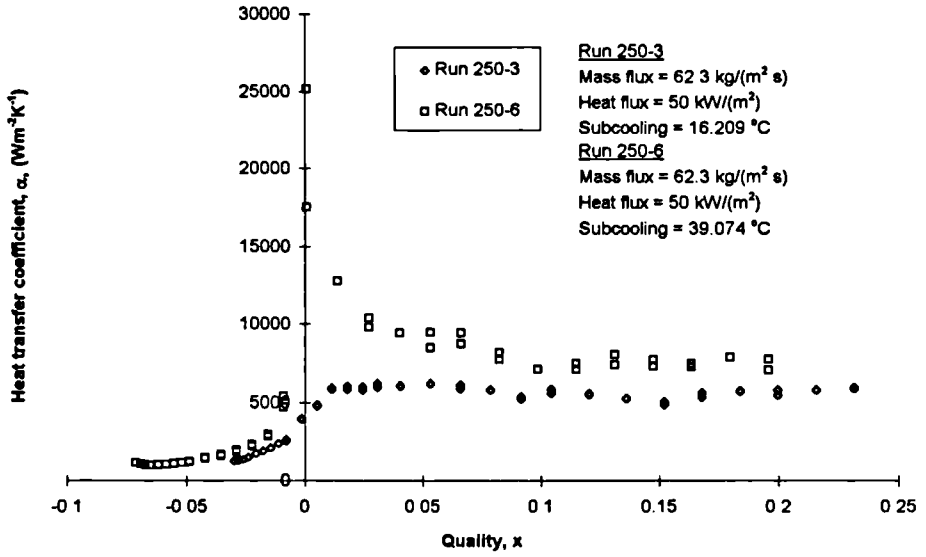

Figure 5.72 Comparison of inlet subcooling variation for Runs 250-4, 250-8A and 250-8B

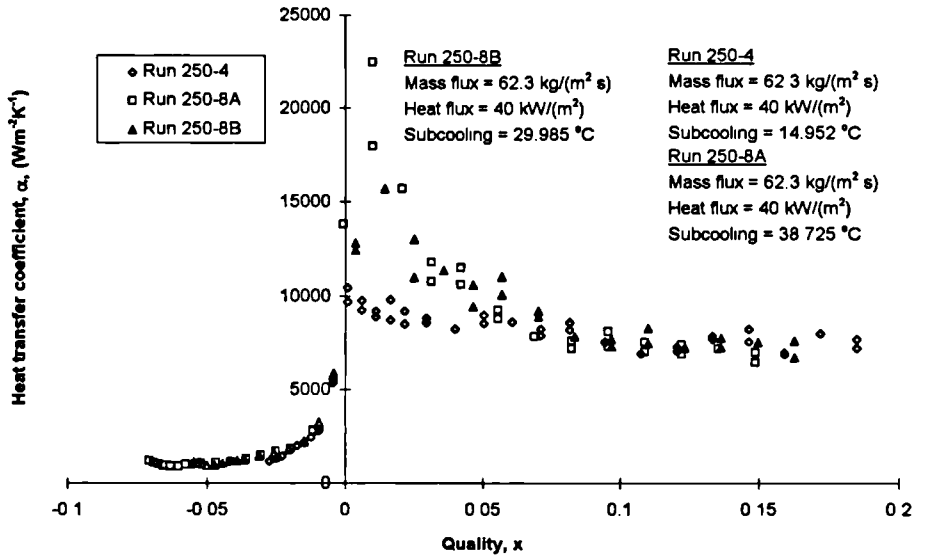

Figure 5.73 Comparison of inlet subcooling variation for Runs 500-1 and 500-5

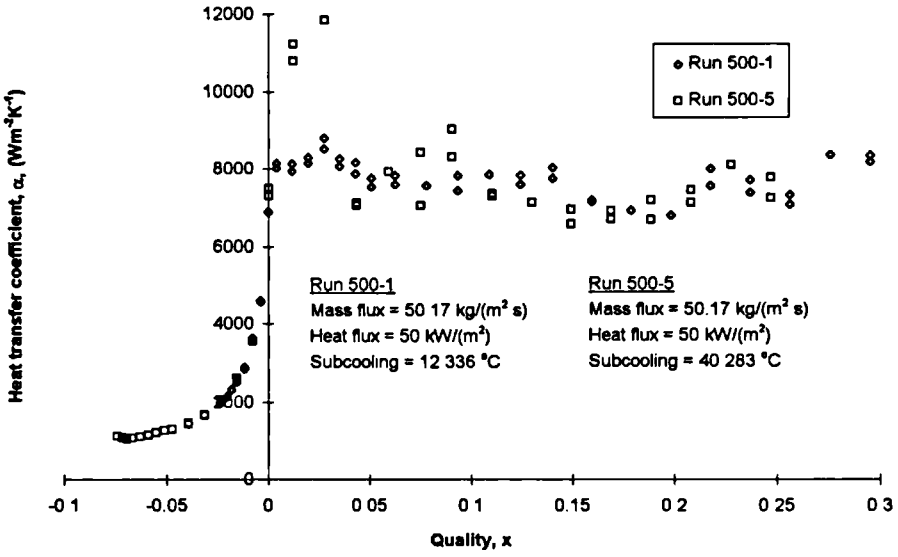

Figure 5.74 Comparison of inlet subcooling variation for Runs 500-2 and 500-7

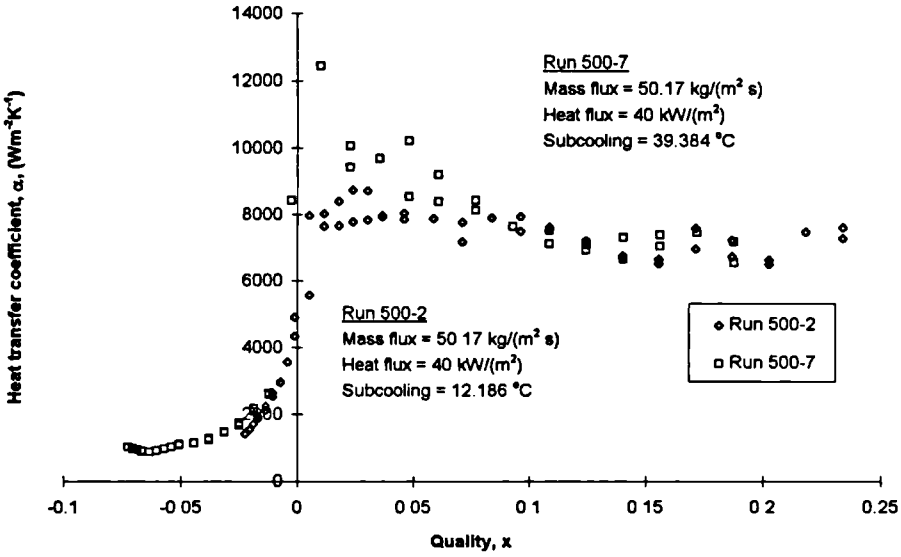

Figure 5.75 Comparison of inlet subcooling variation for Runs 500-3 and 500-6

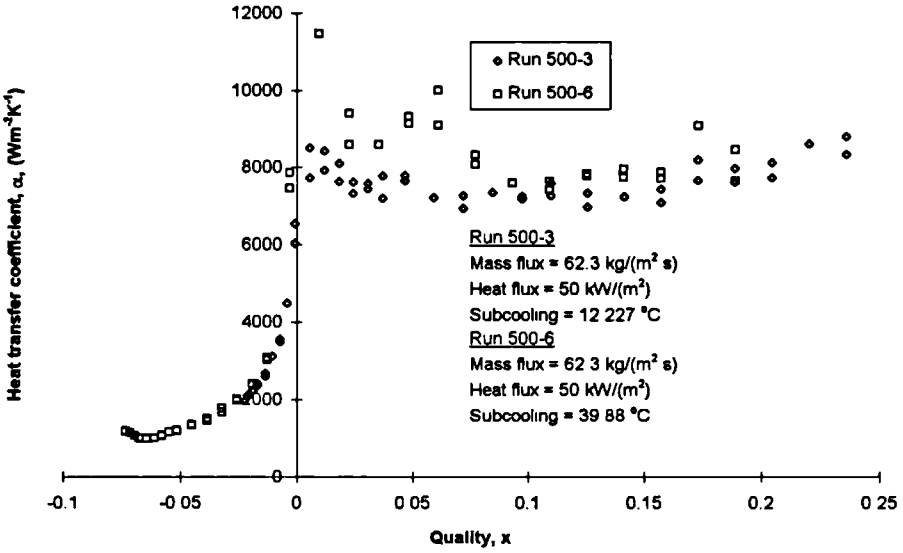

Figure 5.76 Comparison of inlet subcooling variation for Runs 500-4 and 500-8

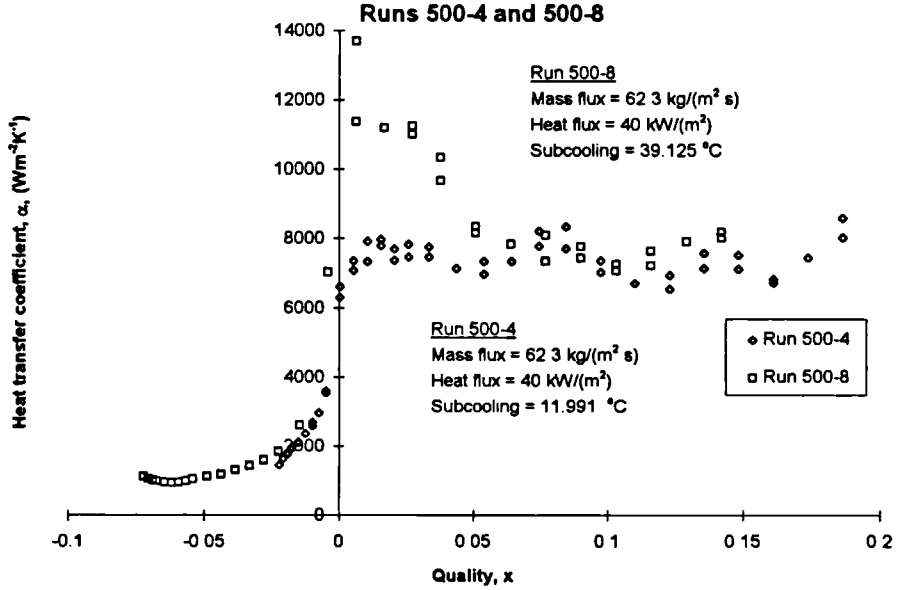

Figure 5.77 Comparison of inlet subcooling variation for Runs 1000-1 and 1000-5

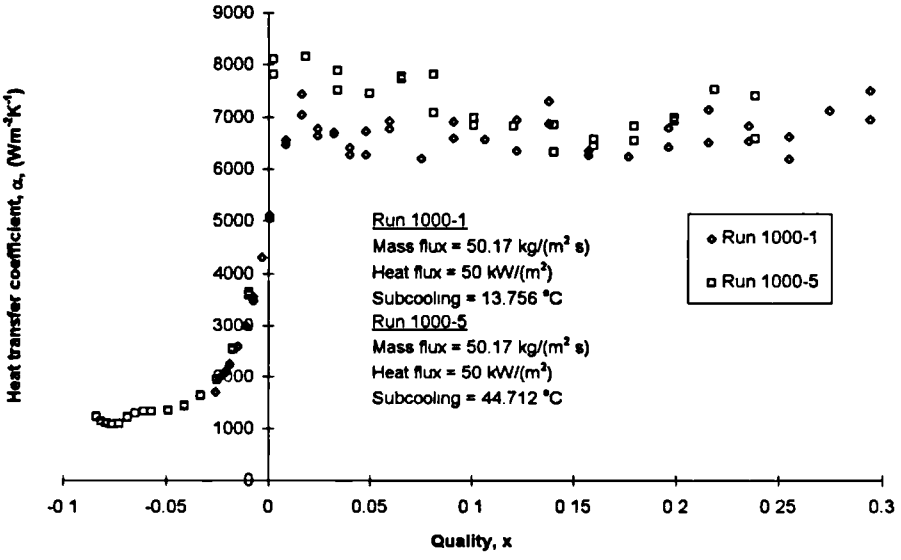

Figure 5.78 Comparison of inlet subcooling variation for Runs 1000-2 and 1000-7

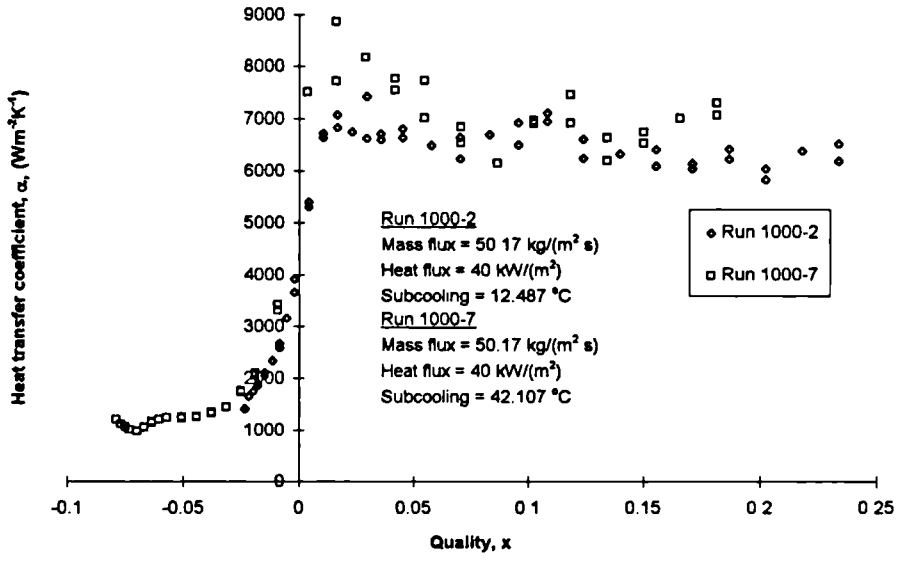

Figure 5.79 Comparison of inlet subcooling variation for Runs 1000-3 and 1000-6

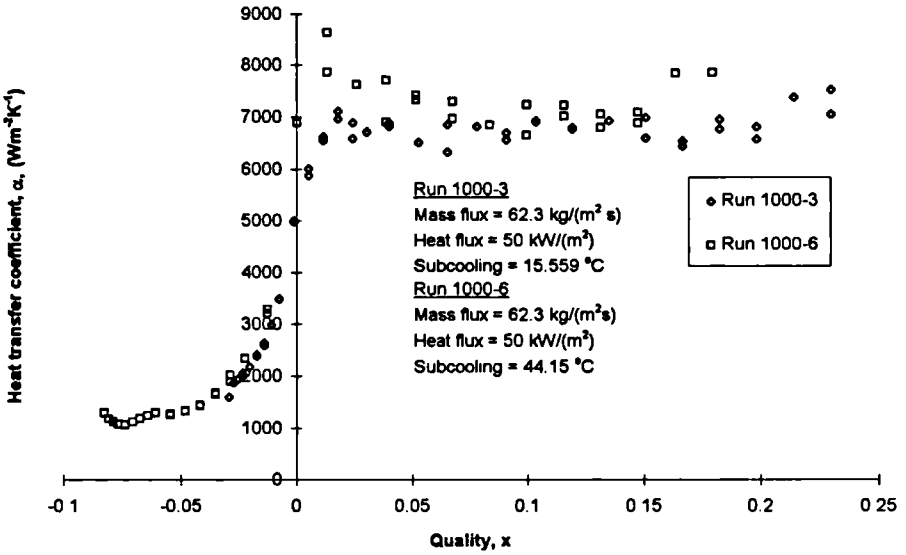

Figure 5.80 Comparison of inlet subcooling variation for Runs 1000-4 and 1000-8

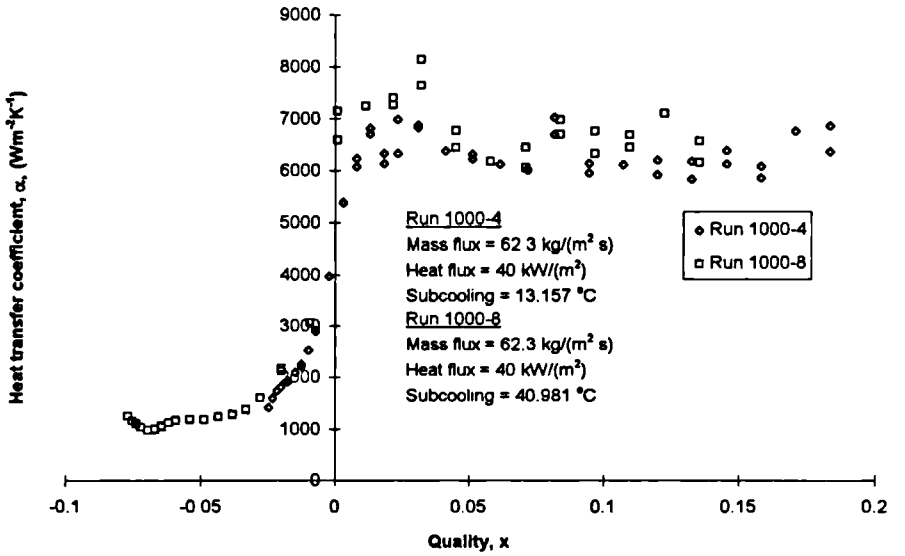

CHAPTER 6

SUB-ATMOSPHERIC EVAPORATOR (SAE) MODELLING

6.1 Introduction

As was mentioned earlier, the three main objectives of the work described in this thesis were the design, construction and commissioning of the SAE rig (as reported in Chapter 4), to obtain new data on sub-atmospheric evaporation using the SAE rig (as reported in Chapter 5) and finally, to provide a modelling/design framework for the SAE system. This third instalment of the research work is presented in this chapter.

The literature review chapters (see Chapters 2 and 3), give a systematic presentation of the background to the present author's proposed modelling framework for a sub-atmospheric evaporator. It should be noted here that the main bulk and thrust of the theoretical discussions and arguments for the various models used in the SAE program has been presented and scrutinised in these earlier chapters. Therefore, this present chapter's function is to primarily list the models used and discuss in detail some of the models where appropriate.

The discussion in this chapter will follow the transitions of the flow regimes, starting with single-phase liquid flow, followed by subcooled flow boiling, bubbly flow, slug flow, churn flow and finally annular flow respectively. The chapter will end with

analyses and discussions on the comparisons of the predicted results with the experimental data.

6.2 SAE program structure and logic

It had been decided at the onset of the research programme that the SAE program would take the final form of a phenomenologically based modelling code written in standard FORTRAN 77. The first step in the development programme, was the creation of a framework and structure (in modular form) that enables the successful recognition and division of flow into different flow regimes, utilising empirical correlations and basic models for some of the flow and heat transfer regimes. Having created a suitable framework, the models were then improved to include more advanced phenomenological approaches. This process of improvement was ongoing in the present research and should continue in the future. It was important to evaluate the SAE program at all stages against experimental database. The concept is to bring together the whole subject of vertical upward flow boiling, from subcooled single-phase liquid up to the dryout or critical heat flux (CHF) point.

A fully operational code is available and the comparison of results from the prediction of the SAE program against the SAE experimental results will be presented later in this chapter. The results are most encouraging but highlight the need for the further future development. At the time of writing of this thesis, the second stage of the SAE code development was started.

Figure 6.1 illustrate schematically the proposed sub-atmospheric evaporator modelling framework. Briefly, the whole modelling framework is centred upon the various flow regime transitions which occur during the upward evaporating flow in a vertical tube. For each of these flow regimes, the hydrodynamic parameters, i.e. void fraction and pressure drop were calculated, followed then by the heat transfer coefficient.

Figure 6.2 shows the logic structure of the program. It mirrors the framework described above. Since the program was coded to be modular, changes can be made to the different flow regimes by introducing and removing subroutine modules as appropriate. However, in its present form, the SAE program suffers from a minor disadvantage in that its transition from one flow regime to ~~the~~ another can be abrupt especially at the transition from single-phase liquid to two-phase gas-liquid flow. In this transitional region, the flow can change directly from single-phase liquid flow or subcooled flow boiling into slug flow, bypassing the bubbly flow regime altogether, especially in the case of highly superheated liquid. These flow regime transition jumps are inevitable in the first incarnation of the SAE program reported here, where the main aim is to ensure that the transitions are detected and acted upon accordingly.

The transitions used to divide the flow into different flow regimes are presented in Table 6.1 below and discussed in the next section. It is intended that for some transitions, there will be detailed discussions, while for others which had already been discussed in detail in the literature review chapters on hydrodynamics and heat transfer, only a statement of their key salient points are made.

The semi-theoretical transitions used in predicting the changeover from one flow regime to the next can be categorised as follows:

Flow Regime Transition	**Transition Criterion**
Single-phase flow to subcooled flow boiling (no bubble detachment)	Onset of nucleate boiling (ONB) criterion proposed by Davis and Anderson (1966).
Subcooled flow boiling (no bubble detachment) to subcooled flow boiling (with bubble detachment)	Net vapour generation (NVG) criterion by Saha and Zuber (1974)

Subcooled flow boiling (with bubble detachment) to equilibrium bubbly flow regime	Thermodynamic equilibrium quality, $x = 0$
Bubbly flow to slug flow regime	Void fraction, ε = 0.30, using the Drift-Flux Model for calculating ε.
Slug flow to churn flow regime	*Flooding* mechanism transition proposed by Jayanti and Hewitt (1992).
Churn flow to annular flow regime	*Flow reversal* criterion with non-dimensionalised superficial gas velocity, $U_G^* = 1.0$

Table 6.1 Flow regime transitions

The chosen variable for dividing the flow into separate flow regimes is the **distance** ,*z*, from the tube entrance. In other words, the positions for the start of each flow regime based on the above transition models are calculated and if they overlap, the higher (later) flow regime will be used, resulting in the lower flow regime being 'squeezed out' of the calculation sequence. Hence, the calculated positions are as follows:

- Position of ONB
- Position of NVG
- Position of vapour quality, $x = 0$
- Position of void fraction greater than 0.30
- Position of modified Jayanti and Hewitt (1992) flooding
- Position of flow reversal

At constant heat flux and pressure, the position of all the above transitions could be calculated *ab initio* in terms of the local quality or distance along the channel.

However, for the present case, the pressure changes significantly along the channel and this will change the physical properties and hence, the location of the transitions. Thus, a stepwise procedure was adopted in which the local pressure is calculated and the *local* conditions for the transitions are determined. A difficulty here is that, within a given region, certain variables may be interpolated between the extremes of the region. For this regions, therefore, the stepwise procedure was carried out iteratively until constant values were obtained within the region.

6.3 Flow regime transitions

Each of the flow regime transitions will be described in the following sub-sections. It should be noted here that these transition are semi-theoretical in nature in that their prediction combines both phenomenological models and theoretical arguments.

6.3.1 Transition from single-phase liquid to subcooled flow boiling (no bubble detachment)

The transition from single-phase liquid flow to the subcooled boiling region (no bubble detachment) is determined by the critical temperature difference between the wall temperature and the liquid saturation temperature, i.e. the critical wall superheat. This minimum temperature difference has to be achieved before active nucleation of bubbles can begin at the nucleation sites at the wall. The position when this criterion is met is known as the point of *onset of nucleate boiling* (ONB). The onset of nucleate boiling (ONB) criterion proposed by Davis and Anderson (1966) is used in the SAE program. It is a modification and extension of the Bergles and Rohsenow (1964) ONB analysis. Full mathematical and analytical details of Davis and Anderson's (1966) model can be found in their paper. It is the intention of this section to highlight the key points and mathematical equations of their model.

Davis and Anderson (1966) made the following assumptions in their model:

(I) The bubble nucleus which develops at the surface cavity has the shape of a truncated sphere.

(II) The equilibrium theory is applied to predict the superheat required to satisfy the force balance on the bubble.

(III) A bubble nucleus will grow if the temperature of the fluid at a distance from the wall equal to the bubble height is greater than the superheat required for bubble equilibrium.

(IV) The bubble nucleus does not alter the temperature profile in the fluid surrounding it.

Davis and Anderson (1966) started their mathematical model by deriving the superheat equation necessary to maintain a stable bubble by combining the Gibbs equation for the pressure difference across a curved surface, the Clausius-Clapeyron equation and the ideal gas law.

Assuming that $\rho_L >> \rho_G$ and that from the ideal gas law, $\rho_G = \frac{p}{RT}$, the Clausius-Clapeyron equation can be written as

$$\frac{dp}{dT} = \frac{h_{LG}\, p}{RT^2} \tag{6.1}$$

where R is the ideal gas constant. Integrating equation (6.1) between the saturation and bubble conditions and substituting the Gibbs equation

$$p_b - p_{sat} = \frac{2\sigma}{r_b} \tag{6.2}$$

where r_b is the bubble radius, into the integrated equation will yield the superheat equation

$$T_b - T_{sat} = \frac{R\, T_b\, T_{sat}}{h_{LG}} \ln\left(1 + \frac{2\,\sigma}{r_b\, p_{sat}}\right) \tag{6.3}$$

Davis and Anderson (1966) suggested that it is more convenient to express the superheat equation in terms of the bubble height or the distance from the wall to the top of the bubble, y_b and relationships linking the bubble radius, bubble height and cavity radius, r_c, see also Figure 6.3a, are as follows

$$y_b = r_b\,(1 + \cos\theta) = C_1\, r_b \tag{6.4}$$

and

$$r_c = r_b \sin\theta = C_2\, r_b \tag{6.5}$$

where θ is the contact angle. Hence, the superheat equation can be written as

$$T_b - T_{sat} = \frac{R\, T_b\, T_{sat}}{h_{LG}} \ln\left(1 + \frac{2\, C_1\, \sigma}{y_b\, p_{sat}}\right) \tag{6.6}$$

To apply assumption (III) that was made earlier, a liquid temperature is required. By assuming that the bubble nuclei population density is small, and that the bubbles develop well within the laminar sublayer where, with a constant liquid thermal conductivity, a linear temperature profile occurs, Davis and Anderson (1966) express the temperature profile as:

$$T_L = T_W - \frac{\dot{q}\, y}{\lambda_L} \tag{6.7}$$

The key criteria for ONB apart from satisfying the superheat and temperature profile is the existence of active cavities. Following Davis and Anderson's (1966) procedures, the critical cavity radius and its corresponding critical bubble height is given by

$$r_c' = \frac{C_2}{C_1} y' \tag{6.8}$$

Hence, the first intersection between the superheat and temperature profile equations, assuming that there is a sufficiently wide range of cavity sizes, will mark the point of ONB. To find this intersection, the slopes from equations (6.9) and (6.10) are calculated respectively as

$$\frac{dT_b}{dy_b} = -\frac{2\,C_1\,R\,T_{sat}^2}{p_{sat}\,y_b^2\,(1+\xi)}\left[1-\frac{R\,T_{sat}}{h_{LG}}\ln(1+\xi)\right]^{-2} \tag{6.9}$$

where $\xi = \dfrac{2\,\sigma\,C_1}{p_{sat}\,y_b}$ and

$$\frac{dT}{dy} = -\frac{\dot{q}}{\lambda_L} \tag{6.10}$$

Davis and Anderson (1966) suggested that equation (6.9) can be simplified with slight loss in accuracy (except for conditions where the wall superheat is very high), since in most cases,

$$1 \;>> \frac{R\,T_{sat}}{h_{LG}}\ln(1+\xi) \tag{6.11}$$

Therefore, equation (6.9) is then simplified to

$$\frac{dT_b}{dy_b} = -\frac{2\,C_1\,\sigma\,T_{sat}}{y_b^2\,h_{LG}\,\rho_G} \tag{6.12}$$

Equating the slopes of the superheat equation and the temperature profile and solving for the critical distance y', which is also the critical bubble height will yield

$$y' = \frac{C_1\,\sigma}{p} + \sqrt{\left(\frac{C_1\,\sigma}{p}\right)^2 + \frac{2\,C_1\,\lambda_L\,\sigma\,T_{sat}}{\dot{q}\,h_{LG}\,\rho_G}} \tag{6.13}$$

and solving with equation (6.6) for y' and eliminating T' will give,

$$\left(T_w - T_{sat}\right)_{ONB} = \frac{\left(RT_{sat}^2/h_{LG}\right)\ln\left(1+\xi'\right)}{1-\left(RT_{sat}/h_{LG}\right)\ln\left(1+\xi'\right)} + \frac{\dot{q}\,y'}{\lambda_L} \tag{6.14}$$

where

$$\xi' = \frac{2C_1\,\sigma}{py'} \tag{6.15}$$

Further simplifications are possible for systems at higher pressure or low surface tension, where,

$$\frac{dT_b}{dy_b} = -\frac{2\,C_1\,\sigma\,T_{sat}}{y_b^2\,h_{LG}\,\rho_G} \tag{6.16}$$

and equation (6.13) can be approximated to

$$y' = \frac{2\,C_1\,\lambda_L\,\sigma\,T_{sat}}{\dot{q}\,h_{LG}\,\rho_G} \tag{6.17}$$

leading to

$$\left(T_w - T_{sat}\right) = \frac{2\,C_1\,\sigma\,T_{sat}}{y'} + \frac{\dot{q}\,y'}{\lambda_L} \tag{6.18}$$

and substituting for y'

$$\dot{q} = \frac{\lambda_L\,h_{LG}\,\rho_G}{8\,C_1\,\sigma\,T_{sat}}\left(T_w - T_{sat}\right)^2 \tag{6.19}$$

Davis and Anderson (1966) found that when $C_1 = 1$, which is the assumption of a hemispherical bubble model, their proposed equation (6.19) can be reduced to that proposed by Sato and Matsumura (1964). Therefore, the minimum required wall superheat $(T_w - T_{sat})$ for the onset of nucleate boiling can be calculated from the equation (6.20) below.

$$(T_w - T_{sat}) = \sqrt{\frac{8\,\sigma\,\dot{q}\,T_{sat}}{\rho_G\,\lambda_L\,h_{LG}}} \tag{6.20}$$

Since the initial wall temperature is not specified, it can be calculated by finding the heat transfer coefficient for single-phase liquid flow from the ESDU (1977) correlation,

$$St = 0.0204\,Re^{-0.195}\,Pr^{-0.585} \tag{6.21}$$

where $St = \frac{\alpha_L\,\dot{m}}{C_{pL}}$, $Re = \frac{\dot{m}\,D}{\eta_L}$, $Pr = \frac{C_{PL}\,\eta_L}{\lambda_L}$ and $\dot{m}$ is the mass flux.

The wall temperature is then calculated from,

$$T_w = T_L + \frac{\dot{q}}{\alpha} \tag{6.22}$$

while the bulk fluid temperature is given by

$$T_L = T_{inlet} + \frac{4\,\dot{q}\,z}{\dot{m}\,D\,C_{pL}} \tag{6.23}$$

By combining equations (6.20), (6.22) and (6.23), the position of ONB can be calculated from equation (6.24) given below and this is used in the SAE program.

$$z_{ONB} = \frac{\dot{m}\, D\, C_{pL}}{4}\left(\sqrt{\frac{8\,\sigma\, T_{sat}}{\dot{q}\,\lambda_L\, h_{LG}\,\rho_G}} - \frac{1}{\alpha_L} + \frac{T_{sat} - T_{inlet}}{\dot{q}}\right) \qquad (6.24)$$

6.3.2 Transition from subcooled flow boiling (no bubble detachment) to subcooled flow boiling (with bubble detachment)

The net vapour generation (NVG) criterion proposed by Saha and Zuber (1974) is used. It was chosen as it represented a wide range of data for a variety of fluids. It is essentially a correlation. Saha and Zuber (1974) conducted an investigation into the prediction of the point of NVG and vapour void fraction in subcooled boiling. They showed that the point of NVG is dependent upon the local conditions - thermal and fluid dynamic. They concluded that at low mass flow rates, NVG is thermally controlled while at high mass flow rates, the phenomenon is hydrodynamically controlled.

They suggested that the thermally controlled region should be represented in terms of the local Nusselt (*Nu*) number while the hydrodynamically controlled region should be represented in terms of the Stanton (*St*) number. In order to link the two regions together, they used the Peclet (*Pe*) number, which is the ratio of the Nusselt and Stanton numbers. They then plotted various experimental data for NVG in terms of *St-Pe* co-ordinate system, and the result of their plot is given in Figure 6.3b.

From their plot, two distinct regions can clearly be identified. Up to a Peclet number of around 70 000, the data plotted fell onto a linear profile with a negative gradient implying a constant value for the local Nusselt number. For Peclet number greater than 70 000, the data fell onto a constant Stanton number. Saha and Zuber (1974) expressed this plot in the following mathematical form,

$$Nu = \frac{\dot{q}\, D}{\lambda_L\, \Delta T_{NVG}} = 455 \qquad (6.25)$$

for $Pe \leq 70\ 000$

and

$$St = \frac{\dot{q}}{\dot{m}\, C_{pL}\, \Delta T_{NVG}} = 0.0065 \qquad (6.26)$$

for $Pe > 70\ 000$

where $\Delta T_{NVG} = T_{sat} - T_L(z_{NVG})$ and $T_L(z_{NVG})$ is the bulk liquid temperature at the NVG point.

Taking into account the equilibrium vapour quality at NVG which is given by,

$$x_{NVG} = -\frac{C_{pL}\, \Delta T_{NVG}}{h_{LG}} \qquad (6.27)$$

Saha and Zuber (1974) also expressed their correlation in terms of x_{NVG}. The following equations given below are slightly modified for use in the SAE program, where the thermal diffusivity and liquid density terms in the first Saha and Zuber (1974) equation were replaced with the liquid specific heat capacity and thermal conductivity terms, while in the second equation, the liquid density and velocity terms was replaced by mass flux. Hence, the modified equations are:

$$x_{NVG} = -0.0022\left(\frac{\dot{q}\, D\, C_{pL}}{h_{LG}\, \lambda_L}\right) \qquad (6.28)$$

for $Pe \leq 70\ 000$

$$x_{NVG} = -154\left(\frac{\dot{q}}{\dot{m}\, h_{LG}}\right) \qquad (6.29)$$

for $Pe > 70\ 000$

In the SAE program, the position of NVG is calculated by using,

$$z_{NVG} = \frac{\dot{m}\, D \left(h_{LG}\, x_{NVG} + \Delta h_{subcool} \right)}{4\, \dot{q}} \tag{6.30}$$

Therefore, by calculating the position of bubble departure and using the above criterion, the subcooled flow boiling regions can be separated into two distinct flow regimes, i.e. with and without bubble detachment from the tube wall.

A more recent study of NVG is that by Zeitoun and Shoukri (1995),who carried out an experimental investigation into low pressure (1.07 to 1.8 barg) subcooled flow boiling in a vertical annular test section and produced a new NVG model based on the balance between vapour generation and condensation rates at the NVG point. They found their model to be consistent with that of Saha and Zuber (1974) model for thermally controlled net vapour generation, as discussed above; clearly, the Zeitoun and Shoukri (1995) model will be a candidate for inclusion in further development of the SAE code.

6.3.3 Transition from subcooled flow boiling (with bubble detachment) to equilibrium bubbly flow

The transition from subcooled boiling to equilibrium bubbly flow is that of the thermodynamic equilibrium quality, $x = 0$. The position along the tube when $x = 0$ occurs, can be evaluated from the following equations,

$$x = \frac{h(z) - h_L}{h_{LG}} \tag{6.31}$$

$$h(z) = h_{inlet} + \frac{4\, \dot{q}\, z}{\dot{m}\, D} \tag{6.32}$$

By substituting the second equation into the first equation and setting $x = 0$, the value for z when $x = 0$, can be calculated.

6.3.4 Transition from bubbly flow to slug flow

Beyond a certain concentration of bubbles, void waves form which give rise to rapid grouping of the bubbles which begin to travel as a group and which then coalesce to form a large bubble , characteristic of slug flow. The conditions for transition are not yet fully established from an analytical point of view, but a commonly used criterion for transition is that the void fraction is approximately 30% (i.e. $\varepsilon = 0.30$) as proposed by Radovcich and Moissis (1962). It should be noted that to a large extent, in an evaporator system, the rate of generation of bubbles from the heated walls is so great that it rapidly exceeds the criterion for the transition between dispersed bubbly flow and slug flow. Full discussions on this criterion and other suggested criteria for this transition were presented in Chapter 2, section 2.2.3.1.

In the SAE program, the void fraction is evaluated using the drift-flux model proposed by Zuber and Findlay (1954), as follows,

$$\varepsilon_G = \frac{x(z)\,\rho_L}{C_0\left\{x(z)\,\rho_L + \left[1 - x(z)\right]\rho_G\right\} + \rho_L\ \rho_G\ u_{GU}/\dot{m}} \tag{6.33}$$

where

$$x(z) = x_e(z) - x_{NVG}\ \exp\left[\frac{x_e(z)}{x_{NVG}} - 1\right] \tag{6.34}$$

and

$$x_e(z) = \frac{h(z) - h_L}{h_{LG}} \tag{6.35}$$

whilst x_{NVG} is calculated from the same equations and criterion as those in the Saha and Zuber (1974) criterion for subcooled boiling with bubble detachment. The value of the distribution constant, C_0 (see Dix, 1971) and the mean relative velocity, u_{GU} can be calculated from:

$$C_0 = \beta\left[1+\left(\frac{1}{\beta}-1\right)^b\right] \tag{6.36}$$

where β is the volumetric flow ratio, which is related to local flow quality by the expression

$$\beta = \frac{x(z)}{x(z)+[1-x(z)]\rho_G/\rho_L} \tag{6.37}$$

The exponent b is related to the density ratio as follows

$$b = \left(\frac{\rho_G}{\rho_L}\right)^{0.1} \tag{6.38}$$

while mean relative velocity, u_{GU} is calculated from:

$$u_{GU} = 2.9\left[\frac{(\rho_L-\rho_G)\,\sigma\, g}{\rho_L^2}\right]^{0.25} \tag{6.39}$$

More details of these equations can be found in Hewitt (1982) and Dix (1971).

6.3.5 Transition from slug flow to churn flow

The slug to churn flow transition had been extensively discussed in Chapter 2, section 2.2.3.2. There is still considerable controversy about the mechanism of this transition. However, the view which seems most consistent with experimental data is that of the *flooding* mechanism. This mechanism was originally proposed by Nicklin and Davidson (1962) and further developed by McQuillan and Whalley (1985) and more recently, by Jayanti and Hewitt (1992). In essence, as the overall superficial velocity is increased, the vapour velocity within the vapour plug is also increased. Since there is a falling film, a condition is ultimately reached when flooding occurs. Flooding is a phenomenon in which the liquid film in counter-current flow of gas and liquid breaks down due to the formation of large interfacial waves.

The model used here is that improved by Jayanti and Hewitt (1992). They had rather extensively surveyed the literature on the different mechanisms of the slug to churn flow transition. They concluded that the flooding mechanism proposed by McQuillan and Whalley (1985) was the most probable mechanism but they noted two shortcomings in McQuillan and Whalley's (1985) model where they had assumed a laminar film surrounding the Taylor bubble and the neglect of the effect of falling film length on the flooding velocity.

Jayanti and Hewitt (1992) then proceeded to introduce their own modifications to the model and it is their modified model which is used as the transition in the SAE program.

The correlation that is used to predict the flooding transition is that originally proposed by Wallis (1961) :

$$\sqrt{U_G^*} + \sqrt{U_L^*} = C \qquad (6.40)$$

where U_G^* and U_L^* are the non-dimensionalised superficial gas and liquid velocities calculated from,

$$U_G^* = U_G \frac{\sqrt{\rho_G}}{\sqrt{g\,D\,(\rho_L - \rho_G)}} \tag{6.41}$$

$$U_L^* = U_L \frac{\sqrt{\rho_L}}{\sqrt{g\,D\,(\rho_L - \rho_G)}} \tag{6.42}$$

where U_G and U_L are the gas and liquid superficial velocities respectively. The constant C has values typically in the range between 0.75 to 1.0. In applying the correlation to the slug-to-churn transition, the recommended value for C is equal to 1.0.

In light of the relationship between flooding and slug-to-churn transition, Jayanti and Hewitt (1992) used the characteristic phase superficial velocities attributed to the superficial Taylor bubble (U_{bs}) velocity and the superficial liquid film (U_{fs}) velocity since flooding occurs in this region. Therefore, modifications to the Wallis equations above are as follows:

$$\sqrt{U_{bs}^*} + m\sqrt{U_{fs}^*} > 1 \tag{6.43}$$

where U_{bs}^* and U_{fs}^* are the non-dimensional superficial velocities of the Taylor bubble and the falling liquid film which can be calculated from,

$$U_{bs}^* = U_{bs}\frac{\sqrt{\rho_G}}{\sqrt{g\,D\,(\rho_L - \rho_G)}} \text{ and } U_{fs}^* = U_{fs}\frac{\sqrt{\rho_L}}{\sqrt{g\,D\,(\rho_L - \rho_G)}} \tag{6.44}$$

The velocities, U_{bs} and U_{fs} are then calculated from

$$U_{bs} = \left(1 - 4\frac{\delta}{D}\right)\left[1.2\left(U_G + U_L\right) + 0.35\sqrt{\frac{g\,D\left(\rho_L - \rho_G\right)}{\rho_L}}\right] \tag{6.45}$$

and

$$U_{fs} = U_{bs} - \left(U_G + U_L\right) \tag{6.46}$$

where

$$U_G = \frac{\dot{m}\,x}{\rho_G} \tag{6.47}$$

and

$$U_L = \frac{\dot{m}\left(1 - x\right)}{\rho_L} \tag{6.48}$$

and solved iteratively for the film thickness δ in the Taylor bubble region by using the empirical correlation proposed by Brotz (1954) which was found to be applicable over a wide range of Reynolds number,

$$\delta\left[\frac{g\left(\rho_L - \rho_G\right)}{\nu_L^2\,\rho_L}\right]^{1/3} = 0.1719 Re_f^{2/3} \text{ where } Re_f = \frac{\Gamma}{\eta_L} \tag{6.49}$$

and Γ is the film flow rate (by mass) per unit wetted perimeter. In terms of superficial falling film velocity,

$$Re_f = \frac{\rho_L\,U_{fs}\,D}{4\,\eta_L} \tag{6.50}$$

An **upper limit** for the film thickness for this model was found, which had not previously been identified and stated by Jayanti and Hewitt (1992) in their paper, is when the falling film superficial velocity, U_{fs} is equal to zero. By setting $U_{fs} = 0$, and substituting it into equation (6.46), and solving equations (6.45) and (6.46) simultaneously for the film thickness yield the following equation,

$$\delta_{max} = \left\{1 - \left(U_G + U_L\right) \Big/ \left(1.2\left(U_G + U_L\right) + 0.35\sqrt{\frac{g\,D\left(\rho_L - \rho_G\right)}{\rho_L}}\right)\right\}\left(\frac{D}{4}\right) \tag{6.51}$$

The constant m in equation (6.43) was obtained by Jayanti and Hewitt (1992) from a quadratic curve-fit on the length-to-diameter ratio of the flooding column data of Hewitt et al. (1965) and were given as

$$m = 0.1928 + 0.01089\left(\frac{L}{D}\right) - 3.754 \times 10^{-5}\left(\frac{L}{D}\right)^2 \qquad \text{if } \frac{L}{D} \le 120 \tag{6.52}$$

$$m = 0.96 \approx 1 \qquad \text{if } \frac{L}{D} > 120 \tag{6.53}$$

The length L was recommended to be that of the Taylor bubble, L_b , which is calculated from

$$L_b = \frac{L_s\,\beta}{1-\beta} \tag{6.54}$$

where

$$\beta = \frac{U_m\left(1-\varepsilon_s\right) - U_L}{U_{fs} + U_m\left(1-\varepsilon_s\right)} \tag{6.55}$$

which were obtained from a liquid phase mass balance equation over a slug unit, given as

$$U_L = U_{sL}\left(1-\varepsilon_s\right)\left(1-\beta\right) - U_{fs}\,\beta \tag{6.56}$$

where U_{sL} is the velocity of the liquid in the slug body and was taken to be equal to the mixture superficial velocity U_m, by Jayanti and Hewitt (1992), while ε_s is the void

fraction in the slug body. Jayanti and Hewitt (1992) recommended that $\varepsilon_s = 0.5$ and $L_s = 12\,D$ [they referred to Moissis and Griffith (1962) who suggested that L_s is between 8 D and 16 D and to Brauner and Barnea (1986) for the void fraction], which they claimed to be typical values in vertical slug flow.

6.3.6 Transition from churn flow to annular flow

The *flow reversal* point is the point when all the liquid injected around the periphery of a channel travels upwards in the form of a liquid film with no downflow below the injector. This point was chosen as the transition point from churn to annular flow, and was characterised by the correlation proposed by Wallis (1961) as

$$U_G^* \cong 1.0 \tag{6.57}$$

where

$$U_G^* = U_G\,\rho_G^{1/2}\left[g\,D\,(\rho_L - \rho_G)\right]^{-1/2} \tag{6.58}$$

Discussions regarding other possible definition of the transition point from churn to annular flow were presented in Chapter 2, section 2.2.3.3.

6.4 Single-phase flow model

For single-phase flow, the SAE program calculates the pressure drop from the following equations,

$$\Delta p_{\text{frictional}} = \frac{2 f \dot{m}^2}{\rho_L D}(\Delta z) \tag{6.59}$$

$$\Delta p_{\text{gravitational}} = \rho_L g \Delta z \tag{6.60}$$

$$\Delta p_{\text{accelerational}} = 0 \tag{6.61}$$

with the total pressure drop being the sum of all the three pressure drop components above. The friction factor, f, term in the frictional pressure drop component, equation (6.59) is calculated from the explicit friction factor correlation proposed by Chen (1979) given below.

$$\frac{1}{\sqrt{f}} = -4.0 \log_{10}\left[\frac{\varepsilon}{3.7065 D} - \frac{5.0452}{Re}\log_{10}\left(\frac{1}{2.8257}\left(\frac{\varepsilon}{D}\right)^{1.1098} + \frac{5.8506}{Re^{0.8981}}\right)\right] \tag{6.62}$$

In the case of heat transfer, the single-phase correlation developed by ESDU (1977) was used. This correlation was presented in the form of Stanton (St) number and was reported to have a r.m.s. error of 11.5% from a large experimental database. The ESDU correlation is given below as

$$St = 0.0204\, Re^{-0.195}\, Pr^{-0.585} \tag{6.63}$$

where

$$St = \frac{\alpha}{\dot{m} C_{pL}} \tag{6.64}$$

6.5 Subcooled flow boiling models

For subcooled flow boiling, the treatment is best divided into two distinguishable sections, i.e.

- Subcooled flow boiling (no bubble detachment)
- Subcooled flow boiling (with bubble detachment)

Subcooled flow boiling (no bubble detachment)

In this region (between ONB and NVG), the following methods were used in SAE program to evaluate the pressure drop and heat transfer coefficient.

- **Pressure drop** The single-phase pressure drop method outlined in the previous section was utilised. It is assumed here that in this region, the emergence of nucleating bubbles will produce effects equivalent to a standard commercial steel pipe roughness of around 2.5×10^{-5}m (see Gersten, 1983).

- **Heat transfer** The Butterworth (1970) extension to the Chen (1966) flow boiling correlation into subcooled boiling was utilised. Details and discussions on this extension had been presented in the literature review on heat transfer (see Chapter 3, section 3.3.2).

Subcooled flow boiling (with bubble detachment)

This is the region classified between the point of NVG and thermodynamic vapour quality, $x = 0$. In this region, the vapour voids is sufficiently significant to merit its inclusion in the hydrodynamic calculations. The actual (non-equilibrium) quality is calculated from equation (6.34).

- **Pressure drop** In this region, the pressure drop is calculated from the separated flow model, with the frictional pressure drop component calculated from Friedel (1979) two-phase multiplier correlation. Both the separated flow model and Friedel (1979) correlation had been extensively reviewed in the literature review on hydrodynamics (see Chapter 2, section 2.3.1.2).

- **Void fraction** The drift flux model used in calculating the void fraction was given earlier in section 6.3.4 during the discussion on the transition from bubbly to slug flow. It should be noted that the expression chosen for the distribution constant C_0 was that proposed by Dix (1971), which was suggested by Hewitt (1982) to fit the appropriate trends for the variation of C_0 with quality.

- **Heat transfer** The Butterworth (1970) extension of the Chen (1966) is applied in this region as well.

6.6 Bubbly flow model

For bubbly flow, the only difference in the models used from those for the subcooled flow boiling with bubble detachment, is the heat transfer model. The Cooper (1984) correlation (see Chapter 3, section 3.2.3 on fully developed nucleate boiling) is used in the SAE program, since in this region, the fully developed saturated nucleate boiling predominates. Discussions on the merits and demerits of different nucleate boiling relationships are given in the literature review.

6.7 Slug flow model

For the slug flow, the SAE program uses the following hydrodynamic and heat transfer models.

- **Pressure drop** The separated flow model with Friedel (1979) frictional two phase multiplier is used. The existence of hydrodynamic phenomenological models for vertical slug flow such as Fernandes et al. (1983), Orell and Rembrand (1986) and Sylvester (1987) has been noted. The implementation of these models is suggested as part of the further development of the SAE program.

- **Void fraction** In slug flow, the study by Nicklin and Davidson (1961) was used to evaluate the void fraction. As described in Hewitt (1982), for slug flow, the mean gas velocity in steady two-phase flow is given by

$$u_G = C_0 \left(U_G + U_L\right) + u_S \tag{6.65}$$

where U_G and U_L are the gas and liquid superficial velocities, u_S is the rise velocity of a single slug flow in a static liquid and C_0 is the distribution parameter. Nicklin et al. (1962) found that the distribution parameter is approximately equal to 1.2 for slug flow.

Hewitt (1982) stated that for low viscosity fluids, e.g. water and in a wide bore tubes (> 1 cm, for example), the rise velocity is given by

$$u_S = 0.345\sqrt{g\,D} \tag{6.66}$$

which can be obtained from potential flow analysis. In order to evaluate the void fraction, Nicklin and Davidson (1961) assumed that bubble velocity is equal to the average velocity of the gas phase which gives

$$\frac{U_G}{\varepsilon_G} = 1.2\left(U_G + U_L\right) + 0.345\sqrt{g\,D} \qquad (6.67)$$

where the void fraction, ε_G can easily be calculated.

- **Heat transfer** Wadekar (1991) proposed a heat transfer model for vertical slug flow. It is an improvement on an earlier model by Wadekar and Kenning (1990) with the key addition of a nucleate boiling component. Both models used the McQuillan and Whalley (1985) model for evaluating the falling film flow rate. In the SAE program, this was changed to the Jayanti and Hewitt (1992) model. Further modification included the assumption of Taylor bubble and liquid slug lengths in the manner suggested by Jayanti and Hewitt (1992) (see earlier section 6.3.5 on the transition from slug flow to churn flow).

  The essence of the Wadekar (1991) model is given as follows. According to Wadekar (1991) the slug flow heat transfer can be estimated by prorating the heat transfer coefficients associated with the Taylor bubble and liquid slug in the following fashion:

$$\alpha_{slug} = \alpha_b\,\beta + \alpha_s\left(1-\beta\right) \qquad (6.68)$$

where

$$\beta = \frac{L_b}{L_b + L_s} \qquad (6.69)$$

and α_{slug}, α_b and α_s are the slug flow, Taylor bubble and liquid slug heat transfer coefficients, L_b and L_s are the Taylor bubble and liquid slug lengths respectively.

The heat transfer coefficients are calculated from the following:

Taylor bubble Wadekar (1991) suggested the use of Chun and Seban (1971) correlation for the turbulent falling liquid film surrounding the Taylor bubble. They chose this correlation on the grounds that when compared to theoretical models, the theoretical models tended to overestimate the heat transfer coefficient. The Chun and Seban (1971) correlation is given as follows,

$$\alpha_b = 0.0038\, Re_f^{0.4} \left(\frac{g\, \lambda_L^3\, \rho_L^2}{\eta_L^2} \right)^{0.333} Pr_L^{0.65} \tag{6.70}$$

Liquid slug For the liquid slug region, Wadekar (1991) chose to treat it as a simplified bubbly flow region. They argued that bubbly flow can be regarded as single-phase liquid flow with the vapour bubbles increasing the two-phase flow velocity. Hence, they used the Dittus and Boelter (1930) equation with a modified Reynolds number to calculate the liquid slug heat transfer coefficient. The equations they recommended are,

$$\alpha_s = 0.023 \frac{\lambda_L}{D} Re_{mix}^{0.8}\, Pr_L^{0.4} \tag{6.71}$$

where,

$$Re_{mix} = \frac{\dot{m}\, D\, \rho_L}{\eta_L} \left(\frac{x}{\rho_G} + \frac{1-x}{\rho_L} \right) \tag{6.72}$$

To account for the **nucleate boiling component**, the reduced pressure based correlation by Cooper (1984) (see also Chapter 3, section 3.2.3) was used as follows:

$$\alpha_{nb} = 35\, \dot{q}^{0.67}\, p_r^{0.12} \left(-\log_{10} p_r \right)^{-0.55} M^{-0.5} \tag{6.73}$$

For boiling of water, Kenning and Cooper (1989) noted that by choosing the higher heat transfer coefficient between the nucleate and convective boiling

components, they were able to reproduce the experimental trends within the accuracy of measurements.

Hence, in this case, the modified Wadekar (1991) model employed the following slug flow heat transfer criteria:

- **At low heat flux,** where $\alpha_{nb} < \alpha_s$, the recommended overall slug flow heat transfer relation is that of equation (6.68).

- **At intermediate heat flux,** where $\alpha_s < \alpha_{nb} < \alpha_b$, the recommended overall slug flow heat transfer relation is as follows:

$$\alpha_{slug} = \alpha_b \beta + \alpha_{nb} (1 - \beta) \tag{6.74}$$

- **At high heat flux,** where $\alpha_{nb} > \alpha_b$, the overall slug flow heat transfer was taken to be that of the fully developed nucleate boiling, equation (6.73).

6.8 Churn flow model

Churn flow occurs in vertical and near-vertical pipes. Hewitt and Hall-Taylor (1970) defined churn flow as a distinct intermediate flow regime that is 'sandwiched' between the slug and annular vertical flow. According to Hewitt (1995c), churn flow has the following unique characteristics:

- The regime is entered from slug flow via the formation of flooding type waves and these persist as a characteristic of the regime. Such waves are absent in both slug flow and annular flow. In fully developed churn flow, such waves are formed repeatedly and transport the liquid upwards.

- In between successive waves, the flow of the liquid phase in the film region near the wall reverses direction and is eventually entrained by the next upward moving wave.

Hence, the existence of flooding waves is a characteristic feature of the churn flow regime. Another feature of churn flow is that the flooding waves become less frequent as the gas velocity increases. The oscillatory up and down motion of the liquid causes the wall shear stress to fluctuate periodically from positive to negative indicating a change in the direction of the liquid film flow. The churn flow regime have not been studied extensively, probably because of its complexity. Nevertheless, some work has been done, e.g. Bharathan (1978), Govan et al. (1991) and more recently, Jayanti and Brauner (1992).

Jayanti and Brauner (1992) introduced, in essence, an annular-type flow model for churn flow. They based the main body of their model on the findings of Bharathan (1978) in air-water countercurrent flow, and of Govan et al. (1991) in flooding and churn flow. Bharathan (1978) conducted air-water countercurrent flow at atmospheric pressures in vertical tubes with internal diameters of 0.025 and 0.051 m and 1.5 m in length. He measured the pressure gradient and liquid holdup (by using quick closing valves). In the churn flow type region, Bharathan (1978) correlated the interfacial friction factor as

$$f_{iB} = 0.005 + 24\left(1-\varepsilon_G\right)^{2\,04} \tag{6.75}$$

where f_{iB} is the interfacial friction factor defined as

$$f_{iB} = \frac{2\,\tau_i}{\rho_G\, u_G^2} \tag{6.76}$$

and τ_i and u_G are the interfacial shear stress and gas velocity respectively.

Govan et al. (1991) showed, in their study on flooding and churn flow in vertical tubes, that the flow in the post-flooding regime, above the liquid injection point, has similar pressure drop and holdup characteristics as in normal churn flow. From their comparisons with the correlations of Bharathan (1978) for countercurrent and Wallis (1969) for annular flow, they found their data lies between the two. Jayanti and Brauner (1992), therefore, suggested that the interfacial friction factor in churn flow may be estimated by simple mean averaging between these two correlations as follows

$$f_i = \frac{f_{iB} + f_{iW}}{2} \tag{6.77}$$

where f_{iW} is the Wallis friction factor given by

$$f_{iW} = 0.005 + 0.375\left(1 - \varepsilon_G\right) \tag{6.78}$$

As noted by Jayanti and Brauner (1992), the above correlation was based on one set of data only, hence its validity for a wider range of data has yet to be established. Jayanti and Brauner (1992) suggested that the average wall shear stress τ in churn flow can be calculated based on the net liquid flow rate alone and, hence its time-varying nature may be neglected. Consequently, churn flow is then treated as an upward cocurrent separated flow with the film flow rate of that of the net liquid flow rate. The wall shear stress is calculated as follows

$$\tau_\omega = \frac{1}{2} f_L \rho_L u_L^2 \tag{6.79}$$

where, the liquid velocity

$$u_L = \frac{U_L}{1 - \varepsilon_G} \tag{6.80}$$

and

$$f_L = \frac{16}{Re_L} \qquad \text{for } Re_L \le 2100 \tag{6.81}$$

$$f_L = 0.079\, Re_L^{-0.25} \qquad \text{for } Re_L > 2100 \tag{6.82}$$

Jayanti and Brauner (1992) then performed a force balance on the gas core and on the tube (noting that the gas is not in contact with the wall) to give

$$-\frac{dp}{dz} = \frac{4\,\tau_i}{D\,\varepsilon_G^{0.5}} + \rho_G\, g \tag{6.83}$$

$$-\frac{dp}{dz} = \frac{4\,\tau_w}{D} + \left[\rho_L\,(1-\varepsilon_G) + \rho_G\,\varepsilon_G\right] g \tag{6.84}$$

Hence, the churn model proposed by Jayanti and Brauner (1992) can be calculated by solving equations (6.83) and (6.84) simultaneously for the pressure gradient and void fraction, using the interfacial and wall shear stresses calculated from equations (6.77) and (6.79) respectively. Jayanti and Brauner (1992) tested their proposed model against the Owen (1986) data and claimed that their prediction lies, for most of the data points, within ±20%.

It should also be noted that the model proposed by Jayanti and Brauner (1992) is for adiabatic flow and does not include the pressure drop term due to acceleration as required in the SAE program which deals with diabatic flow.

From the point of view of the present work, the Jayanti and Brauner model has the major disadvantage of giving discontinuities at the slug/churn and churn/annular boundaries. In fact, it is easier and sufficiently accurate (in terms of physical description) to treat churn flow like a slug flow at the point of transition from slug to churn flow and like annular flow at the *flow reversal* point, interpolating between the two extremes for the churn flow region itself.

In the work described in this thesis, the dimensionless gas superficial velocity, U_G^* is used as an interpolation parameter. To recapitulate, U_G^* is defined as follows,

$$U_G^* = U_G \frac{\sqrt{\rho_G}}{\sqrt{g\,D\,(\rho_L - \rho_G)}} \tag{6.85}$$

where U_G is the gas superficial velocity. The following are limits of the churn flow regime:

1. At the **onset** of churn flow, i.e. *flooding* within the Taylor bubble, U_G^* is one of the 2 variables (the other being U_L^*) that determines the transition point, (see section 6.3.5 above) and is therefore known in the model.

2. At the **demise** of churn flow, i.e. *flow reversal*, U_G^* was evaluated to be equal to unity.

Therefore, the new interpolation procedure for churn flow based on the dimensionless gas superficial velocity, U_G^* can be written as

$$Ch = \frac{U_G^*(z) - U_G^*\left(z_{\text{flooding}}\right)}{U_G^*\left(z_{\text{flow reversal}}\right) - U_G^*\left(z_{\text{flooding}}\right)} \tag{6.86}$$

where

$U_G^*(z)$	is the value of U_G^* at position z, as the flow progresses from the flooding to the flow reversal points, i.e. through the churn flow regime.
$U_G^*\left(z_{\text{flooding}}\right)$	is the value of U_G^* at the flooding point.
$U_G^*\left(z_{\text{flow reversal}}\right)$	is the value of U_G^* at the flow reversal point.
Ch	is christened the *'churn flow'* ratio (dimensionless).

Hence, the hydrodynamic and heat transfer parameters for the churn flow regime in the SAE program are calculated as follows:

$$\tau_w = \left(\tau_{w(annular)}\ Ch\right) + \left(\tau_{w(slug)}\ [1 - Ch]\right) \tag{6.87}$$

$$\varepsilon_G = \left(\varepsilon_{G\ annular}\ Ch\right) + \left(\varepsilon_{G\ slug}\ [1 - Ch]\right) \tag{6.88}$$

The slug wall shear stress can be evaluated by utilising the following equations below together with the flooding model proposed by Jayanti and Hewitt (1992) for the falling film thickness and Taylor bubble and liquid slug lengths.

$$\tau_{w(slug)} = \left(\frac{L_b}{L_b + L_s}\right) \tau_{wb} + \left(\frac{L_s}{L_b + L_s}\right) \tau_{ws} \tag{6.89}$$

and assuming that there is no interfacial shear in the Taylor bubble,

$$\tau_{wb} = -\rho_L\ g\ \delta \tag{6.90}$$

and homogeneous flow in the liquid slug,

$$\tau_{ws} = \frac{f_s\ \rho_L\ U^2}{2} \tag{6.91}$$

where the friction factor is calculated from standard friction factor correlations and U is the total superficial velocity.

Therefore, in the SAE program, the pressure gradient is calculated from the separated flow model as

$$-\frac{dp}{dz} = \frac{4\ \tau_w}{D} + \dot{m}^2\ \frac{d}{dz}\left\{\frac{(1-x)^2}{\rho_L\ (1-\varepsilon_G)} + \frac{x^2}{\rho_G\ \varepsilon_G}\right\} + g\left\{\rho_G\ \varepsilon_G + \rho_L\ (1-\varepsilon_G)\right\} \tag{6.92}$$

For heat transfer,

$$\alpha_{churn} = \left(\alpha_{annular}\ Ch\right) + \left(\alpha_{slug}\ \left[1 - Ch\right]\right) \tag{6.93}$$

Validation of the proposed procedure against the existing adiabatic churn flow data of Govan (1990) and Owen (1986) was difficult to achieve since the experimental limits of the regime were not defined in these studies. However, partial validation against this adiabatic churn flow database is strongly suggested for future work. The current interpolation procedure was specially designed and tailored for use in the SAE code and may require modifications in the future. Though the emphasis has been on developing a smooth transition model from slug, through churn, to annular flow, one may have to recognise that the slug/churn transition is, by its very nature, *not smooth* and to take account of this fact in any modelling.

It should be noted here that the accuracy of the U_G^* interpolation procedure described above is fully dependent upon the accuracy of the slug and annular flow models chosen. Consequently, it is not a fully independent model in its own right, but is actually a combination of separate flow models with an interpolation method.

6.9 Annular flow model

Annular flow is one of the major flow regimes found in the chemical industry especially in boiling and evaporation processes, where it predominates. Consequently, it is also one of the most studied and phenomenologically modelled, especially in relation to the nuclear power generation industry. Some of the most recent studies are those of Owen (1986), Govan (1990) and Wolf (1995).

Figure 6.4 shows the main characteristics of annular flow. Essentially, the gas (vapour) flows up the core of the tube with the liquid film on the periphery. It is the rule rather than the exception for a proportion of the liquid phase to be entrained as

droplets in the gas core. Furthermore, there is continuous interchange of liquid between the gas core and the liquid film. Consequently, it is this fraction of droplet entrainment and deposition that is a principal problem in predicting annular flow. In addition, the surface of the liquid film is wavy and this presents to the gas phase an effectively rough surface, with roughness enhancing the interfacial friction. Therefore, the principle variables in annular flow are the pressure gradient (related directly to interfacial friction), the thickness of the liquid film and the flow rate in the liquid film (or the fraction of the liquid phase entrained).

In any model of annular flow, what is required is:

- A relationship allowing the calculation of film thickness if the interfacial shear stress and liquid film flow rate (total liquid flow rate less the entrained liquid flow rate) are known. This relationship is known as *the triangular relationship* since it allows the prediction of any one of these variables if the other two are known.

- An expression for interfacial shear stress. This can be related to an interfacial friction factor which, in turn, may be related to the film thickness with the wave heights being approximately scaled by the film thickness.

- An expression for the film flow rate, namely a relationship between flow parameters and the fraction of the liquid which is entrained.

Certainly the first two of these relationships (and sometimes all three) are inter-related and must be solved implicitly. Detailed discussions of the methodologies involved are given by Hewitt and Hall-Taylor (1970), Hewitt (1982) and Whalley et al. (1974). A crucial feature of prediction in annular flow is that the entrained droplet fraction is rarely at equilibrium. Many hundreds of diameters are needed to reach equilibrium between the rate of entrainment of droplets and the rate of deposition of droplets, even in an adiabatic flow. In an evaporating flow, the flow conditions are also changing because of the increasing quality and, though equilibrium conditions may be passed through, they can never be permanently attained. An extreme of this, of course, is

when the liquid film flow rate becomes zero due to the preponderance of evaporation and entrainment over deposition; under such conditions, film dryout or critical heat flux (CHF) occurs.

For the annular flow region, the computer code HANA (Harwell Annular Flow) and its associated manual (Whalley, 1975), which embodied the Harwell programme of research on annular flow, was used. The original HANA code has limitations on the relationships used for interfacial friction and entrainment/deposition. Since then, recent work on developing better relationships has been proceeding, most notably those carried out in the Ph.D. studies of D.G. Owen (Owen, 1986 and Owen and Hewitt, 1987) and A.H. Govan (Govan, 1990 and Govan et al. 1988). Owen and Hewitt (1987) described an improved model for interface friction and Govan et al. (1988) concentrate on improved relationships for deposition and entrainment. Govan (1990) modified the HANA code to include the new deposition and entrainment relationships and it is this modified version of the code that has been used. In the SAE program scheme, a small subroutine was specially written to link and filter between the sub-annular flow (SUBANA) models and HANA. This is to ensure modularity and consistency of the SAE program.

The fundamentals of the HANA code and its equations are discussed in the following sub-section.

6.9.1 Harwell Annular Flow (HANA) code

The HANA code is designed and written for vertical upward flow in pipes. It treats the flow as having a homogeneous core (vapour-droplet mixture) and a film characterised by a mean thickness δ.

The fundamental equation in HANA is the mass balance on the liquid film

$$\frac{d\dot{m}_{LF}}{dz} = \frac{4}{d_i}\left(D - E - \frac{\dot{q}}{h_{LG}}\right) \tag{6.94}$$

where $\dot{m}$ is the mass flux (based on the total cross sectional area of the tube), z is the axial distance, D and E are the deposition and entrainment rates per unit peripheral area, d_i is the internal tube diameter, $\dot{q}$ is the heat flux and h_{LG} is the latent heat of vaporisation. According to Whalley (1975), both D and E are based on the surface area at the tube wall rather than the surface area of the actual film. The difference is not usually significant.

The rate of deposition of the liquid droplets from the turbulent gas stream onto the liquid film is calculated from the equation

$$D = k\,C \tag{6.95}$$

where k is the droplet mass transfer coefficient (ms^{-1}) and C is the homogeneous concentration of droplets in the core given by

$$C = \frac{\dot{m}_{LE}}{\frac{\dot{m}_G}{\rho_G} + \frac{\dot{m}_{LE}}{\rho_L}} \tag{6.96}$$

where $\dot{m}_G$ and $\dot{m}_{LE}$ are the mass fluxes for the vapour and entrained liquid and ρ_L and ρ_G are the liquid and vapour densities respectively. The deposition rate relationships developed by Govan et al. (1988) and Govan (1990) are as follows:

$$k\left(\sqrt{\frac{\rho_G d_i}{\sigma}}\right) = 0.18 \qquad \text{if } \frac{C}{\rho_G} < 0.3 \tag{6.97}$$

$$k\left(\sqrt{\frac{\rho_G d_i}{\sigma}}\right) = 0.083\left(\frac{C}{\rho_G}\right)^{0.65} \qquad \text{if } \frac{C}{\rho_G} > 0.3 \tag{6.98}$$

In correlating the entrainment rate, Govan et al. (1988) followed the route of deducing E from the equilibrium data (i.e. where D=E) but used a wide range of sources, covering many fluids, tube diameters and operating pressures. Many correlations ignore the fact that E=0 if $\dot{m}_{LF} < \dot{m}_{LFC}$ where $\dot{m}_{LFC}$ is the critical film flow rate for the onset of entrainment. $\dot{m}_{LFC}$ has been correlated by Owen and Hewitt (1987) as follows:

$$\frac{\dot{m}_{LFC}\, d_i}{\eta_L} = Re_{LFC} = \exp\left(5.8405 + 0.4249\left(\frac{\eta_G}{\eta_L}\right)\left(\sqrt{\frac{\rho_L}{\rho_G}}\right)\right) \tag{6.99}$$

where η_L and η_G are the dynamic viscosities of the liquid and vapour phases respectively. After investigating a number of alternatives, the following correlation was found by Govan et al. (1988) to give a reasonable fit:

$$\frac{E}{\dot{m}_G} = 5.75 \times 10^{-5}\left\{\left(\dot{m}_{LF} - \dot{m}_{LFC}\right)^2 \frac{d_i\, \rho_L}{\rho_G}\right\}^{0.316} \qquad \text{for } \dot{m}_{LF} > \dot{m}_{LFC} \tag{6.100}$$

Integration of equation (6.94) allows the estimation of the profile of film flow rate along the tube and thus the information can be used to calculate the film thickness and

interfacial shear stress via the triangular and interfacial roughness correlations. The HANA code uses the following simplified version of the triangular relationship (applicable for thin films and approximately constant shear stress in the film):

$$\frac{4\,\delta}{d_i} = \sqrt{\frac{(dp/dz)_{LF}}{(dp/dz)_F}} \tag{6.101}$$

where $(dp/dz)_F$ is the two-phase frictional pressure gradient and $(dp/dz)_{LF}$ is the frictional pressure gradient which would occur if the liquid film flow were to occupy the whole cross section in single-phase flow. $(dp/dz)_{LF}$ is given by:

$$\left(\frac{dp}{dz}\right)_{LF} = \frac{2\,f_{LF}\,\dot{m}_{LF}^2}{\rho_L\,d_i} \tag{6.102}$$

and f_{LF} is a single-phase friction factor, and in HANA, it is calculated from the following relationships for fully laminar and fully turbulent flow:

For laminar flow, where $Re_{LF} < 200$,

$$f_{LF} = \frac{16}{Re_{LF}} \tag{6.103}$$

For turbulent flow, where $Re_{LF} > 8000$,

$$f_{LF} = 0.079\,Re_{LF}^{-0.25} \tag{6.104}$$

where

$$Re_{LF} = \frac{\dot{m}_{LF}\,d_i}{\eta_L} \tag{6.105}$$

Hewitt and Hall-Taylor (1970) showed that in the intermediate (transition) region $200 < Re_{LF} < 8000$, a different relationship was necessary. This may be approximated as

$$f_{LF} = 0.001069 + \frac{143.8}{(\ln Re_{LF})^{4.5}} \tag{6.106}$$

The frictional pressure gradient is given by:

$$\left(\frac{dp}{dz}\right)_F = \frac{4\,\tau_i}{d_i} \tag{6.107}$$

where τ_i is the interfacial shear stress. τ_i is related to the interfacial friction factor, f_i by the relationship

$$\tau_i = \frac{f_i\,\rho_{GC}\,U_{GC}^2}{2} \tag{6.108}$$

where ρ_{GC} is the mean density of the droplet vapour mixture in the core of the annular flow and is given by:

$$\rho_{GC} = \frac{\dot{m}_{LE} + \dot{m}_G}{\frac{\dot{m}_{LE}}{\rho_L} + \frac{\dot{m}_G}{\rho_G}} = C + \rho_G \tag{6.109}$$

U_{GC} is the superficial velocity of the gas core material given by:

$$U_{GC} = \frac{(\dot{m}_{LE}/\rho_L) + (\dot{m}_G/\rho_G)}{A} \tag{6.110}$$

where A is the cross sectional area of the channel. The interfacial friction, f_i is calculated from the expression due to Wallis (1968):

$$f_i = f_{GC}\left(1 + 360\frac{\delta}{d_i}\right) \tag{6.111}$$

where f_{GC} is the friction factor for the gas core material flowing in single-phase flow in a smooth tube. f_{GC} is a function of the Reynolds number for the gas core given by:

$$Re_{GC} = \frac{\rho_{GC}\, U_{GC}\, d_i}{\eta_G} \tag{6.112}$$

where η_G is the vapour dynamic viscosity. f_{GC} is calculated from the Blasius equation:

$$f_{GC} = 0.079\, Re_{GC}^{-0.25} \tag{6.113}$$

At any given point along the channel, $\dot{m}_{LF}$ is known from the integration of equation (6.94). Equation (6.101) to (6.113) can be solved iteratively to give the frictional pressure gradient. The HANA code also integrates the expression for total pressure gradient

$$-\frac{dp}{dz} = -\frac{dp_F}{dz} - \frac{dp_A}{dz} - \frac{dp_G}{dz} \tag{6.114}$$

along the channel where the frictional pressure gradient, $\frac{dp_F}{dz}$ (the frictional pressure gradient) is given by equation (6.107). $\frac{dp_A}{dz}$ is the accelerational pressure gradient and $\frac{dp_G}{dz}$ is the gravitational pressure gradient. The latter two terms are given by:

$$-\frac{dp_A}{dz} = \frac{dM_T}{dz} \tag{6.115}$$

and

$$-\frac{dp_G}{dz} = g\left[\varepsilon_G\, \rho_{GC} + (1-\varepsilon_G)\, \rho_L\right] \tag{6.116}$$

where the void fraction is calculated in HANA from:

$$\varepsilon_G = \frac{\rho_L \left(1 - \frac{4\,\delta}{d_i} + \frac{4\,\delta^2}{d_i^2}\right)}{\dot{m}_{LE}\left(\frac{\rho_L}{\dot{m}_{LE}} + \frac{\rho_G}{\dot{m}_G}\right)} \tag{6.117}$$

The total momentum flux, M_T, is derived from the following 3 components:

- Momentum flux due to the liquid film
- Momentum flux due to the gas core
- Momentum flux due to the entrained liquid at the same velocity as the gas core.

These momentum fluxes are calculated from the following expressions:

$$M_T = M_{LF} + M_{GC} + M_{LE} \tag{6.118}$$

$$M_{LF} = \frac{\dot{m}_{LF}}{\rho_L \left(1 - \left(1 - \frac{4\,\delta}{d_i} + \frac{4\,\delta^2}{d_i^2}\right)\right)} \tag{6.119}$$

$$M_{GC} = \frac{\dot{m}_G^2\, \dot{m}_{LE}\left(\frac{\rho_L}{\dot{m}_{LE}} + \frac{\rho_G}{\dot{m}_G}\right)}{\rho_L\, \rho_G \left(1 - \left(1 - \frac{4\,\delta}{d_i} + \frac{4\,\delta^2}{d_i^2}\right)\right)} \tag{6.120}$$

$$M_{LE} = \frac{\dot{m}_{LE}^2\, \dot{m}_G\left(\frac{\rho_L}{\dot{m}_{LE}} + \frac{\rho_G}{\dot{m}_G}\right)}{\rho_L\, \rho_G \left(1 - \left(1 - \frac{4\,\delta}{d_i} + \frac{4\,\delta^2}{d_i^2}\right)\right)} \tag{6.121}$$

Each of the pressure gradient terms is estimated at each incremental distance along the channel. Thus, the hydrodynamic annular flow calculations were completed

6.9.2 Heat transfer in annular flow

In the present SAE modelling program, the Liu and Winterton (1991) correlation was used to evaluate the heat transfer in annular flow. The Liu and Winterton (1991) heat transfer correlation was discussed in section 3.3.4. The essence of their proposed model can be written as follows:

$$\alpha_{TP} = \left[\left(E\,\alpha_L \right)^2 + \left(S\,\alpha_{nb} \right)^2 \right]^{1/2} \tag{6.122}$$

$$E = \left[1 + x\,Pr_L \left(\frac{\rho_L}{\rho_G} - 1 \right) \right]^{0.35} \tag{6.123}$$

$$S = \frac{1}{\left(1 + 0.055\,E^{0.1}\,Re_L^{0.16} \right)} \tag{6.124}$$

where E and S are the enhancement and suppression factors and Re_L is the Reynolds number for liquid flowing alone in the tube. The nucleate boiling α_{nb} and forced convective α_L components are calculated from the Cooper (1984) and Dittus and Boelter (1930) correlations respectively.

6.10 Comparison of experimental and modelling results

The 3 key parameters being compared between the SAE experimental and SAE modelling results are:

- Exit flow pattern
- Total pressure drop
- Heat transfer coefficient

Each of these parameters and their comparative results will be discussed in detail in the following sections.

6.10.1 Exit flow pattern

In agreement with the observed SAE experimental results, the exit flow pattern predicted for all the runs modelled are churn / annular.

6.10.2 SAE total pressure drop

The comparison of the total pressure drop results between the SAE experiments and SAE modelling program is tabulated below in Table 6.2, 6.3 and 6.4. In these tables, the percentage deviation in the total pressure drop are presented. The final overall mean deviation for all the runs are calculated as follows:

$$Mean\ deviation = \frac{1}{n}\sum \left| \frac{\Delta p_{predicted} - \Delta p_{experiment}}{\Delta p_{experiment}} \times 100\% \right|$$

where n is the number of runs sampled.

The **overall mean deviation** was calculated to be **approximately 20.64 %.** This is most encouraging especially when one considers the prospect of improving the hydrodynamic models for slug and bubbly flows even further. Naturally, this level of deviation will also serve as a benchmark and standard for future comparisons in the SAE code development programme.

Run No	SAE experiment Δp (mbar abs.)	SAE modelling Δp (mbar abs.)	Percentage deviation $\left(\frac{\Delta p_{predicted} - \Delta p_{experiment}}{\Delta p_{experiment}} \times 100\%\right)$
250-1	132	100.4	-23.94
250-2	130	98.3	-24.38
250-3	132	121.9	-7.65
250-4	131	113.3	-13.51
250-5	160	134.9	-15.69
250-6	181	155.7	-13.98
250-7A	181	141.5	-21.82
250-7B	160	122.3	-23.56
250-8A	190	160.3	-15.63
250-8B	175	141.5	-19.14

Table 6.2 Pressure drop comparisons for 250 mbar abs. exit pressure experimental runs

Run No	SAE experiment Δp (mbar abs.)	SAE modelling Δp (mbar abs.)	Percentage deviation $\left(\frac{\Delta p_{predicted} - \Delta p_{experiment}}{\Delta p_{experiment}}\right) \times 100\%$
500-1	120	81.7	-31.92
500-2	120	80.9	-32.58
500-3	124	92.7	-25.24
500-4	122	91.0	-25.40
500-5	160	128.7	-19.56
500-6	173	148.0	-14.45
500-7	168	138.0	-17.86
500-8	194	158.1	-18.51

Table 6.3 Pressure drop comparisons for 500 mbar abs. exit pressure experimental runs

Run No	SAE experiment Δp (mbar abs.)	SAE modelling Δp (mbar abs.)	Percentage deviation $\left(\frac{\Delta p_{predicted} - \Delta p_{experiment}}{\Delta p_{experiment}}\right) \times 100\%$
1000-1	119	77.5	-34.87
1000-2	118	79.8	-32.37
1000-3	119	90.8	-23.70
1000-4	119	91.07	-23.47
1000-5	160	134	-16.25
1000-6	179	157.82	-11.83
1000-7	182	153.18	-15.84
1000-8	201	174.08	-13.39

Table 6.4 Pressure drop comparisons for 1000 mbar abs. exit pressure experimental runs

6.10.3 SAE heat transfer coefficient

The results from the heat transfer modelling for the SAE program are shown in Figures 6.5, 6.8 and 6.11 for 250, 500 and 1000 mbar abs. exit pressure respectively. The following observations and conclusions can be seen and drawn.

- In Figures 6.5 (for all 250 mbar abs. exit pressure runs), there is a wide scatter in the deviation (with the majority of the data points lying between ±60%) between the predicted heat transfer coefficients from the SAE model and those from the SAE experiments. While this is disappointing, it is hardly surprising nor unexpected when one considers the following points:

  (i) **SAE experimental data scatter and flow instabilities** especially at 250 mbar abs. as discussed in the previous experimental results chapter. These effects will certainly cause a large deviation. It can be seen that for low vapour qualities, nearly all the modelling results under predicted (shown by the negative deviation) the heat transfer coefficients. Clearly, this showed that the current models *do not account for the local heat transfer coefficient maxima at low vapour qualities*. This point is further strengthened by Figures 6.6. and 6.7, which compared the Chen (1966) [with Butterworth (1970) extension into the subcooling boiling region] and the Liu and Winterton (1991) general flow boiling correlations against the SAE experimental data respectively.

  (ii) **Limited validity range of present models and correlations** will affect their applicability into sub-atmospheric systems. The validity range of the heat transfer models used in the current SAE program as well as those of Chen (1966) and Liu and Winterton (1991) are more suited to atmospheric or high pressure

systems since they were correlated and derived from a larger database of data at those higher pressure conditions. This fact, can be clearly seen when one considers the reduction in deviation as one increases the exit pressure, see Figures 6.5 to 6.13.

For SAE models: compare Figures 6.5, 6.8 and 6.11
For Chen (1966): compare Figures 6.6, 6.9 and 6.12
For Liu and Winterton (1991): compare Figures 6.7, 6.10 and 6.13.

- In Figures 6.8 (for all 500 mbar abs. exit pressure runs), there is still a wide scatter in the deviation (with the majority of the data points lying between ±40%) between the predicted heat transfer coefficients from the SAE model and those from the SAE experiments. The deviations are less due to the reduced influences of the two possible causes discussed above.

- In Figures 6.11 (for all 1000 mbar abs. exit pressure runs), the scatter in the deviation (with the majority of the data points lying between ±30%) between the predicted heat transfer coefficients from the SAE model and those from the SAE experiments is even lower. The deviations are lessened more due to the reduced influences of the two possible causes as discussed for the 250 mbar abs. exit pressure case above. In the case of the local heat transfer coefficient maxima, as discussed in the previous chapter (Chapter 5), they are almost non-existence at this pressure, and consequently, the improvement in reduced magnitude of heat transfer coefficient deviation is more profound.

Figures 6.14 to 6.16 showed some typical SAE modelling program heat transfer coefficient profiles. The 'kinks' observed occur at the flow regime transitions when different heat transfer models are used, especially when the changes occur from subcooled boiling to slug flow, bypassing the bubble flow regime altogether, see Figures 6.15 and 6.16.

6.11 Conclusion

This chapter presented the SAE modelling framework and the models that were used for the hydrodynamic and heat transfer modelling of a vertical sub-atmospheric evaporator. Results from the SAE program were compared with those of the experiments, and these were encouraging especially for pressure drop prediction while more work is needed on the heat transfer front. The existing heat transfer models are clearly not adequate to predict the sub-atmospheric evaporator system, especially when the local heat transfer coefficient maxima at low vapour qualities occur.

A proposal for a new interpolative concept for churn flow based on the dimensionless gas superficial velocity, U_G^* was also introduced but validation against existing adiabatic churn flow data of Govan (1990) and Owen (1986) had yet to be completed. The current interpolative procedure was designed for use in the SAE code and may require modifications before extending into adiabatic systems. Nevertheless, the main principle and idea remained the same, which is to monitor the variation of U_G^*, since it is one of the key variables that determines the onset and demise of churn flow.

Flow Regime	Heat transfer model	Transition		Void Fraction	Pressure Drop
Annular	Liu and Winterton (1991)	$U_G^* = 1$ Flow reversal	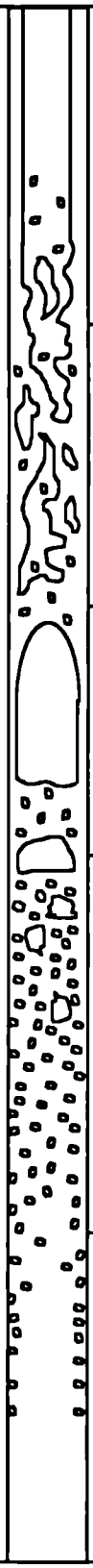	HANA	HANA
Churn	U_G^* ratio interpolation	Jayanti and Hewitt (1992) Flooding		U_G^* ratio inter-polation	U_G^* ratio interpolation
Slug	Wadekar (1991)	$\varepsilon = 0.3$		Nicklin and Davidson (1961)	Separated Flow Model using Friedel (1979) correlation for frictional component
Bubbly	Cooper (1984)	$x = 0$		Drift flux model	
Subcooled Boiling (with bubble detachment)	Butterworth extension to Chen (1966)	NVG - Saha and Zuber (1974)			
Subcooled Boiling (no bubble detachment)		ONB - Davis and Anderson (1966)		None	Single-phase pressure drop with Chen (1979) friction factor correlation
Single phase	ESDU				

Figure 6.1 SAE program framework

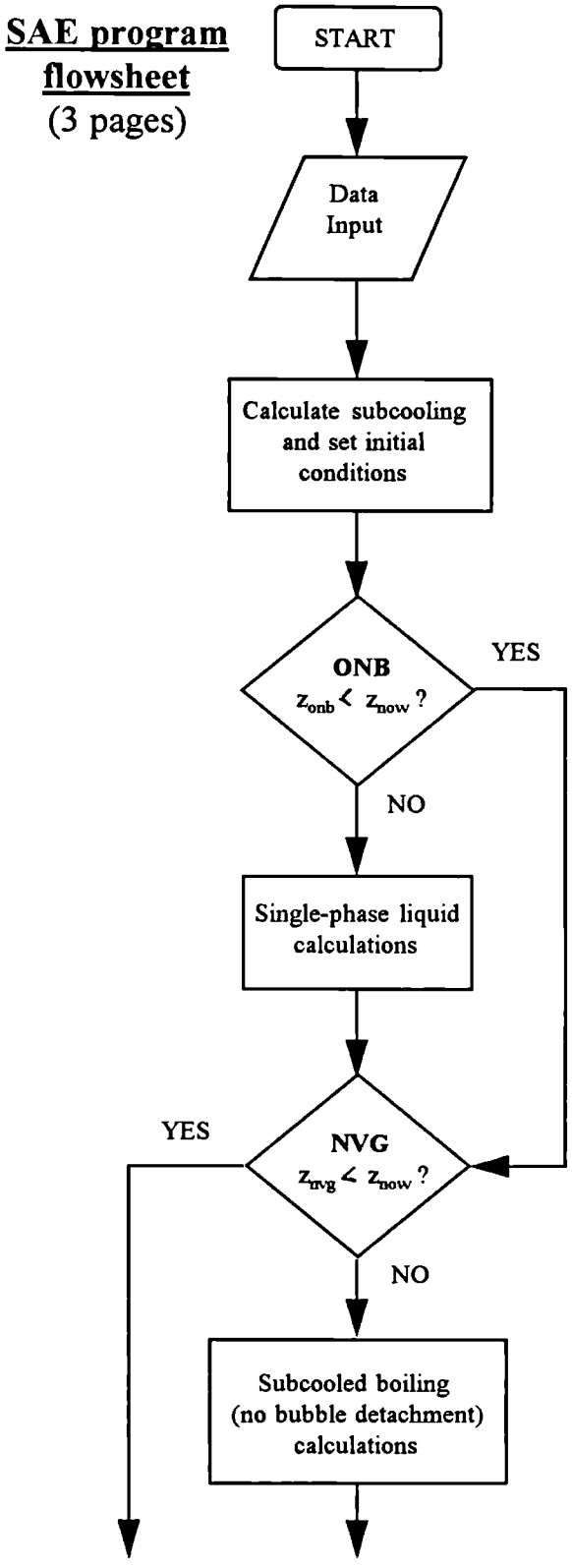

Figure 6.2 SAE program logic (page 1/3)

(Continued from page 1)

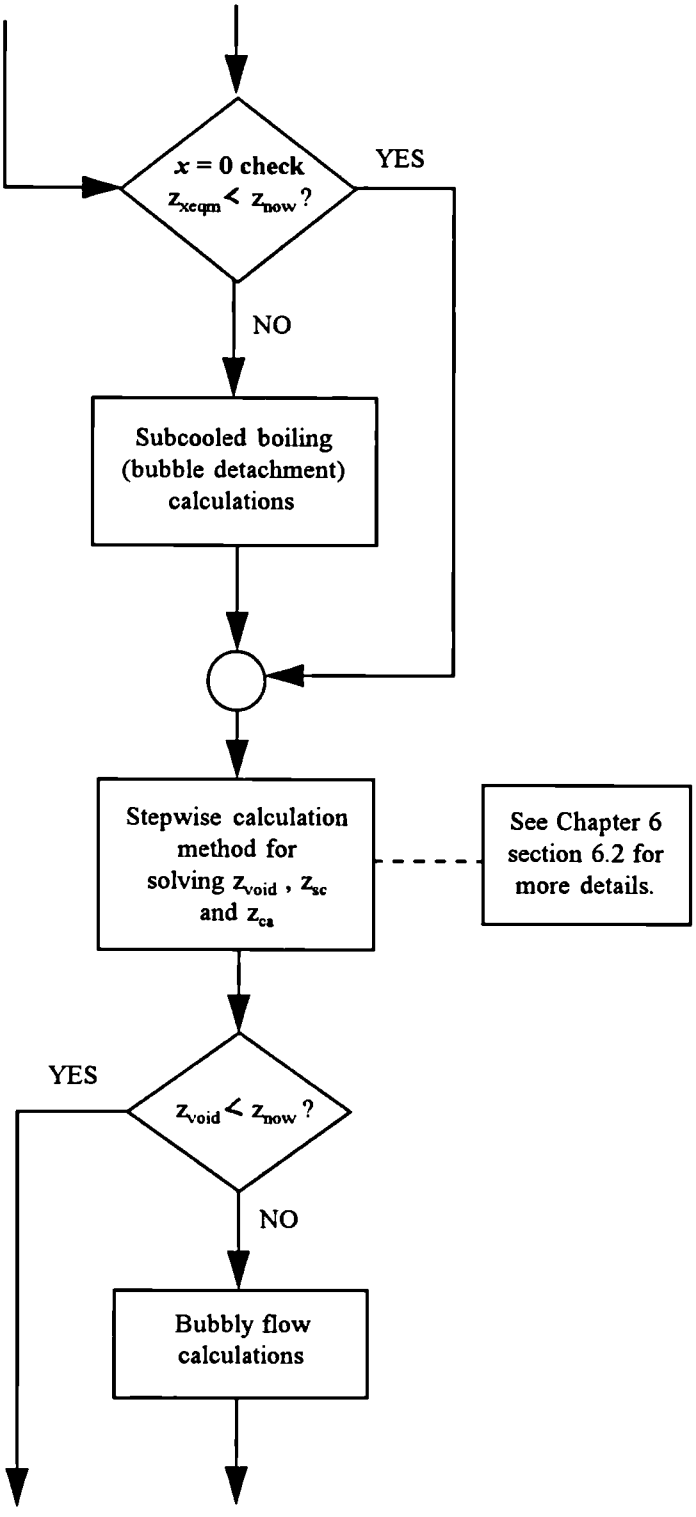

Figure 6.2 SAE program logic (page 2/3)

(Continued from page 2)

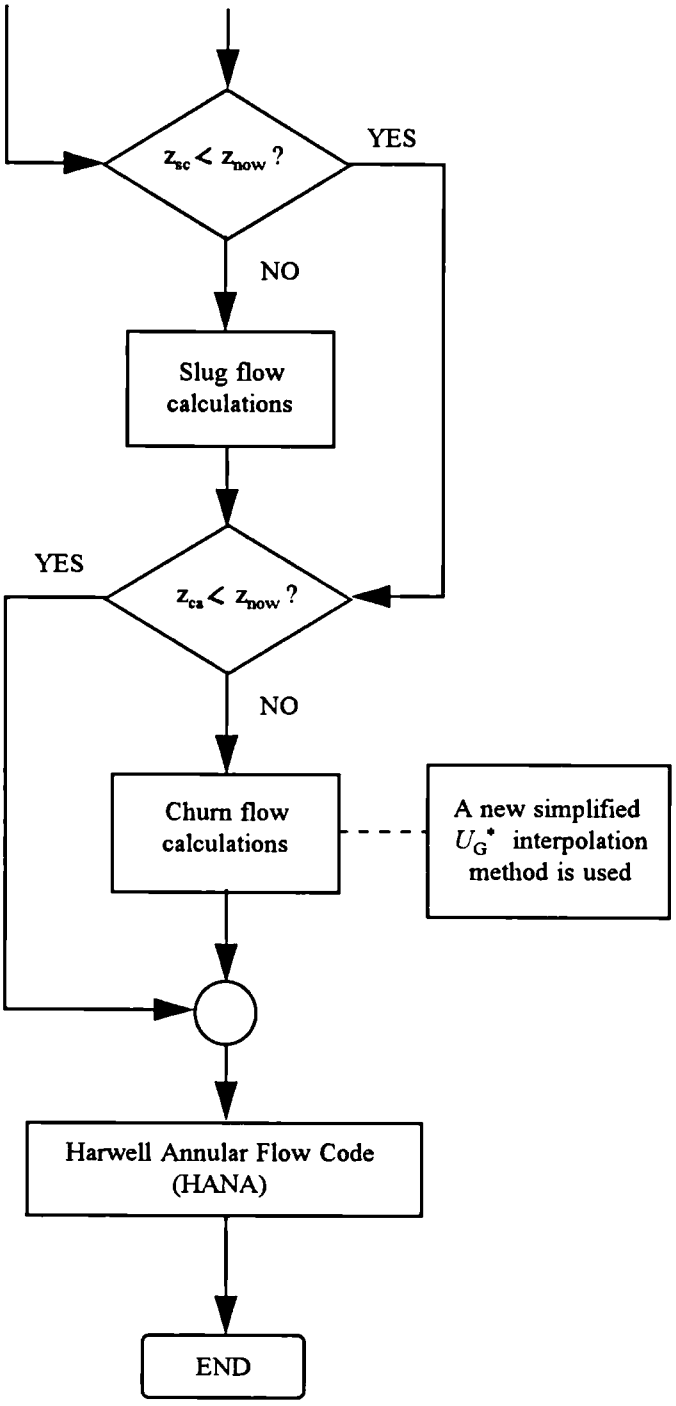

Figure 6.2 SAE program logic (page 3/3)

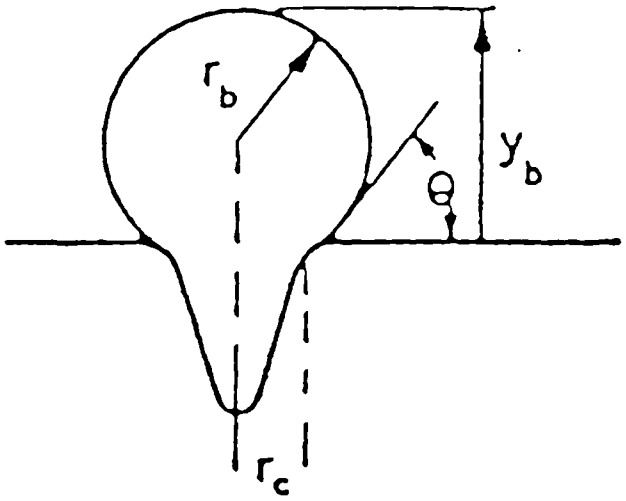

Figure 6.3a Davis and Anderson (1966) truncated sphere bubble nucleus

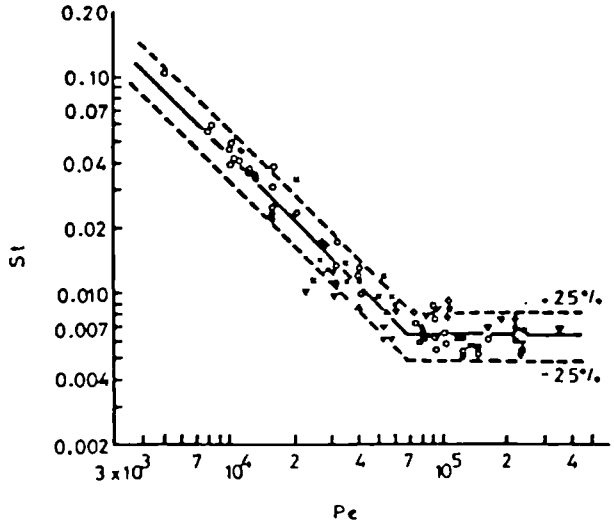

Figure 6.3b Stanton Number versus Peclet Number for bubble detachment in subcooled boiling (Saha and Zuber, 1974)

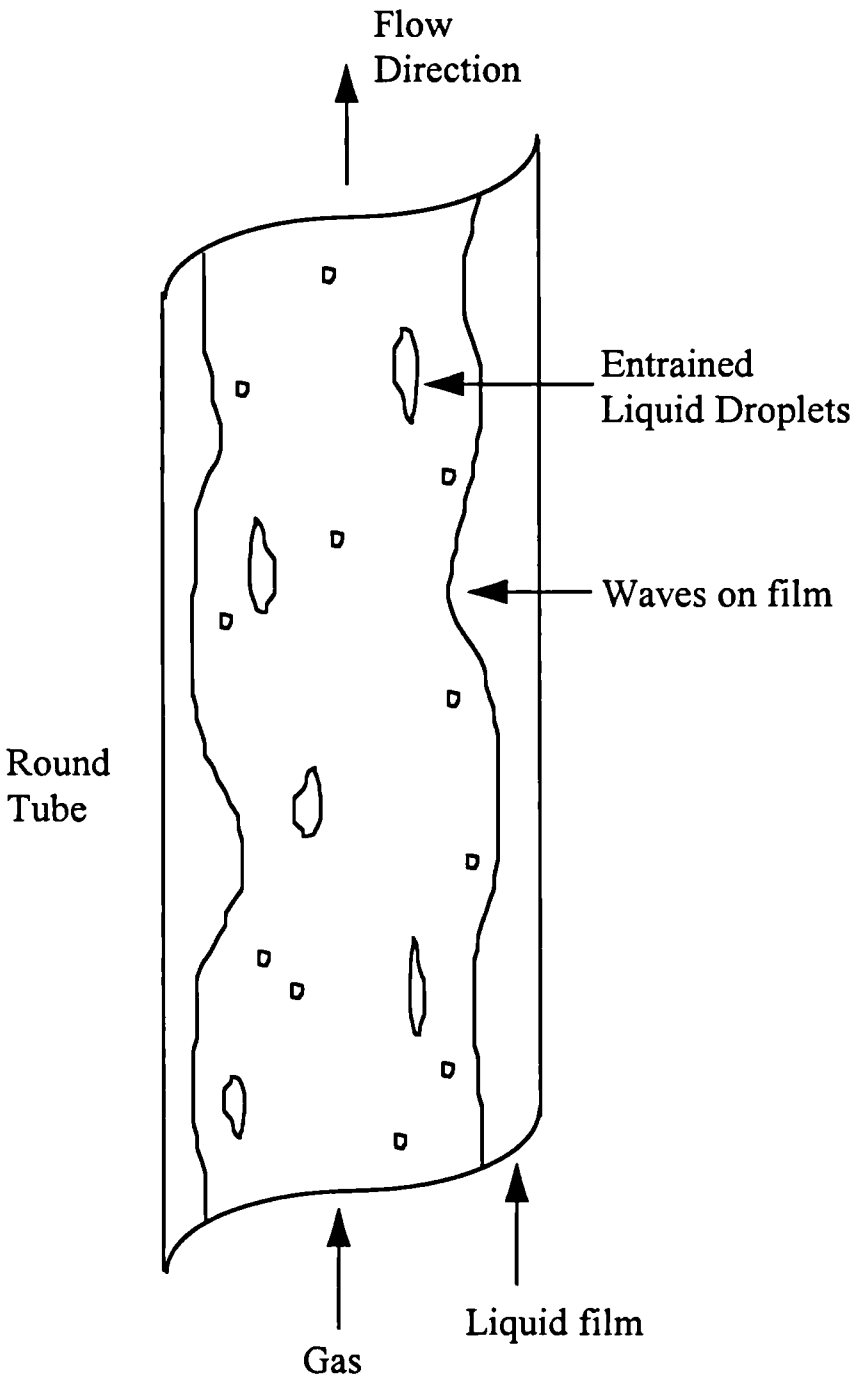

Figure 6.4 Two-phase gas-liquid annular flow

Figure 6.5 SAE prediction of heat transfer coefficient for all 250 mbar abs. experimental runs

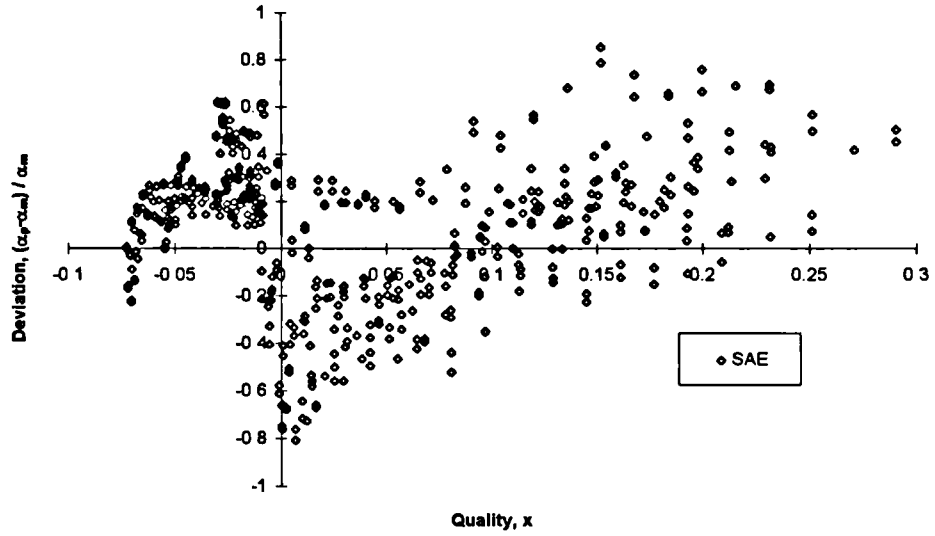

Figure 6.6 Chen (1966) prediction of heat transfer coefficient for all 250 mbar abs. experimental runs

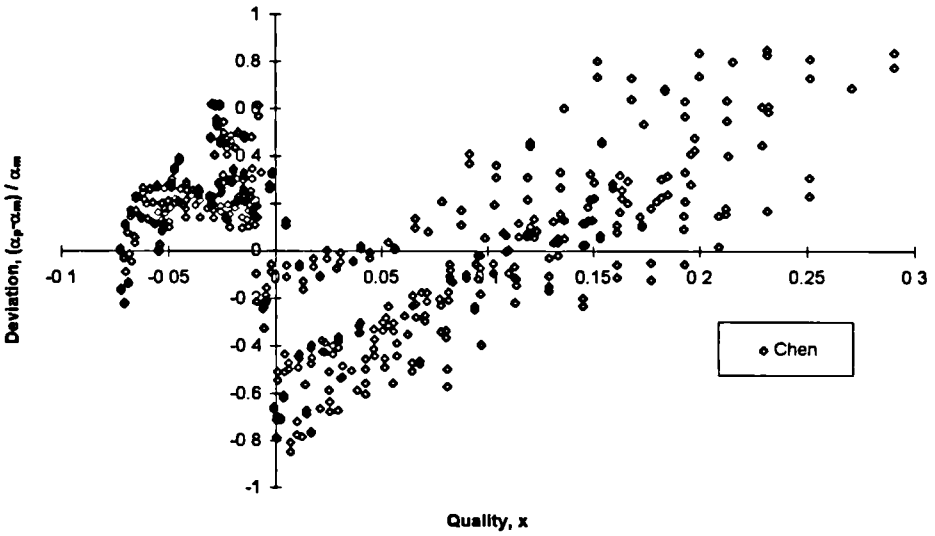

Figure 6.7 Liu-Winterton (1991) prediction of heat transfer coefficient for all 250 mbar abs. experimental runs

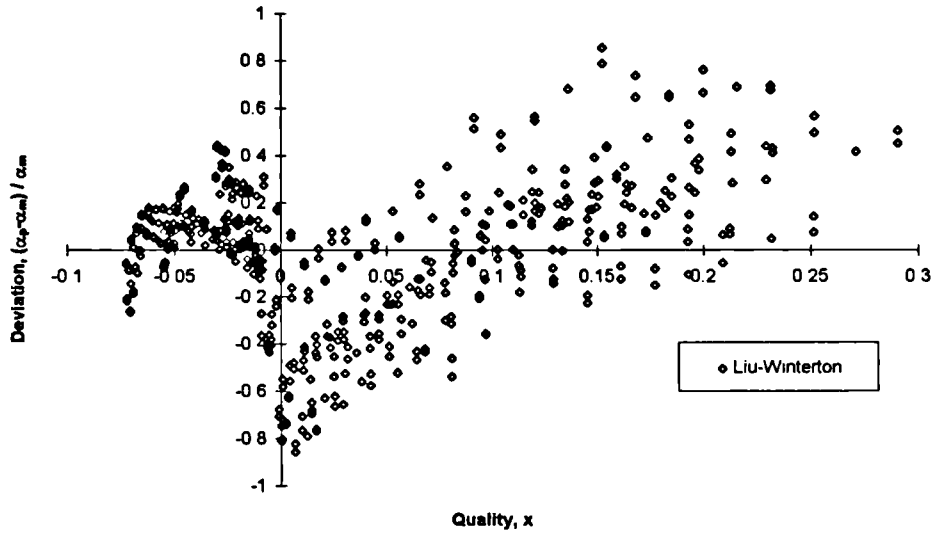

Figure 6.8 SAE prediction of heat transfer coefficient for all 500 mbar abs. experimental runs

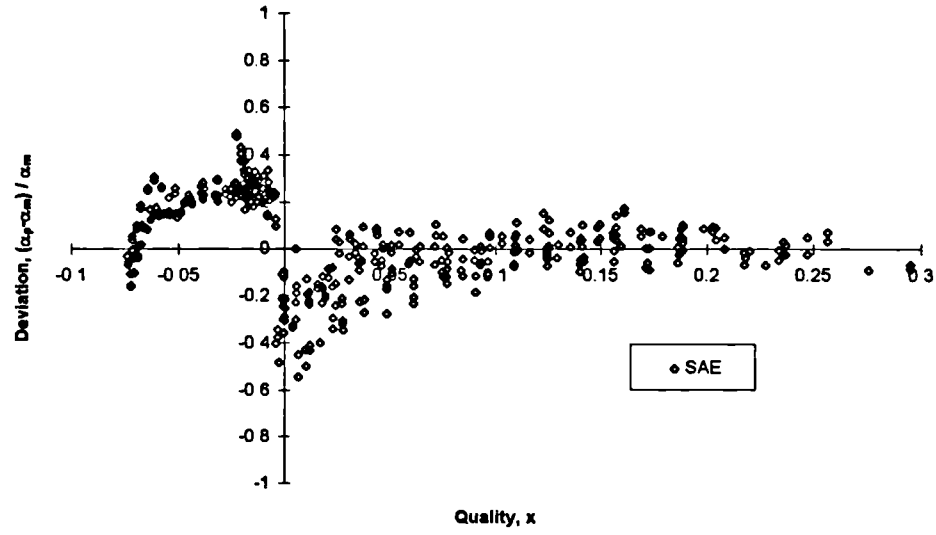

Figure 6.9 Chen (1966) prediction of heat transfer coefficient for all 500 mbar abs. experimental runs

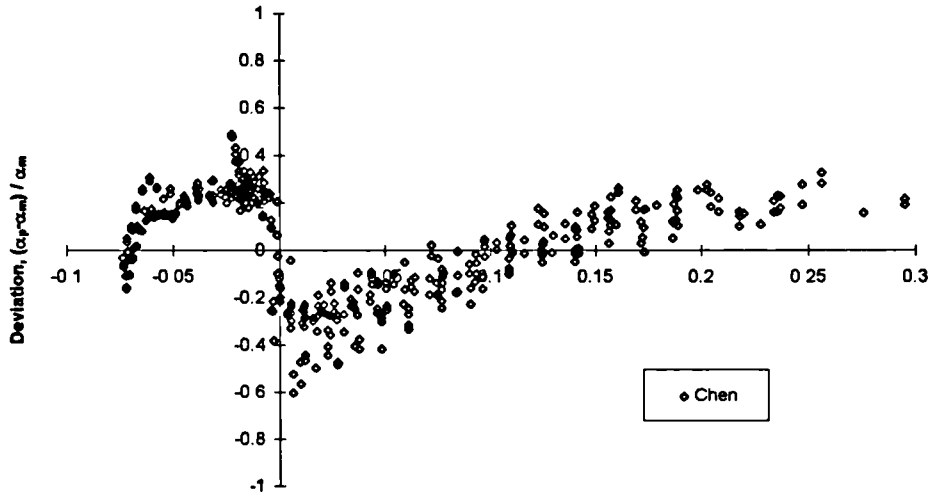

Figure 6.10 Liu-Winterton (1991) prediction of heat transfer coefficient for all 500 mbar abs. experimental runs

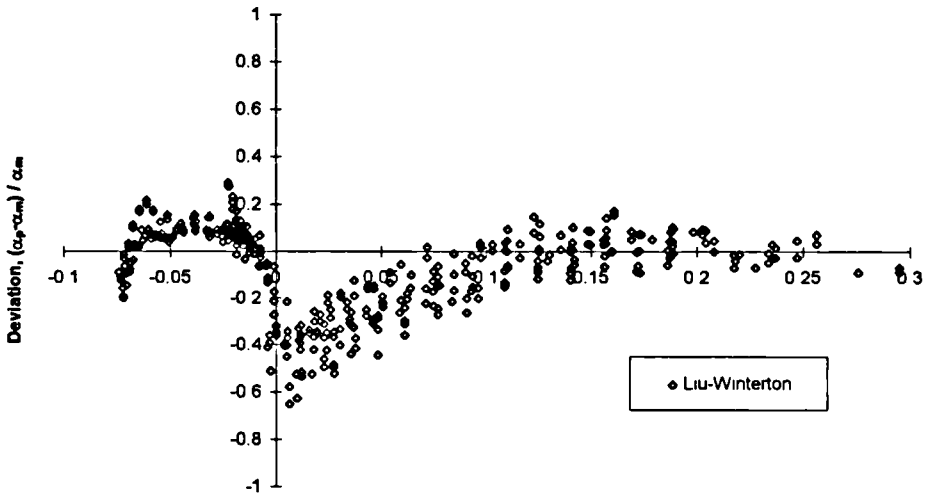

Figure 6.11 SAE prediction of heat transfer coefficient for all 1000 mbar abs. experimental runs

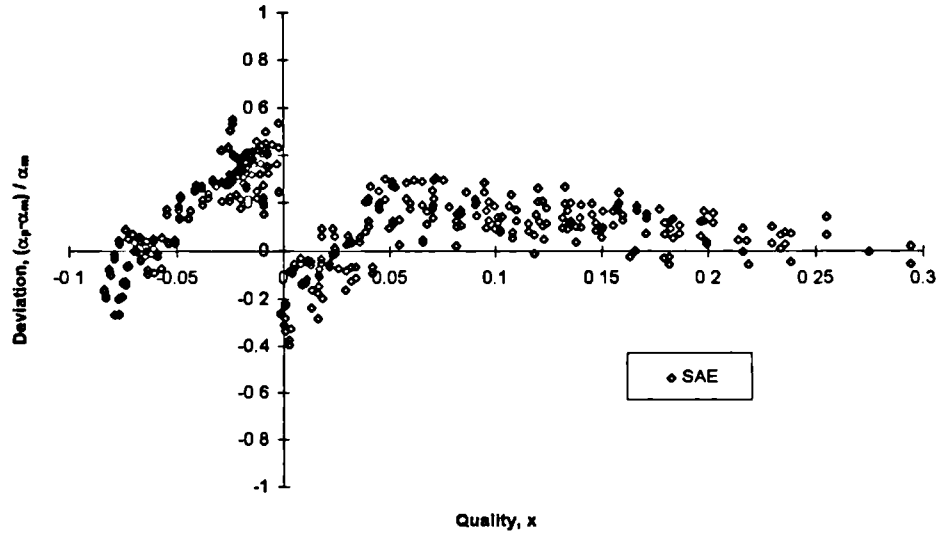

Figure 6.12 Chen (1966) prediction of heat transfer coefficient for all 1000 mbar abs. experimental runs

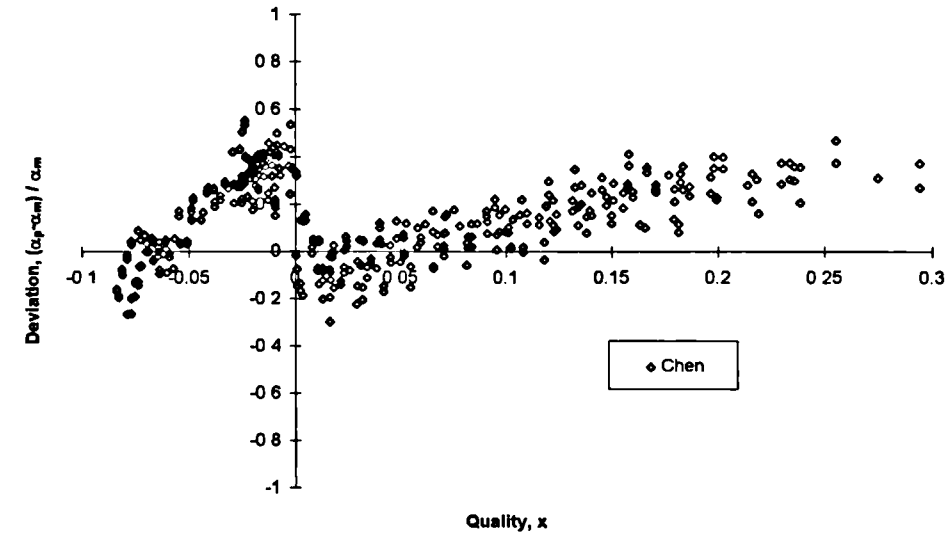

Figure 6.13 Liu-Winterton (1991) prediction of heat transfer coefficient for all 1000 mbar abs. experimental runs

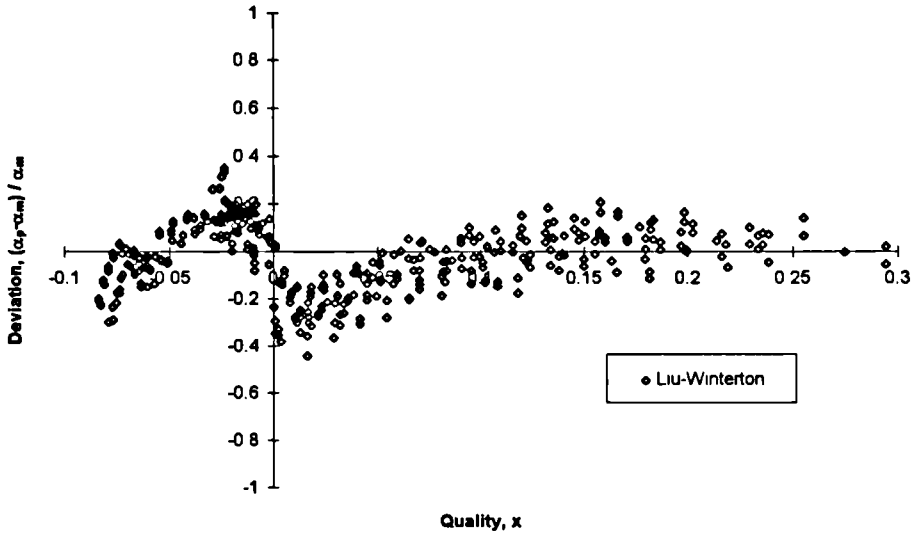

Figure 6.14 Typical SAE modelling profile (Run 250-1) and comparison with experimental run

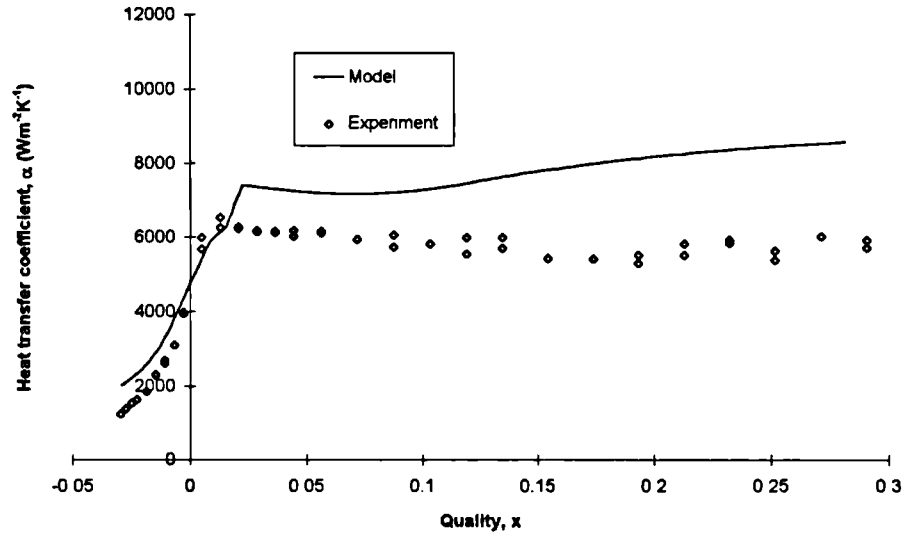

Figure 6.15 Typical SAE modelling profile (Run 500-1) and comparison with experimental run

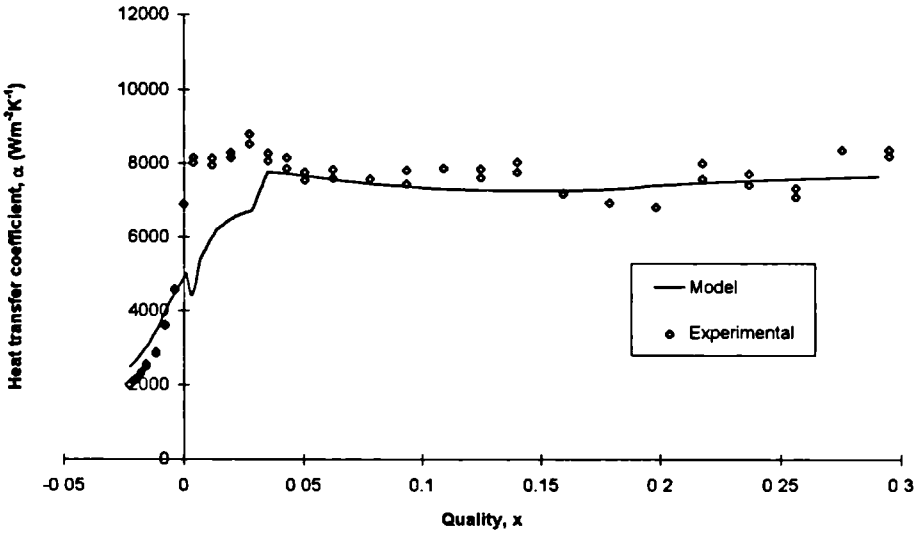

Figure 6.16 Typical SAE modelling profile (Run 1000-1) and comparison with experimental run

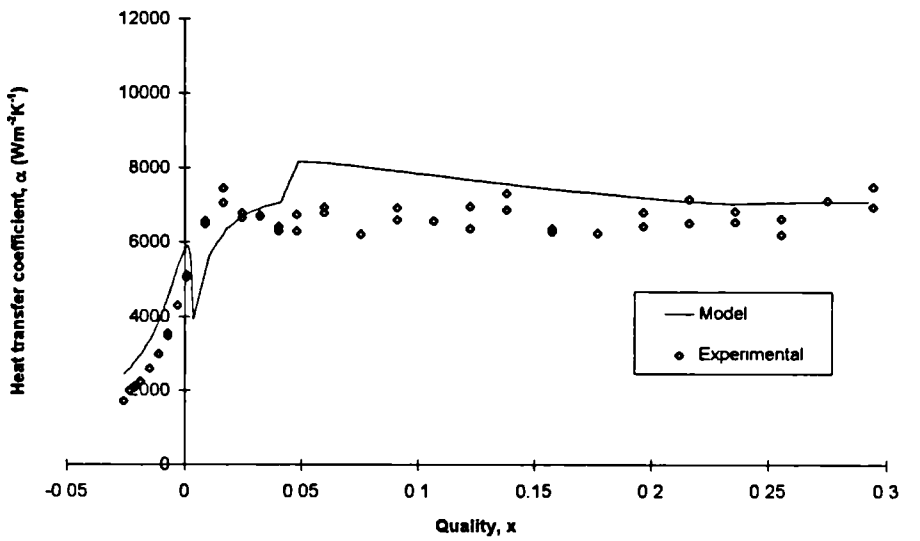

CHAPTER 7

CONCLUSIONS AND FUTURE WORK

This is the final and concluding chapter of this thesis. The objectives of this Ph.D. programme have been successfully fulfilled and the main conclusions drawn during the course of this work are presented in the following section. This is then followed by the recommendations for future experimental and theoretical/modelling work.

7.1 Conclusions

The objectives of this Ph.D. research programme have been successful achieved. To recapitulate, they are as follows:

1) To design, construct, commission and operate a new sub-atmospheric evaporator (SAE) rig and its instrumentation.

2) To perform and collect experimental data at sub-atmospheric pressures, as low as 250 mbar abs.

3) To design and code a framework/methodology for the phenomenological modelling of two-phase flow.

From the successful completion of these objectives, the following key conclusions were made:

(I) The SAE experiments were found to be **nucleate boiling dominant** for vapour quality, $x \geq 0.05$

(II) **Heat transfer coefficient maxima** were observed at around zero quality for the results at high inlet subcoolings and low sub-atmospheric pressures. The *localised thermal non-equilibrium instability* hypothesis presented by Jeglic and Grace (1965) provided an explanation.

(III) An unexpected increase in heat transfer coefficient (at the lowest pressure studied) with decreasing heat flux, which is contrary to the expected trend for nucleate boiling was observed. The **flow boiling hysteresis** hypothesis by Abdelmessih et al. (1973, 1974) provided an explanation for these anomalies.

(IV) The **system pressure and inlet subcoolings** were shown to influence flow stability in accordance with Jeglic and Grace (1965) hypothesis.

(V) From the SAE modelling code results and comparison against the SAE experimental data, it was concluded that existing heat transfer models, namely Chen (1966) (with Butterworth (1970) extension into subcooled boiling) and Liu and Winterton (1991) **flow boiling correlations were inadequate** to predict the heat transfer coefficients for sub-atmospheric pressure system, especially with the presence of local heat transfer coefficient maxima.

(VI) The **overall pressure drop predictions** from the SAE modelling code was found to be reasonably good with an overall mean deviation of 20.64%.

(VII) Finally, a proposal for a **new interpolative concept for churn flow** based on the dimensionless gas superficial velocity, U_G^* was tabled but needed validation

against existing adiabatic churn flow data of Govan (1990) and Owen (1986). A churn flow ratio, *Ch* was introduced as follows,

$$Ch = \frac{U_G^*(z) - U_G^*\left(z_{\text{flooding}}\right)}{U_G^*\left(z_{\text{flow reversal}}\right) - U_G^*\left(z_{\text{flooding}}\right)} \tag{7.1}$$

where

$U_G^*(z)$ is the value of U_G^* at position z, as the flow progresses from the flooding to the flow reversal points, i.e. through the churn flow regime.

$U_G^*\left(z_{\text{flooding}}\right)$ is the value of U_G^* at the flooding point.

$U_G^*\left(z_{\text{flow reversal}}\right)$ is the value of U_G^* at the flow reversal point.

7.2 Future work

The recommendations for future work can be divided into an experimental component and a theoretical/modelling component.

7.2.1 Experimental

The followings are recommendations for future experimental work:

(I) In view of the several heat transfer effects that had occurred, i.e. local heat transfer coefficient maxima at low vapour qualities and hysteresis observed, it is highly recommended that further and a wider range of sub-atmospheric experiments be conducted to investigate these effects. This would involve increasing the SAE rig's power rating as a first priority and improve the

temperature control system with the inclusion of a condenser to regulate the inlet subcoolings.

(II) To investigate the local heat transfer coefficient maxima at low vapour qualities, which is attributed to local flow instabilities as postulated by Jeglic and Grace (1965), better instrumentation and recording system are required, i.e. high speed data logging.

(III) To investigate the effects of hysteresis as postulated by Abdelmessih et al. (1973, 1974), a wider range of heat fluxes are necessary and needed as well as an increased in the number of thermocouples used. Additional power must be added to the current SAE rig configuration in order to achieve higher heat fluxes.

(IV) To increase the experimental database by performing additional experiments at different sub-atmospheric pressures, mass fluxes, heat fluxes and inlet subcoolings for water. This is highly recommended to both confirm the findings here as well as providing more data for use in future modelling or correlation developments.

(V) To conduct sub-atmospheric flow boiling experiments for other fluids including nitric acid solutions as found extant in BNFL reboilers. The SAE rig was built using high corrosion resistant stainless steel for this possible eventuality.

7.3.2 Theoretical / modelling

The followings are theoretical / modelling recommendations for future work.

(I) To validate and test the current SAE program with external experimental database.

(II) To compare the prediction of the heat transfer coefficients from the SAE program against other additional general flow boiling correlations, e.g. Gungor and Winterton (1986, 1987), Kandlikar (1992) and Steiner and Taborek (1992). This is currently in progress.

(III) To improve and extend the following flow regime developments in the SAE program:

Bubbly flow development It had been discussed and recommended that the key future flow pattern development for this flow regime will be a merger of the present SAE *subcooled flow boiling* (with bubble detachment) and *bubbly* flow regimes. This will be in line with the hydrodynamic flow regime of bubbly flow and should remove the current 'kinks' near zero quality in the SAE modelling code.

Slug flow development The improvement on the hydrodynamic model is the key recommendation for slug flow with models proposed by many researchers available for evaluation and testing, e.g. Fernandes et al. (1983), Orell and Rembrand (1986) and Sylvester (1987).

Churn flow model development Although a simplified interpolative method based on U_G^* was introduced in this thesis for churn flow, the validity of this procedure has yet to be rigorously tested against the adiabatic churn flow database of Owen (1986) and Govan (1990). During the writing of this thesis, an alternative model for churn flow was formulated but not implemented. In this new scheme, the key features of the proposals of Jayanti and Brauner (1992) and the U_G^* interpolation method could be brought together in the following manner.

Using essentially the churn flow model proposed by Jayanti and Brauner (1992), the key modification is the replacement of their assumption for

calculating the average wall shear stress based on a net liquid flow rate alone, with the U_G^* interpolation method for the wall shear stress. However, the problem with validating the U_G^* interpolation method against existing adiabatic churn flow database remained. The need to know *a priori* the flooding and flow reversal conditions and a reliable and robust procedure to extrapolate these conditions for the existing churn flow database is, therefore, of the utmost importance in the next phase of the development of churn flow model, should this methodology continue to be pursued.

Annular flow development The key development and recommendation for annular flow is to replace the existing general flow boiling correlation of Liu and Winterton (1991) with a heat transfer model that accounts for its phenomenological features. Heat transfer models by Kosky and Staub (1971) and Sun et al. (1995) are recommended for further evaluation.

(IV) As Thome (1995) noted that there is no model currently available that enables the prediction of the local heat transfer coefficient maxima near zero quality at low sub-atmospheric pressures found in the current SAE experiments. Therefore, an attempt to model this effect is highly recommended. A starting point would be a better understanding and development of local thermal non-equilibrium induced flow instability as proposed by Jeglic and Grace (1965).

It should be noted that the development of SAE program is a continuous process of improvement and refinement. The recommendations given above are currently being implemented and are at various stages of progress.

References

Abdelmessih, A.H., Fakhri, A. and Yin, S.T. (1974) Hysteresis effects in incipient boiling superheat of Freon 11. *Proc. of the 5th. Int. Heat Transfer Conf.*, Tokyo, Japan, vol. 4, pp. 165-169.

Abdelmessih, A.H., Yin, S.T. and Fakhri, A. (1973) Hysteresis effects and hydrodynamic oscillations in incipient boiling of Freon 11. *Proc. of Int. Meeting of Reactor Heat Transfer*, Karlsrühe, Deutschland, pp. 331-350.

Aounallah, Y., Kenning, D.B.R., Whalley, P.B. and Hewitt, G.F. (1982) Boiling heat transfer in annular flow. *Proc. of the 7th. Int. Heat Transfer Conf.*, München, Deutschland, vol. 4, pp. 193-199.

ASM Metals Handbook : Properties and Selection : Stainless Steels, Tool Materials and Special Purpose Metals, vol. 3, 9th. Edition, 1980.

Badiuzzaman, M. (1967) Correlation of subcooled boiling data. *Pakistan Eng.*, vol. 7, pp. 759-764, (see also Moles and Shaw, 1972).

Bankoff, S.G. and Lee, S.C. (1986) A critical review of the flooding literature. In *Multiphase Science and Technology*, vol. 2, Chap. 1 (Edited by Hewitt, G.F., Delhaye, J.M. and Zuber, N.), Hemisphere Pub. Corp., Washington DC, USA.

Barnea, D. (1986) Transition from annular flow and from dispersed-bubble flow unified models for the whole range of pipe inclination. *Int. J. Multiphase Flow*, vol. 5, pp. 733-744.

Barnea, D. (1987) A unified model for prediction of flow pattern transitions in the whole range of pipe inclination. *Int. J. Multiphase Flow*, vol. 13, pp. 1-12.

Barnea, D., Shoham, O. and Taitel, Y. (1982a) Flow pattern transition for vertical downward two-phase flow. *Chem. Eng. Sci.*, vol. 37, pp. 741-744.

Barnea, D., Shoham, O. and Taitel, Y. (1982b) Flow pattern transition for downward inclined two-phase flow; horizontal to vertical. *Chem. Eng. Sci.*, vol. 37, pp. 735-740.

Baroczy, C.J. (1966) A systematic correlation for two-phase pressure drop. *Chem. Eng. Prog. Symp. Ser.*, vol. 62, no. 64, pp. 232-249.

Beaton, C.F. (1990) Thermal and mechanical properties of heat exchanger construction material. Chapter 5.5.12 of *Hemisphere Handbook of Heat Exchanger Design* (Ed. G.F. Hewitt), Hemisphere Publishing Corp., New York.

Beisheuvel, A. (1984) On void fraction waves in dilute mixtures of gas and liquid bubbles. Ph.D. thesis, University of Twente, Netherlands. (see also Hewitt 1990).

Beisheuvel, A. and Gorissen, W.C.M. (1990) Void fraction disturbances in a uniform bubbly fluid. *Int. J. Multiphase Flow*, vol. 16, pp. 211-233. (see also Hewitt 1990).

Bennett, A.W., Hewitt, G.F., Kearsey, H.A., Keeys, R.K.F. and Lacey, P.M.C. (1965) Flow visualisation studies of boiling at high-pressure. *AERE*-R4874, UK Atomic Energy Agency, Harwell, England. (see also Hewitt and Roberts 1969).

Bennett, D.L. and Chen, J.C. (1980) Forced convection boiling in vertical tubes for saturated pure fluids and binary mixtures. *AIChE J.*, vol. 26, no. 3, pp. 454-464.

Bennett, J.A.R., Collier, J.G., Pratt, H.T.C. and Thornton, J.D. (1961) Heat transfer to two-phase gas-liquid systems. Part I: Steam/water mixtures in the liquid dispersed region in an annulus. *Trans. IChemE*, vol. 39, pp. 113. Also *AERE*-R 3519 (1959), UK Atomic Energy Agency, Harwell, England.

Bergles, A.E. and Rohsenow, W.M. (1964) The determination of forced-convection surface-boiling heat transfer. *J. Heat Transfer*, vol. 86, pp. 365-372.

Bharathan, D. (1978) Air-water countercurrent annular flow in vertical tubes. *EPRI Report* No. EPRI NP-786.

Bjorge, R.W., Hall, G.R. and Rohsenow, W.M. (1982) Correlation of forced convection boiling heat transfer data. *Int. J. Heat Mass Transfer*, vol. 25, no. 6, pp. 753-757.

Blasius, H. (1913) Mitt. Forschungsarb., no. 131 (see also Govier and Aziz, 1972).

Bowring, R.W. (1962) Physical model based on bubble detachment and calculation of steam voidage in the subcooled region of a heated channel. *OECD Halden Reactor Project Report* HPR-10. (see also Carey, 1992).

Brauner, N. and Barnea, D. (1986) Slug/churn transition in upward gas-liquid flow. *Chem. Eng. Sci.*, vol. 41, pp. 159-163.

Brotz, W. (1954) Uber die vorausberchnung der absorptiongeschwindeigkeit von gasen in stromenden flussigkeitsschichten. *Chem. Ing. Tech.*, vol. 26, pp. 470. (see also Jayanti and Hewitt, 1992).

BS 4937 : Part 4 : 1973. British Standard, London, England.

Butterworth, D. (1970) Private communication. (see Collier and Thome 1994).

Butterworth, D. (1977) Empirical methods for pressure drop, Chapter 4 of *Two-phase Flow and Heat Transfer* (edited by Butterworth, D. and Hewitt, G.F.), UKAEA Harwell Series, Oxford University Press.

Butterworth, D. (1979) The correlation of cross flow pressure drop data by means of permeability concept. *AERE* - R9435, UK Atomic Energy Agency, Harwell, England.

Butterworth, D. and Shock, R.A.W. (1982) Flow boiling. *Proc. of the 7th. Int. Heat Transfer Conf.*, München, Deutschland, vol. 1, pp. 11-30.

Carey, V.P. (1992) Liquid-vapor phase change phenomena. Hemisphere Pub. Corp., Washington DC, USA.

Chan, W.H.G.T. (1990) Evaporation and condensation in annular vertical upward flow of water-steam. Ph.D. thesis, University of London, England.

Chaudhry, A.B., Emerton, A.C. and Jackson, R. (1965) Flow regimes in the co-current upwards flow of water and air. *Symp. on Two-phase Flow*, Exeter, paper B2, pp. B201-B208.

Cheah, L.W. (1989) Nucleate pool boiling of refrigerant-12/Oil mixtures. *3rd Year Link-Project* Report, Imperial College of Science, Technology and Medicine, Dept. of Chem. Eng. and Chem. Tech., London, England.

Cheah, L.W. and Hewitt, G.F. (1992a) Steady state experiments Series # 1 Progress Report. Imperial College of Science, Technology and Medicine, Dept. of Chem. Eng. and Chem. Tech., *Multiphase Flow Systems Programme Report* (MPS) 22., London, England.

Cheah, L.W. and Hewitt, G.F. (1992b) Calculations on steady state flow and heat transfer. Imperial College of Science, Technology and Medicine, Dept. of Chem. Eng.

and Chem. Tech., *Multiphase Flow Systems Programme Report* (MPS) 1., London, England.

Chen, J.C. (1963) A correlation for boiling heat transfer to saturated fluids in convective flow. *ASME pre-print 63-HT-34* presented at 6th. National Heat Transfer Conference, Boston, 11-14 August. (see also Chen, 1966).

Chen, J.C. (1966) Correlation for boiling heat transfer to saturated fluids in convective flow. *Ind. Eng. Chem. Proc. Design. and Dev.*, vol. 5, no. 3, pp. 322-339. Reprint of Chen (1963) *ASME paper 63-HT-34.*

Chen, J.C. and Tuzla, K. (1995) Contributions of convection and boiling to convective flow boiling. *Convective Flow Boiling Conf.*, Banff, Alberta, Canada, Paper IV-10.

Chexal, B. and Lellouche, G.S. (1991) The Chexal-Lellouche void fraction correlation for generalised applications. *NSAC-139*, USA.

Chisholm, D. (1967) A theoretical basis for the Lockhart-Martinelli correlation for two-phase flow. *Int. J. Heat Mass Transfer*, vol. 10, pp. 1767-1778.

Chisholm, D. (1973) Pressure gradients due to friction during the flow of evaporating two-phase mixtures in smooth tubes and channels. *Int. J. Heat Mass Transfer*, vol. 16, pp. 347-358.

Chun, K.R. and Seban, R.A. (1971) Heat transfer to evaporating liquid films. J. Heat Transfer, vol. 93, pp. 391-396.

Churchill, S.W. and Usagi, R. (1972) A general expression for the correlation of rates of transfer and other phenomena. *AIChE J.*, vol. 18, no. 6, pp.1121-1128.

Cicchitti, A., Lombardi, C., Silvestri, M., Soldaini, G. and Zavattarelli, R. (1960) Two-phase cooling experiments : Pressure drop, heat transfer and burnout measurements. *Energ. Nucl.*, vol. 7, pp. 407-425 (see also Hewitt 1982).

Colburn, A.P. (1933) A method of correlating forced convection heat transfer data and a comparison with fluid friction. *Trans. AIChE*, vol. 29, pp. 174-210.

Colebrook, C.F. (1939) Turbulent flows in pipes, with particular reference to the transition region between smooth and rough pipe laws. *J. Inst. Civil Engrs.* , London, vol. 11, pp. 133-156.

Collier, J.G. (1972) Convective boiling and condensation. 1st Edition, Clarendon Press, Oxford, England.

Collier, J.G. and Thome, J.R. (1994) Convective boiling and condensation. 3rd Edition, Clarendon Press, Oxford, England.

Cooper, M.G. (1982) Correlation for nucleate boiling - formulation using reduced properties. *Physiochem. Hydrodynam.*, vol. 3, no. 4, pp. 89.

Cooper, M.G. (1984) Heat flow rates in saturated nucleate pool boiling - a wide ranging examination using reduced properties. *Advances in Heat Transfer*, vol. 16, pp. 157-239. Abstract published as **Saturation Nucleate Pool Boiling - A Simple Correlation**, in *Proc. 1st. UK Natl. Heat Transfer Conf.*, vol. 2, pp. 785-793., IChemE Symp. Ser. No. 86, London, 1984.

Cooper, M.G. (1989) Flow boiling - the 'apparently nucleate' regime. *Int. J. Heat Mass Transfer*, vol. 32, no. 3, pp. 459-464.

Davidson, W.F. (1943) Studies of heat transmission through boiler tubing at pressures from 500 to 3300 psi. *ASME Trans.*, vol. 65, pp. 551-554.

Davis, E.J. and Anderson, G.H. (1966) The incipience of nucleate boiling in forced convection flow. *AIChE Journal*, vol. 12, no. 4, pp. 774-780.

Davis, R.M. and Taylor, G.I. (1950) The mechanism of large bubbles rising through extended liquids and through liquids in tubes. *Proc. of the Royal Society*, London, vol. 200, series A, pp. 375-390.

Dengler, C.E. and Addoms, J.N. (1956) Heat transfer mechanism for vaporization of water in a vertical tube. *Chem. Eng. Prog. Symp. Series*, vol. 52, no. 18, pp. 95-103.

Dittus, F.W. and Boelter, L.M.K. (1930) University of California Publications on Engineering, vol. 2, pp. 443, Berkeley, USA.

Dix, G.E. (1971) Vapour void fractions for forced convection with subcooled boiling at low flow rates. *Rept. NEDO-10491, General Electric Co.*, USA.

Dukler, A.E. and Taitel, Y. (1986) Flow pattern transitions in gas-liquid systems: Measurement and modelling. In *Multiphase Science and Technology*, vol. 2 (Edited by Hewitt, G.F., Delhaye, J.M. and Zuber, N.), pp. 1-94, Hemisphere Pub. Corp., Washington DC, USA.

Engelberg-Forester, K. and Greif, R. (1959) Heat transfer to a boiling liquid - Mechanism and Correlations. *Trans. ASME*, J. Heat Transfer, vol. 81, pp. 43-53.

ESDU International Plc. (1967) Forced convection heat transfer in circular tubes, Part I : Correlations for fully developed turbulent flow - their scopes and limitations.

ESDU International Plc. (1977) Forced convection heat transfer in circular tubes, Part I : Correlations for fully developed turbulent flow - their scopes and limitations - Amendment to 1967.

Forster, H.K. and Zuber, N. (1955) Dynamics of vapor bubbles and boiling heat transfer. *AIChE Journal*, vol. 1, no. 4, pp. 531-535.

Fréchou, D. (1986) Etude de l'écoulement ascendant à trois fluide en conduite verticale. Thèse Inst. Natl. Polytech., Toulouse, France.

Friedel, L. (1979) Improved friction pressure drop correlations for horizontal and vertical two-phase flow. *European Two-Phase Flow Group Meeting*, Ispra, Italy, paper E2.

Fulford, G.D. (1964) The flow of liquids in thin films. In *Advances in Chemical Engineering*, vol. 5, (Edited by Drew, T.B., Hoopes, J.W. and Vermeulen, T.), pp. 151-236, Academic Press Inc., New York.

Galegar, W.C., Stovall, W.B. and Huntington, R.L. (1954) More data on two-phase vertical flow. *Petroleum Refiner*, vol. 33, pp. 208. (see also Chaudhry et al. 1965).

Gersten, K. (1983) Ducts. *Chapter 2.2.2 of Heat Exchanger Design Handbook* (HEDH), Hemisphere Publishing Corp., USA

Gnielinski, V. (1976) New equations for heat and mass transfer in turbulent pipe and channel flow. *Int. Chem. Eng.*, vol. 16, no. 2, pp. 359-368.

Gorenflo, D. (1993) Pool boiling. *VDI-Wärmeatlas*, VDI-Verlag, Düsseldorf, Deutschland (see Steiner and Taborek 1992 & Collier and Thome 1994).

Gouse, S.W. Jr. (1964) An introduction to two-phase gas-liquid flow. Report No 8734-3, Engr. Projects Lab., MIT, USA.

Govan, A.H. (1990) Modelling of vertical annular and disperse two-phase flows. Ph.D. thesis, University of London, England.

Govan, A.H., Hewitt, G.F., Owen, D.G. and Bott, T.R. (1988) An improved CHF modelling code. *Proc. of the Second UK National Conf. on Heat Transfer*, Glasgow, vol. 1, pp. 33-48.

Govan, A.H., Hewitt, G.F., Richter, H.J. and Scott, A. (1991) Flooding and churn flow in vertical pipes. *Int. J. Multiphase Flow*, vol. 17, pp. 27-44.

Govier, G.W. and Aziz, K. (1972) The flow of complex mixtures in pipes. Van Nostrand Reinhold, New York.

Govier, G.W., Radford, B.A. and Dunn, J.S.C. (1957) Upwards vertical flow of air-water mixtures. *Can. J. Chem. Eng*, vol. 35, pp. 58-70. (see also Chaudhry et al. 1965).

Griffith, P. and Synder, G.A. (1964) The bubbly-slug transition in a high velocity two-phase flow. MIT Report no. 5008-29. (see also Hewitt and Hall-Taylor 1970).

Griffith, P. and Wallis, G.B. (1961) Two-phase slug flow. *J. Heat Transfer*, Trans. ASME, vol. 83, pp. 307-320.

Guerrieri, S.A. and Talty, R.D. (1956) A study of heat transfer to organic liquids in single tube, natural circulation vertical tube boilers. *Chem. Eng. Prog.Symp. Series*, vol. 52, no. 18, pp. 69-77.

Gungor, K.E. and Winterton, R.H.S. (1986) A general correlation for flow boiling in tubes and annuli. *Int. J. Heat Mass Transfer*, vol. 29, no. 3, pp. 351-358.

Gungor, K.E. and Winterton, R.H.S. (1987) Simplified general correlation for saturated flow boiling and comparison of correlations with data. *Chem. Eng. Res. Des.*, vol. 65, pp. 148-156.

Haaland, S.E. (1983) Simple and explicit formulas for the friction factor in turbulent pipe flow. *ASME J. Fluids Eng.*, vol. 105, pp. 89-90.

Hahne, E., Spindler, K. and Shen, N. (1990) Incipience of flow boiling in subcooled well-wetting fluids. *Proc. of the 9th. Int. Heat Transfer Conf.*, Jerusalem, Israel, vol. 2, pp. 69-74.

Hanson, A. and Parr, G. (1965) The Engineer's Guide to Steels. Addison-Wesley Pub. Company Inc.

Hewitt, G.F. (1978) Measurements of two-phase flow parameters. Academic Press Inc. New York.

Hewitt, G.F. (1982) Pressure drop. Chapter 2.2 of *Handbook of Multiphase Systems*, (Editor-in-Chief: Hestroni, G.), Hemisphere Pub. Corp., Washington DC, USA.

Hewitt, G.F. (1989) Countercurrent two-phase flow. *Proc. of NURETH* (4th. Int. Mtg. on Nuclear Reactor Thermal Hydraulics), vol. 2.

Hewitt, G.F. (1990) Non-equilibrium two-phase flow. *Proc. 9th. Int. Heat Transfer Conf.*, Jerusalem, Israel, vol. 1, pp. 383-394.

Hewitt, G.F. (1995a) Forced convective boiling. To be published and presented as *Invited Lecture, 4th. UK National Heat Transfer Conf (Sept. 26-27th, 1995).*, UMIST, Manchester, England.

Hewitt, G.F. (1995b) Phenomenological issues in forced convective boiling. *Convective Flow Boiling Conf.*, Banff, Alberta, Canada, Keynote Lecture II.

Hewitt, G.F. (1995c) Phenomenological modelling: Churn and Annular flows. Workshop on Computation and Modelling of Multiphase Flows, January 9-13, Santa Barbara, CA, USA.

Hewitt, G.F. and Hall-Taylor, N.S. (1970) Annular two-phase flow. Pergamon Press, Oxford, England.

Hewitt, G.F. and Jayanti, S. (1993) To churn or not to churn. *Int. J. Multiphase Flow*, vol. 19, no. 3, pp. 527-529.

Hewitt, G.F. and Roberts, D.N. (1969) Studies of two-phase flow patterns by simultaneous X-ray and flash photography. *AERE*-M2159, UK Atomic Energy Agency, Harwell, England.

Hewitt, G.F. and Wallis, G.B. (1963) Flooding and associated phenomena in falling film flow in a vertical tube. *AERE*-R4022, UK Atomic Energy Agency, Harwell, England.

Hewitt, G.F., Kersey, H.A., Lacey, P.M.C. and Pulling, D.J. (1965) Burnout and nucleation in climbing film flow. *Int. J. Heat Mass Transfer*, vol. 8, pp. 793-814.

Hewitt, G.F., Lacey, P.M.C. and Nicholls, B. (1965) Transitions in the film flow in a vertical tube. In *Proc. Symp. on Two-phase Flow*, Exeter, England, vol. 2, pp. B401-B430.

Hewitt, G.F., Shires, G.L. and Bott, T.R. (1994) Process heat transfer. CRC Press Inc., USA

Hino, R. and Ueda, T. (1985) Studies on heat transfer and flow characteristics in subcooled flow boiling - Part 1 : Boiling characteristics. *Int. J. Multiphase Flow*, vol. 11, no. 3, pp. 269-281.

Hsu, Y.Y. (1962) On the size range of active nucleation cavities on a heating surface. *J. Heat Transfer*, vol. 83, pp. 207-216.

Incropera, F.P. and DeWitt, D.P. (1990) Fundamentals of Heat and Mass Transfer. 3rd. Edition, John Wiley and Sons, New York.

Ishii, M. (1982) Wave phenomena and two-phase flow instabilities. Chapter 2.4 of *Handbook of Multiphase Systems*, (Editor-in-Chief: Hestroni, G.), Hemisphere Pub. Corp., Washington DC, USA.

Jayanti, S. and Brauner, N. (1992) Churn flow. *Proc. 3rd. Int. Workshop on Two-phase Flow Fundamentals*, London, England.

Jayanti, S. and Hewitt, G.F. (1992) Prediction of the slug-to-churn flow transition in vertical two-phase flow. *Int. J. Multiphase Flow*, vol. 18, no. 6, pp. 847-860.

Jeglic, F.A. and Grace, T.M. (1965) Onset of flow oscillations in forced-flow subcooled boiling. *NASA Technical Note* TN D-2821, Lewis Research Center, Cleveland, Ohio, USA.

Jensen, M.K. and Hsu, J.T. (1987) A parametric study of boiling heat transfer in a tube bundle. *Proc. 1987 ASME-JSME Thermal Engineering Joint Conf.*, vol. 3, pp. 133-140.

Jones, O.C. and Zuber, N. (1978) Slug-annular transition with particular reference to narrow rectangular ducts. *Int. Seminar, Momentum, Heat and Mass Transfer in Two-phase Energy and Chemical Systems*, Dubrovnik, Yugoslavia. (see also Collier and Thome 1994).

Kandlikar, S.G. (1990) A general correlation for saturated two-phase flow boiling heat transfer inside horizontal and vertical tubes. *J. Heat Transfer*, vol. 112, pp. 219-228.

Kandlikar, S.G., Cartwright, M.D. and Mizo, V.R. (1995) A photographic study of nucleation characteristics of cavities in flow boiling. *Convective Flow Boiling Conf.*, Banff, Alberta, Canada, Paper II-1.

Kapteijn, C. (1989) Measurement on concentration waves in bubbly liquids. Ph.D. thesis, University of Twente, Netherlands. (see also Hewitt 1990).

Kattan, N., Thome, J.R. and Favrat, D. (1995) R-502 and two near-azeotropic alternatives, Part I: In tube flow boiling tests. *ASHRAE Trans.*, vol. 101, no. 1, paper CH-95-12-3.

Kenning, D.B.R. (1990) Wall temperatures in nucleate boiling: Spatial and temporal variations. *Proc. of the 9th. Int. Heat Transfer Conf.*, Jerusalem, Israel, vol. 3, pp. 33-38.

Kenning, D.B.R. (1992) Wall temperature patterns in nucleate boiling. *Int. J. Heat Mass Transfer*, vol. 35, no. 1, pp. 73-86.

Kenning, D.B.R. and Cooper, M.G. (1965) Flow patterns near nuclei and the initiation of boiling during forced convection heat transfer. Paper 11, presented at *Symp. on Boiling Heat Transfer in Steam Generating Units and Heat Exchangers* held in Manchester, IMechE (London), 15-16 Sept.

Kenning, D.B.R. and Cooper, M.G. (1989) Saturated flow boiling of water in vertical tubes. *Int. J. Heat Mass Transfer*, vol. 32, no. 3, pp. 445-458.

Kenning, D.B.R. and Hewitt, G.F. (1986) Boiling heat transfer in the annular flow regime. *Proc. of the 8th. Int. Heat Transfer Conf.*, San Francisco, USA, vol. 5, pp. 2185-2190.

Klausner, J.F. and Mei, R. (1995) Suppression of nucleation sites in flow boiling. *Convective Flow Boiling Conf.*, Banff, Alberta, Canada, Paper IV-6.

Kosky, P.G. and Staub, F.W. (1971) Local condensing heat transfer coefficients in the annular flow regime. *AIChE J*, vol. 17, no. 5, pp. 1037-1043.

Kosterin, S.I. (1949) An investigation of the influence of the diameter and the position of a tube on the hydraulic resistance and the structure of flow of a gas-liquid mixture (translated from Russian). *Ivestiya Akademii Nauk S.S.S.R.*, Otdelenie Tekhnicheskikh Nauk, No 12, pp. 1824-1831.

Kozlov, B.K. (1954) Forms of flow of gas-liquid mixtures and their stability limits in vertical tubes. *Zh. Tekh. Fiz.*, vol. 24, pp. 2285-2288. (see also Weisman and Kang 1981).

Kutateladze, S.S. (1961) Boiling heat transfer. *Int. J. Heat Mass Transfer*, vol. 4, pp. 31-45.

LABFACILITY Ltd. (1987) Temperature sensing with thermocouples and resistance thermometers - A practical handbook. 2nd Edition, Labfacility Ltd., England.

Lahey, R.T. and Moody, F.J. (1977) The thermal hydraulics of a boiling water nuclear reactor. *American Nuclear Society*, USA.

Levy, S. (1967) Forced convection subcooled boiling - Prediction of vapor volumetric fraction. *Int. J. Heat Mass Transfer*, vol. 10, pp. 951-965.

Lide, D.R. (Editor-in-Chief) (1991) Handbook of Chemistry and Physics. 72nd. Edition, CRC Press Inc., USA

Lienhard, J.H. (1994) Snares of pool boiling research : Putting our history to use. *Proc. 10th. Int. Heat Trans. Conf.*, Brighton, England, vol. 1, pp. 333-348.

Liu, Z. and Winterton, R.H.S. (1991) A general correlation for saturated and subcooled flow boiling in tubes and annuli, based on a nucleate pool boiling equation. *Int. J. Heat Mass Transfer*, vol. 34, no. 11, pp. 2759-2766.

Lockhart, R.W. and Martinelli, R.C. (1949) Proposed correlation of data for isothermal two-phase two-component flow in pipes. *Chem. Eng. Prog.*, vol. 45, pp. 39-48.

Mao, Z.S. and Dukler, A.E. (1989) An experimental study of gas-liquid slug flow. *Expts. Fluids*, vol. 8, pp. 169-182.

Mao, Z.S. and Dukler, A.E. (1993) The myth of churn flow? *Int. J. Multiphase Flow*, vol. 19, pp. 377-383.

Martinelli, R.C. and Nelson, D.B. (1948) Prediction of pressure drop during forced circulation boiling of water. *Trans. ASME*, vol. 70, pp. 695-702.

McQuillan, K.W. and Whalley, P.B. (1985) Flow patterns in vertical two-phase flow. *Int. J. Multiphase Flow*, vol. 11, no. 2, pp. 161-175.

McQuillan, K.W., Whalley, P.B. and Hewitt, G.F. (1985) Flooding in vertical two-phase flow. *Int. J. Multiphase Flow*, vol. 11, no. 6, pp. 741-760.

Mesler, R.B. (1973) An alternative to the Dengler and Addoms convective concept of forced convective boiling heat transfer. *AIChE J*, vol. 27, pp. 448-453.

Mishima, K. and Ishii, M. (1984) Flow regime transition criteria for upward two-phase flow in vertical tubes. *Int. J. Heat Mass Transfer*, vol. 27, no. 5, pp. 723-737.

Moissis, R. and Griffith, P. (1962) Entrance effects in a two-phase slug flow. *J. HeatTransfer*, vol. 84, pp. 29-39.

Moles, F.D. and Shaw, J.F.G. (1972) Boiling heat transfer to subcooled liquids under conditions of forced convection. *Trans. IChemE*, vol. 50, pp. 76-84.

Moody L.F. (1944) Friction factors for pipe flow. *Trans. ASME*, vol. 66, pp. 641. (see also Incropera and DeWitt 1990).

Mostinski, I.L. (1963) Calculation of heat transfer and critical heat fluxes in liquids. *Teploenergetika*, vol. 10, no. 4, pp. 66. (see also Hewitt, Shires and Bott 1994).

Nicklin, D.J. (1961) Two-phase flow in vertical tube. Ph.D. thesis, University of Cambridge, England. (see also Chaudhry et al. 1965).

Nicklin, D.J. and Davidson, J.F. (1962) The onset of instability in two-phase slug flow. Presented at the *Symp. on Two-phase Flow*, Inst. Mech. Engrs., London, paper no. 4.

Nicklin, D.J., Wilkes, J.O. and Davidson, J.F. (1962) Two-phase flow in vertical tubes. *Trans. Inst. Chem. Eng.*, vol. 40, pp. 61-68.

Nikuradse, J. (1932) Gesetzmässigkeiten der turbulenten Strömung in glatten Rohren, Forschungsheft no. 356, VDI., Verlag, Berlin. (see also Govier and Aziz 1972).

Nishikawa, K. (1995) Development of boiling heat transfer and its app.lications. *Proc. of the 2nd. Int. Conf. on Multiphase Flow*, Kyoto, Japan, vol. 3, pp. PL3-1 to PL3-12.

Nukiyama, S. (1934) The maximum and minimum values of the heat Q transmitted from metal to boiling water under atmospheric pressure (translated by C.J. Lee from

Jap. Soc. Mech. Engr., vol. 37, 1934, pp. 367-374). *Int. J. Heat Mass Transfer*, vol. 9, 1966, pp. 1419-1433.

Nusselt, W. (1916) Die Oberflachenkondensation des Wasserdampfes (Surface condensation of water). *Z. Ver. Deut. Ing.*, vol. 60 ,(26), pp. 569-575, vol. 60 ,(27), pp. 541-546. (see also Jayanti and Hewitt 1992).

Ohnuki, A., Akimoto, H. and Sudo, Y. (1995) Flow pattern and its transition in gas-liquid two-phase flow along a large vertical pipe. *Proc. of the 2nd. Int. Conf. on Multiphase Flow*, Kyoto, Japan, vol. 3, pp. FT1-17 to FT1-23.

Oshinowo, T. and Charles, M.E. (1974) Vertical two-phase flow: Part I. Flow pattern correlations. *Can. J. Chem. Eng.*, vol. 52, pp. 25-35.

Owen, D.G. (1986) An experimental and theoretical analysis of equilibrium annular flows. Ph.D. thesis, University of Birmingham, England.

Owen, D.G. and Hewitt, G.F. (1987) An improved annular two-phase flow model. Proc. 3rd. Int. Symp. on Multiphase Flow, The Hague, Published by BHRA.

Papell, S.S. (1963) Subcooled boiling heat transfer under forced convection in a heated tube. *NASA Technical Note* TN D-1583, Lewis Research Center, Cleveland, Ohio, USA.

Pethukov, B.S. (1970) Heat transfer and friction in turbulent pipe flow with variable physical properties. *Advances in Heat Transfer*, vol. 6, pp. 503-564, Academic Press, New York, USA.

Pethukov, B.S., Genin, L.G. and Kovalve, S.A. (1986) Heat transfer in nuclear power plants. *Energoatomizdat (in Russian).* (see also Yagov 1995).

Pickering, P.F. (1994) Instabilities in low pressure boiling systems. Ph.D. thesis, University of London, England.

Polley, G.T., Ralston, T. and Grant, I.D.R. (1980) Forced crossflow boiling in an ideal in-line tube bundle. *ASME paper 80-HT-46.*

Premoli, A., Francesco, D. and Prina, A. (1971) A dimensionless correlation for determining the density of two-phase mixtures. *Termotecnica*, vol. 25, pp. 17-26.

Radovcich, N.A. and Moissis, R. (1962) The transition from two-phase bubble flow to slug flow. *MIT Report* no. 7-7673-22.

Rohsenow, W.M. (1952) A method of correlating heat transfer data for surface boiling of liquids. *Trans. ASME*, vol. 74, pp. 969-975.

Rohsenow, W.M. (1953) Heat transfer with evaporation. *Heat Transfer - A Symposium held at the University of Michigan During The Summer of 1952.* University of Michigan Press, pp 101-150.

Ross, H.D. and Radermacher, R. (1987) Suppression of nucleate boiling of pure and mixed refrigerants in turbulent annular flow. *Int. J. Multiphase Flow*, vol. 13, no. 6, pp. 759-772.

Rouhani, S.Z. (1969) Modified correlations for void and two-phase pressure drop. *AB Atomenergi*, Rept. AE-RTV 841, Sweden.

Saha, P. and Zuber, N. (1974) Point of net vapor generation and vapor void fraction in subcooled boiling. *Proc. of the 5th. Int. Heat Transfer Conf.*, Tokyo, Japan, vol. 4, pp. 175-179.

Sani, R.L. (1960) Downflow boiling and nonboiling heat transfer in a uniformly heated tube. *Univ. California Radiation Lab.*, Report UCRL-9023. (see Chen 1966).

Sato, T. and Matsumura, H. (1964) On the conditions of incipient subcooled boiling with forced convection. *Bulletin of JSME*, vol. 7, no. 26, pp. 392-398.

Schrock, V.E. and Grossman, L.M. (1962) Forced convection boiling in tubes. *Nuclear Sci. Eng.*, vol. 12, pp. 474-480.

Shah, M.M. (1976) A new correlation for heat transfer during boiling flow through pipes. *ASHRAE Trans.*, vol. 82, no. 2, pp. 66-86.

Shah, M.M. (1982) Chart correlation for saturated boiling heat transfer: Equations and further study. *ASHRAE Trans.*, vol. 88, part 1, no. 2673, pp. 185-196.

Sieder, E.N. and Tate, G.E. (1936) Heat transfer and pressure drop of liquids in tubes. *Ind. Eng. Chem.*, vol. 28, pp. 1429-1435.

Spindler, K. (1994) Flow boiling. *Proc. of the 10th. Int. Heat Transfer Conf.*, Brighton, England, vol. 1, pp. 349-368.

Steiner, D. and Taborek, J. (1992) Flow boiling heat transfer in vertical tubes correlated by an asymptotic model. *Heat Transfer Eng.*, vol. 13, no. 2, pp. 43-69.

Stephan, K. and Abdelsalam, M. (1980) Heat transfer correlations for natural convection boiling. *Int. J. Heat Mass Transfer*, vol. 23, pp. 73-87.

Stone, J.R. (1971) Subcooled and net boiling heat transfer to low pressure water in electrically heated tubes. *NASA Technical Note* TN D-6402, Lewis Research Center, Cleveland, Ohio, USA.

Sun, G., Chan, W.H.G.T. and Hewitt, G.F. (1995) A general heat transfer model for two-phase annular flow. *Convective Flow Boiling Conf.*, Banff, Alberta, Canada. Paper IV-12.

Taitel, Y. (1990) Flow pattern transition in two-phase flow. *Proc. 9th. Int. Heat Transfer Conf.*, Jerusalem, Israel, vol. 1, pp. 237-254.

Taitel, Y. and Dukler, A.E. (1976) A model for prediction of flow regime transitions in horizontal and near-horizontal gas-liquid flow. *AIChE J.*, vol. 22, pp. 47-55.

Taitel, Y., Barnea, D. and Dukler, A.E. (1980) Modelling flow pattern transitions for steady upward gas-liquid flow in vertical tubes. *AIChE J.*, vol. 26, pp. 345-354.

Thom, J.R.S. (1964) Prediction of pressure drop during forced circulation boiling of water. *Int. J. Heat Mass Transfer*, vol. 7, pp. 709-724.

Thome, J.R. (1995) Flow boiling in horizontal tubes: A critical assessment of current methodologies. *Two-Phase Flow Modelling and Experimentation*, vol. 1, pp. 41-52.

van Wijgaarden, L. (1989) Flow of bubbly liquids. In *Theoretical and Applied Mechanics* (IUTAM, 1989), (Edited by Germain, P. et al.), Elsevier Science Publishers, Netherlands, pp. 387-406. (see also Hewitt 1990).

Von Karman, T. (1930) Nachr. Ges. Wiss. Göttingen, *Math-physik.* Kl. (see also Govier and Aziz 1972).

Wadekar, V. (1995) An alternative model for flow boiling heat transfer. *Convective Flow Boiling Conf.*, Banff, Alberta, Canada, Paper IV-11.

Wadekar, V.V. (1991) Vertical slug flow heat transfer with nucleate boiling. *Phase Change Heat Transfer, 28th. Nat. Heat Transfer Conf.*, Minneapolis, MN, USA. ASME, HTD, vol. 159, pp. 157-161.

Wadekar, V.V. (1992) A model for addition of convective and nucleate boiling heat transfer in flow boiling. Proc. of 3rd. UK National Heat Transfer Conference, Birmingham, England, vol. 1, pp. 181-187.

Wadekar, V.V. (1994) A flow boiling model based on suppression of convective heat transfer, First ISHMT-ASME Heat and Mass Transfer Conf., Bombay, India, Paper No. TPF-23.

Wadekar, V.V. and Kenning, D.B.R. (1990) Flow boiling heat transfer in vertical slug and churn flow region. *Proc. of the 9th. Int. Heat Transfer Conf.*, Jerusalem, Israel, vol. 3, pp. 449-454.

Wallis, G.B. (1961) Flooding velocities for air and water in vertical tubes. *AEEW*-R123.

Wallis, G.B. (1962) The transition from flooding to co-current annular flow in a vertical tube. *AEEW*-R142.

Wallis, G.B. (1969) One-dimensional two-phase flow. McGraw-Hill, New York.

Webb, R.L. and Neelkanth, S.G. (1992) A critical review of correlations for convective vaporization in tubes and tube banks. *Heat Transfer Eng.*, vol.. 13, no. 3, pp. 58-81.

Weisman, J. and Kang, S.Y. (1981) Flow pattern transitions in vertical and upwardly inclined lines. *Int. J. Multiphase Flow*, vol. 7, pp. 271-291.

Weisman, J., Duncan, D., Gibson, J. and Crawford, T. (1979) Effects of fluid properties and pipe diameter on two-phase flow patterns in horizontal lines. *Int. J. Multiphase Flow*, vol. 5, pp. 437-462. (see also Weisman and Kang 1981).

Whalley, P.B. (1975) HTFS-UM7-HANA users manual, Harwell Annular Flow Program, AERE-R-7994.

Whalley, P.B. (1990) Boiling, condensation and gas-liquid flow. Clarendon Press, Oxford, England.

Whalley, P.B., Hutchinson, P. and Hewitt, G.F. (1974) The calculation of critical heat flux in forced convective boiling. *Proc. of the 5th. Int. Heat Transfer Conf.*, Tokyo, Japan, vol. 4, pp. 290-294.

Willetts, I.P., Azzopardi, B.J. and Whalley, P.B. (1986) A study of the effect of gas and liquid properties on annular two-phase flow. *AERE* - R-11976, UK Atomic Energy Agency, Harwell, England.

Wolf, A. (1995) Film structure of vertical annular flow. Ph.D. thesis, University of London, England.

Wood, D.J. (1966) An explicit friction factor relationship. *Civil Eng., ASCE*, vol. 36, pp. 60-61. (see also N.H. Chen 1979).

Wright, R.M. (1961) Downflow forced-convection boiling of water in uniformly heated tubes. Ph.D. thesis, *Univ. California Radiation Lab.*, Report UCRL-9744.

Yagov, V.V. (1995) The principal mechanisms of the flow boiling heat transfer. *Convective Flow Boiling Conf.*, Banff, Alberta, Canada, Paper IV-9.

Zabaras, G.J. and Dukler, A.E. (1988) Counter-current gas-liquid annular flow including the flooding state. *AIChE. J.*, vol. 34, pp. 389-396.

Zeitoun, O. (1994) Subcooled flow boiling and condensation. Ph.D. Thesis, McMaster University, Hamilton, Ontario, Canada (see also Zeitoun and Shoukri 1995).

Zeitoun, O. and Shoukri, M. (1995) On the net vapour generation phenomenon in low pressure and low mass flux subcooled flow boiling. *Convective Flow Boiling Conf.*, Banff, Alberta, Canada, Paper II-3.

Zigrang, D.J. and Sylvester, N.D. (1985) A review of explicit friction factor equations. *Trans ASME, J. Energy Resources Technology*, vol. 107, no. 2, pp. 280-283.

Zuber, N. and Findlay, J.A. (1965) Average volumetric concentration in two-phase flow systems. *J. Heat Transfer*, vol. 87, pp. 453-468.

APPENDIX A

Calculation of temperature difference across the test-section wall

Although the outside surface wall temperature was measured experimentally, it is the difference in temperature between the **inside surface wall** and the boiling fluid temperatures that is used in the heat transfer coefficient calculations and analysis. Since heat is generated in the wall by passing a high electric current through it, it is necessary to calculate the temperature difference across the test section wall in order to estimate the inside surface wall temperature.

This temperature difference can be estimated from the one-dimensional heat conduction analysis (see for instance Incropera and DeWitt, 1990). In such an analysis, the following assumptions were made:

- No axial heat conduction
- Uniform heat generation
- Uniform wall thickness
- Constant test section properties

For heat conduction in a cylinder of thermal conductivity, λ and volumetric heat generation rate, $\dot{q}_V$, the following one-dimensional heat conduction equation can be written

$$\frac{1}{r}\frac{d}{dr}\left(r\frac{dT}{dr}\right)+\frac{\dot{q}_V}{\lambda}=0 \qquad \text{(A-1)}$$

where T is the temperature at radius r. Integrating the equation (A-1), will give

$$r\frac{dT}{dr}=-\frac{\dot{q}_V r^2}{2\lambda}+C_1 \qquad \text{(A-2)}$$

where C_1 is an integration constant. Since the test section is a cylinder with an outer radius of, say, r_2 and an inner radius of r_1, and as the outer surface is also insulated, then when $r = r_2$, $dT/dr = 0$ and thus:

$$C_1=\frac{\dot{q}_V r_2^2}{2\lambda} \qquad \text{(A-3)}$$

It then follows that:

$$dT=-\frac{\dot{q}_V}{2\lambda}\left(r-\frac{r_2^2}{r}\right)dr \qquad \text{(A-4)}$$

which can be integrated to give:

$$T=-\frac{\dot{q}_V}{2\lambda}\left(\frac{r^2}{2}-r_2^2\ln r\right)+C_2 \qquad \text{(A-5)}$$

Recognising that at $r = r_2$, $T = T_2$, the above equation can be written as:

$$T_2=-\frac{\dot{q}_V}{2\lambda}\left(\frac{r_2^2}{2}-r_2^2\ln r_2\right)+C_2 \qquad \text{(A-6)}$$

By subtracting equation (A-5) from (A-6), the integration constant C_2 is eliminated giving the following equation:

$$T_2 - T = \frac{\dot{q}_V}{2\lambda}\left(\frac{r_2^{\,2} - r^2}{2} - r_2^2 \ln\left(\frac{r_2}{r}\right)\right) \qquad \text{(A-7)}$$

The inner surface heat flux, $\dot{q}$ of the test section can be related to the volumetric heat generation rate $\dot{q}_V$ by the following expression:

$$\dot{q} = -\frac{\dot{q}_V \pi \left(r_2^2 - r_1^2\right)}{2\,\pi\, r_1} \qquad \text{(A-8)}$$

and hence

$$\dot{q}_V = -\frac{2\, r_1\, \dot{q}}{\left(r_2^2 - r_1^2\right)} \qquad \text{(A-9)}$$

Substituting for the volumetric heat generation rate $\dot{q}_V$ into equation (A-7) for the inner surface position will give:

$$T_2 - T_1 = -\frac{2\, r_1\, \dot{q}}{2\,\lambda\left(r_2^2 - r_1^2\right)}\left(\frac{r_2^{\,2} - r_1^{\,2}}{2} - r_2^2 \ln\left(\frac{r_2}{r_1}\right)\right) \qquad \text{(A-10)}$$

or simplified as

$$T_2 - T_1 = -\frac{\dot{q}\, r_1}{\lambda}\left(\frac{1}{2} - \frac{r_2^{\,2}}{\left(r_2^2 - r_1^2\right)} \ln\left(\frac{r_2}{r_1}\right)\right) \qquad \text{(A-11)}$$

which is the required expression relating the temperature difference across the heated test section wall to the inner surface heat flux. It should be noted that in this particular set of coordinates, $\dot{q}$ is taken as positive in the outwards direction and , therefore, negative in the inwards direction.

APPENDIX B

Thermocouple calibration results

The whole temperature measurement system (i.e. thermocouples, compensating cables and leads, data logging computer and software) was calibrated using a constant temperature hot water bath (as heat source for the hot junction) and the prepared isothermal box (reference junction). For an accurate and sensitive independent reference temperature measurement of the hot water bath, a Platinum probe connected to a Fluke Multimeter (tested and accurate to ± 0.001 °C, and was calibrated by the Electronics Section of the Chemical Engineering Department) was used. A schematic block diagram of the calibration arrangement is given in Figure 4.9 of Chapter 4.

The EMFs for each thermocouple at different temperature settings were logged and plotted. The temperature settings were staggered by first raising the temperature settings (i.e. measurements at 10, 30, 50, 70 and 90°C) and then followed by a gradual decrease (i.e. measurements at 80, 60, 40 and 20°C). This procedure was followed to detect any possible hysteresis in the data-logging system, which fortunately, there wasn't. Each plot for each thermocouple was then curve-fitted using linear regression and an almost perfect linear (R^2 value ≅ 1) equation was obtained for each of the thermocouples in the general form of,

$$y = mx + c$$

confirming the linear response expected of the K-type thermocouples. The coefficients, *m* and *c*, of the thermocouple calibrations and the location of each thermocouple relative to the first point of measurement are given below:

Calibration coefficients for fluid thermocouples

Fluid Thermocouple Position	*m*	*c*
0.0	0.02437	-0.37422
0.03	0.02444	-0.65216
0.06	0.02388	-0.14387
0.09	0.02400	-0.31208
0.34	0.02439	-0.33643
1.09	0.02351	0.04925
2.09	0.02251	1.14260
3.09	0.02443	-0.58998
4.09	0.02444	-0.59663

Calibration coefficients for wall thermocouples

Wall Thermocouple Position	*m*	*c*
0.0	0.02484	-0.83784
0.0	0.02483	-0.80627
0.03	0.02432	-0.45934
0.03	0.02541	-1.20294
0.06	0.02491	-0.90684
0.06	0.02429	-0.45706
0.09	0.02400	-0.23714
0.09	0.02410	-0.21131

0.14	0.02393	-0.16972
0.14	0.02458	-0.62615
0.19	0.02437	-0.48156
0.19	0.02448	-0.71591
0.24	0.02434	-0.57007
0.24	0.02417	-0.40468
0.29*	0.02474	-0.76259
0.29	0.02474	-0.69797
0.34	0.02473	-0.65492
0.34	0.02379	-0.12969
0.44	0.02459	-0.45153
0.44	0.02450	-0.57645
0.54	0.02492	-0.78439
0.54	0.02560	-1.36272
0.64	0.02376	-0.03852
0.64	0.02418	-0.35495
0.74	0.02434	-0.53034
0.74	0.02383	-0.26503
0.84	0.02399	-0.32805
0.84	0.02561	-1.04637
0.94	0.02458	-0.67927
0.94	0.02338	0.29341
1.09	0.02343	0.19004
1.09	0.02529	-1.10439
1.29*	0.02541	-1.19236
1.29	0.02356	-0.07013
1.49	0.02480	-0.85607
1.49	0.02441	-0.60226
1.69*	0.02319	0.19725
1.69	0.02351	0.00955
1.89	0.02388	-0.31790

1.89	0.02525	-0.87872
2.09	0.02466	-0.65499
2.09	0.02461	-0.70427
2.34	0.02538	-0.98528
2.34	0.02432	-0.44316
2.59*	0.02462	-0.57649
2.59	0.02458	-0.58668
2.84	0.02470	-0.66355
2.84	0.02443	-0.47542
3.09	0.02488	-0.87131
3.09	0.02460	-0.54581
3.34	0.02425	-0.47088
3.34	0.02519	-0.92662
3.59	0.02457	-0.69977
3.59	0.02475	-0.72198
3.84	0.02447	-0.77248
4.09	0.02445	-0.48452
4.09	0.02443	-0.36621

NB: The thermocouples with an asterisk (*) marked beside them were not used in the final analysis since they were tested to be faulty i.e. their readings were *faulty* due to EMF pickup from the test section (see Chapter 4 for discussion).

APPENDIX C

Experimental error estimation and analysis

The measured value of any physical quantity such as pressure and temperature has little meaning unless it is accompanied by a statement of its uncertainty. Therefore, it is the objective of this appendix to furnish the experimental work reported in this thesis with such a statement. By conducting an error estimation and analysis on each of the measuring instrument used, the final combined result will then provide a value, with which the data obtained from the SAE experiments can be utilised with confidence.

The final combined result showed that the random r.m.s error associated with the heat transfer coefficient in the saturated two-phase flow region is:

$$\left(\frac{d\alpha}{\alpha}\right) = \pm 0.132$$

The following sections will analyse each stage of the error analysis process that was performed which eventually led to the above statement.

Error in pressure measurement:

The high stability pressure transducers used were manufactured and calibrated by Maywood Instruments Ltd. These calibrations were checked at atmospheric pressure

against that of a highly accurate mercury barometer and was found to be in good agreement by Pickering (1994). It was found that the transducers' response was very repeatable and linear with an estimated accuracy of ± 3 mbar. The calibrations were checked *in situ* before and after each set of runs based on hydrostatic head calculations and vacuum checks for calibration drifts (where with no fluid flow, all the transducers will show the same readings). Fortunately, no drifts were detected due to the high stability of the transducers used.

During the course of the experiments, a small oscillation of ± 10 mbar were noted. These oscillations, however, had not impaired neither the accuracy nor stability of the transducers in any way as it was initially feared. Hence, in the worse case scenario, the error in the pressure measurement is estimated to be ± 13 mbar.

Error in thermocouple calibration:

From the linear regression correlations for each of the thermocouples (see Appendix B) used in the SAE experiments, one could conclude that from the high value of R-squared, i.e. R^2 value ≅ 1, the linearity of the thermocouple response is of the highest order as one would expect.

Taking into account of the wall thermocouple mounting and the mock-up test conducted to check on the viability of this form of mounting as described and illustrated in Chapter 4, an estimate of the thermocouple accuracy was ±0.01 °C, which is a whole magnitude higher than the accuracy of the reference platinum resistance probe (±0.001 °C) against which the thermocouples were calibrated.

Error in heat flux:

The amount of electrical power dissipated in the test section during the steady state forced convective experiments was measured using an AC Watt-meter (manufactured

by H.W. Sullivan). As the power measurements were read off directly from the watt-meter, care must be taken to avoid any parallax misreading. The power readings can be read to an accuracy of ±1 W before multiplying with the scaling factor of 125, which will result in an overall accuracy of ±125 W.

The total error in the heat flux used can then be estimated from the following equation:

$$\dot{q} = \frac{\mathrm{P}}{\pi D L} \tag{C-1}$$

where P, D and L are the power reading (W), test section diameter (m) and test section length (m) respectively. Complete differential of equation (C-1) will give,

$$d\dot{q} = \frac{\partial \dot{q}}{\partial \mathrm{P}} d\mathrm{P} + \frac{\partial \dot{q}}{\partial D} \mathrm{d}D + \frac{\partial \dot{q}}{\partial L} dL \tag{C-2}$$

Solving for each of the partial differential terms yield the following results:

$$\frac{\partial \dot{q}}{\partial P} = \frac{1}{\pi D L} \tag{C-3}$$

$$\frac{\partial \dot{q}}{\partial D} = -\frac{P}{\pi D^2 L} \tag{C-4}$$

$$\frac{\partial \dot{q}}{\partial L} = -\frac{P}{\pi D L^2} \tag{C-5}$$

Hence, to evaluate the random error, equation (C-2) is first divided by equation (C-1) and then squared to give:

$$\therefore \quad \left(\frac{d\dot{q}}{\dot{q}}\right)^2 = \left(\frac{dP}{P}\right)^2 + \left(\frac{dD}{D}\right)^2 + \left(\frac{dL}{L}\right)^2 \tag{C-6}$$

Estimating the variation in each term of equation (C-6):

$\frac{dP}{P} = \pm 0.00962$ ± 125W accuracy from 12 994.8 W (lowest experiment setting).

$\frac{dD}{D} = \pm 0.00087$ $\pm 2 \times 10^{-5}$ m from a test section diameter of 2.298×10^{-2}m

$\frac{dL}{L} = \pm 0.00023$ $\pm 1 \times 10^{-3}$ m from an effective test section length of 4.34 m.

The calculated mean squared error in heat flux:

$$\left(\frac{d\dot{q}}{\dot{q}}\right)^2 = 9.335 \times 10^{-5} \qquad \text{(C-7)}$$

∴Random r.m.s. error in heat flux:

$$\underline{\underline{\left(\frac{d\dot{q}}{\dot{q}}\right) = \pm 9.66 \times 10^{-3}}} \qquad \text{(C-8)}$$

Error in saturation temperature:

The estimated value for the variation in the saturation temperature was evaluated in the following manner. From a pressure-saturation temperature correlation for steam-water,

$$T_{sat} = \frac{3842.56}{23.2189 - \ln p} - 228.6 \qquad \text{(C-9)}$$

and taking its complete differential,

$$dT_{sat} = \frac{\partial T_{sat}}{\partial p} dp \qquad \text{(C-10)}$$

Solving the above equation and dividing with T_{sat} on both sides of the equation will yield,

$$\frac{dT_{sat}}{T_{sat}} = \left(\frac{1}{T_{sat}}\right)\left(\frac{3842.56}{(23.2189 - \ln p)^2}\right)\left(\frac{dp}{p}\right) \qquad \text{(C-11)}$$

The averaged exit pressure (441.357 mbar abs) and averaged saturation temperature (78.725°C) obtained from all the experimental runs performed were used. The variation in pressure is then estimated to be

$\left(\frac{dp}{p}\right) = \pm 0.0295$ ± 13 mbar abs accuracy from an averaged experimental exit pressure value of 441.357 mbar abs.

Hence, using the value of $\left(\frac{dp}{p}\right)$ and the averaged experimental values of exit pressure and saturation temperature, the error due to the variation of saturation temperature can be estimated from equation (C-11) to be:

$$\underline{\underline{\left(\frac{dT_{sat}}{T_{sat}}\right) = \pm 9.16 \times 10^{-3}}} \qquad \text{(C-12)}$$

Error in wall superheat:

The possible errors associated with the wall superheat in saturated two-phase flow are slightly more complex to evaluate since its values change with quality along the test section, with different operating conditions and the uncertainties in the test section thermal conductivity. Nevertheless, it is still possible to provide an estimate of the error, albeit with some simplifications listed below:

- The **average wall and saturation temperature values** were used. These average values were obtained from all the 42 experimental runs in both the main and repeated databases.

- The **average pressure** for the whole experimental database is taken to be that at 441.357 mbar abs.

- Due to the lack of precise data for the **thermal conductivity** of ASTM 316 stainless steel, an estimate of **10%** variation based on the linear interpolation of its values (12.7 $Wm^{-1}K^{-1}$ at 0°C and 14.0 $Wm^{-1}K^{-1}$ at 100°C by Beaton, 1990) is deemed to be fair.

The total error in the wall superheat used can then be estimated from the following equations:

$$\Delta T_{sat} = T_{w_{inside}} - T_{sat} \tag{C-13}$$

which is related to the experimentally measured wall temperature as:

$$\Delta T_{sat} = T_{w_{measured}} - \left(\frac{\dot{q}\, r_1}{\lambda}\right)\left(\frac{1}{2} - \frac{r_2^2}{\left(r_2^2 - r_1^2\right)}\ln\left(\frac{r_2}{r_1}\right)\right) - T_{sat} \tag{C-14}$$

where r_1 and r_2 are the inner and outer radius of the test section. In subsequent equations, $T_{w_{measured}}$ will be simplified as T_w, purely for the purpose of shortening the equations. Taking the complete differential of equation (C-14) gives:

$$\begin{aligned} d\Delta T_{sat} = {} & \frac{\partial \Delta T_{sat}}{\partial T_w} dT_w + \frac{\partial \Delta T_{sat}}{\partial \dot{q}} d\dot{q} + \frac{\partial \Delta T_{sat}}{\partial \lambda} d\lambda \\ & + \frac{\partial \Delta T_{sat}}{\partial r_1} dr_1 + \frac{\partial \Delta T_{sat}}{\partial r_2} dr_2 + \frac{\partial \Delta T_{sat}}{\partial T_{sat}} dT_{sat} \end{aligned} \tag{C-15}$$

Solving for each of the partial differential terms yield the following results:

$$\frac{\partial \Delta T_{sat}}{\partial T_w} = 1 \tag{C-16}$$

$$\frac{\partial \Delta T_{sat}}{\partial \dot{q}} = -\frac{r_1}{\lambda}\left[\frac{1}{2} - \frac{r_2^2}{\left(r_2^2 - r_1^2\right)}\ln\left(\frac{r_2}{r_1}\right)\right] \tag{C-17}$$

$$\frac{\partial \Delta T_{sat}}{\partial \lambda} = \frac{\dot{q}\, r_1}{\lambda^2}\left[\frac{1}{2} - \frac{r_2^2}{\left(r_2^2 - r_1^2\right)}\ln\left(\frac{r_2}{r_1}\right)\right] \tag{C-18}$$

$$\frac{\partial \Delta T_{sat}}{\partial r_1} = -\left(\frac{\dot{q}\, r_1}{\lambda}\right)\left[\frac{r_2^2}{r_1\left(r_2^2 - r_1^2\right)} - \frac{2\, r_1\, r_2^2}{\left(r_2^2 - r_1^2\right)^2}\ln\left(\frac{r_2}{r_1}\right)\right] - \left(\frac{\dot{q}}{\lambda}\right)\left[\frac{1}{2} - \frac{r_2^2}{\left(r_2^2 - r_1^2\right)}\ln\left(\frac{r_2}{r_1}\right)\right] \tag{C-19}$$

$$\frac{\partial \Delta T_{sat}}{\partial r_2} = -\left(\frac{\dot{q}\, r_1}{\lambda}\right)\left[\frac{2\, r_2^3}{\left(r_2^2 - r_1^2\right)^2}\ln\left(\frac{r_2}{r_1}\right) - \frac{2\, r_2}{\left(r_2^2 - r_1^2\right)}\ln\left(\frac{r_2}{r_1}\right) - \frac{r_2}{\left(r_2^2 - r_1^2\right)}\right] \tag{C-20}$$

$$\frac{\partial \Delta T_{sat}}{\partial T_{sat}} = -1 \tag{C-21}$$

In a similar procedure used earlier for the evaluation of the error associated with the heat flux, with the above mentioned simplifications, equation (C-15) can be worked on and the resultant equation is written as follows:

$$\begin{aligned}\frac{d\Delta T_{sat}}{\Delta T_{sat}} = &\left\{\left(\frac{\partial \Delta T_{sat}}{\partial T_w}\right)\left(\frac{T_w}{\Delta T_{sat}}\right)\left(\frac{dT_w}{T_W}\right)\right\} + \left\{\left(\frac{\partial \Delta T_{sat}}{\partial \dot{q}}\right)\left(\frac{\dot{q}}{\Delta T_{sat}}\right)\left(\frac{d\dot{q}}{\dot{q}}\right)\right\} \\ &+\left\{\left(\frac{\partial \Delta T_{sat}}{\partial \lambda}\right)\left(\frac{\lambda}{\Delta T_{sat}}\right)\left(\frac{d\lambda}{\lambda}\right)\right\} + \left\{\left(\frac{\partial \Delta T_{sat}}{\partial r_1}\right)\left(\frac{r_1}{\Delta T_{sat}}\right)\left(\frac{dr_1}{r_1}\right)\right\} \\ &+\left\{\left(\frac{\partial \Delta T_{sat}}{\partial r_2}\right)\left(\frac{r_2}{\Delta T_{sat}}\right)\left(\frac{dr_2}{r_2}\right)\right\} + \left\{\left(\frac{\partial \Delta T_{sat}}{\partial T_{sat}}\right)\left(\frac{T_{sat}}{\Delta T_{sat}}\right)\left(\frac{dT_{sat}}{T_{sat}}\right)\right\}\end{aligned} \tag{C-22}$$

Estimating the variation of the each term of equation (C-22)

$\frac{dT_w}{T_w} = \pm 0.00011$ $\pm$ 0.01 °C from the averaged wall temperature of 87.404°C.

$\frac{d\dot{q}}{\dot{q}} = \pm 9.66 \times 10^{-3}$ calculated from the error analysis of heat flux.

$\frac{d\lambda}{\lambda} = \pm 0.10$ the thermal conductivity was assumed to vary by 10%.

$\frac{dr_1}{r_1} = \pm 0.00174$ ± 0.02 mm from an inner test section radius of 11.49 mm.

$\frac{dr_2}{r_2} = \pm 0.00151$ ± 0.02 mm from an outer test section radius of 13.25 mm.

$\frac{dT_{sat}}{T_{sat}} = \pm 9.16 \times 10^{-3}$ calculated from the error analysis on saturation temperature.

In order to evaluate the random error, each term in equation (C-18) is squared, and its sum will give the mean squared error for the wall superheat. To compute each of these term, the following averaged values were used:

Averaged values

- $\dot{q}$ = 45 000 Wm^{-2}
- p = 44 135.7 Nm^{-2} (441.357 mbar abs)
- λ = 13.717 $Wm^{-1}K^{-1}$
- r_1 = 0.01149 m
- r_2 = 0.01325 m
- ΔT_{sat} = 5.907 °C
- T_{sat} = 78.725 °C
- T_w = 87.404 °C

$$\left(\frac{d\Delta T_{sat}}{\Delta T_{sat}}\right)^2 = \left\{\left(\frac{\partial \Delta T_{sat}}{\partial T_w}\right)\left(\frac{T_w}{\Delta T_{sat}}\right)\left(\frac{dT_w}{T_W}\right)\right\}^2 + \left\{\left(\frac{\partial \Delta T_{sat}}{\partial \dot{q}}\right)\left(\frac{\dot{q}}{\Delta T_{sat}}\right)\left(\frac{d\dot{q}}{\dot{q}}\right)\right\}^2$$
$$+\left\{\left(\frac{\partial \Delta T_{sat}}{\partial \lambda}\right)\left(\frac{\lambda}{\Delta T_{sat}}\right)\left(\frac{d\lambda}{\lambda}\right)\right\}^2 + \left\{\left(\frac{\partial \Delta T_{sat}}{\partial r_1}\right)\left(\frac{r_1}{\Delta T_{sat}}\right)\left(\frac{dr_1}{r_1}\right)\right\}^2$$
$$+\left\{\left(\frac{\partial \Delta T_{sat}}{\partial r_2}\right)\left(\frac{r_2}{\Delta T_{sat}}\right)\left(\frac{dr_2}{r_2}\right)\right\}^2 + \left\{\left(\frac{\partial \Delta T_{sat}}{\partial T_{sat}}\right)\left(\frac{T_{sat}}{\Delta T_{sat}}\right)\left(\frac{dT_{sat}}{T_{sat}}\right)\right\}^2 \quad \text{(C-23)}$$

Writing the above equation (C-23) in its entirety will give,

$$\left(\frac{d\Delta T_{sat}}{\Delta T_{sat}}\right)^2 = \left\{\left(\frac{T_w}{\Delta T_{sat}}\right)\left(\frac{dT_w}{T_W}\right)\right\}^2 + \left\{-\frac{r_1}{\lambda}\left[\frac{1}{2} - \frac{r_2^2}{\left(r_2^2 - r_1^2\right)}\ln\left(\frac{r_2}{r_1}\right)\right]\left(\frac{\dot{q}}{\Delta T_{sat}}\right)\left(\frac{d\dot{q}}{\dot{q}}\right)\right\}^2$$
$$+\left\{\frac{\dot{q}\, r_1}{\lambda}\left[\frac{1}{2} - \frac{r_2^2}{\left(r_2^2 - r_1^2\right)}\ln\left(\frac{r_2}{r_1}\right)\right]\left(\frac{1}{\Delta T_{sat}}\right)\left(\frac{d\lambda}{\lambda}\right)\right\}^2$$
$$+\left\{-\left[\begin{array}{l}\left(\frac{\dot{q}\, r_1}{\lambda}\right)\left[\frac{r_2^2}{r_1\left(r_2^2 - r_1^2\right)} - \frac{2\, r_1\, r_2^2}{\left(r_2^2 - r_1^2\right)^2}\ln\left(\frac{r_2}{r_1}\right)\right] - \\ \left(\frac{\dot{q}}{\lambda}\right)\left[\frac{1}{2} - \frac{r_2^2}{\left(r_2^2 - r_1^2\right)}\ln\left(\frac{r_2}{r_1}\right)\right]\end{array}\right]\left(\frac{r_1}{\Delta T_{sat}}\right)\left(\frac{dr_1}{r_1}\right)\right\}^2$$
$$+\left\{-\left(\frac{\dot{q}\, r_1}{\lambda}\right)\left[\frac{2\, r_2^3}{\left(r_2^2 - r_1^2\right)^2}\ln\left(\frac{r_2}{r_1}\right) - \frac{2\, r_2}{\left(r_2^2 - r_1^2\right)}\ln\left(\frac{r_2}{r_1}\right) - \frac{r_2}{\left(r_2^2 - r_1^2\right)}\right]\left(\frac{r_2}{\Delta T_{sat}}\right)\left(\frac{dr_2}{r_2}\right)\right\}^2$$
$$+\left\{-\left(\frac{T_{sat}}{\Delta T_{sat}}\right)\left(\frac{dT_{sat}}{T_{sat}}\right)\right\}^2 \quad \text{(C-24)}$$

Solving equation (C-24) using the averaged values will give the calculated mean squared error in wall superheat as,

$$\left(\frac{d\Delta T_{sat}}{\Delta T_{sat}}\right)^2 = 0.0173 \quad \text{(C-25)}$$

∴Random r.m.s. error in wall superheat:

$$\frac{d\Delta T_{sat}}{\Delta T_{sat}} = \pm 0.132 \qquad \text{(C-26)}$$

Error in heat transfer coefficient in saturated two-phase flow:

The total error of the heat transfer coefficient in the saturated two-phase flow region can be calculated from the following equation:

$$\alpha = \frac{\dot{q}}{\Delta T_{sat}} \qquad \text{(C-27)}$$

Taking a complete differential of the above equation will give

$$d\alpha = \left(\frac{\partial \alpha}{\partial \dot{q}}\right) d\dot{q} + \left(\frac{\partial \alpha}{\partial \Delta T_{sat}}\right) d\Delta T_{sat} \qquad \text{(C-28)}$$

Solving for each of the partial differential terms yield the following results:

$$\left(\frac{\partial \alpha}{\partial \dot{q}}\right) = \frac{1}{\Delta T_{sat}} \qquad \text{(C-29)}$$

$$\left(\frac{\partial \alpha}{\partial \Delta T_{sat}}\right) = -\frac{\dot{q}}{(\Delta T_{sat})^2} \qquad \text{(C-30)}$$

Equation (C-28) can be re-written as equation (C-31) after some algebraic manipulation, before being squared (equation (C-32)) to enable the evaluation of the mean squared error.

$$\left(\frac{d\alpha}{\alpha}\right) = \left\{\left(\frac{\partial \alpha}{\partial \dot{q}}\right)\left(\frac{\dot{q}}{\alpha}\right)\left(\frac{d\dot{q}}{\dot{q}}\right)\right\} + \left\{\left(\frac{\partial \alpha}{\partial \Delta T_{sat}}\right)\left(\frac{\Delta T_{sat}}{\alpha}\right)\left(\frac{d\Delta T_{sat}}{\Delta T_{sat}}\right)\right\} \quad \text{(C-31)}$$

$$\left(\frac{d\alpha}{\alpha}\right)^2 = \left\{\left(\frac{\partial \alpha}{\partial \dot{q}}\right)\left(\frac{\dot{q}}{\alpha}\right)\left(\frac{d\dot{q}}{\dot{q}}\right)\right\}^2 + \left\{\left(\frac{\partial \alpha}{\partial \Delta T_{sat}}\right)\left(\frac{\Delta T_{sat}}{\alpha}\right)\left(\frac{d\Delta T_{sat}}{\Delta T_{sat}}\right)\right\}^2 \quad \text{(C-32)}$$

Simplifying equation (C-32)using equations (C-27), (C-29) and (C-30) will give:

$$\left(\frac{d\alpha}{\alpha}\right)^2 = \left(\frac{d\dot{q}}{\dot{q}}\right)^2 + \left(\frac{d\Delta T_{sat}}{\Delta T_{sat}}\right)^2 \quad \text{(C-33)}$$

where the variations in the heat flux and wall superheat terms are:

$\left(\frac{d\dot{q}}{\dot{q}}\right) = \pm 9.66 \times 10^{-3}$ calculated from the error analysis on heat flux.

$\left(\frac{d\Delta T_{sat}}{\Delta T_{sat}}\right) = \pm 0.132$ calculated from the error analysis on wall superheat.

Hence, the calculated mean squared error in heat transfer coefficient:

$$\left(\frac{d\alpha}{\alpha}\right)^2 = 0.0174 \quad \text{(C-34)}$$

$\therefore$ **Random r.m.s. error in heat transfer coefficient:**

$$\underline{\underline{\left(\frac{d\alpha}{\alpha}\right) = \pm 0.132}} \quad \text{(C-35)}$$

APPENDIX D

Determination of experimental matrix

For the given test section tube diameter and power supply available for heating, only a limited range of flow and operating parameters can be used to obtain annular flow (at least at the test section exit) in the sub-atmospheric experiments. The criterion selected for the transition to annular flow is that when the dimensionless gas superficial velocity, U_G^* reaches the value of unity. The equations used to determine the feasible operating range are as follows:

$$U_G^* = U_G \sqrt{\frac{\rho_G}{g\,D\,(\rho_L - \rho_G)}} \tag{D-1}$$

For $U_G^* = 1$,

$$U_G = \dot{m}\,x = \sqrt{\frac{g\,D\,(\rho_L - \rho_G)}{\rho_G}} \tag{D-2}$$

which can be re-written as

$$x = \frac{1}{\dot{m}} \sqrt{\frac{g\,D\,(\rho_L - \rho_G)}{\rho_G}} \tag{D-3}$$

This is the quality that will theoretically cause annular flow to occur at the test section outlet. In the case of a heated system, the thermodynamic quality is calculated from the following equation,

$$x = \frac{4\,\dot{q}\,z}{\dot{m}\,D\,h_{LG}} - \frac{C_{pL}\,\Delta T_{subcool}}{h_{LG}} \qquad \text{(D-4)}$$

By solving both equations (D-3) and (D-4) for different values of mass fluxes, heat fluxes and subcoolings, the following operating parameters were calculated and utilised in the sub-atmospheric experiments.

Range of mass flux

For annular flow : 50.17 and 62.3 $kgm^{-2}s^{-1}$

Range of heat flux

For annular flow : 40 and 50 kWm^{-2}

Range of outlet pressure

For annular flow : 250, 500 and 1000 mbar abs.

Range of inlet subcooling

For annular flow : ≈ 15 °C and ≈ 40 °C

APPENDIX E

Experimental runs

The experimental runs conducted in the annular flow series of the SAE experiments are listed below, giving their run names and operating conditions.

Run Name	Outlet Pressure (mbar abs)	$\dot{m}\left(\mathrm{kgm^{-2}s^{-1}}\right)$	$\dot{q}\left(\mathrm{kWm^{-2}}\right)$	$\Delta T_{subcool}\left(^{\circ}\mathrm{C}\right)$
250-1	251	50.17	50	16.282
250-2	250	50.17	40	16.489
250-3	249	62.3	50	16.209
250-4	250	62.3	40	14.952
250-5	251	50.17	50	39.893
250-6	250	62.3	50	39.074
250-7A	251	50.17	40	39.66
250-7B	250	50.17	40	29.704
250-8A	250	62.3	40	38.725
250-8B	250	62.3	40	29.985
500-1	501	50.17	50	12.336
500-2	500	50.17	40	12.186
500-3	501	62.3	50	12.227
500-4	499	62.3	40	11.991
500-5	500	50.17	50	40.283

500-6	502	62.3	50	39.88
500-7	501	50.17	40	39.384
500-8	501	62.3	40	39.125
1000-1	997	50.17	50	13.756
1000-2	998	50.17	40	12.487
1000-3	999	62.3	50	15.559
1000-4	998	62.3	40	13.157
1000-5	1000	50.17	50	44.712
1000-6	1001	62.3	50	44.15
1000-7	998	50.17	40	42.107
1000-8	999	62.3	40	40.981

Table E-1 SAE experimental runs

On top of the 26 experimental runs conducted above, 16 additional re-runs at 250 mbar abs outlet pressure were performed to check and confirm on the repeatability and accuracy of the measurements. The following table lists the key operating parameters of these 16 experimental runs.

Run Name	Outlet Pressure (mbar abs)	$\dot{m}\left(\mathrm{kgm^{-2}s^{-1}}\right)$	$\dot{q}\left(\mathrm{kWm^{-2}}\right)$	$\Delta T_{subcool}\left(^{\circ}\mathrm{C}\right)$
250-1A	250	50.17	50	14.766
250-1B	265	50.17	50	25.12
250-1C	268	50.17	50	21.489
250-1D	267	50.17	50	22.099
250-2A	220	50.17	40	26.798
250-2B	220	50.17	40	27.064
250-2C	257	50.17	40	20.941
250-2D	256	50.17	40	20.846
250-3A	265	62.3	50	29.323
250-3B	265	62.3	50	29.695

250-3C	265	62.3	50	27.317
250-3D	268	62.3	50	27.833
250-4A	225	62.3	40	28.807
250-4B	225	62.3	40	28.736
250-4C	263	62.3	40	21.425
250-4D	261	62.3	40	21.406

Table E-2 SAE repeatability runs

ADDENDA

The following points are included for completeness of this thesis:

- In reference to Chapter 4, it was stated that the SAE rig's key components, i.e. the heating system, pumps, tanks and data logging equipment, were salvaged tested and recommissioned from a UKAEA boiling rig. Apart from the collaboration with Dr. Pickering to clean and test all these components, the author's other main responsibities and contributions during the SAE rig's design, construction and commissioning were as follows:

  (i) The full design of the cooling water and the safety pressure relief systems and joint effort in the building of the remainder of the SAE rig pipe work, drawing up the operating procedures and HAZOP study.

  (ii) The full design and calibration of the instrumentation for the steady state mode operation with the exception of the calibration of the pressure transducers; this was done by Dr. Pickering (1994). The author also wrote the data acquisition software for the steady state experiments.

  (iii) The complete commissioning tests of the SAE rig for the steady state operations and revision of the operating procedures.

- In reference to flow boiling hysteresis, there was no provision made during the experiments for the control or measurement of the dissolved gas content in the test fluid. Consequently, the proposed hypothesis on the expected effects and type of interactions of dissolved gas (as discussed in page 196) on flow boiling hysteresis is therefore *strictly* qualitative.

- Since the test section was built from commercially available stainless steel (ASTM 316) and its surface was not specially prepared in any way, it is assumed that a wide range of cavity sizes are available for nucleate boiling. Typical cavity sizes which nucleation occurs are normally very small of the order of 1 μm in diameter (see Hewitt et al., 1994).

Table 5.11 (page 190) is extended to include the surface tension and the p-T_{SAT} variation for the key physical properties of water to reflect their roles via the dissolved gas effects on bubble nucleation in flow boiling hysteresis.

p (mbar abs.)	ρ_L (kgm^{-3})	ρ_G (kgm^{-3})	ρ_L/ρ_G ratio	h_{LG} (J/kg)	λ_L ($Wm^{-1}K^{-1}$)
250	980.490	0.161	6090	2.346×10^6	0.658
500	970.780	0.309	3142	2.306×10^6	0.670
1000	958.405	0.590	1624	2.259×10^6	0.678

p (mbar abs.)	T_{SAT} (°C)	σ (Nm^{-1})
250	65.0	6.54×10^{-2}
500	81.3	6.24×10^{-2}
1000	99.6	5.90×10^{-2}

- An additional reference to the flow boiling hysteresis is that of Wadekar (1993) who conducted experiments on in-tube flow boiling of cyclohexane. His paper focused on the describing and classifying various temperature profiles and hysteresis effects. He noted that the hysteresis effects were more pronounced at lower flow rates and attributed this observation to:

    1. The effect of bubble activity is more pronounced at lower flow rate due to a lower single phase heat transfer rate.

    2. At low flow rates, the bubbles generated at the point of onset tends to slide along the tube wall over a longer downstream length, thereby altering the rate of heat transfer over a longer length.

Reference: **Wadekar, V.V.** (1993) Onset of boiling in vertical upflow. *AIChE Symp. Series No. 295, Vol. 89*, pp. 293-299.

- In reference to the proposed hypothesis on thermal nonequilibrium causing the local heat transfer coefficient maxima (see Chapter 5), it is stressed that there is *no direct evidence in the form of measurements* to support the hypothesis, except for qualitative arguments as presented.

CORRIGENDA

The following are major corrigenda to the thesis:

- The Baker (1954) dimensionless scaling parameter (see page 38) for his horizontal flow pattern map are best re-written as follows:

$$\lambda = \left[\left(\frac{\rho_G}{\rho_A}\right)\left(\frac{\rho_L}{\rho_W}\right)\right]^{0.5} \tag{2.1}$$

$$\psi = \left(\frac{\sigma_W}{\sigma}\right)\left[\left(\frac{\eta_L}{\eta_W}\right)\left(\frac{\rho_W}{\rho_L}\right)^2\right]^{1/3} \tag{2.2}$$

where the subscripts A and W denote the air and water physical properties are the standard atmospheric pressure and room temperature (20°C).

- page 99 (after equation 3.36 and before the preceeding text) **Missing text:**
Yagov (1995) suggested that for subcooled flow boiling, an asymptotic form of the heat transfer coefficient correlation be used as follows,

$$\alpha = \left(\alpha_{nb}^2 + \alpha_L^2\right)^{1/2} \tag{3.36a}$$

- Figure 5.11, page 207 is corrected to include the data points for Tfluid (measured) as given below.

Figure 5.11 Comparison of measured and calculated fluid temperature profiles for a typical run at 1000 mbar abs exit pressure (Run 1000-1)